

I. A COVALENT/COMPUTATIONAL APPROACH FOR SENSING CHIRALITY
II. OXIDATIVE FUNCTIONALIZATION OF THE INDOLE CORE
III. DESIGN AND SYNTHESIS OF NOVEL CYANINE DYES AS PHOTORECEPTORS
FOR PHOTOVOLTAICS

By

Jun Zhang

A DISSERTATION

Submitted to
Michigan State University
in partial fulfillment of the requirements
for the degree of

Chemistry – Doctor of Philosophy

2018

ABSTRACT

- I. A COVALENT/COMPUTATIONAL APPROACH FOR SENSING CHIRALITY
- II. OXIDATIVE FUNCTIONALIZATION OF THE INDOLE CORE
- III. DESIGN AND SYNTHESIS OF NOVEL CYANINE DYES AS PHOTORECEPTORS FOR PHOTOVOLTAICS

By

Jun Zhang

In the first part, a simple and efficient protocol for sensing the absolute stereochemistry and enantiomeric excess of chiral monoamines is described. Preparation of the sample requires a single-step reaction of the 1,1'-(bromomethylene)dinaphthalene with the chiral amine. Analysis of the exciton coupled circular dichroism (ECCD) generated from the derivatized chiral amine sample, along with comparison to conformational analysis performed computationally, yields the absolute stereochemistry of the parent chiral monoamine. Expansion of this methodology also leads to the absolute stereochemical determination of chiral carboxylic acids.

In the second part, a tunable reaction between 3-oxindole formation and selective C-H oxidation or amination under a mild condition is described. Substituted alkyl position on the indole directs the reaction to different pathways under similar conditions. Mechanistic studies reveal the oxidation cycle of Cu(I)/Cu(II), hydroxylamine and air play different roles in this reaction.

In the third part, a simple method to tune the Stokes shift of heptamethine cyanine dyes is introduced. After various computational studies, we were able to build a theoretical model to predict the photophysical properties of cyanine dyes. Cyanine analogs were synthesized as fluorophores for luminescent solar concentrators (LSCs) to harvest solar

energy. The absorption range of the synthesized dyes were from 600 nm to 780 nm, with Stokes shift as large as 180 nm.

To my Mom and Dad

ACKNOWLEDGMENTS

I want to first thank my family for the support and love during my graduate school in Michigan State University.

I am really grateful of being a graduate student in Babak's lab. It's really an enjoyable journey to learn and enjoy chemistry here. Our group is like a big family; we really enjoy the summer camping as well as summer soccer games. Although most of the time I scored the most on the soccer field. Babak is a really cool friend, he gave very good insights to my projects and encouraged me to pursue my own chemistry. Whenever I came up with a new idea, he always supported me to pursue them. Chrysoula has done amazing jobs. I believe she has been "impressed" by my manuscripts many times.

I would like to thank all my lab members, they are really helpful and kind. I want to thank Hadi for the collaboration on the porphyrin ECCD projects, Ding and Wei for daily chemistry discussion, my undergraduate student Minji for assistance. Even outside the lab, we also had lot of fun: summer tennis games with Debarshi, Pokémon hunting with Liz, etc. Huge fun with these guys!

I would also like to thank Prof. Tatuso for the collaboration on the CD calculation part, Dr. Staples for the amazing X-Ray help and Prof. Lunt for the collaboration on the exciting LSCs projects. All of these cool things makes my graduate school journey unforgettable and invaluable.

TABLE OF CONTENTS

LIST OF TABLES.....	x
LIST OF FIGURES.....	xiii
LIST OF SCHEMES.....	xix
KEY TO SYMBOLS AND ABBREVIATIONS.....	xxi
Chapter I: Determination of Absolute Stereochemistry and Enantiomeric Excess.	1
I.1. Introduction to chirality.....	1
I.1.1 Fluorescent method for absolute stereochemical determination.....	3
I.1.2 Microwave method for absolute stereochemical determination.....	4
I.1.3 Vibrational circular dichroism for absolute stereochemical determination.....	5
I.1.4 Electronic circular dichroism method for absolute stereochemical determination.....	6
I.1.4.1 Electronic circular dichroism coupled with calculations.....	7
I.1.4.2 Exciton Coupled Circular Dichroism method for absolute stereochemical determination.....	9
I.1.4.3 Exciton Coupled Circular Dichroism for absolute stereochemical determination.....	12
I.2. Introduction to measuring enantiomeric excess.....	16
I.2.1 Improving chromatographic separation for rapid <i>ee</i> determination.....	17
I.2.2 Optical methods for <i>ee</i> analysis.....	18
I.3 Accomplishments from the Borhan's group.....	22
REFERENCES.....	23
Chapter II: Computationally Aided Absolute Stereochemical Determination of Enantioenriched Amines.	28
II.1. Introduction of chemical derivatization method.....	28
II.1.1 Design goals of the new chemical derivatization method.....	30
II.1.2 Initial reporter design.....	31
II.1.3 Literature precedence.....	33
II.2 Preliminary study.....	34
II.3 Reaction rate and additive study.....	38
II.4 Absolute stereochemical determination of aromatic amines.....	41
II.4.1 Computational analysis.....	43
II.4.2 Crystallography study.....	49
II.5 Absolute stereochemical determination of aliphatic amines.....	50
II.6 Analysis of amino alcohols.....	52
II.7 Analysis of secondary amines.....	53
II.8 Rapid <i>ee</i> analysis.....	57

II.8.1 Effect of impurity on <i>ee</i> analysis.....	57
II.8.2 Standard curve for <i>ee</i> analysis.....	60
II.9 Experimental section.....	63
II.9.1 Materials and general instrumentations.....	63
II.9.2 General procedure for analysis of absolute stereochemistry of amines.....	63
II.9.3 Synthesis of the compounds.....	64
II.9.3.1 General procedures for the synthesis of II-1 amine derivatives.....	66
II.9.4 HPLC data for chiral amines.....	81
II.9.5 Crystal structure of II-3-D	83
II.9.6 ECCD spectra of II-1 derivatized chiral amines.....	86
REFERENCES.....	97

Chapter III: Di(1-Naphthyl) Methanol Ester of Carboxylic Acids for Absolute Stereochemical Determination.....

III.1. Introduction.....	104
III.1.1 Strategies towards the chiral carboxylic acids sensing.....	107
III.2 Absolute stereochemical determination of chiral aliphatic carboxylic acids.....	110
III.3 Absolute stereochemical determination of chiral aromatic carboxylic acids.....	114
III.4 High level computation and crystal structure study.....	118
III.5 Use of a standard curve for <i>ee</i> determination.....	120
III.6 Future work.....	122
III.6.1 Absolute stereochemical determination of chiral alcohols.....	122
III.6.2 A non-derivatizing host for absolute stereochemical determinations.....	124
III.6.3 More red-shifted chromophores.....	128
III.7 Experimental section.....	130
III.7.1 Materials and general instruments.....	130
III.7.2 General procedure for CD measurements.....	130
III.7.3 Synthesis of the starting materials.....	131
III.7.4 General synthesis of esters for absolute stereochemical determination..	137
III.7.5 Molecular modeling and CD calculations (represented with III-12-D)....	147
III.7.6 Crystal structure.....	148
III.7.7 ECCD spectra of III-1 derivatized chiral carboxylic acids.....	152
REFERENCES.....	160

Chapter IV: Tuning Indole Oxidation by Copper Catalyst.....

IV.1. Introduction	164
IV.1.1. Intramolecular oxindole core construction.....	165
IV.1.2. Intermolecular oxindole core construction.....	168
IV.1.3. Indole selective C-H functionalization.....	171
IV.2. Discovery of the new reaction	172
IV.2.1. Brief introduction to the reactions.....	172
IV.2.2. The initial proposed reaction.....	174
IV.2.3. Initial reaction discovery.....	176
IV.3 Reaction screening.....	179
IV.3.1 Indole alkyl position screening.....	179

IV.3.2 Oxindole reaction condition screening.....	180
IV.4 Indole dearomatization reaction.....	182
IV.4.1 Reaction substrate scope.....	182
IV.4.2 Important note regarding the reaction.....	183
IV.4.3 Substrates that do not work.....	184
IV.4.4 Photo physical properties of the oxindole product.....	186
IV.4.5 Photophysical calculations	188
IV.4.6 Mechanistic studies.....	189
IV.4.7 Proposed mechanism.....	193
IV.5 Selective C-H functionalization	194
IV.5.1 Reaction optimization.....	195
IV.5.2 Reaction substrate scope.....	196
IV.5.3 Exploring ring fused indoles	199
IV.5.4. Attempts towards enantioselective C-H functionalization	200
IV.5.5. Reaction mechanism.....	201
IV.6 Summary and conclusion.....	202
IV.7 Experimental section.....	204
IV.7.1 Materials and general instrumentations.....	204
IV.7.2 Preparation of starting materials.....	205
IV.7.2.1 Procedure 1	205
IV.7.2.2 Procedure 2.....	206
IV.7.2.3 Procedure 3.....	207
IV.7.2.4 Procedure 4.....	209
IV.7.2.5 Procedure 5.....	210
IV.7.2.6 Procedure 6.....	212
IV.7.2.7 Procedure 7.....	214
IV.7.2.8 Procedure 8.....	215
IV.7.2.9 Procedure 9.....	218
IV.7.3 Oxindole product characterization.....	218
IV.7.4 Indole C-H functionalization product characterization.....	231
IV.7.5 Ring fused indoles substrates.....	246
IV.7.6 X-Ray crystallographic data.....	248
REFERENCES.....	258

Chapter V: Engineering Large Stokes Shift Heptamethine Cyanine Dyes for Transparent Luminescent Solar Concentrators (LSCs)	265
V.1 Introduction of LSCs.....	265
V.2 Literature precedence for large Stokes shift cyanine dyes.....	267
V.2.1 Literature precedence on improving quantum yield.....	269
V.3 Engineering large Stokes shift cyanine dyes.....	270
V.3.1 Series 1 cyanine dyes.....	270
V.3.2 Series 2 cyanine dyes.....	278
V.4 Theoretical calculation.....	280
V.4.1 Cyanine <i>s-trans</i> and <i>s-cis</i> geometries.....	280
V.4.2 Effect of twisting and bending.....	282

V.4.3 Geometry at the nitrogen atom.....	293
V.5 Experimental Section.....	301
V.5.1 Materials and general instrumentations.....	301
V.5.2 Computational analysis.....	301
V.5.3 General dye synthesis.....	301
REFERENCES.....	314

LIST OF TABLES

Table II-1. All CD measurements were recorded in acetonitrile (10 μM) at rt.....	42
Table II-2. Theoretical <i>P</i> and <i>M</i> predictions were obtained by tabulating the population of conformations that yield <i>P</i> or <i>M</i> helicity by DFT at the B3LYP/6-31G* level.....	46
Table II-3. Chiral aliphatic amines ECCD analysis. All CD measurements were recorded in acetonitrile (10 μM) at rt. Theoretical <i>P</i> and <i>M</i> predictions were obtained by tabulating the population of conformations that yield <i>P</i> or <i>M</i> helicity by DFT at the B3LYP/6-31G* level.....	51
Table II-4. Chiral amino alcohols ECCD analysis. All CD measurements were recorded in acetonitrile (10 μM) at rt. Theoretical <i>P</i> and <i>M</i> predictions were obtained by tabulating the population of conformations that yield <i>P</i> or <i>M</i> helicity by DFT at the B3LYP/6-31G* level.	52
Table II-5. Chiral secondary amines ECCD analysis. All CD measurements were recorded in acetonitrile (10 μM) at rt.	56
Table II-6. ECCD signal recorded at 227 nm with different equivalent of HCl.....	59
Table II-7. Measured <i>ees</i> of unknown amine samples.....	62
Table II-8. Crystal data and structure refinement for II-3-D	84
Table II-9. Fractional atomic coordinates ($\times 10^4$) and equivalent isotropic displacement parameters ($\text{\AA}^2 \times 10^3$) for II-3-D . U_{eq} is defined as 1/3 of the trace of the orthogonalised U_{ij}	85
Table III-1. ^a All CD measurements were recorded with 10 μM ester derivative in acetonitrile at rt. ^b Calculated populations of <i>P</i> and <i>M</i> helical conformers were obtained via tabulating the population of conformations that yield positive and negative helicity....	113
Table III-2. ^a All CD measurement were recorded with 10 μM ester derivative in acetonitrile at rt. ^b Calculated populations of <i>P</i> and <i>M</i> helical conformers were obtained via tabulating the population of conformations that yield positive and negative helicity.....	117
Table III-3. Summarized calculation data.....	148
Table III-4. Crystal data and structure refinement for III-12-D	150

Table III-5. Fractional atomic coordinates ($\times 10^4$) and equivalent isotropic displacement parameters ($\text{\AA}^2 \times 10^3$) for III-12-D . U_{eq} is defined as 1/3 of the trace of the orthogonalised U_{ij}	151
Table IV-1. Oxindole formation optimization. ^a Determined by ¹ H-NMR using MTBE as an internal standard. All reactions were performed at 0.1 mmol scale.....	181
Table IV-2. Reaction optimization. ^a Determined by ¹ H-NMR using MTBE as an internal standard, all reactions were performed at 0.1 mmol scale.....	195
Table IV-3. Crystal data and structure refinement for IV-19	250
Table IV-4: Fractional atomic coordinates ($\times 10^4$) and equivalent isotropic displacement parameters ($\text{\AA}^2 \times 10^3$) for IV-19 . U_{eq} is defined as 1/3 of the trace of the orthogonalised U_{ij}	251
Table IV-5. Crystal data and structure refinement for IV-41-O	252
Table IV-6: Fractional atomic coordinates ($\times 10^4$) and equivalent isotropic displacement parameters ($\text{\AA}^2 \times 10^3$) for IV-41-O . U_{eq} is defined as 1/3 of the trace of the orthogonalised U_{ij}	253
Table IV-7. Crystal data and structure refinement for IV-41-N	254
Table IV-8: Fractional atomic coordinates ($\times 10^4$) and equivalent isotropic displacement parameters ($\text{\AA}^2 \times 10^3$) for IV-41-N . U_{eq} is defined as 1/3 of the trace of the orthogonalised U_{ij}	255
Table IV-9. Crystal data and structure refinement for IV-55	256
Table IV-10: Fractional atomic coordinates ($\times 10^4$) and equivalent isotropic displacement parameters ($\text{\AA}^2 \times 10^3$) for IV-55 . U_{eq} is defined as 1/3 of the trace of the orthogonalised U_{ij}	257
Table V-1. Spectroscopic data for series 1 cyanine dyes. Absorption, emission and quantum yield were measured in DCM. QY = quantum yield.....	276
Table V-2. Spectroscopic data for series 2 cyanine dyes. Absorption, emission and quantum yield were measured in DCM. QY = quantum yield.....	279
Table V-3. Screening computation functionals of cyanine dye V-4 . ^a Optimized geometry from MP2 level was subject to energy calculation at B3LYP/6-31+G*/CPCM level. Water is chosen for all the solvation models. E(S0) was calculated as singlet at ground state. E(S1) was calculated as singlet at excited state.....	283

Table V-4. Summarized 3 parameters data for series 1 cyanine dyes at DFT/B3LYP/6-31G*/CPCM(H₂O) level. Calculated results from SPARTAN 16 software..... 292

Table V-5. Summarized 3 parameters data for series 1 cyanine dyes at MP2 level. Calculated results from SPARTAN 16 software..... 293

Table V-6. Summarized data for series 1 cyanine dyes. ^aFully sp² and sp³ hybridized angles were obtained from SPRATN 16 at MP2/6-31G* level. ^bCyanine ∠_{C-N-C} angle was measure at PBE-D3/6-31G*/CPCM(H₂O) level..... 296

Table V-7. Summarized data for series 1 cyanine dyes. ^aFully sp² and sp³ hybridized angles were obtained from SPRATN 16 at MP2/6-31G* level. ^bCyanine ∠_{C-N-C} angle was measured at B3LYP-D3/6-31G*/CPCM(H₂O) level..... 297

LIST OF FIGURES

Figure I-1. Imine metathesis reaction between 2-aminonaphthalene condensed chiral imine with the guest chiral amine. Dual fluorescence emissions were observed.....	4
Figure I-2. Principal of microwave chiral sensing. μ_a , μ_b and μ_c are the dipole moments of the chiral propane-1,2-diol. A, B, C are the rotational constants.....	6
Figure I-3. Energy splitting between two identical chromophores in the excited state. Two chromophores <i>i</i> and <i>j</i> are coupled with each other and lead to two new energy states..	10
Figure I-4. Davydov splitting in the UV-Vis and ECCD.	10
Figure I-5. ECCD cotton effects. The black bars indicate two separate chromophore dipoles. Two different ECCD signals are observed.....	11
Figure I-6. Using porphyrin tweezer to sense chiral diamines. Upon binding with the guest diamine, the helical twist of the tweezer leads to the observed ECCD signal.....	13
Figure I-7. MAPOL host for ECCD analysis.....	15
Figure I-8. Sensing chiral amines through Fe(II) complex. Δ -(<i>S</i>)- <i>fac</i> and Δ -(<i>R</i>)- <i>fac</i> lead to negative and positive ECCD signals.	19
Figure I-9. Working model for the Pd complex to sense chiral amino acids and a direct mixture analysis of asymmetric imine hydrogenation reaction by UV-Vis and CD.....	20
Figure I-10. Oxo-vanadium (V) aminotriphenolate complex binds to the chiral analytes to yield the CD signal.....	21
Figure II-1. Derivatization of chiral monoamines with II-1 yields ECCD active derivatives.....	34
Figure II-2. Synthesis of compound II-1 . Both II-2 and II-1 can be easily synthesized in gram scales.....	35
Figure II-3. ECCD spectra obtained with derivatized chiral amines II-3-D and II-4-D (10^{-5} M) in acetonitrile at room temperature. The CD spectrum of II-1 , as expected, is silent. Naph = 1-naphthyl.	36
Figure II-4. ECCD solvents study: five different solvents were used to test the chiral amine derivative II-3-D (10^{-5} M concentration) at rt.....	37

Figure II-5. Interval scans study of (<i>S</i>)-methylbenzylamine II-3 and II-1 at room temperature. Top figure: reaction without additive, bottom figure: in presence of 2 equiv of AgNO ₃ .	39
Figure II-6. Rate study of the reaction of (<i>S</i>)-methylbenzylamine II-3 and II-1 at 10 μM in acetonitrile at room temperature. Top: rate profile based on CD read out, Bottom: comparison based on conversion.	40
Figure II-7. Common symbols for the ECCD study.	41
Figure II-8. ECCD spectrum of II-5-D , recorded at 10 ⁻⁵ M in acetonitrile at rt. Crystal structure of II-5-D , clearly shows a <i>P</i> helicity.	50
Figure II-9. ECCD spectra of enantiomeric II-1 derivatized benzyl protected aromatic amines (10 ⁻⁵ M) in acetonitrile at rt show opposite ECCD spectra.	54
Figure II-10. ECCD spectra of II-5-D and II-20-D (10 ⁻⁵ M) in acetonitrile at rt show different ECCD amplitudes.	55
Figure II-11. ECCD spectra of enantiomeric II-1 derivatized benzyl protected aliphatic amines (10 ⁻⁵ M) in acetonitrile at rt show opposite ECCD spectra. Cy = cyclohexyl.	56
Figure II-12. Acid impurity study. Pure II-3 amine yielded ECCD signal, amine II-3 HCl salt yielded no signal.	58
Figure II-13. Treatment of II-4-D with different equivalents of HCl. Signal decreased upon addition of HCl from 1 equivalent up to 50 equivalents, however, after addition of solid K ₂ CO ₃ , the CD signal was recovered.	58
Figure II-14. Treatment of II-4-D with H ₂ O ₂ stock solution at different equivalents. The ECCD signal remained unchanged.	60
Figure II-15. CD spectra of chiral amines II-5 and II-6 at various <i>ees</i> .	61
Figure II-16. Linear correlation of the CD signal with <i>ee</i> values of chiral amines.	61
Figure II-17. HPLC data for chiral amines.	82
Figure II-18. Crystal structure of II-3-D	83
Figure II-19. ECCD spectra of II-1 derivatized chiral amines.	84
Figure III-1. (a) Chiral amine sensing. (b) Working models for the carboxylic acids sensing. <i>P</i> and <i>M</i> helical conformations of the chiral ester. (c) Breaking down the chiral ester.	108
Figure III-2. A CD spectra of chiral aliphatic carboxylic esters III-2-D and III-3-D show the opposite ECCD signals. Np = 1-naphthyl.	111

Figure III-3. Distance differences between the chiral amines and chiral carboxylic acids. <i>d</i> refers to distance.....	112
Figure III-4. CD spectra of chiral aromatic carboxylic esters III-9-D and III-10-D show the opposite ECCD signals. Np = 1-naphthyl.....	115
Figure III-5. A correlation is observed between the strength of the ECCD spectra ($\Delta\epsilon$ of the high wavelength Cotton effect) and the population difference calculated for <i>P</i> and <i>M</i> helicities.....	118
Figure III-6. Theoretical calculation of ECCD for III-11-D overlapped with the experimentally observed spectrum.....	119
Figure III-7. Crystal structure of compound III-11-D exhibits the <i>P</i> helicity that would yield a positive ECCD signal.....	119
Figure III-8. ECCD spectra of chiral carboxylic acids III-11-D and III-12-D at various <i>ees</i>	121
Figure III-9. Linear correlation of the ECCD signals at 227 nm with exact <i>ee</i> values of chiral carboxylic acids.	121
Figure III-10. CD spectra of chiral mono alcohol ethers III-18-D and III-19-D show the opposite ECCD signals. Np = 1-naphthyl.....	123
Figure III-11. ECCD spectrum of enantio-enriched amino alcohol III-21 with new host III-20 in acetonitrile at 0 °C.....	126
Figure III-12. Potential chiral guests for ECCD study.....	127
Figure III-13. Theoretical CD spectra of III-12-D conformers calculated at B3LYP/cc-pVDZ level.....	148
Figure III-14. Crystal structure of III-12-D	149
Figure III-15. ECCD spectra of III-1 derivatized chiral carboxylic acids.....	152
Figure IV-1. Visible light induced aerobic dearomatization of indole.....	167
Figure IV-2. Copper catalyzed oxidative dearomatization/spirocyclization of indole..	168
Figure IV-3. Oxidative dearomatization of indole by Pd catalyst.....	169
Figure IV-4. Copper catalyzed aerobic oxidation of indole.....	170
Figure IV-5. Thionium mediated indole functionalization.....	171

- Figure IV-6.** Proposed indole substrates **IV-15** and **IV-16**. Reaction intermediates were computed at DFT/B3LYP 6-31+G* level (vacuum), with relative energies shown in the figure..... 177
- Figure IV-7.** Screening of the alkyl positions on indole. Substrates marked as “X” indicate no reaction. Substrates marked as “star” indicate there was a reaction..... 179
- Figure IV-8.** Indole dearomatization substrate scope. Reactions were conducted on 0.1 mmol scale and isolated by Prep-TLC. ^a1 equiv CuCl and 4 equiv of **IV-19** were used..... 183
- Figure IV-9.** Hydroxylamines or indole substrates that did not work under the optimal conditions. NR stands for no reaction. 185
- Figure IV-10.** UV-Vis spectra of compound **IV-19**, 30 μM in acetonitrile at rt..... 187
- Figure IV-11.** Fluorescent spectra of compound **IV-19** in various solutions at rt. Excited at 407 nm..... 187
- Figure IV-12.** HOMO and LUMO of compound **IV-19**. Left is HOMO, right is LUMO. Calculated results are shown below at PBE0-6-311+G** level. S0 is the ground state, S1 is the first excited state..... 188
- Figure IV-13.** C2 position CD₃ remained unchanged after the reaction. Top picture: starting material with deuterated C2 position. Bottom picture: After the reaction, product was analyzed by ¹H-NMR, integration of the area only indicated the Boc group..... 192
- Figure IV-14.** Proposed mechanism for indole dearomatization reaction..... 193
- Figure IV-15.** Unexpected indole allylic functionalization reaction. Crystal structures of compound **IV-41-O** is on the left and **IV-41-N** is on the right..... 194
- Figure IV-16.** Indole selective C-H functionalization scope. a) Reactions were conducted on a 0.1 mmol scale in 1 mL THF (with 20 equiv H₂O) and yield was measured by NMR with internal standard MTBE. *ar*_{O:N} defined as the oxidation to amination product ratio. b) 6 mol% pyridine was used. c) 4 mol% pyridine was used.....197
- Figure IV-17.** Obtaining both products in decent amount of yield. Reaction were conducted on a 0.2 mmol scale with 4 equivalent **IV-13** in 4 mL THF open to air..... 198
- Figure IV-18.** Ring fused indoles substrate scope. Reactions were conducted on a 0.2 mmol scale with 4 equivalent **IV-13** open to air. Crystal structure of **IV-55** was confirmed by X-Ray and crystal structure is shown above..... 199
- Figure IV-19.** Possible reaction mechanism to yield **IV-55**. Intermediates **IV-55-InA** and **IV-55-InB** are possible intermediates which can trap water to yield final product..... 200

Figure IV-20. Attempts to the enantioselective allylic indole functionalization. 4 equivalent of IV-13 were used. ^a Reaction conversion and product yield were measured by ¹ H-NMR. ^b ee value was measured by chiral HPLC equipped with OD-H column.....	201
Figure IV-21. Indole C-H functionalization mechanism.....	202
Figure IV-22. Crystal structure of IV-19	250
Figure IV-23. Crystal structure of IV-41-O	252
Figure IV-24. Crystal structure of IV-41-N	254
Figure IV-25. Crystal structure of IV-55	256
Figure V-1. Working model of LSCs. Both UV and near IR light can be harvested. S stands for Stokes shift and W stands for dye emission width.....	265
Figure V-2. Calculated Stokes shift impact on LSCs.....	267
Figure V-3. Large Stokes shift cyanine dyes. Absorption and emission were measured in methanol solution.....	268
Figure V-4. Bis-dipole form of cyanine dyes.....	269
Figure V-5. Spectroscopic data of different rhodamine derivate. ϕ , quantum yield; τ , fluorescence lifetime. V-2-B did not show appreciable absorption or emission.....	270
Figure V-6. Spectroscopic data for dye V-4 and V-5 . Absorption, emission and quantum yield were measured in DCM. SS= Stokes shift.....	274
Figure V-7. Spectroscopic data for dye V-8 and V-9 . Absorption, emission and quantum yield were measured in DCM. SS= Stokes shift.....	275
Figure V-8. Spectroscopic data of dye V-6 in various solvents.....	277
Figure V-9. Spectroscopic data for similar dye V-13 and V-4 . Absorption, emission and quantum yield were measured in DCM.....	279
Figure V-10. Two possible <i>s-cis</i> and <i>s-trans</i> conformers of dye V-4 . The lowest energies of these two conformers are computed at DFT/B3LYP/6-31G*/CPCM(H ₂ O) level from SPARTAN 16 software.....	281
Figure V-11. Calculated relative energy difference between the most stable <i>s-cis</i> and <i>s-trans</i> conformation at DFT/B3LYP/6-31G*/CPCM (H ₂ O) level.....	282
Figure V-12. Using different parameters to evaluate series 1 cyanine dyes.....	288

Figure V-13. Optimized ground state geometries of dye V-4 , V-8 and V-5 from SPARTAN 16.....	291
Figure V-14. Calculated Mulliken charge and electrostatic values of series 1 cyanine dyes at PBE-D3/6-31G*/CPCM(H ₂ O) level. No clear trend was observed in these attempts.....	292
Figure V-15. Linear correlation between the angle subtraction ($\text{angle}_{\text{donation}}$) and Stokes shift at DFT-D3 and PBE-D3 levels. Top figures: cyclic ring substrates; bottom figures: open chain substrates.....	295
Figure V-16. Linear correlation between the angle subtraction ($\text{angle}_{\text{donation}}$) and Stokes shift at DFT-D3 and PBE-D3 levels. Top figures: DFT-D3/B3LYP/6-31G*/CPCM(H ₂ O) level; bottom figures: PBE-D3/B3LYP/6-31G*/CPCM(H ₂ O) level.....	296

LIST OF SCHEMES

Scheme I-1. Enantiomers of chiral drugs can have different biological activities.....	1
Scheme I-2. Selected chiral drugs approved by FDA in 2017.....	2
Scheme I-3. Steps to assign absolute configuration by TDDFT assisted ECD analysis..	8
Scheme II-1. Four component covalent assembly for chiral alcohol CD sensing.....	30
Scheme II-2. Proposal of the initial structures. II-E to II-J are the potential structures for chiral sensing. M stands for the metal, Ar refers to different aromatic rings. L is the linker which can provide covalent bond with chiral guests. LG is the leaving group.....	31
Scheme II-3. Dinaphthyl ketals as chiral sensors.....	33
Scheme II-4. Step by step procedure for computational studies via DFT calculation...	45
Scheme II-5. Step by step demonstration of II-8-D predicted ECCD analysis.....	48
Scheme II-6: General procedure for preparation of samples for CD analysis.....	64
Scheme II-7: General procedure to sense chiral secondary benzyl protected amines..	64
Scheme III-1. Biphenyl chromophore probe for carboxylic acids absolute stereochemistry assignment. EDC = 1-ethyl-3-(3-dimethylaminopropyl)carbodiimide. DMAP = 4-dimethylaminopyridine.....	106
Scheme III-2. Anslyn's host for carboxylic acids absolute stereochemistry determination.....	107
Scheme III-3. Bis(porphyrin) tweezer for remote chirality sensing. TFA = trifluoroacetic acid.	108
Scheme III-4. Synthesis of compound III-1 and simple esterification of the carboxylic acids for the ECCD study. DCC = N,N'-Dicyclohexylcarbodiimide. DMAP = 4-dimethylaminopyridine.	111
Scheme III-5. Chiral mono-alcohol sensing method.	124
Scheme III-6. Design of new hosts. M refers to metal, B refers to boron, R refers to the substituents that can red shift the chromophores, L is the ligand.	125
Scheme III-7. Synthesis of the new host.....	126

Scheme III-8. Improve the reactivity of the new boron host. LG = leaving group.....	129
Scheme III-9. Two chromophores that can yield a redshifted CD signals.....	130
Scheme IV-1. Selected marketed drugs with indole core.....	164
Scheme IV-2. Selected indole functionalization reactions.....	165
Scheme IV-3. Biologically active compounds which contain 3-oxindole moiety.....	166
Scheme IV-4. Different types of the Pictet-Spengler reactions.....	172
Scheme IV-5. Versatile applications of the nitroso compound.....	173
Scheme IV-6. Mechanism for nitroso ene reaction.....	174
Scheme IV-7. Initial proposed reaction.....	175
Scheme IV-8. Mild nitroso generation. Py = pyridine.....	176
Scheme IV-9. Initial test reactions to validate the nitroso ene-aromatization proposal.	176
Scheme IV-10. Unexpected results of the indole test reactions.....	178
Scheme IV-11. Indole dearomatization reaction.....	189
Scheme IV-12. Control experiments for copper and air oxidation pathway.....	189
Scheme IV-13. Nitroso trapping experiments.....	190
Scheme IV-14. Deuterium labeling experiment was carried out to exclude an ene type reaction mechanism.....	191
Scheme IV-15. Overall reaction scheme.....	203
Scheme V-1. Positions on the cyanine dyes that can be modified.....	271
Scheme V-2. General scheme for cyanine dyes synthesis. DIPEA = N,N-Diisopropylethylamine.....	272
Scheme V-3. Series 1 cyanine dyes.....	273
Scheme V-4. Series 2 cyanine dyes.....	278
Scheme V-5. New parameter is established to quantify the electron donation from different nitrogen substituents.....	293

KEY TO SYMBOLS AND ABBREVIATIONS

$[\alpha]_D^{20}$	Specific optical rotation
ACN	Acetonitrile
Ar	Argon, aryl groups
Bn	Benzyl
Boc	<i>tert</i> -Butyloxycarbonyl
Pyr	Pyridine
<i>n</i> BuLi	<i>n</i> -Butyllithium
<i>t</i> BuLi	<i>t</i> -Butyllithium
CD	Circular Dichroism
CHCl ₃	Chloroform
DCM	Dichloromethane
ECCD	Exciton Coupled Circular Dichroism
ee	Enantiomeric excess
equiv	Equivalent
g	Gram
h	Hour
HOMO	Highest Occupied Molecular Orbital
Hz	Hertz
HRMS	High resolution mass spectrometry
<i>J</i>	Coupling constant

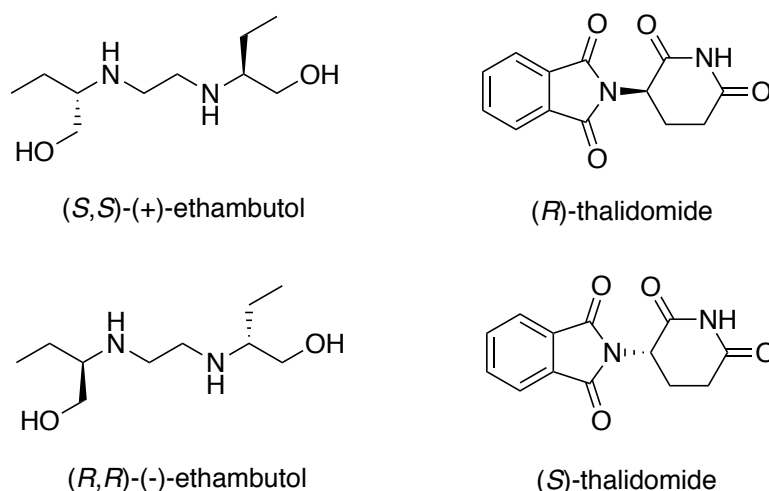
λ	Wavelength
λ_{abs}	Absorption wavelength
λ_{em}	Emission wavelength
LAH	Lithium aluminum hydride
LUMO	Lowest Unoccupied Molecular Orbital
LG	leaving group
m	Multiplet
M	Molar
mg	Milligram
min	Minute
mmol	Milimole
mol	Mole
MS	Molecule Sieve
Mol. CD	Molecular CD
N.R	No Reaction
NMR	Nuclear Magnetic Resonance
<i>p</i>	Para position
ppm	Parts per million
rt	Room temperature
s	Singlet
t	Triplet
Tf	Triflate group

TFA	Trifluoroacetic acid
THF	Tetrahydrofuran
TLC	Thin Layer Chromatography
Ts	Tosyl group
UV-Vis	Ultraviolet-Visible Spectroscopy
μM	Micro Molar
VCD	Vibrational Circular Dichroism

Chapter I: Determination of Absolute Stereochemistry and Enantiomeric Excess

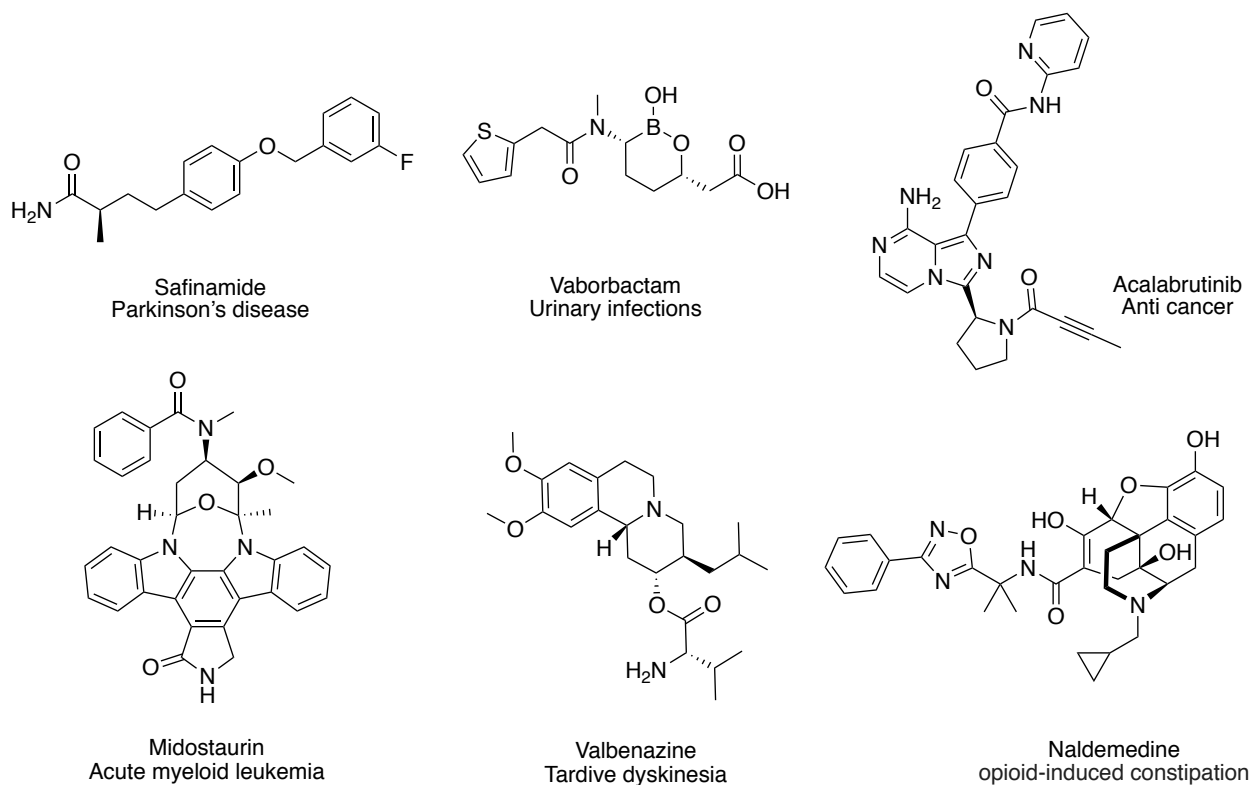
I.1. Introduction to chirality

Chirality is one of the most fundamental molecular properties in chemistry and biochemistry. It is critical as a determinant of activity in biological systems. Over the years, it has drawn significant attention in the process of drug development, since enantiomers of drug candidates may cause off-target problems or other serious issues in the biological systems.¹ For example, the (*S,S*)-(+)-ethambutol can be used to treat tuberculosis, while its enantiomer (*R,R*)-(-)-ethambutol may cause blindness; Another example is thalidomide, a drug that has caused serious birth defects back in the late 1950s and early 1960s. The (*R*)-thalidomide can be used to treat morning sickness during pregnancy, whereas the (*S*) enantiomer leads to birth defects. It is important to note that this drug epimerizes in the human body, so even if dosed with a highly enantiomerically pure (*R*)-thalidomide does not eliminate the side effect (**Scheme I-1**).²



Scheme I-1. Enantiomers of chiral drugs can have different biological activities.

In recent years, the U.S. Food and Drug Administration (FDA) has also required the manufacturers to identify each individual drug isomers' effect prior to clinical application. Drugs with enantiomers but without side effects are allowed to be produced in the racemic form while the others have to be produced in enantiomerically pure form. Here is the list of some new enantiomerically pure drugs which were approved in 2017 by FDA (**Scheme I-2**).³



Scheme I-2. Selected chiral drugs approved by FDA in 2017.

Thus, a rapid and convenient way to sense the absolute chirality of organic molecules is highly desired for the pharmaceutical industries. As for organic chemists, rapid chirality sensing can also accelerate the development of methodologies.

Common methods to determine the absolute stereochemistry rely heavily on X-ray crystallography and NMR spectroscopy. These are routine methods to assign chiral

structures and are widely accepted for scientific publication. However, these methods suffer their own limitations. For X-ray crystallography, presence of heavy atoms and a fine crystal is required, which is not always easy to obtain. As for NMR, milligram scale sample is needed to perform a reaction with a chiral analyte to form a diastereotopic complex which can be distinguished by NMR. Most of the time, the sample can not be recycled due to an irreversible chemical reaction. On the other hand, the use of chiroptical methods to assign the stereochemistry is emerging in recent years due to the rapid analysis time and minimum sample requirement. Methods using Fluorescent, Microwave, Vibrational Circular Dichroism (VCD) or Electronic Circular Dichroism (ECD) detection with empirical or non-empirical rules could serve as the alternatives for current methodologies.

I.1.1 Fluorescent method for absolute stereochemical determination

Recent development of fluorescent sensors for chiral sensing was pioneered by Pu's and other groups.⁴⁻⁵ Single and dual fluorescent responsive systems have been developed in the past few years. For single responsive system, normally a chiral host is needed to form a complex with the chiral analytes. The matched in terms of chirality complex normally exhibits a higher fluorescence intensity than the mismatched complex. Dual responsive system was first developed by Pu's group and the mechanism is shown below (**Figure I-1**).

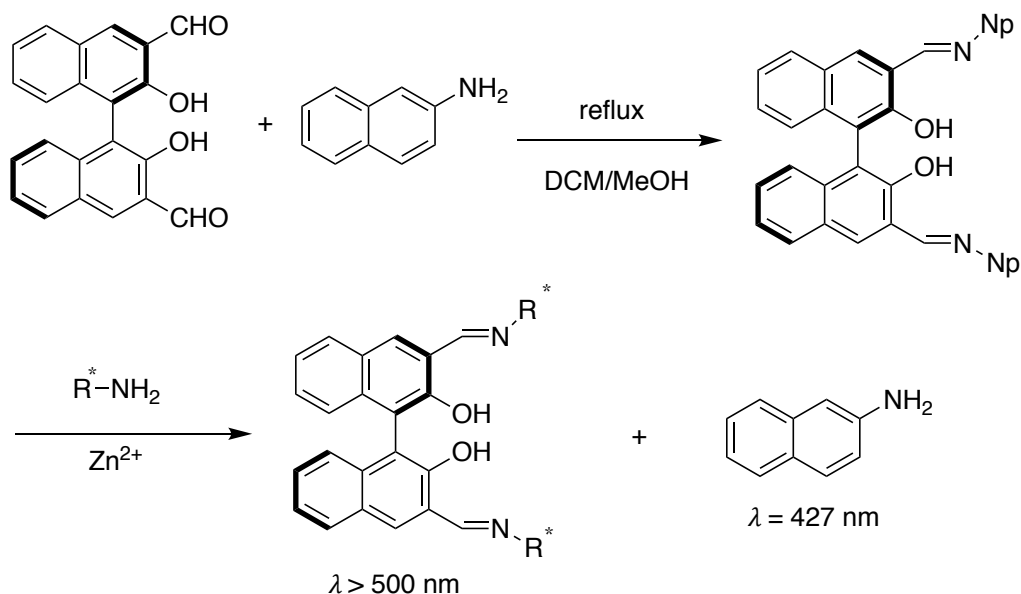


Figure I-1. Imine metathesis reaction between 2-aminonaphthalene condensed chiral imine with the guest chiral amine. Dual fluorescence emissions were observed.

A chiral dinaphthalene aldehyde was first condensed with the fluorescent molecule 2-aminonaphthalene to yield a fluorescent quenched chiral imine. Using this chiral imine as the probe to carry out imine metathesis can form a highly fluorescent compound with the exchanged 2-aminonaphthalene for the chirality matched amines. Fluorescence emission at two different wavelengths was observed: the new imine shows a strong fluorescence above 500 nm and the 2-aminonaphthalene fluorescence at 427 nm. If the chirality mismatched amine enantiomer is formed, only the exchanged 2-aminonaphthalene peak is observed.

I.1.2 Microwave method for absolute stereochemical determination

This new method uses microwave spectroscopy to determine absolute stereochemistry and was first introduced by Dr. Doyle in 2013.⁶ The principal for this detection is based on the enantiomer dependent Hamiltonian of the rigid molecule. For most chiral molecules (**Figure I-2**), rotational constants A, B and C, the magnitude of the

dipole moment components $|\mu_a|$, $|\mu_b|$, $|\mu_c|$, are the same. However, the combined quantity sign of the $\mu_a\mu_b\mu_c$ is distinct from its enantiomer. Under a sequence of specialized electric fields (microwave), the signal can be achieved to differentiate the enantiomers of small chiral molecules. Further development of this technology could be used to measure the enantiomeric excess ratio.⁷

This technology, however, suffers from a huge hurdle. This complicated system could only detect the absolute stereochemistry of a few chiral organic molecules, while requiring extreme conditions (gas phase and low temperature $\sim 7\text{K}$) for the analysis.

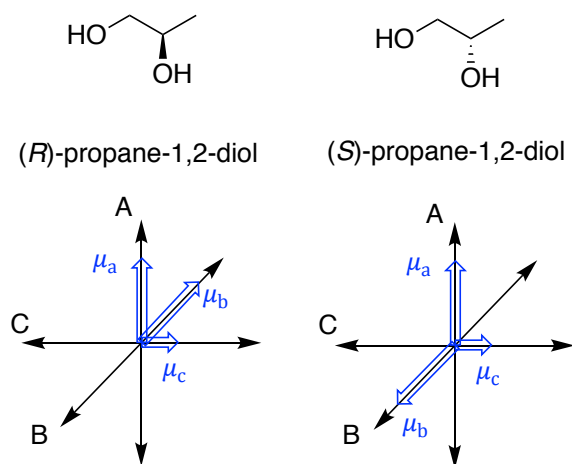


Figure I-2. Principal of microwave chiral sensing. μ_a , μ_b and μ_c are the dipole moments of the chiral propane-1,2-diol. A, B, C are the rotational constants.

I.1.3 Vibrational circular dichroism for absolute stereochemical determination

Vibrational Circular Dichroism (VCD) detects the absorption differences when the circularly polarized IR light passes through a sample. It is an extension of the Electronic Circular Dichroism (ECD) method, which will be discussed below. VCD has been used to assign the stereochemistry of moderately complex molecules.

To determine the stereochemistry of the chiral analytes, a good quality VCD spectrum must be recorded first, followed by the computational calculation of the VCD spectrum. By comparing the signs of the experimental result with the results of the calculation, the chirality can be assigned. General computational level is carried out with DFT, hybrid B3LYP functional and 6-31GD basis set. For higher accuracy, larger basis set such as cc-pVTZ can be used to yield better results. Computational calculations start by optimizing the geometry of the chiral molecule. The Boltzmann population of conformers generated is then assessed, followed by the calculation of vibration modes for the major conformers. This technique has a broad application in determining the stereochemistry of chiral centers.⁸⁻⁹

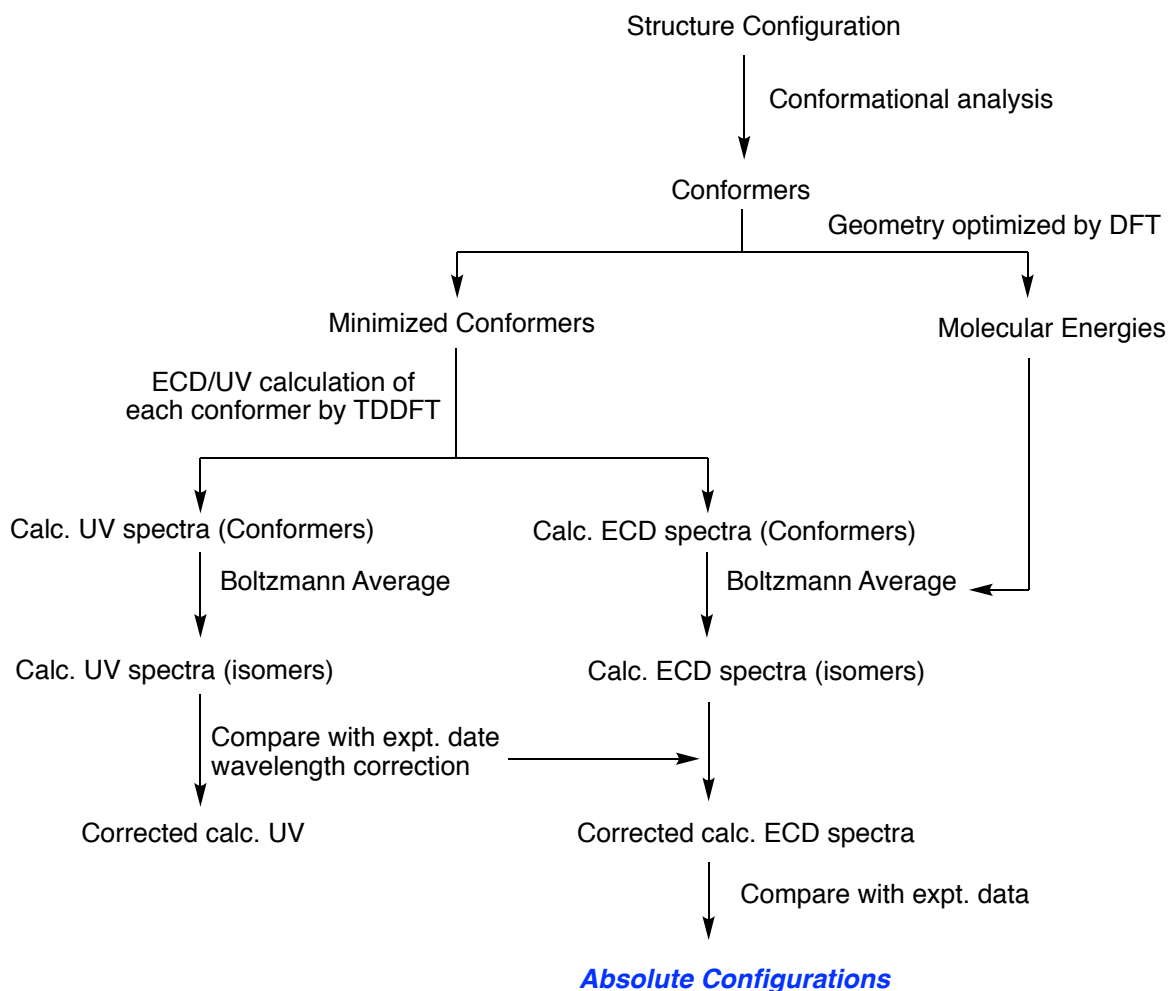
I.1.4 Electronic circular dichroism method for absolute stereochemical determination

Electronic Circular Dichroism (ECD) shares a similar principal as VCD described above. It utilizes the difference in interaction between the circularly polarized UV or visible light with the chiral sample. Due in part to the fact that most organic molecules contain UV-Vis active chromophores, ECD has attracted significant attention for small organic molecule chiral determination. ECD relies on the electron transitions from the molecule to yield ECD signal. The positive or negative peaks recorded by the ECD instrument are called Cotton effects. Multiple chromophores in the structure can couple with each other, thus multiple electron transition bands can be observed.¹⁰ Simply relying on the ECD spectrum only affords chiral determination in an empirical fashion. In other words, by comparing the reported ECD spectrum with the experimental results, chiral centers can

be assigned. For example, (*S*)-camphor-10-sulfonic acid yields a positive peak around 290 nm whereas (*R*)-camphor-10-sulfonic acid yields a negative peak around 290 nm. If there is an unknown camphor-10-sulfonic acid, its ECD spectrum can be compared with the spectra from (*R*) and (*S*) camphor sulfonic acid leading to the assignment of chirality in an empirical manner.

I.1.4.1 Electronic circular dichroism coupled with calculations

Combined with high level calculations, ECD is an emerging area for stereochemical assignment in natural products in recent years. The calculation for ECD analysis is based on time-dependent density functional theory (TDDFT). A general scheme to assign the structure of the unknown analyte via calculation assisted ECD method is shown below (**Scheme I-3**).¹¹⁻¹²



Scheme I-3. Steps to assign absolute configuration by TDDFT assisted ECD analysis.

ECD calculations normally contain 2 parts: first part begins with the conformer search. It is generally done with Monte Carlo methods using molecular mechanics or semi empirical methods (MMFF or other higher levels). Generated conformers from the conformer search are subjected to DFT calculation (B3LYP or higher basis sets) to obtain the optimized geometry at lower energy state. During the second part, TDDFT is used to calculate the optimized conformers to yield UV and ECD spectra. The calculated UV or ECD spectra of the isomers are obtained through Boltzmann averaging. After comparing

the result from calculation with the experimental ECD data, the absolute configuration of the sample can be determined.

The accuracy of the analysis is highly dependent on the calculation basis sets and functions. Common function and basis sets to achieve good calculation results are B3LYP/6-31GD level. Larger basis sets such as 6-311+G(d,p) or aug-cc-pVDZ yield better calculation results, but prolong the calculation time and increase the cost.

I.1.4.2 Exciton Coupled Circular Dichroism method for absolute stereochemical determination

Exciton Coupled Circular Dichroism (ECCD) is observed when the excited state dipole moments of two or more chromophores, arranged in a helical fashion, couple through space.¹³⁻¹⁴ ECCD is a phenomenon which is detected with a circular dichroic (CD) instrument and is a sub part of the electronic circular dichroism (ECD). Its use was pioneered by Nakanishi and Harada. ECCD arises from the dipole-dipole interaction between two or more chromophores. An energy split occurs to afford two new energy states, α and β at the excited state(**Figure I-3**). Thus, two new absorption peaks are expected (Davydov splitting).

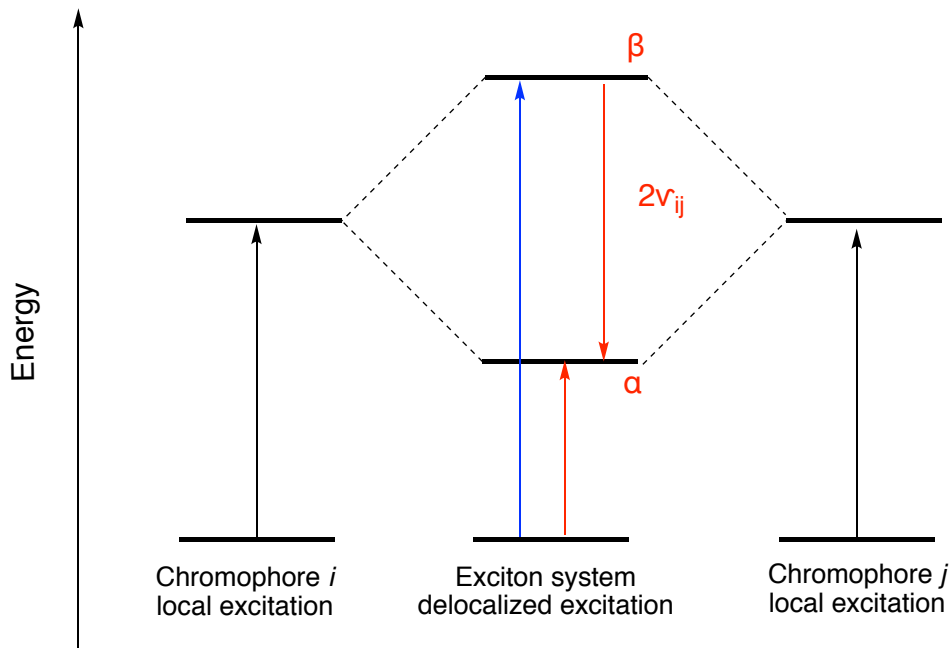


Figure I-3. Energy splitting between two identical chromophores in the excited state. Two chromophores i and j are coupled with each other and lead to two new energy states.

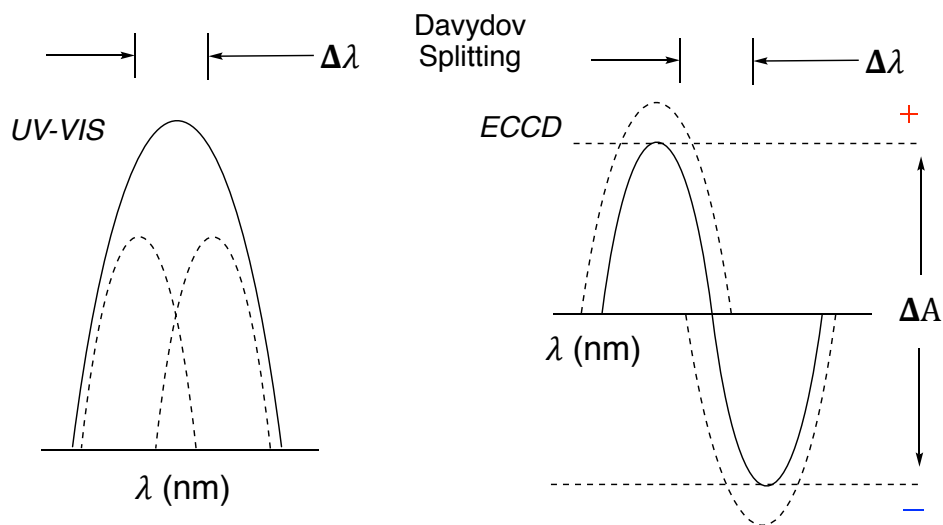


Figure I-4. Davydov splitting in the UV-Vis and ECCD.

In the UV spectrum, both absorptions are of the same phase, thus their overlap results usually in a single peak without any noticeable difference (**Figure I-4**). Their CD, however, results in two peaks of opposite cotton effect. The combined amplitudes of the observed Cotton effects are proportional to the square of the magnitude of the transition

dipole moment, μ . Therefore, chromophores with strong electron transition lead to a stronger signal. The distance (r) between the chromophores should be relatively small since the efficiency in coupling is proportional to the $1/r^3$.

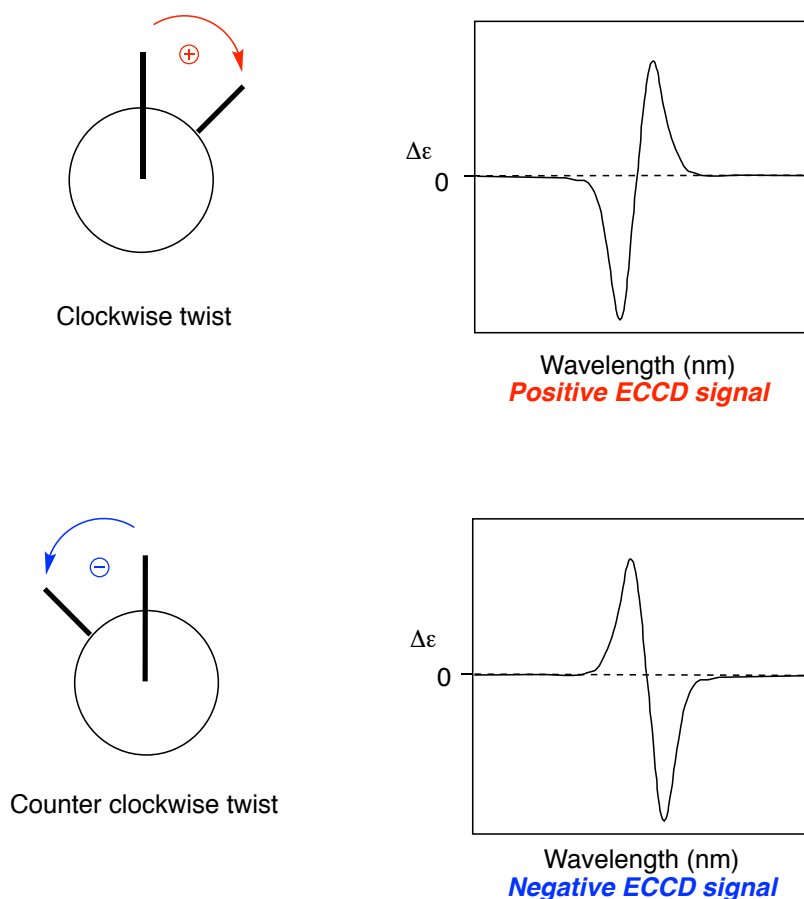


Figure I-5. ECCD Cotton effects. The black bars indicate two separate chromophore dipoles. Two different ECCD signals are observed.

The helical twist between the two chromophores leads to two opposite signals (**Figure I-5**). If two chromophores form a clockwise twist, they yield a positive ECCD signal. The positive sign is defined as: the higher wavelength Cotton effect is a positive peak whereas the lower wavelength Cotton effect is a negative peak. For counter clockwise twist, a negative ECCD signal is observed. This phenomenon is the result of

the electric transition dipole moment multiplication. Commonly, a clockwise twist coupling leads to a positive ECCD signal whereas a counter-clockwise coupling leads to a negative ECCD signal. Utilizing this ECCD method, a series of host molecules have been designed for the determination of the absolute stereochemistry of a variety of guests in a non-empirical fashion.¹⁵

I.1.4.3 Exciton Coupled Circular Dichroism for absolute stereochemical determination

Porphyrin tweezers were developed as chromophoric host molecules to sense the absolute stereochemistry of small chiral organic molecules. A variety of elegant porphyrin-based host molecules have been designed by the Nakanishi lab. Porphyrins as host chromophores have several advantages: 1) Porphyrin is a large and flat structure. Even with a small twist, we can still observe ECCD signal. 2) Porphyrin has a visible UV absorption peak centered around 420 nm. Most organic analytes do not have strong electron transitions at such wavelengths, so they can not interfere with the ECCD signal. 3) The porphyrin center can be easily metalated to provide a new binding site for the guest molecules.

The general working model of the porphyrin tweezers is described below: after complexation with the guest chiral molecule, the porphyrin tweezers adopt a specific helicity due to the steric interaction between the host and the chiral guest. Depending on the chirality of the guest, a clockwise or counter-clockwise helical twist is favored which translates into a positive or negative ECCD signal. Based on proposed working model of

the tweezer system, the observed ECCD signal can be correlated to the chiral center of the guest molecule in the non-empirical fashion.

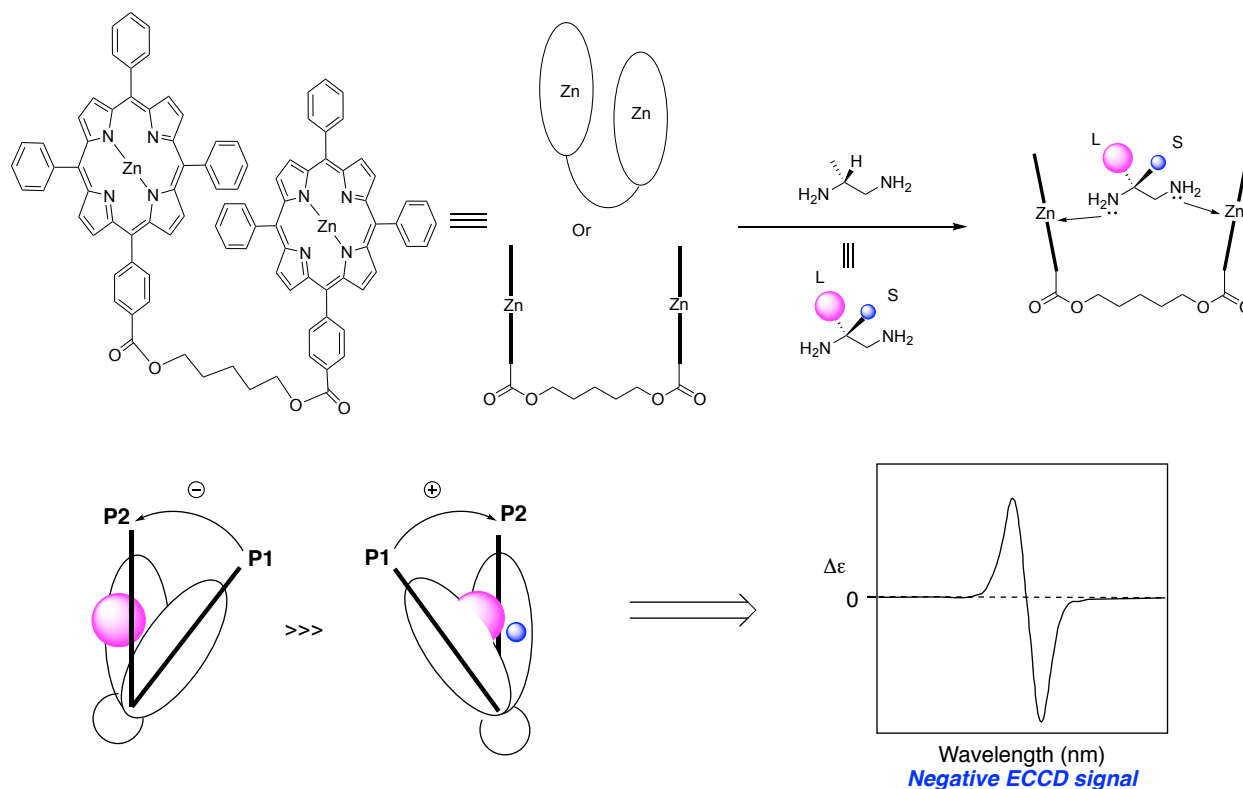
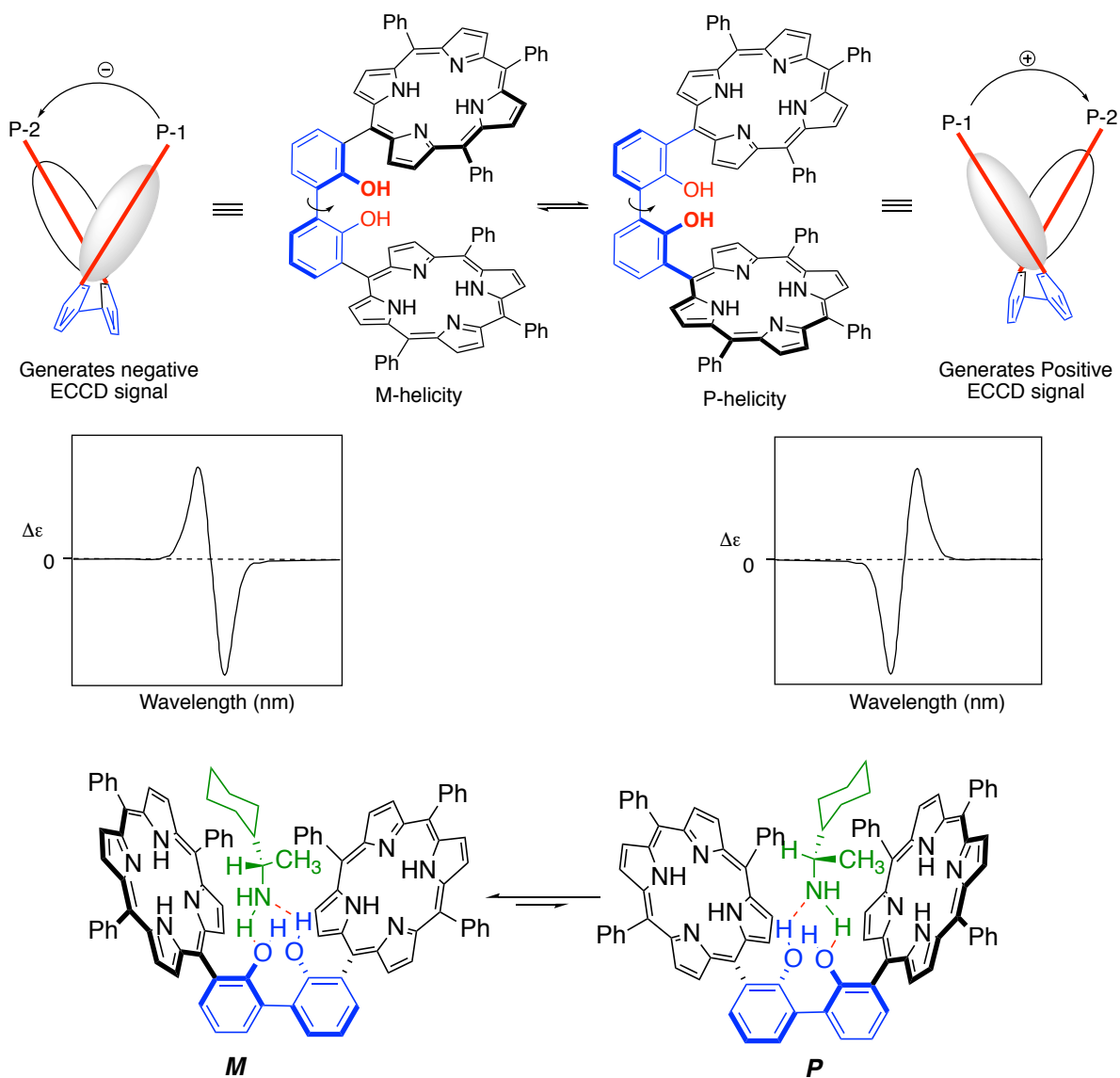


Figure I-6. Using porphyrin tweezer to sense chiral diamines. Upon binding with the guest diamine, the helical twist of the tweezer leads to the observed ECCD signal.

An example of porphyrin tweezer is shown in **Figure I-6**.¹⁶ Two porphyrins are connected through an alkyl chain. The zinc metals in the middle of the porphyrins provide two binding sites for the guest molecule. The chiral guest, i.e. (*R*)-propane-1,2-diamine binds to the tweezer through amine-Zn coordination. The large group is the methyl group and the small group is the H atom. Upon coordination, the diamines bring the two porphyrins close to each other and steric interaction occurs between the host tweezer and the guest diamine. To minimize the energy of the newly formed complex, a twist occurs to avoid steric interactions. To avoid the collision between the large methyl group

with the porphyrin tweezer, a counter clockwise twist for the tweezer is preferred, leading to a negative ECCD signal. By analyzing the experimental result, the absolute stereochemistry of the chiral diamines can be determined in a non-empirical fashion. In addition to this system, many other elegant tweezers have been developed to work with other functionalities present in organic compounds.

Our lab has focused on the ECCD studies for almost 20 years.¹⁷⁻²¹ During that time, we have designed a variety of tweezers to determine the absolute stereochemistry of different chiral guests. Recently, we published a new bis-porphyrin system (MAPOL) by using bi-phenol as the linker (**Figure I-7**).²² It shares similar mechanism as the tweezer system, but it has a significant advantage over the previous systems. The tweezer systems can only sense chiral guests with dual binding site. For molecules with a single binding site, a chemical derivatization is needed to provide a second binding site for ECCD analysis. The new MAPOL system has a biphenyl core as the binding element. In this manner, MAPOL is capable of binding guests such as chiral amines or carboxylic acids. The H-bonding between the two OH on the bisphenol locks the two porphyrins on the same side. Without a guest molecule, MAPOL has an equal distribution of P and M helicities, thus it is ECCD silent. When the guest molecule binds to the MAPOL, a helical twist leads to either a positive or negative ECCD signal. For example, (*S*)-1-cyclohexylethan-1-amine binds to the MAPOL through H-bonding. The *M* helical complex has the least steric interaction due to the fact that the large cyclohexane group is facing towards the open space, while the small methyl group faces the porphyrin ring. A negative ECCD obtained experimentally matches the working model.



Chiral Guests

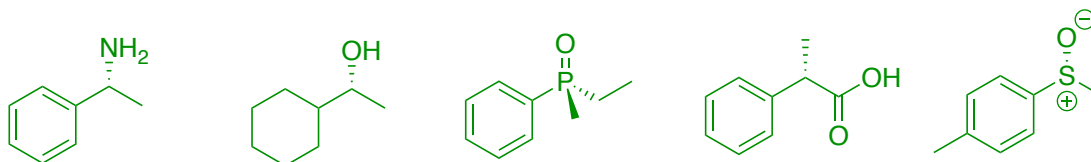


Figure I-7. MAPOL host for ECCD analysis.

Using this MAPOL system, we were able to assign the absolute stereochemistry of chiral amines and carboxylic acids. For more challenging sulfoxides and cyanohydrins, we were able to sense the chirality through a modified (Zn)-MAPOL host system. There

are many exciting projects ongoing with the modification of the MAPOL system to analyze more challenging chiral guests such as chiral phosphines and phosphine oxides.

I.2. Introduction to measuring enantiomeric excess

Enantiomeric excess (*ee*) is one of the most important standards to evaluate the purity of a chiral mixture. This number is commonly expressed in % ratio ($ee = [(R-S)/(R+S)] \times 100\%$). Highly enantiomerically pure intermediates or products enjoy great appreciation in organic synthesis and pharmaceutical industry. In the past few decades, chiral sensing techniques have developed tremendously in various subjects. To date, there are many methods to determine the *ee* values. These include high-performance liquid chromatography (HPLC), gas chromatography (GC), nuclear magnetic resonance spectroscopy (NMR), fluorescence, ultraviolet-visible spectroscopy (UV-Vis) and circular dichroism (CD).²³⁻²⁵ Amongst these, the chromatographic methods (HPLC, GC) enjoy broad application due to their easy operation and high reliability. The reported *ee* value by chromatography is also widely accepted for scientific publications. On the other hand, using spectroscopic methods to report *ee* value has attracted great attention in the past few decades due to their potential for rapid analysis. Spectroscopic methods normally require a host molecule which can form a covalent or non-covalent bond with the guest molecule to yield a complex. Complex formation causes a change in the spectrum which can be directly correlated to the *ee* value. A variety of elegant sensors for *ee* sensing have been developed in the past few years.

The driving force for the fast *ee* analysis comes from chemical and pharmaceutical research development. In industry, time is considered as one of the most important limits

for projects. Thus, a fast screening method to analyze reaction results is highly desired. High Throughput Screening (HTS) is the method to accelerate research progress. Aided by the fast development of the robotics and engineering, thousands to millions samples can be analyzed in a short time through HTS systems. Many different systems have been developed to analyze the reaction yields and are widely used in the pharmaceutical industry. However, since most of the HTS systems are focused on reaction yield analysis, there are rare examples that analyze the asymmetric reaction *ee* values in a HTS manner. Thus, an increasing interest of developing a HTS method for *ee* analysis has been addressed in recent years. Developing chromatography or spectroscopy methods to meet HTS criteria screening has become an attractive area of research.

I.2.1 Improving chromatographic separation for rapid *ee* determination

Traditional chromatography based chiral separation (HPLC) has been widely used in the research labs. HPLC uses chiral stationary phases to separate chiral mixtures. Normally, around 10-20 min analysis time is required for each sample in routine HPLC systems. In addition, choosing the right columns and right eluent ratio and flow rate requires a large amount of time. General ways to improve chromatographic separations are based on five key factors: 1) Spherical particles work better than irregular particles. 2) Regular packing of ideal spheres also improves the efficiency. 3) Smaller particles separate better than large particles. 4) Decreasing connection volumes between the injector and column yields better result. 5) Sample injection volume needs to be as little as possible. Recent improvement on chiral separation allows enantiomeric pairs to be separated in less than 1 min. Fast separations have been demonstrated by Merck,

University of Texas Arlington and University of Rome, some certain chiral enantiomers can be completed within few seconds by using short columns (0.5 to 5 cm). However, these columns normally are packed with smaller particles and are used under a high flow rate. Thus, a high back column pressure is a challenging issue that needs to be solved.²⁶

Another approach for ultrafast enantioseparation is by employing super critical fluid chromatography (SFC). It provides faster separation as compared to liquid chromatography. The eluent for SFC is condensed carbon dioxide, which has a lower viscosity and enhanced diffusivity. Thus, a high flow rate can be applied to accelerate the separation. Thanks to new stationary phases, column length, particle size, pressure, column design and improvement in equipment, the speed for the chiral separation by chromatography has increased dramatically.

I.2.2 Optical methods for ee analysis

Using optical spectroscopic methods to determine ee values is another attractive approach for HTS screening.²⁷ A significant advantage in comparison to chromatography methods is the low instrument cost. A general spectroscopic scan only takes few seconds; such short time scale is also ideal for HTS screening analysis. Among all spectroscopic methods, circular dichroism (CD) is the most powerful.²⁸⁻²⁹ The readouts from the CD are the Cotton effects, which are dependent on the analytes. Impurities normally have weak Cotton effects in CD analysis, thus a higher accuracy can be achieved by CD analysis, whereas UV-Vis or fluorescence based systems could have a larger error due to the impurities that may interfere with the signal.

A variety of systems based on CD methods to analyze the *ee* values have been developed by Anslyn, Wolf, Canary, Borhan and other groups.^{18, 30-32} An example of such is using in situ generation of Fe(II) complexes to sense chiral amines was shown below (**Figure I-8**).³³ A fast derivatization of chiral amines with 2-pyridinecarbaldehyde yields chiral imines (< 10 s) which can be coordinated to the Fe(II) metal center. The newly formed octahedral iron complex can form up to 24 stereoisomers (result from helical isomerism, configurational isomerism and *R*, *S* amines). Due to the fast equilibria between the isomers, the complexity does not interfere with the ECCD signal, thus signal can be correlated to *ee* values. After a concentration independent calibration curve is made, the *ee* values of the chiral guests can be easily determined. The average error for this method is about $\pm 5\%$.

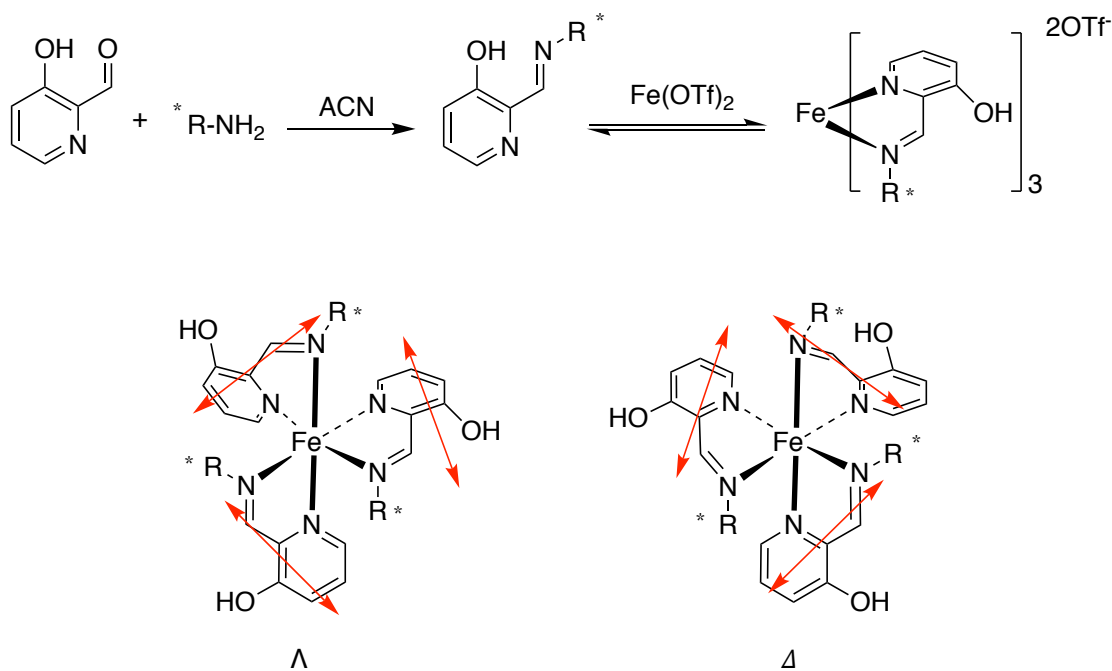


Figure I-8. Sensing chiral amines through Fe(II) complex. Λ -(*S*)-*fac* and Δ -(*R*)-*fac* lead to negative and positive ECCD signals.

Wolf's lab is also active in designing different host molecules for rapid *ee* sensing as well as yield sensing via spectroscopic methods. An example is shown here, where achiral phosphine aldehydes can complex with chiral guests in the presence of Pd(OAc)₂ and tetrabutylammonium hydroxide (TBAOH) in acetonitrile (**Figure I-9**).³⁴ This Pd complexation is completed within 15 mins. This new probe can be used to sense amino acids, mono amines and amino alcohols. Cotton effects occur typically around 310 nm to 420 nm. *Ee* values can be correlated to the CD signals whereas the UV-Vis change can be correlated to the concentration of the guest molecule. Thus, two readouts can be achieved through a combination of UV-Vis and CD spectroscopy, leading to the measurement of the reaction yield and *ee*.

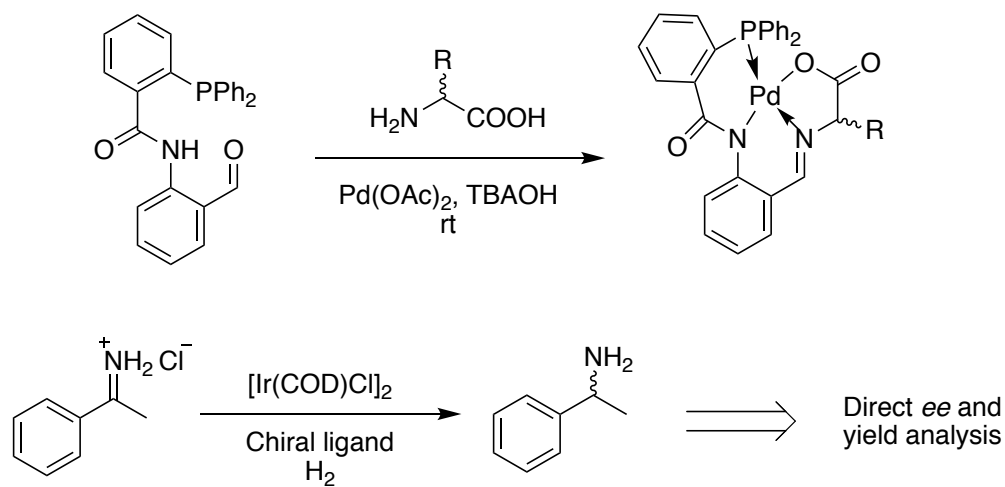


Figure I-9. Working model for the Pd complex to sense chiral amino acids and a direct mixture analysis of asymmetric imine hydrogenation reaction by UV-Vis and CD.

This method also features a fast determination for crude yield and *ee* demonstrated for the reduction of imines. They were able to determine the yield through UV-Vis and *ee* value through CD analysis even in presence of the Ir catalyst and the chiral

phosphine ligand. The chiroptical sensing is also in good agreement with the traditional HPLC analysis.

However, most of the host systems for the *ee* analysis rely on the knowledge of either probe or analyte concentration. The error in the concentration directly influences the *ee* readout. Thus a precise concentration control is required for the *ee* study and this limits practical applications. Recently, a group from Italy reported the first probe and analyte concentration independent host for the *ee* determination via a new oxo-vanadium (V) aminotriphenolate complex (**Figure I-10**).³⁵

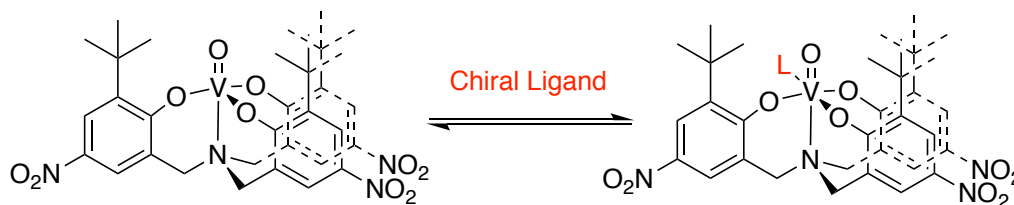


Figure I-10. Oxo-vanadium (V) aminotriphenolate complex binds to the chiral analytes to yield the CD signal.

This unique vanadium complex has a broad UV absorption range (up to 800 nm). The strong UV absorption bands are observed at 308 and 450 nm due to ligand to metal charge transfer. Upon mixing the vanadium complex with coordination solvents, a red shift of the 450 nm peak to 600 nm is observed. The wavelength above 600nm in the UV-Vis is caused by the octahedral vanadium adduct. Thus, by introducing the anisotropic *g*-factor ($g = \Delta\varepsilon/\varepsilon$), which can be calculated based on the dichroic signal ($\Delta\varepsilon$) and absorbance (ε), an independence of the octahedral species concentration is observed, but the key point is that this *g* factor is proportional to the *ee* values. Using this *g* factor instead of the CD signal (mdeg) leads to the independence of both probe and analyte.

This paper also demonstrated that a broad range of guest molecules can be analyzed such as amines, sulfoxides, amino alcohols and some protected amines.

There is a growing interest in rapid *ee* sensing via spectroscopic methods. We are excited to see more and more new host molecules being designed to meet different requirements.

I.3 Accomplishments from the Borhan's group

Our group's efforts is focused on designing new systems to tackle the problems which have not been solved in the CD area. We have been active in the new porphyrin hosts design area. Recently, we have successfully used the MAPOL system to determine the absolute stereochemistry of cyanohydrins and sulfoxides in a non-empirical fashion.³⁶⁻
³⁷ We were the first group to solve these problems through ECCD analysis. Now, we are addressing more challenging chiral problems, such as chiral phosphine oxides, boronic acids and boronic esters. We believe these problems will be solved by our hosts in the near future.

We are also interested in using simple designs to solve problems in chiral determination. Such techniques can be used by more research labs to accelerate research development, especially for asymmetric reaction development. In the next chapter, a simple BDN and DNM system for the chiral sensing of amines, alcohols and carboxylic acids will be described. This system can be also used for *ee* sensing.

REFERENCES

REFERENCES

1. Ribeiro, C.; Santos, C.; Goncalves, V.; Ramos, A.; Afonso, C.; Tiritan, M. E., Chiral Drug Analysis in Forensic Chemistry: An Overview. *Molecules* **2018**, *23* (2).
2. Smith, S. W., Chiral Toxicology: It's the Same Thing...Only Different. *Toxicol Sci* **2009**, *110* (1), 4-30.
3. Mullard, A., 2017 FDA drug approvals The FDA approved 46 new drugs last year, the highest total in more than two decades. *Nat Rev Drug Discov* **2018**, *17* (2), 81-85.
4. Wen, K. L.; Yu, S. S.; Huang, Z.; Chen, L. M.; Xiao, M.; Yu, X. Q.; Pu, L., Rational Design of a Fluorescent Sensor to Simultaneously Determine Both the Enantiomeric Composition and the Concentration of Chiral Functional Amines. *J Am Chem Soc* **2015**, *137* (13), 4517-4524.
5. Pu, L., Fluorescence of organic molecules in chiral recognition. *Chem Rev* **2004**, *104* (3), 1687-1716.
6. Patterson, D.; Schnell, M.; Doyle, J. M., Enantiomer-specific detection of chiral molecules via microwave spectroscopy. *Nature* **2013**, *497* (7450), 475-+.
7. Shubert, V. A.; Schmitz, D.; Patterson, D.; Doyle, J. M.; Schnell, M., Identifying Enantiomers in Mixtures of Chiral Molecules with Broadband Microwave Spectroscopy. *Angew Chem Int Edit* **2014**, *53* (4), 1152-1155.
8. Freedman, T. B.; Cao, X. L.; Dukor, R. K.; Nafie, L. A., Absolute configuration determination of chiral molecules in the solution state using vibrational circular dichroism. *Chirality* **2003**, *15* (9), 743-758.
9. He, Y. A.; Wang, B.; Dukor, R. K.; Nafie, L. A., Determination of Absolute Configuration of Chiral Molecules Using Vibrational Optical Activity: A Review. *Appl Spectrosc* **2011**, *65* (7), 699-723.
10. Pescitelli, G.; Di Bari, L.; Berova, N., Conformational aspects in the studies of organic compounds by electronic circular dichroism. *Chem Soc Rev* **2011**, *40* (9), 4603-4625.
11. Nugroho, A. E.; Morita, H., Circular dichroism calculation for natural products. *J Nat Med-Tokyo* **2014**, *68* (1), 1-10.
12. Telfer, S. G.; McLean, T. M.; Waterland, M. R., Exciton coupling in coordination compounds. *Dalton T* **2011**, *40* (13), 3097-3108.

13. Harada, N.; Nakanishi, K. j., *Circular dichroic spectroscopy : exciton coupling in organic stereochemistry*. University Science Books: Mill Valley, CA, 1983; p xiii, 460.
14. Berova, N.; Polavarapu, P. L.; Nakanishi, K.; Woody, R. W., *Comprehensive Chiroptical Spectroscopy, Applications in Stereochemical Analysis of Synthetic Compounds, Natural Products, and Biomolecules. Volume 2*. Wiley Imprint John Wiley & Sons, Incorporated.: Hoboken, 2012.
15. Berova, N.; Di Bari, L.; Pescitelli, G., Application of electronic circular dichroism in configurational and conformational analysis of organic compounds. *Chem Soc Rev* **2007**, *36* (6), 914-931.
16. Huang, X.; Rickman, B. H.; Borhan, B.; Berova, N.; Nakanishi, K., Zinc porphyrin tweezer in host-guest complexation: determination of absolute configurations of diamines, amino acids, and amino alcohols by circular dichroism. *J Am Chem Soc* **1998**, *120* (24), 6185-6186.
17. Tanasova, M.; Borhan, B., Conformational Preference in Bis (porphyrin) Tweezer Complexes: A Versatile Chirality Sensor for α -Chiral Carboxylic Acids. *Euro J Org Chem* **2012**, *2012* (17), 3261-3269.
18. Yang, Q.; Olmsted, C.; Borhan, B., Absolute stereochemical determination of chiral carboxylic acids. *Org Lett* **2002**, *4* (20), 3423-3426.
19. Li, X.; Borhan, B., Prompt Determination of Absolute Configuration for Epoxy Alcohols via Exciton Chirality Protocol. *J Am Chem Soc* **2008**, *130* (48), 16126-16127.
20. Li, X.; Burrell, C. E.; Staples, R. J.; Borhan, B., Absolute configuration for 1, n-glycols: A nonempirical approach to long-range stereochemical determination. *J Am Chem Soc* **2012**, *134* (22), 9026-9029.
21. Tanasova, M.; Anyika, M.; Borhan, B., Sensing Remote Chirality: Stereochemical Determination of beta-, gamma-, and delta-Chiral Carboxylic Acids. *Angew Chem Int Edit* **2015**, *54* (14), 4274-4278.
22. Anyika, M.; Gholami, H.; Ashtekar, K. D.; Acho, R.; Borhan, B., Point-to-Axial Chirality Transfer A New Probe for "Sensing" the Absolute Configurations of Monoamines. *J Am Chem Soc* **2014**, *136* (2), 550-553.
23. Jung, S. H.; Kim, K. Y.; Ahn, A.; Lee, S. S.; Choi, M. Y.; Jaworski, J.; Jung, J. H., NMR detection of chirality and enantiopurity of amines by using benzene tricarboxamide-based hydrogelators as chiral solvating agents. *New J Chem* **2016**, *40* (9), 7917-7922.

24. Labuta, J.; Ishihara, S.; Sikorsky, T.; Futera, Z.; Shundo, A.; Hanykova, L.; Burda, J. V.; Ariga, K.; Hill, J. P., NMR spectroscopic detection of chirality and enantiopurity in referenced systems without formation of diastereomers. *Nat Commun* **2013**, *4*.
25. Zhang, X.; Yin, J.; Yoon, J., Recent Advances in Development of Chiral Fluorescent and Colorimetric Sensors. *Chem Rev* **2014**, *114* (9), 4918-4959.
26. Welch, C. J., Are We Approaching a Speed Limit for the Chromatographic Separation of Enantiomers? *Acs Central Sci* **2017**, *3* (8), 823-829.
27. You, L.; Zha, D. J.; Anslyn, E. V., Recent Advances in Supramolecular Analytical Chemistry Using Optical Sensing. *Chem Rev* **2015**, *115* (15), 7840-7892.
28. Jo, H. H.; Lin, C. Y.; Anslyn, E. V., Rapid Optical Methods for Enantiomeric Excess Analysis: From Enantioselective Indicator Displacement Assays to Exciton-Coupled Circular Dichroism. *Accounts Chem Res* **2014**, *47* (7), 2212-2221.
29. Leung, D.; Kang, S. O.; Anslyn, E. V., Rapid determination of enantiomeric excess: a focus on optical approaches. *Chem Soc Rev* **2012**, *41* (1), 448-479.
30. Proni, G.; Pescitelli, G.; Huang, X.; Quraishi, N. Q.; Nakanishi, K.; Berova, N., Configurational assignment of α -chiral carboxylic acids by complexation to dimeric Zn-porphyrin: host-guest structure, chiral recognition and circular dichroism. *Chem Comm* **2002**, (15), 1590-1591.
31. Mei, X.; Wolf, C., Enantioselective sensing of chiral carboxylic acids. *J Am Chem Soc* **2004**, *126* (45), 14736-14737.
32. Joyce, L. A.; Maynor, M. S.; Dragna, J. M.; da Cruz, G. M.; Lynch, V. M.; Canary, J. W.; Anslyn, E. V., A simple method for the determination of enantiomeric excess and identity of chiral carboxylic acids. *J Am Chem Soc* **2011**, *133* (34), 13746-13752.
33. Dragna, J. M.; Pescitelli, G.; Tran, L.; Lynch, V. M.; Anslyn, E. V.; Di Bari, L., In Situ Assembly of Octahedral Fe(II) Complexes for the Enantiomeric Excess Determination of Chiral Amines Using Circular Dichroism Spectroscopy. *J Am Chem Soc* **2012**, *134* (9), 4398-4407.
34. De los Santos, Z. A.; Wolf, C., Chiroptical Asymmetric Reaction Screening via Multicomponent Self-Assembly. *J Am Chem Soc* **2016**, *138* (41), 13517-13520.
35. Zardi, P.; Wurst, K.; Licini, G.; Zonta, C., Concentration-Independent Stereodynamic g-Probe for Chiroptical Enantiomeric Excess Determination. *J Am Chem Soc* **2017**, *139* (44), 15616-15619.

36. Gholami, H.; Zhang, J.; Anyika, M.; Borhan, B., Absolute Stereochemical Determination of Asymmetric Sulfoxides via Central to Axial Induction of Chirality. *Organic Letters* **2017**, *19* (7), 1722-1725.
37. Gholami, H.; Anyika, M.; Zhang, J.; Vasileiou, C.; Borhan, B., Host-Guest Assembly of a Molecular Reporter with Chiral Cyanohydrins for Assignment of Absolute Stereochemistry. *Chem-Eur J* **2016**, *22* (27), 9235-9239.

Chapter II: Computationally Aided Absolute Stereochemical Determination of Enantioenriched Amines

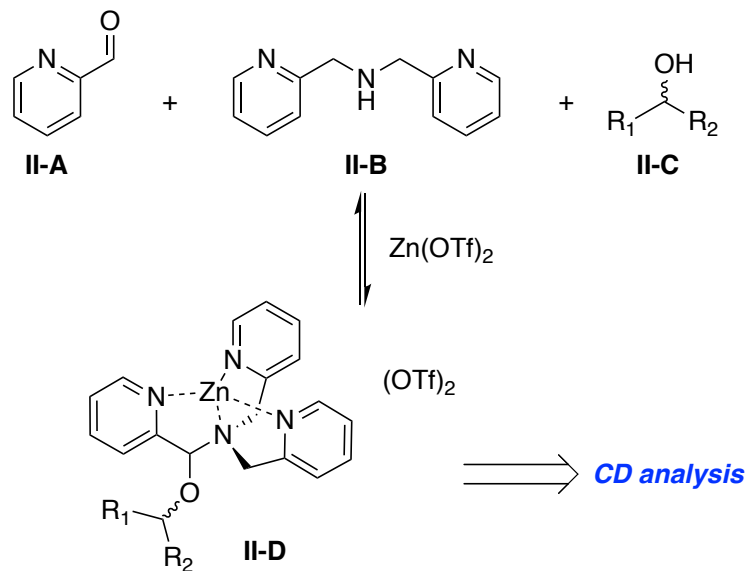
II.1. Introduction of chemical derivatization method

Organic chemistry and the disciplines it serves rely heavily on methods for the absolute stereochemical assignment of organic molecules. Many elegant methods have been developed to tackle this problem. Chiroptical spectroscopy, and in particular circular dichroism (CD), plays a prominent role in this respect due to its inherent sensitivity to asymmetry.¹ Yet, direct methods for analysis are often complicated with either difficult derivatizations or analyses of convoluted spectra that are beyond the expertise of a practitioner not versed in CD spectroscopy. During the past 20 years, a number of groups have designed a variety of elegant sensors to address these problems.²⁻¹⁸ Exciton coupled circular dichroism (ECCD), a method based on the through-space electronic coupling between two or more non-conjugated chromophores, has been utilized extensively for this purpose to assign the absolute stereochemistry of chiral molecules in a non-empirical manner.¹⁹⁻²⁰ This is possible because the sign of the ECCD signal is the direct consequence of the helicity of the coupled chromophores. Examples of ECCD-based methodologies for absolute stereochemical determinations in a non-empirical fashion include, but are not limited to, amino acids, diamines, amino alcohols, epoxy alcohols, amines, alcohols, and carboxylic acids.²¹⁻³⁷ Our lab has been focused on chiral sensing via ECCD method for over 15 years.

In addition to chiroptical methods, chemical derivatizations, such as Mosher ester analysis, have been the workhorse for absolute stereochemical determinations.³⁸⁻⁴² This

method normally requires a chiral compound which can form a covalent bond with the chiral analytes. After the complexation, the diastereotopic pairs can be differentiated through NMR. Nonetheless, besides the fact that NMR is not inherently sensitive to chirality, these methods have their distinct disadvantages, requiring derivatization with chiral reagents and performing reactions that are often not microscale. Furthermore, the assignment of absolute stereochemistry depends on correct assumptions for predicting the highest populating conformers. These analyses are not always routine or predictable since the derivatized molecules contain multiple single bonds that are energetically close-lying conformations and would not be able to solve the problems for complicated molecules.⁴³⁻⁴⁴

A less explored area for absolute stereochemical analyses is a methodology that combines the strengths of each individual technique, i.e., the chiroptically sensitive nature of ECCD, with the strength of covalent modification that results in a robust molecular framework used in NMR studies. There are a few elegant approaches that have highlighted the marriage of these strategies for absolute stereochemical identification of chiral amines. The reader is referred to the work of Anslyn and co-workers for a demonstration of this using an in situ imine derivatization with different guest molecules (**Scheme II-1**).⁴⁵⁻⁴⁶ Upon mixing the pyridine aldehyde (**II-A**) with the secondary pyridine amine (**II-B**), the newly formed imine can trap a chiral alcohol (**II-C**) to yield the tripod complex (**II-D**) in the presence of $\text{Zn}(\text{OTf})_2$. This tripod complex yields an active ECCD signal which can be correlated to the absolute stereochemistry of the alcohol.



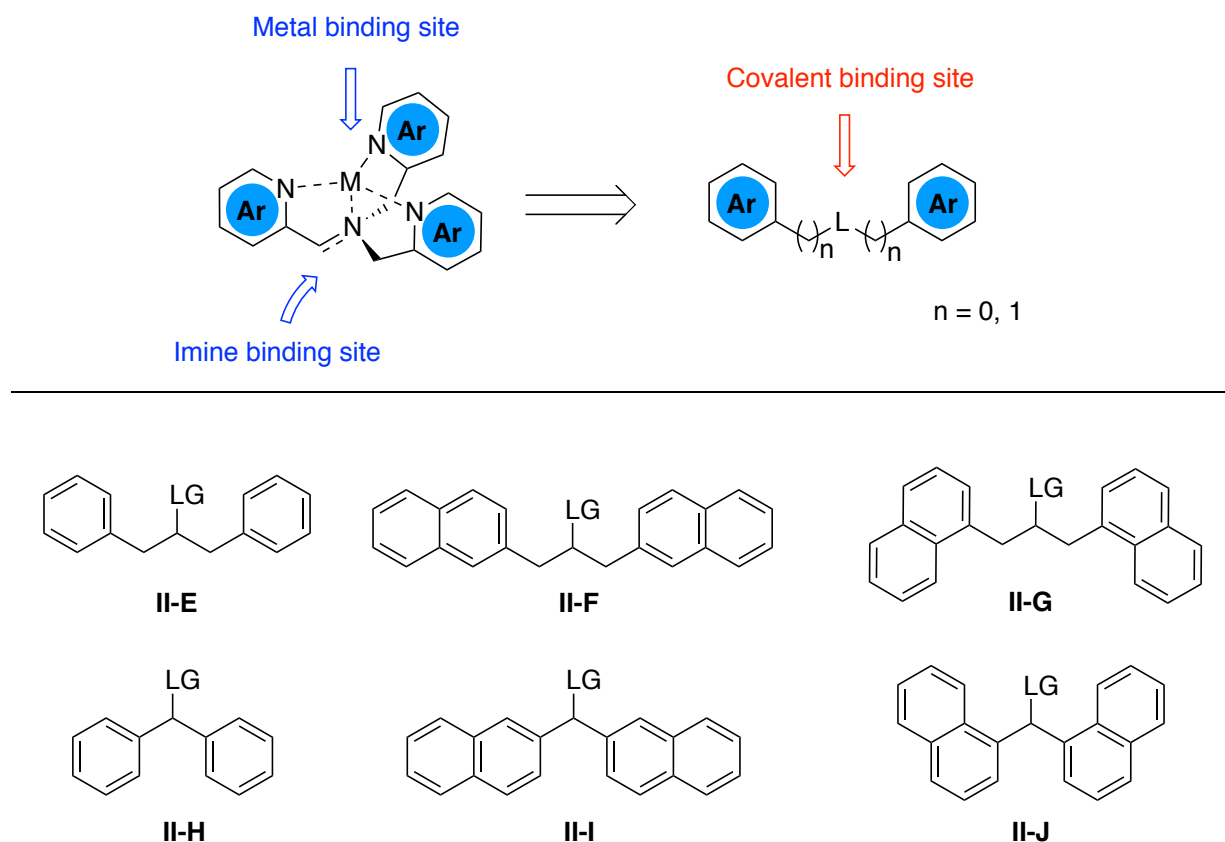
Scheme II-1. Four component covalent assembly for chiral alcohol CD sensing.

II.1.1 Design goals of the new chemical derivatization method

We set our sights on developing a simple, routine, and robust methodology that utilizes a chromophoric reporter, which can be readily derivatized with a chiral molecule. Toward this goal, we chose to first explore chiral amines as a prototypical example of one of the most common synthons in organic chemistry. The following were the goals set for this project. The derivatization must be simple, efficient, and proceed in high yields so that microscale analyses are possible. Ideally, the derivative can be used without the need for further purification, saving both time and effort, with an eye for future development as a platform for High Throughput Screening (HTS). Finally, the results could be obtained within a short time period, while the predictions to match the experimentally observed signals must be accessed via routinely available molecular modeling software.

II.1.2 Initial reporter design

Origins of our thought with regards to design find their roots in the tripod structures. Generally, there are two binding sites for tripod hosts: one is from the metal center in the pocket, the other is the imine bond located on the bottom of the host.^{24, 47-49} Both sites can be used to bind to chiral molecules to induce a chiral twist. Thus, active ECCD signals can be obtained.



Scheme II-2. Proposal of the initial structures. **II-E** to **II-J** are the potential structures for chiral sensing. M stands for the metal, Ar refers to different aromatic rings. L is the linker which can provide covalent bond with chiral guests. LG is the leaving group.

We propose that a tripod host with two aromatic rings to two aromatic “arms” can generate active ECCD signals. Upon attaching a chiral guest to the two “armed” host

through a covalent bond, the chirality from the guest molecule can be transferred to the two aromatic arms. Thus, active ECCD signals can be recorded (**Scheme II-2**).

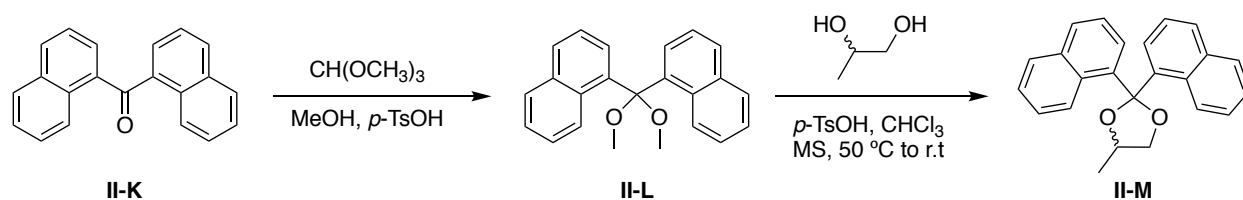
Several initial structures were proposed at this point (**II-E** to **II-J**). With the leaving group in the middle, chiral amine guests can be easily attached to the host via a S_N2 reaction. Compound **II-E** has two phenyl arms while compound **II-F** and compound **II-G** use naphthalene as chromophores. By comparing **II-E** and **II-F**, there are two major advantages for using naphthalene as the chromophore: 1) The naphthalene ring is bigger than phenyl, thus it leads to better interaction with chiral guests. 2) Naphthalene is a more redshifted chromophore with higher extinction coefficient to yield better ECCD signal. Between **II-F** and **II-G**, the difference is the attachment position on the naphthalene ring. **II-E** is attached at the β position of the naphthalene, while **II-G** is attached to the α position. Geometrically, **II-E** host is more flat and the distance between the two chromophores are more separated than in structure **II-G**. As we have discussed in **Chapter I**, the distance between the chromophores is important since the strength of the ECCD signal depends on it (proportional to the $1/r^3$).⁵⁰ Thus, in theory, structure **II-G** should yield a stronger ECCD signal than **II-E**.

Based on the distance argument, we proposed three more structures: **II-H**, **II-I** and **II-J**. We thought that a 3 carbon linker between the two aromatic groups may not be necessary. As long as the chiral guest can be attached to the middle carbon, the chirality can be transferred to the two chromophores. Thus, we believed that a one carbon linker should suffice for chiral sensing. Besides, host with one carbon linker not only brings two chromophores closer to each other, but also shortens the distance to the center of

asymmetry. After all these considerations, we believe structure **II-J** as the best candidate for our new system.

II.1.3 Literature precedence

After the proposal of the initial structures, we visited the literature to check if there was any evidence to support our idea. The best example we found to support our proposal was the work from Rosini's group.⁵¹ In his report, dinaphthyl ketal (**II-L**) was synthesized in presence of *p*-TsOH and trimethyl orthoformate in MeOH. This dinaphthyl ketal (**II-L**) was subjected to a ketal exchange reaction with chiral diols to yield chiral ketal structures (**II-M**). The chiral ketal (**II-M**) was isolated and its ECCD spectrum was recorded. In their paper, a DFT level calculation method was introduced to predict the absolute stereochemistry of the chiral diols. Eight different chiral diols were analyzed in this ECCD study (**Scheme II-3**). Their study was elegant, yet we were surprised that there was no follow up to their initial report. In response, we set our mind to make more improvements on this system for different chiral sensing applications.



Scheme II-3. Dinaphthyl ketals as chiral sensors.

We analyzed that the major drawback of the chiral ketals approach is the harsh conditions under which the chiral diol exchange is carried out. It requires heating for more than 12 h to complete the reaction. We aimed for a new system that required mild derivatization reaction conditions and resulted in higher yields and shorter reaction times.

Ideally, no purification should be needed for such a reaction so that microscale reactions are possible.

II.2 Preliminary study

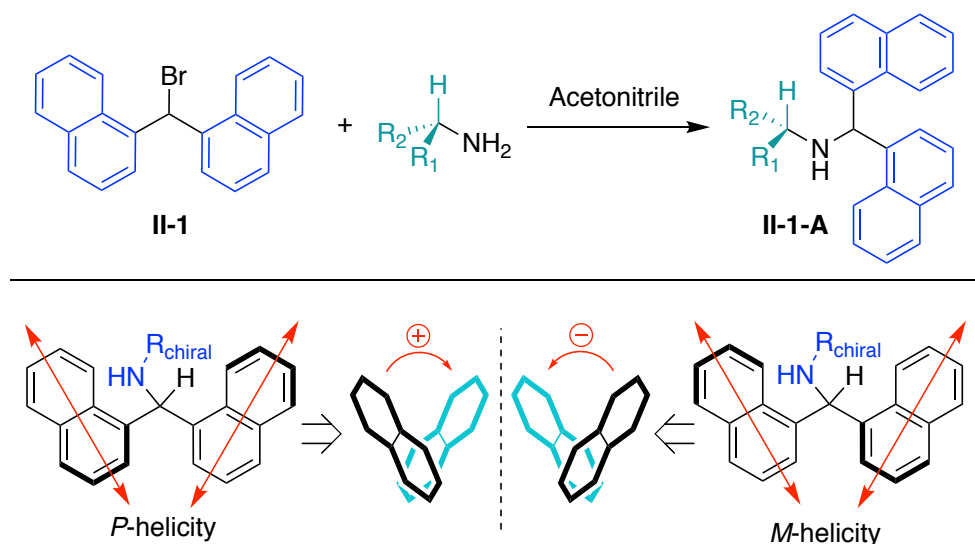


Figure II-1. Derivatization of chiral monoamines with **II-1** yields ECCD active derivatives.

Based on Rosini's work and our initial proposal, we believed that the best leaving group for our system **II-F** is bromide. Herein, we introduced the easily prepared reagent, 1,1'-(bromomethylene)dinaphthalene **II-1**, which reacts readily with chiral monoamines to yield the general structures (**II-1-A**). The methine group in **II-1** not only provides a handle for derivatization, but also aids in reducing the rotational barrier for the two aryl groups, thus enabling them to adopt a preferred conformation as dictated by the chirality of the derivatized chiral amine. The diastereomeric pairs of **II-1** derivatives (central chirality of the amine and the helicity of the naphthyl groups) will have different energetics and thus result in population imbalance that leads to an observable ECCD signal (**Figure II-1**). *P* helicity leads to a positive ECCD signal whereas *M* helicity leads to negative ECCD signal. Naphthyl groups can adopt both *P* and *M* helicity, the population of which is dictated by

the nature of the amine's chirality.

Compound **II-1** can be easily prepared in gram scale via 2 steps with overall 63 % yield. The Grignard of 1-bromonaphthalene was easily prepared by treating it with Mg metal. Addition of ethyl formate provided compound **II-2**. The hydroxyl group on **II-2** is converted to bromide with PBr_3 (**Figure II-2**). It is noteworthy that compound **II-1** decomposes on silica gel columns. Thus, purification by recrystallization is highly preferred.

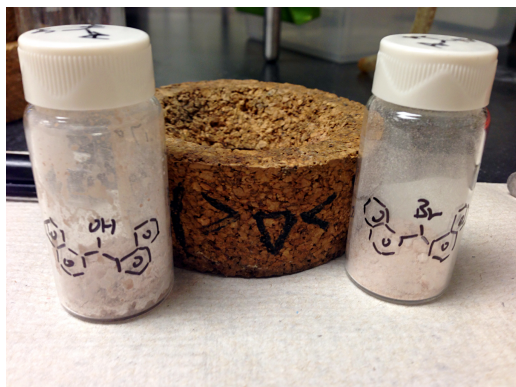
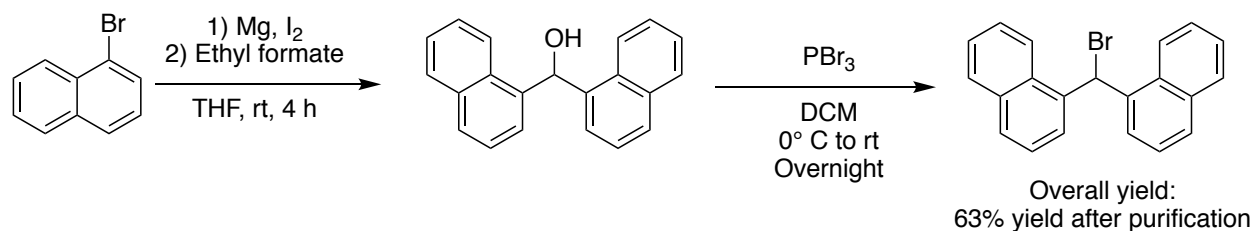


Figure II-2. Synthesis of compound **II-1**. Both **II-2** and **II-1** can be easily synthesized in gram scales.

With compound **II-1** in hand, we first tested our system with *S* and *R* methylbenzylamines. Under the standard conditions, both *S* and *R* amine derivatives can be synthesized under mild conditions (**Figure II-3**).

Owing to the equal population of *P* and *M* helicities, **II-1** is CD silent in acetonitrile. Gratifyingly, *S*-methylbenzylamine derivative **II-3-D** exhibits a positive ECCD spectrum,

while its enantiomeric derivative **II-4-D** produces the expected opposite signal (**Figure II-3**). These results illustrate the ability of the naphthyl rings to adopt a specific helicity due to interactions with the nearby asymmetric center. Consistent with previous reports, the ECCD spectra resulting from the through-space interaction of naphthalene-based chromophores are not symmetric.⁵¹⁻⁵²

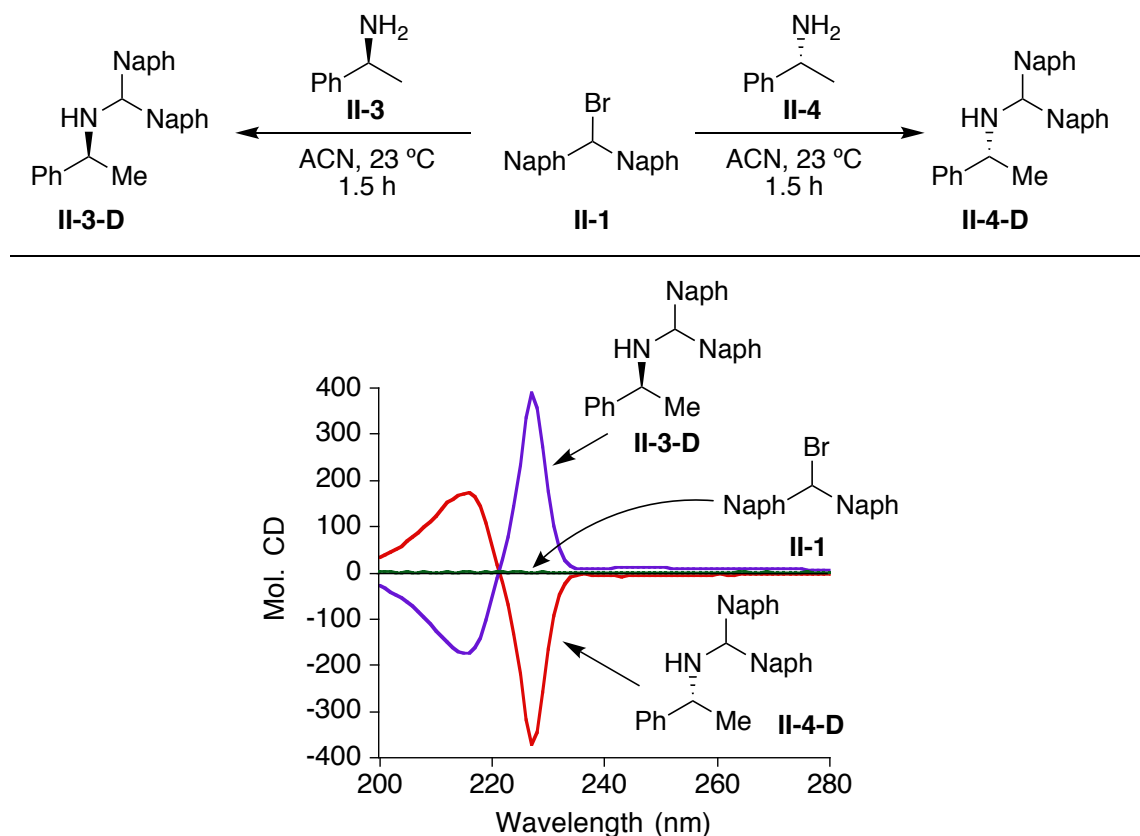


Figure II-3. ECCD spectra obtained with derivatized chiral amines **II-3-D** and **II-4-D** (10^{-5} M) in acetonitrile at room temperature. The CD spectrum of **II-1**, as expected, is silent. Naph = 1-naphthyl.

Next, we explored the best solvent to obtain the strongest ECCD. Due to the absorption of naphthyl reporter groups between 200 nm to 235 nm, low UV cutoffs solvents were chosen for the analysis so that the signal is not obscured. Five different solvents were tested with the standard compound **II-3-D** (10^{-5} M concentration) at room

temperature: acetonitrile, cyclohexane, hexane, methanol and methyl cyclohexane. ECCD signal was observed in all five solvents, however cyclohexane exhibited the poorest spectrum (**Figure II-4**). Although both hexane and methyl cyclohexane provided good spectra, these non-polar solvents are not good choices for the S_N2 type amination reactions. Between acetonitrile and methanol, acetonitrile provided slightly weaker ECCD signal than methanol but it has a much lower UV cutoff (190 nm for acetonitrile, 205 nm for methanol). This solvent property is important to reduce the noise for later high throughput screening analysis. After all these considerations, we chose acetonitrile for our ECCD study.

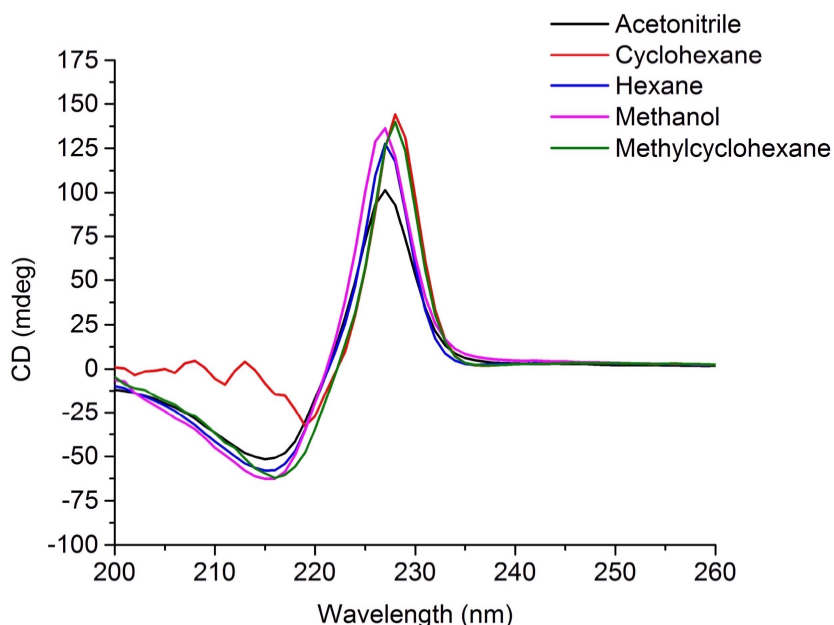


Figure II-4. ECCD solvents study: five different solvents were used to test the chiral amine derivative **II-3-D** (10^{-5} M concentration) at rt.

II.3 Reaction rate and additive study

In order to estimate the general reaction time for the amination, a CD monitored study was carried out. We also performed a parallel study by using AgNO₃ as an additive to examine if this reaction can be accelerated.

Freshly recrystallized **II-1** was first dissolved in anhydrous DCM to obtain a 0.01 M stock solution. (*S*)-Methylbenzylamine (**II-3**) was dissolved in anhydrous DCM to obtain a 0.01 M stock solution. To the spectra grade acetonitrile (1 mL) in a CD cuvette was added 1 μL **II-1** solution, followed by the addition of 10 μL **II-3** solution (10 equiv). The reaction was analyzed by CD at 2 min intervals (100 nm/min scan rate). For the additive study, addition of AgNO₃ solution (2 equiv) in acetonitrile (0.01 M, 2 μL) to a duplicate reaction mixture prepared as described above was used for comparison. Both reactions were monitored by CD.

Comparison of rates was performed by plotting the CD signal (mdeg) at 227 nm for each interval scan as a function of time (min). Both reactions were completed within 2 h. As shown in **Figure II-5** and **Figure II-6**, AgNO₃ accelerated the initial reaction rate, but the overall completion time remained the same (around 1 h). The relatively short reaction time bodes well for the potential of this methodology for HTS applications, as will be discussed later (**II.6.2**).

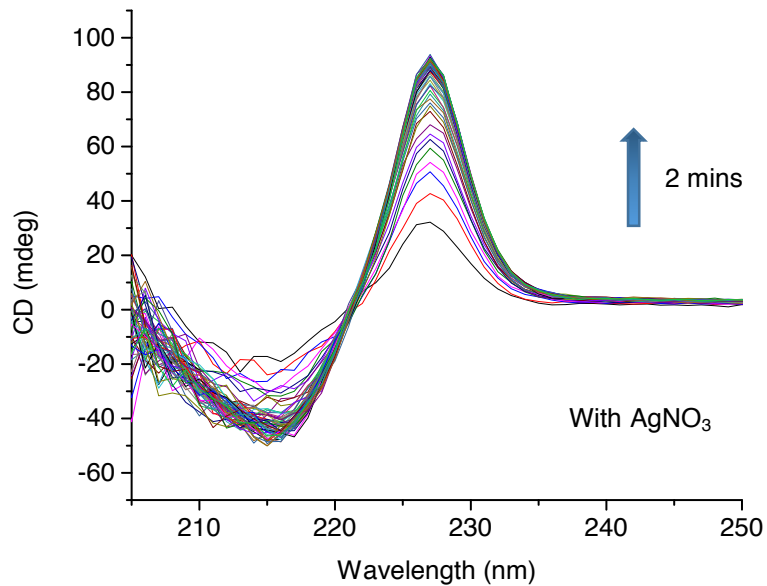
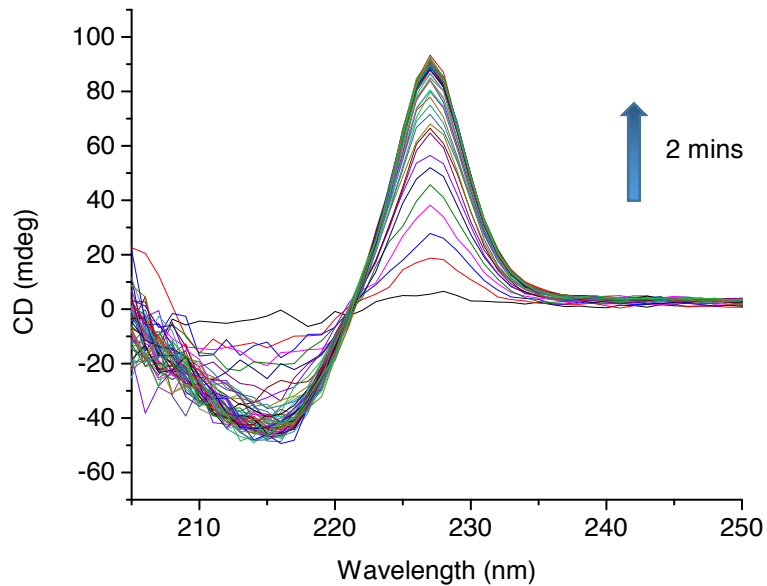


Figure II-5. Interval scans study of (*S*)-methylbenzylamine **II-3** and **II-1** at room temperature. Top figure: reaction without additive, bottom figure: in presence of 2 equiv of AgNO_3 .

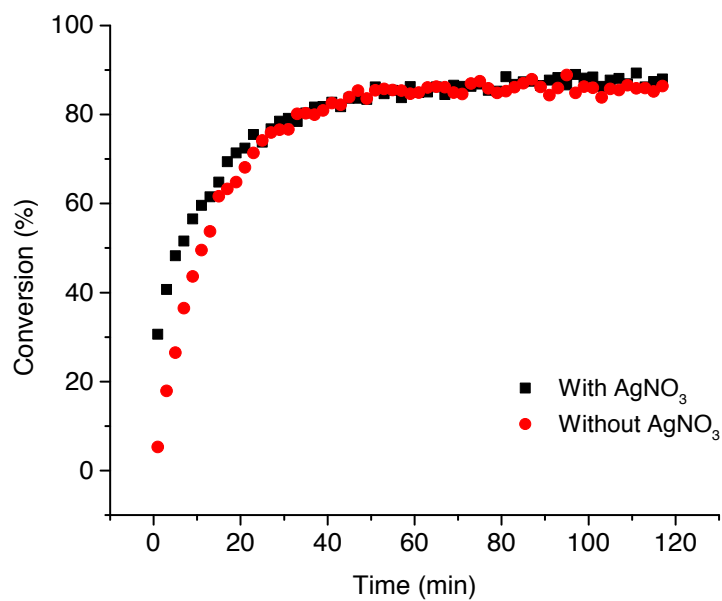
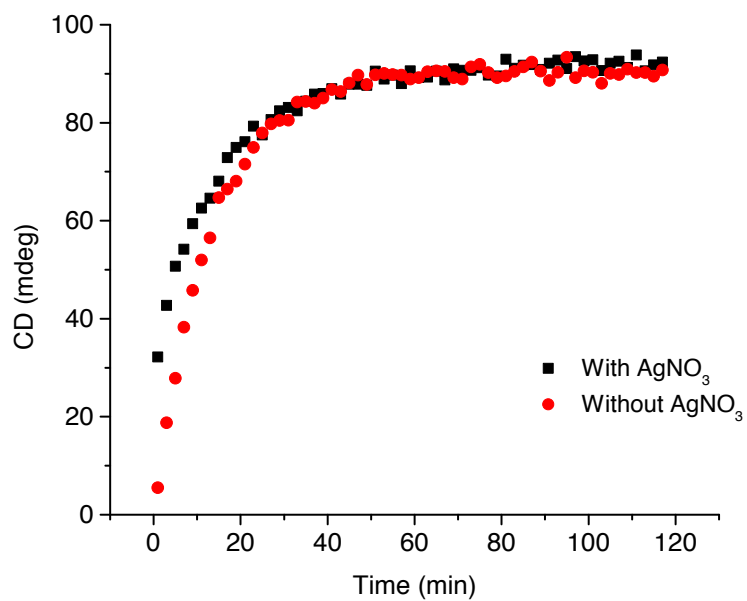


Figure II-6. Rate study of the reaction of (S)-methylbenzylamine II-3 and II-1 at 10 μ M in acetonitrile at room temperature. Top: rate profile based on CD read out, Bottom: comparison based on conversion.

II.4 Absolute stereochemical determination of aromatic amines

After establishing the conditions for CD analysis, we turned our attention to the absolute stereochemical determination of chiral aromatic amines. All the chiral amines were derivatized as their **II-1** derivatives and analyzed by CD in pure form. The ECCD spectra were recorded in millidegrees and normalized based on the concentration of the derivatized **II-1** samples to obtain the molecular CD (Mol CD). General terms for the ECCD studies for **Chapter II** and **Chapter III** are $\Delta\varepsilon$ and A . $\Delta\varepsilon_1$ and $\Delta\varepsilon_2$ are the maximum intensities of the lower and higher energy bands, respectively (higher and lower wavelengths accordingly, **Figure II-7**). A stands for the amplitude, which is expressed as $A = \Delta\varepsilon_1 - \Delta\varepsilon_2$.

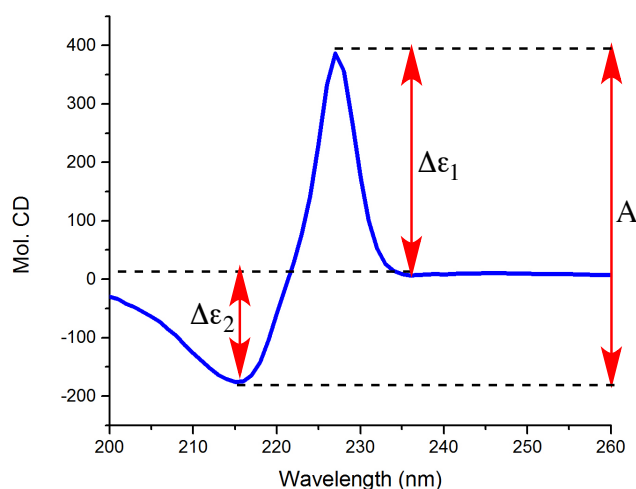


Figure II-7. Common symbols for the ECCD study.

As shown in **Table II-1**, extension of the study to a set of diverse chiral arylamines derivatized with **II-1** (entries 1–7, **Table II-1**) produces ECCD-active species. The system works well for both benzyl- and naphthyl-amines (**II-7**, **II-8**), yielding high amplitude

signals. The amplitudes for all the aromatic amines tested were greater than 150. Such high A values can significantly reduce the noise interference for the analysis. As expected, their corresponding enantiomeric amines leads to the opposite ECCD signal. For example, **II-5** yields a positive sign (+393) at 227 nm and a negative sign (-182) at 216 nm, its enantiomer **II-6** yields negative sign (-403) at 227 nm and a positive sign (+190) at 216 nm.

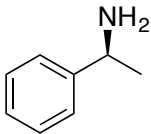
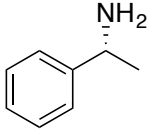
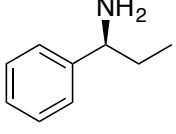
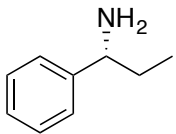
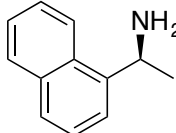
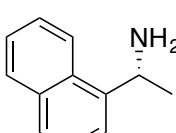
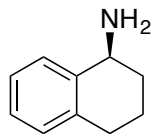
Entry	Amine	$\lambda_1(\text{nm}), \Delta\epsilon_2$	$\lambda_2(\text{nm}), \Delta\epsilon_2$	ECCD Signal	A
1	 II-3	228 (+356)	215 (-176)	Pos	+532
2	 II-4	228 (-345)	216 (+173)	Neg	-518
3	 II-5	227 (+393)	216 (-182)	Pos	+575
4	 II-6	227 (-403)	216 (+190)	Neg	-593
5	 II-7	228 (+305)	217 (-139)	Pos	+444
6	 II-8	228 (-342)	217 (+153)	Neg	-495
7	 II-9	228 (+112)	215 (-62)	Pos	+174

Table II-1. All CD measurements were recorded in acetonitrile (10 μM) at rt.

A general trend for the arylamines was observed: *S* arylamines yield positive ECCD signal and *R* arylamines yield negative ECCD signal. Although this is not a mnemonic and should not be generalized. Thus, we decided to use computational analysis to guide the prediction of the anticipated ECCD.

II.4.1 Computational analysis

Computational analysis is one of the fastest growing research areas in the past few years. It provides unique insights for organic chemists to investigate the reaction mechanism, pathways, and geometries of intermediates.⁵³ There are a number of computational software on the market for chemists to choose from. Due in part to the user friendly interface, which leads to easy setup of experiments, SPARTAN software turns to be one of the most popular software for organic chemists.⁵⁴ In this chapter, we describe the use of SPARTAN software to help elucidate the absolute stereochemistry of the analytes.

The diastereomeric pairs of the **II-1** derivatives (central chirality of the amine and the helicity of the naphthyl groups, **Figure II-3**) will have different energetics and thus result in population imbalance that leads to an observable ECCD signal. The challenge lies in determining the preponderance of either the *P* or *M* helicity as a function of the chiral amine attached to **II-1**. Thus, we turned our attention to the low-cost conformer distribution analysis (DFT, B3LYP/6-31G*) to predict the abundance of populations that lead to either the *P* or *M* helicity of the bisnaphthyl core via SPARTAN software. Comparison with the experimentally obtained ECCD signals leads to the absolute stereochemical determination of the derivatized chiral amine.

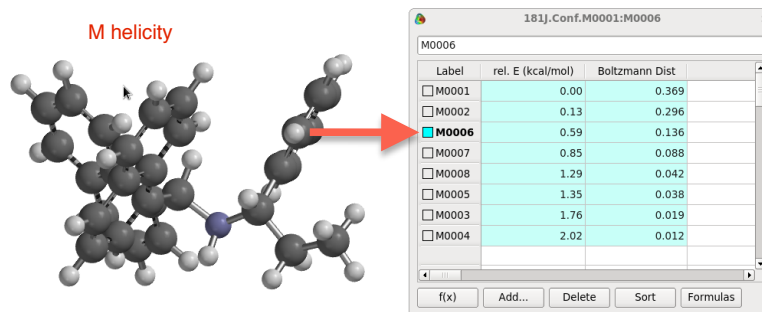
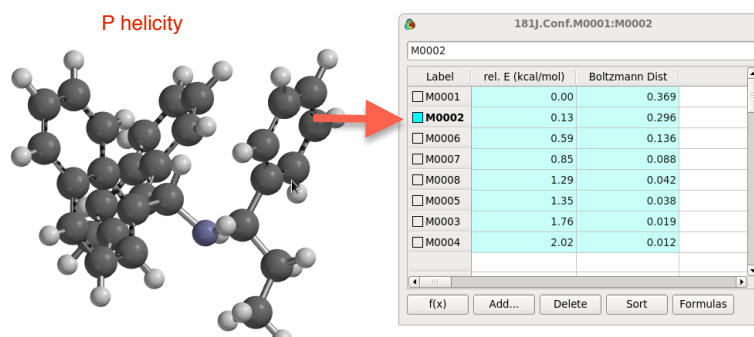
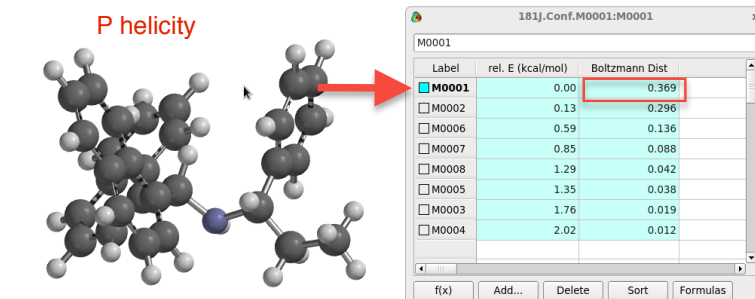
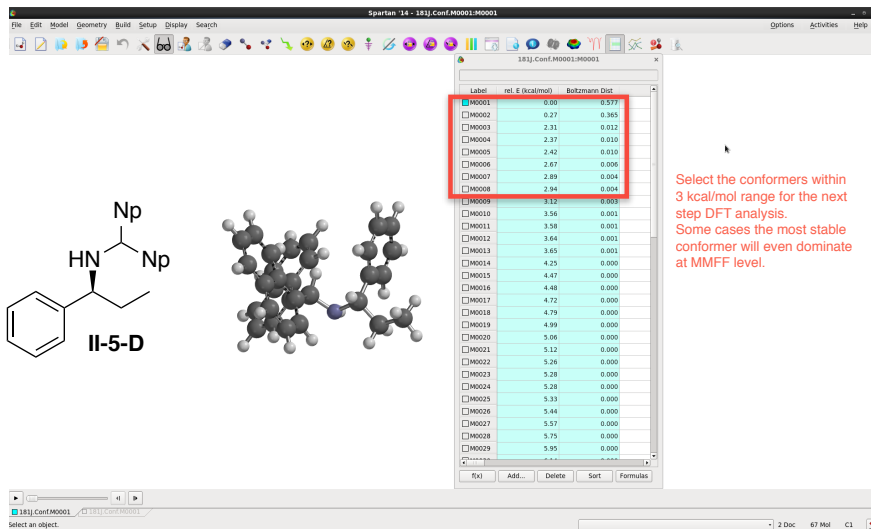
A PC with 15 core Intel Xeon X5647 @2.93 GHz with 48 GB memory on a Kernel Linux platform, equipped with SPARTAN 14 software was used for conformational calculations. Conformer distribution was performed at the MMFF level of theory utilizing Monte Carlo search parameters, starting from 10,000 K. All stable conformers (within 3 Kcal for aromatic compounds and within 2 Kcal for aliphatic compounds) were subject to further optimization by density functional theory at B3LYP/6-31G* level in vacuum. The resulting geometries for each conformer were analyzed and scored to yield either the *P* or *M* helicity by considering the calculated Boltzmann distribution values. A detailed step by step procedure for computational studies performed to obtain the anticipated ECCD signs for the derivatized chiral amines **II-5-D** is shown below (**Scheme II-3**):

Step 1: Perform a conformer distribution calculation with the MMFF force field. From the list of generated conformer structures, select all within 3 Kcal/mol for DFT geometry optimization.

Step 2: Upon geometry optimization (DFT, B3LYP/6-31G*), the helicity of the two naphthyl rings is assigned for each conformer.

Step 3: Sum up the Boltzmann values for all structures that lead to *P* and *M* helicities.

In this example (**II-5-D**), the *P*:*M* ratio is 70.3:29.7, thus predicting that the *P* helicity will dominate in the CD spectra and leads to a positive ECCD signal. This prediction is in agreement with experimental result.



Scheme II-4. Step by step procedure for computational studies via DFT calculation.

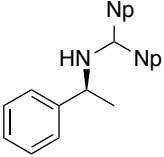
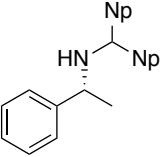
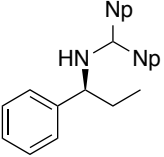
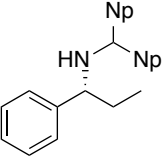
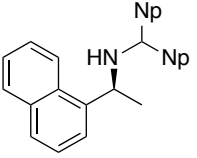
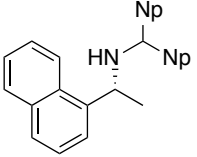
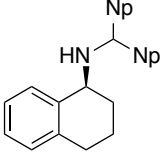
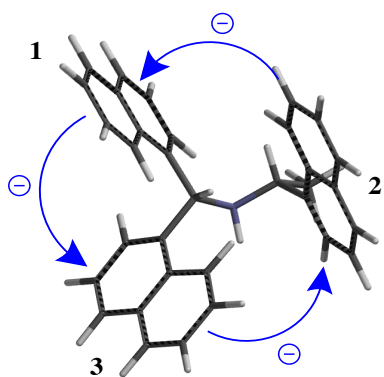
Entry	Amine ^a	Predicted Sign <i>P/M</i> ratio ^b	$\lambda(\text{nm}), \Delta_2$	A
1	 II-3-D	Pos (80.9/19.1)	228 (+356) 215 (-176)	+532
2	 II-4-D	Neg (17.2/82.8)	228 (-345) 216 (+173)	-518
3	 II-5-D	Pos (70.3/29.7)	227 (+393) 216 (-182)	+575
4	 II-6-D	Neg (17.4/82.6)	227 (-403) 216 (+190)	-593
5	 II-7-D	Pos (65.7/34.3)	228 (+305) 217 (-139)	+444
6	 II-8-D	Neg (19.3/80.7)	228 (-342) 217 (+153)	-495
7	 II-9-D	Pos (80.9/19.1)	228 (+112) 215 (-62)	+174

Table II-2. Theoretical *P* and *M* predictions were obtained by tabulating the population of conformations that yield *P* or *M* helicity by DFT at the B3LYP/6-31G* level.

Assisted with the computational study, we were more confident to assign the absolute stereochemistry of chiral amines. Looking back to the previous arylamines (**Table II-1**), we calculated all the *P:M* ratios for each. Gratifyingly, the predicted results from calculations match well with the experimentally recorded ECCD signals. The

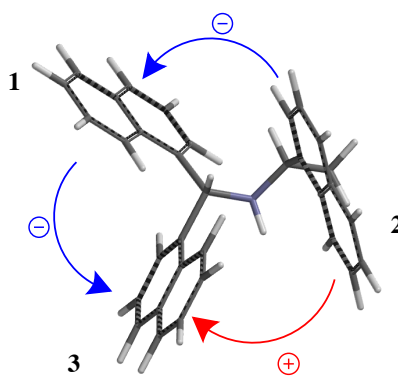
predicted ECCD signs shown in **Table II-2** are arrived at by considering conformational distribution of populations that adopt either the *P* (leading to positive ECCD) or *M* (leading to negative ECCD) helicities by the steps demonstrated in **Scheme II-4**. Among all these 7 chiral amines in **Table II-2**, **II-7-D** and **II-8-D** are the most complicated amines due to the contribution of the naphthyl group from the substrate. The pairwise coupling of three naphthyl groups (one from the substrate and two from **II-1**) is used to arrive at a prediction. The following is a step by step demonstration (**Scheme II-5**) of how to calculate the predicted ECCD for **II-8-D**. As before, the energy minimized conformations are considered. The prediction is based on assigning the helicities of each interacting naphthyl group. For example, in the first conformer the ECCD for all three interactions: i.e, 1→2, 2→3, and 1→3, predict a negative ECCD. Thus, all 45% population of that conformer is assigned as *M*-helicity. In contrast, for the second structure, the 1→2 and 1→3 interactions are negative, while the 2→3 interaction yield a positive helicity. The aggregate of all these calculations leads to the overall predicted helicity *M:P* = 80.7:19.3 for the system. Overall, the calculation predicts a negative ECCD signal which is in agreement with the experimental result.



M1

Label	rel. E (kcal/mol)	Boltzmann Dist
<input checked="" type="checkbox"/> M0001	0.00	0.451
<input type="checkbox"/> M0002	0.85	0.108
<input type="checkbox"/> M0003	0.08	0.393
<input type="checkbox"/> M0004	1.98	0.016
<input type="checkbox"/> M0005	1.57	0.032

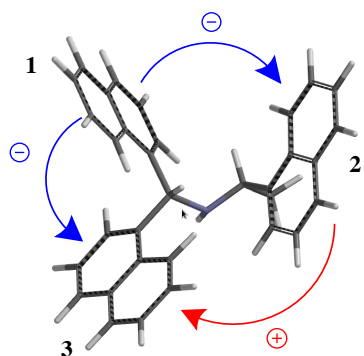
$M = 45.1 \times 100\% = 45.1$ $P = 0 \times 100\% = 0$



M2

Label	rel. E (kcal/mol)	Boltzmann Dist
<input type="checkbox"/> M0001	0.00	0.451
<input checked="" type="checkbox"/> M0002	0.85	0.108
<input type="checkbox"/> M0003	0.08	0.393
<input type="checkbox"/> M0004	1.98	0.016
<input type="checkbox"/> M0005	1.57	0.032

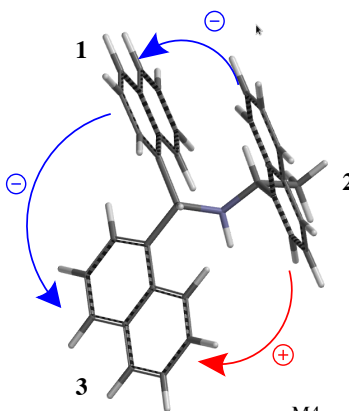
$M = 10.8 \times 66.6\% = 7.2$ $P = 10.8 \times 33.3\% = 3.6$



M3

Label	rel. E (kcal/mol)	Boltzmann Dist
<input type="checkbox"/> M0001	0.00	0.451
<input type="checkbox"/> M0002	0.85	0.108
<input checked="" type="checkbox"/> M0003	0.08	0.393
<input type="checkbox"/> M0004	1.98	0.016
<input type="checkbox"/> M0005	1.57	0.032

$M = 39.3 \times 66.6\% = 26.2$ $P = 39.3 \times 33.3\% = 13.1$



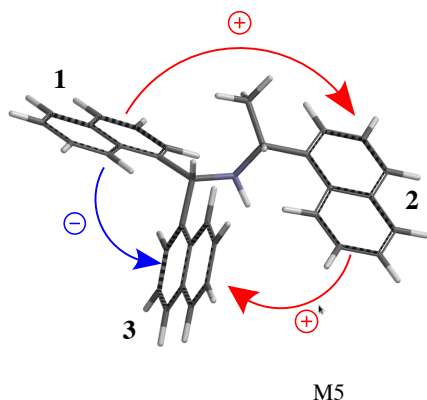
M4

Label	rel. E (kcal/mol)	Boltzmann Dist
<input type="checkbox"/> M0001	0.00	0.451
<input type="checkbox"/> M0002	0.85	0.108
<input type="checkbox"/> M0003	0.08	0.393
<input checked="" type="checkbox"/> M0004	1.98	0.016
<input type="checkbox"/> M0005	1.57	0.032

$M = 1.98 \times 66.6\% = 1.1$ $P = 1.98 \times 33.3\% = 0.5$

Scheme II-5. Step by step demonstration of **II-8-D** predicted ECCD analysis.

Scheme II-5 (cont'd)



F-Spart			
M0005			
Label	rel. E (kcal/mol)	Boltzmann Dist	
<input type="checkbox"/> M0001	0.00	0.451	
<input type="checkbox"/> M0002	0.85	0.108	
<input type="checkbox"/> M0003	0.08	0.393	
<input type="checkbox"/> M0004	1.98	0.016	
<input checked="" type="checkbox"/> M0005	1.57	0.032	

$$M = 3.2 \times 33.3\% = 1.1 \quad P = 3.2 \times 66.6\% = 2.1$$

Conformer Entry	<i>M</i> helicity	<i>P</i> helicity
M1	45.1	0
M2	7.2	3.6
M3	26.2	13.1
M4	1.1	0.5
M5	1.1	2.1
Overall	80.7	19.3

II.4.2 Crystallography study

After we successfully demonstrated the computational assisted analysis for the chiral amines, we were curious about whether the crystal structure of the derivatived amine can support our conformational predictions. Luckily, we were able to obtain the crystal structure of compound **II-5-D**. **II-5-D** yields a positive ECCD signal which indicates the *P* helicity is dominant among all conformers (**Figure II-8**). The obtained crystal structure also exhibits the *P* helicity, indicating a positive ECCD signal. This result is in line with our calculation (*P*:*M* = 70.3: 29.7).

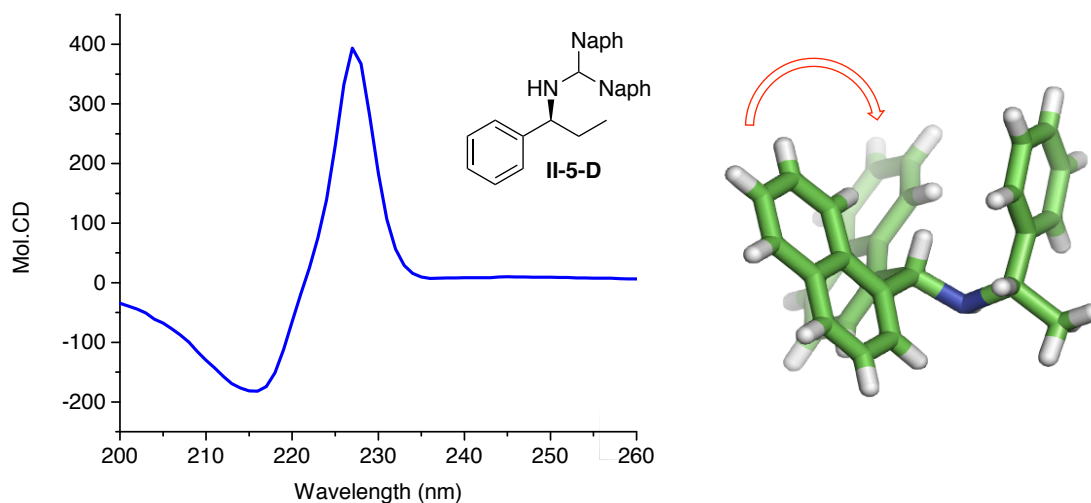


Figure II-8. ECCD spectrum of **II-5-D**, recorded at 10^{-5} M in acetonitrile at rt. Crystal structure of **II-5-D**, clearly shows a *P* helicity.

II.5 Absolute stereochemical determination of aliphatic amines

After screening the chiral aromatic amines, we moved to examining chiral aliphatic amines. In summary, similar results were obtained for aliphatic amines, albeit with lower overall ECCD amplitudes (**Table II-3**, entries 1-6). The average amplitude for chiral aliphatic amines is around 100, with a maximum amplitude of 193 for entry 6, **Table II-3**. Aliphatic amines have a much lower amplitude as compared with aromatic amines (average 500 amplitudes). Presumably, this is the result of more favorable interactions of the bisnaphthyl group with the aryl substituents.

As expected, enantiomeric alkyl amines result in opposite ECCD signals (**Table II-3**). Substituents on the amine with similar size, such as cyclohexyl and isopropyl ($A_{\text{value}} = 2.15$, entries 1 and 5), result in similar CD amplitudes (86–87), while larger substituents such as *t*-butyl ($A_{\text{value}} > 4$, entry 6) result in predictably larger signals.

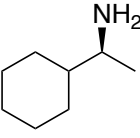
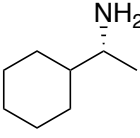
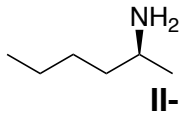
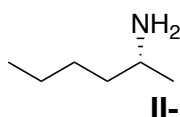
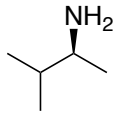
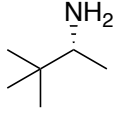
Entry	Amine	Predicted Sign <i>P/M</i> ratio	$\lambda(\text{nm}), \Delta\epsilon$	A
1	 II-10	Neg (37.2/62.8)	227 (-56) 217 (+30)	-86
2	 II-11	Pos (55.1/44.9)	227 (+61) 217 (-31)	+92
3	 II-12	Neg (42.0/58.0)	227 (-79) 216 (+38)	-117
4	 II-13	Pos (61.8/38.2)	227 (+77) 216 (-39)	+116
5	 II-14	Neg (13.8/86.2)	227 (-56) 216 (+31)	-87
6	 II-15	Pos (99.9/0.1)	228 (+130) 217 (-63)	+193

Table II-3. Chiral aliphatic amines ECCD analysis. All CD measurements were recorded in acetonitrile (10 μM) at rt. Theoretical *P* and *M* predictions were obtained by tabulating the population of conformations that yield *P* or *M* helicity by DFT at the B3LYP/6-31G* level.

Interestingly, during the course of the study, we found alkyl amine derivatives yield the opposite ECCD in comparison to aryl amines for the same pseudo-enantiomeric system. For example, **II-3** (Table II-1, entry 1) yields a positive ECCD signal while **II-10** (Table II-3, entry 1) produces a negative ECCD. Gratifyingly, computational analysis as described above, leads to the correct prediction for all substrates examined, irrespective of the nature of the substituents. The induced helicity of the naphthyl rings is the consequence of the asymmetric environment that constitutes both steric and electronic influences; simply considering only sterics or electronics will not lead to the correct

prediction. In fact, application of various linear free energy relationships such as A_{values} ,⁵⁵ Charton values,⁵⁶ and sterimol analysis⁵⁷ failed to provide a guide to develop a routine mnemonic. Thus, the use of an inexpensive conformational calculation, coupled with ECCD spectral analyses, provides a route to determine the absolute stereochemistry of chiral monoamines in an empirical manner.

II.6 Analysis of amino alcohols

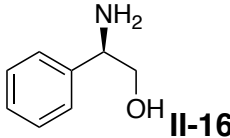
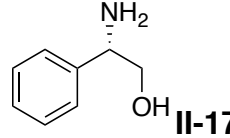
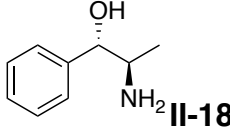
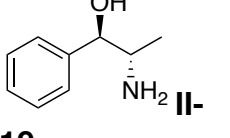
Entry	Amine	Predicted Sign <i>P/M</i> ratio	$\lambda(\text{nm}), \Delta\epsilon$	A
1	 II-16	Pos (83.6/16.4)	227 (+264) 215 (-133)	+397
2	 II-17	Neg (19.1/80.9)	227 (-288) 215 (+147)	-435
3	 II-18	Neg (12.2/87.8)	226 (-61) 215 (+27)	-88
4	 II-19	Pos (89.7/10.3)	226 (+77) 215 (-30)	+107

Table II-4. Chiral amino alcohols ECCD analysis. All CD measurements were recorded in acetonitrile (10 μM) at rt. Theoretical *P* and *M* predictions were obtained by tabulating the population of conformations that yield *P* or *M* helicity by DFT at the B3LYP/6-31G* level.

To further investigate the validity of our working model, chiral amino alcohols were tested. Gratifyingly, both enantiomers of phenylglycinol and norephedrine yield ECCD spectra which coincide with the results from calculation predictions (**Table II-4**). This demonstrates the applicability of the current method not only for chiral amines but also for amino alcohols, including a case (**II-16**, **Table II-4**) where a second stereogenic center

is present. It is important to note that the Cahn–Ingold–Prelog designations do not necessarily correlate with the expected ECCD sign since substitutions can change priorities. An example is **II-16**, in which the hydroxyl group effects the designation, yet it produces the same ECCD as **II-5** since the amine groups are disposed in the same manner.

The amplitudes of the amino alcohols also caught our attention. Phenylglycinol enantiomers (**II-16** and **II-17**, **Table II-4**) exhibit much larger amplitudes than the norephedrine enantiomers (**II-18** and **II-19**, **Table II-4**). Although both compounds have phenyl rings, the position of the phenyl leads to significant difference in the amplitudes. We believe the interactions between the naphthalene rings and phenyl groups were reduced in the norephedrine case due to the chiral center being one more carbon away from the phenyl ring.

II.7 Analysis of secondary amines

Next, we turned our attention to the case of secondary amines. Although these have been challenging for most chiroptical techniques, arguably the most successful and important accomplishment has been that of Anslyn and co-workers. They demonstrated a metal-templated assembly for sensing the chirality of secondary amines by using a tripod system (**Scheme II-1**).⁵⁸ However, the best signal was only achieved for the 2-(methoxymethyl)pyrrolidine. They also tried a secondary amine (*S*-N, α -dimethylbenzylamine), but the signal obtained was weak. To the best of our knowledge, there were no general ECCD methods for protected chiral secondary amines sensing before our method was published.

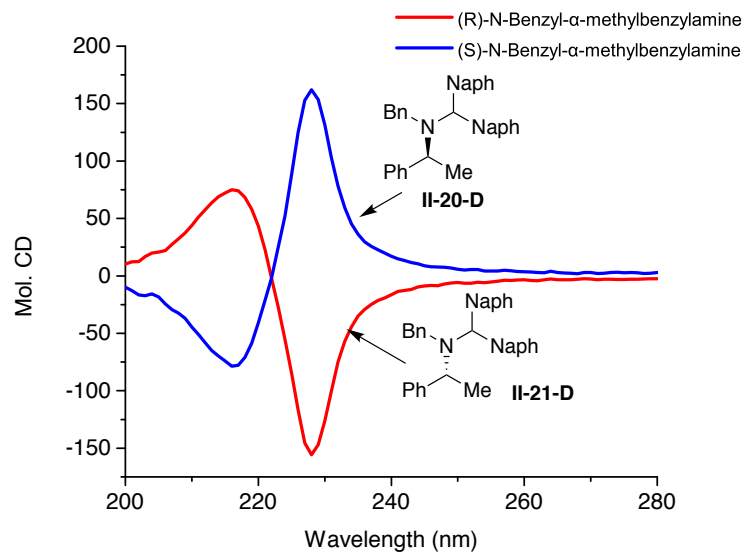


Figure II-9. ECCD spectra of enantiomeric **II-1** derivatized benzyl protected aromatic amines (10^{-5} M) in acetonitrile at rt show opposite ECCD spectra.

Our attempts commenced with the derivatization of amines substituted with electron-withdrawing groups (Boc, Cbz, Ac, Bz) with **II-1**. Under our standard derivatization protocol, these molecules remained unreactive. Nonetheless, benzyl-protected amines react with **II-1** to yield an ECCD active species. As shown in **Figure II-9**, the derivatized R-N-benzylmethylbenzylamine **II-21** yields a negative ECCD signal, while its enantiomer **II-20** yields a positive signal. It is also interesting to point out that the benzyl protected amines yield lower ECCD signal as compared to un-protected amines (**Figure II-10**). Compound **II-5-D** shows a significant higher amplitude as compared to the benzyl protected amine **II-20-D**. Due to the fact that benzyl and phenyl groups are similar in size, chiral sensing of these amines is challenging, but was accomplished by our method.

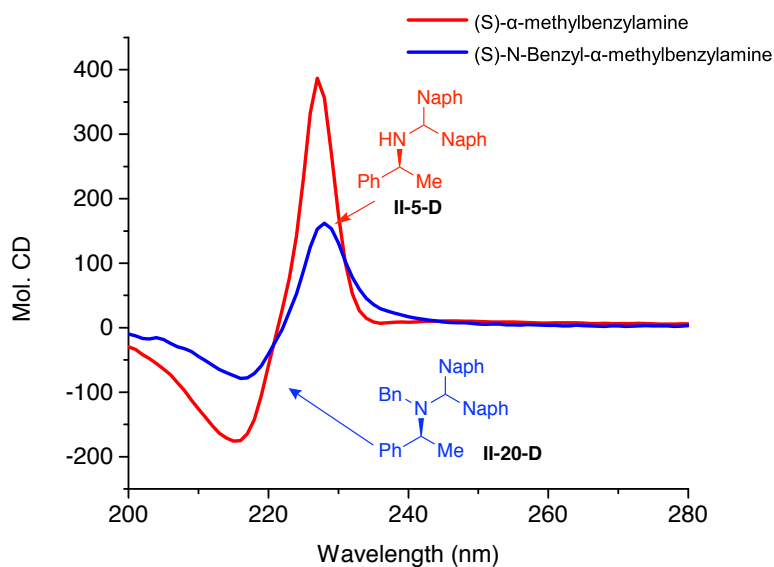


Figure II-10. ECCD spectra of **II-5-D** and **II-20-D** (10^{-5} M) in acetonitrile at rt show different ECCD amplitudes.

We also tested our method with chiral secondary aliphatic amines. Enantiomers of N-benzyl-protected methylcyclohexyl amines resulted in opposite ECCD signals, as expected (**Figure II-11**). To our delight, the calculation predictions match well with the experimental results (**Table II-5**).

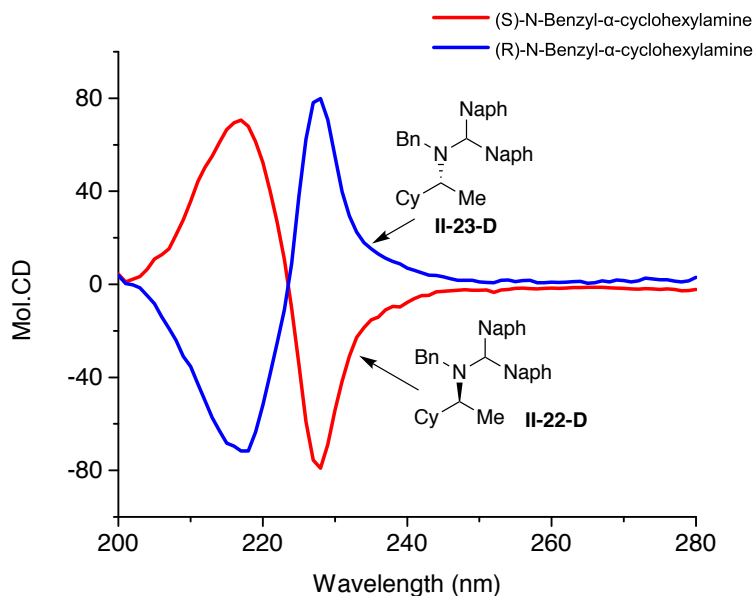


Figure II-11. ECCD spectra of enantiomeric **II-1** derivatized benzyl protected aliphatic amines (10^{-5} M) in acetonitrile at rt show opposite ECCD spectra. Cy = cyclohexyl.

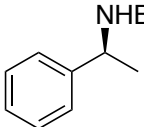
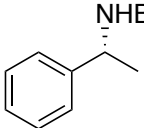
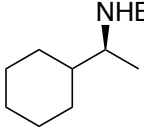
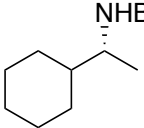
Entry	Amine	Predicted Sign <i>P/M</i> ratio	λ (nm), $\Delta\epsilon$	A
1	 II-20	Pos (95.8/4.2)	228 (+162) 216 (-78)	+240
2	 II-21	Neg (13.0/87.0)	228 (-156) 216 (+75)	-231
3	 II-22	Neg (42.3/57.6)	228 (-79) 217 (+70)	-149
4	 II-23	Pos (77.4/22.6)	227 (+80) 217 (-71)	+151

Table II-5. Chiral secondary amines ECCD analysis. All CD measurements were recorded in acetonitrile ($10 \mu\text{M}$) at rt.

II.8 Rapid *ee* analysis

A rapid measure of *ee* is invaluable to organic chemists and using CD spectroscopy has found traction in this area.⁵⁹ Thus, after demonstrating that our method is capable of analyzing a variety of chiral amines, we extended its capability for an easy way to measure *ee*.

II.8.1 Effect of impurity on *ee* analysis

In order to build a system for *ee* analysis, we have to understand the weakness of the system. Most amines can be easily contaminated by acids or form peroxides under oxygen, thus a detailed study of how the impurities may affect the system is necessary. We first tested acid contamination.

To test if impure chiral amines would react with **II-1**, a control experiment was designed in which (*S*)-methylbenzylamine **II-3** and its HCl salt were reacted with **II-1** (**Figure II-12**). To acetonitrile (1 mL) was added 1-BDN solution (1 μ L, 0.005 M), followed by the addition of **II-3** solution (10 μ L, 10 equiv) and **II-3** HCl salt solution (10 μ L, 10 equiv) in two vials. After incubating for 1.5 h at rt, the mixtures were directly analyzed by CD (100 nm/min scan rate). The pure amine **II-3** yielded a strong ECCD signal, while the amine salt was CD silent. This clearly suggests the need for using free base for derivatization with **II-1**.

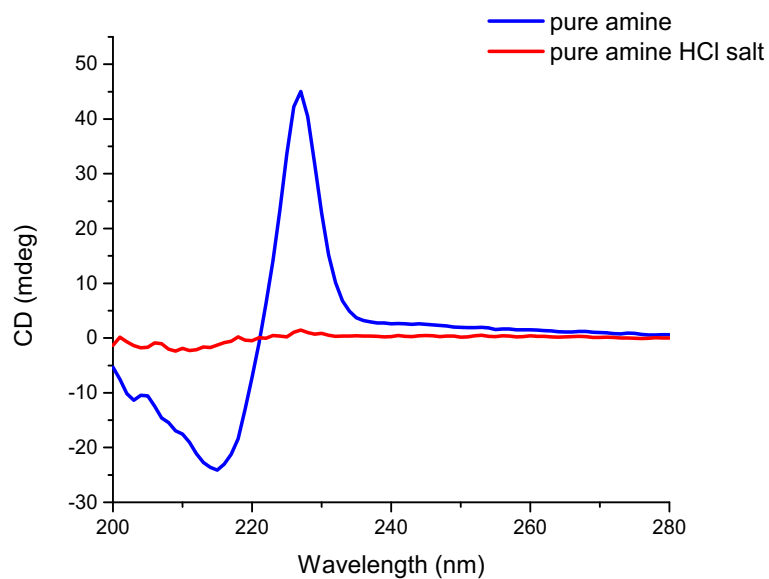


Figure II-12. Acid impurity study. Pure **II-3** amine yielded ECCD signal, amine **II-3** HCl salt yielded no signal.

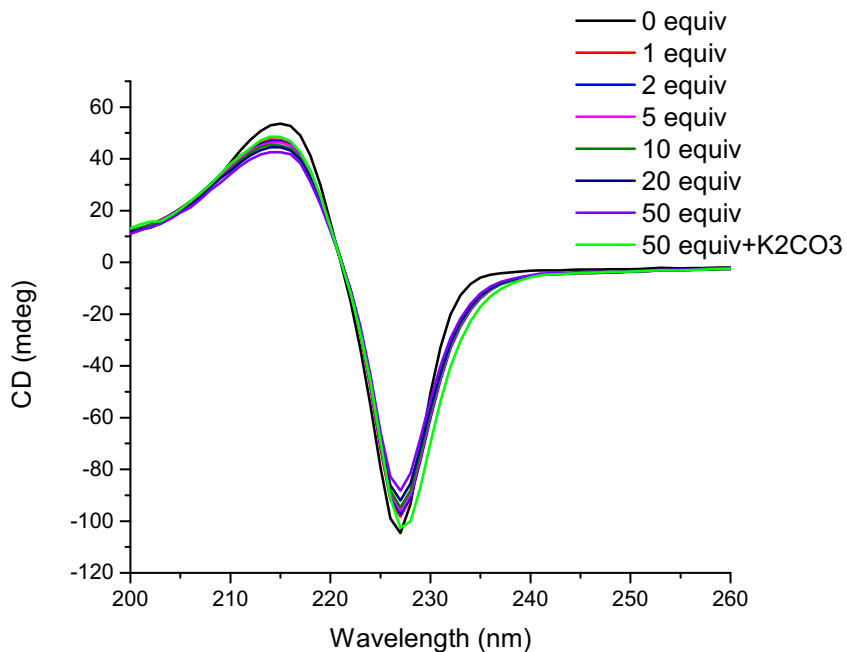


Figure II-13. Treatment of **II-4-D** with different equivalents of HCl. Signal decreased upon addition of HCl from 1 equivalent up to 50 equivalents, however, after addition of solid K₂CO₃, the CD signal was recovered.

Next, we investigated the tolerance of the **II-1** derivatized chiral amines under acidic or oxidative conditions. To the derivatized **II-4** was added HCl acid and H₂O₂ separately. Treating pure **II-4-D** with different equivalents of HCl led to a slight decrease in ECCD (6 % loss with 1 equiv HCl and up to 15 % loss with 50 equiv HCl, **Figure II-13**). However, the original ECCD signal was fully recovered after addition of solid K₂CO₃ (see **Table II-6** for details).

HCl equivalent	CD (mdeg) at 227 nm
0	-104.57
1	-98.261
2	-97.274
5	-95.917
10	-94.689
20	-92.079
50	-88.196
Treating with K ₂ CO ₃	-102.63

Table II-6. ECCD signal recorded at 227 nm with different equivalent of HCl.

For peroxide study, treating **II-4-D** with up to 50 equiv of H₂O₂ stock solution resulted in no change in the signal. Extending the exposure of **II-4-D** to 50 equiv H₂O₂ for 1.5 h also did not result in deterioration of the ECCD signal (**Figure II-14**).

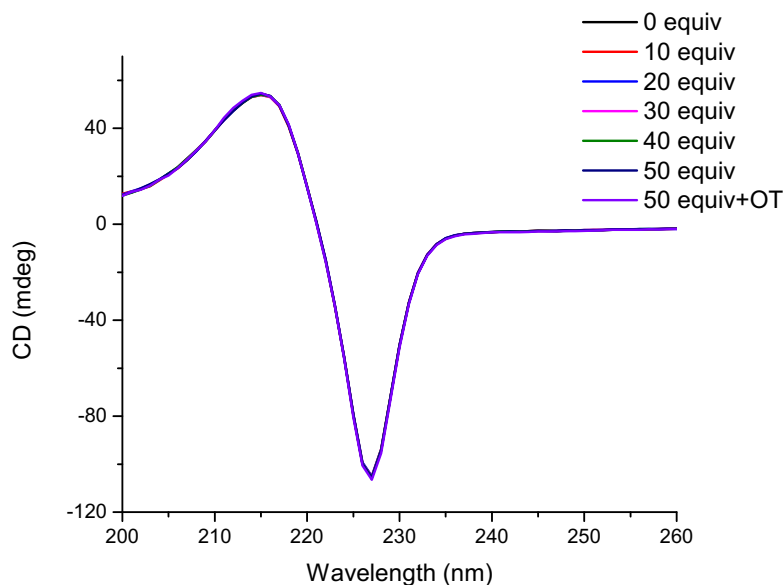


Figure II-14. Treatment of **II-4-D** with H_2O_2 stock solution at different equivalents. The ECCD signal remained unchanged.

II.8.2 Standard curve for *ee* analysis

In order to make a standard curve for *ee* analysis, stock solutions of various *ees* (-100, -80, -60, -40, -20, 0, +20, +40, +60, +80, +100% *ee* for *R* enantiomer) were prepared (0.01 M solution in DCM). Here, we chose chiral ethylbenzylamine **II-5** and **II-6** for *ee* analysis. Actual *ee* value for each standard was measured by HPLC analysis of carbamate derivatized analog for each prepared sample. After incubating for 1.5 h at room temperature, the mixture was directly analyzed by CD (**Figure II-15**). Due to the signal at 215 nm being noisy, we chose the CD signal at 227 nm to derive the standard curve.

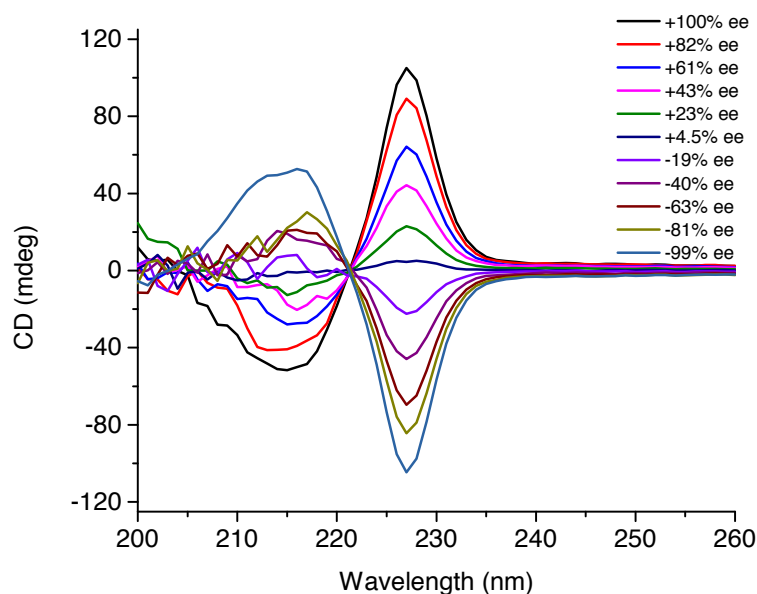


Figure II-15. CD spectra of chiral amines **II-5** and **II-6** at various *ees*.

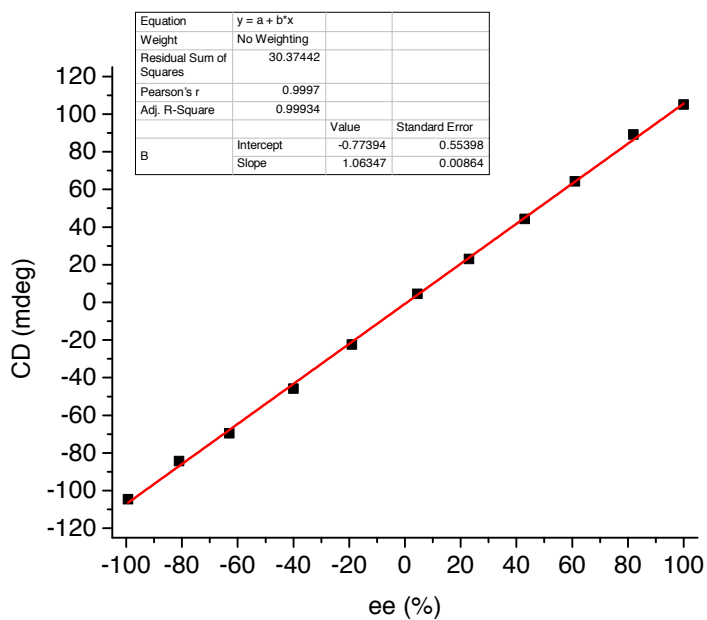


Figure II-16. Linear correlation of the CD signal with *ee* values of chiral amines.

A linear relationship between the CD amplitude at 227 nm and the enantiomeric excess of the analytes was obtained as shown in **Figure II-16**, with a fit that perfectly fits with the data ($R^2 = 0.999$).

We further verified the method by measuring the *ee* of five unknown samples (double-blind study), derivatized under identical conditions. The experimentally derived *ee* values of the unknown samples, obtained with one scan (1 min acquisition time), were in excellent agreement with the known concentrations, with an average error of 0.48% (**Table II-7**). It is also noteworthy that CD scan can be reduced to less than 5 s for a single wavelength. The expedient reactivity of **II-1**, leading to a routine derivatization procedure, and the method's excellent reproducibility lends itself to a potentially suitable methodology for adoption in high-throughput screening (HTS) format.

Entry	1 Scan (< 1 min)		
	<i>ee</i> (%) known	<i>ee</i> (%) measured	Error (%)
A	+71.2	+71.5	0.3
B	+55.4	+55.7	0.3
C	+14.4	+14.9	0.5
D	-81.2	-81.2	0.0
E	-75.7	-74.4	1.3

Table II-7. Measured *ees* of unknown amine samples.

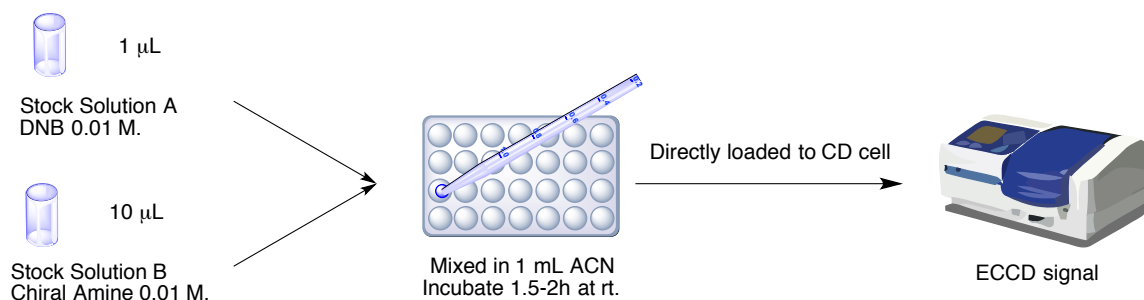
II.9 Experimental section

II.9.1 Materials and general instrumentations

Spectra grade solvents used for Circular Dichroism measurements were purchased from Sigma Aldrich. Column chromatography was performed using SiliCycle silica gel (230-400 mesh). $^1\text{H-NMR}$ and $^{13}\text{C-NMR}$ spectra were obtained on Varian 500 MHz instrument and are reported in parts per million (ppm) relative to the solvent resonances (δ), with coupling constants (J) in Hertz (Hz). CD spectra were recorded on a JASCO J-810 spectropolarimeter, equipped with a temperature controller (Neslab 111) and are reported as λ [nm] ($\Delta\epsilon_{\text{max}}$ [$\text{mol}^{-1} \text{cm}^{-1}$]). All chiral primary amines were purchased from commercial sources and were used without further purification. HRMS analysis was performed on a Q-TOF Ultima system using electrospray ionization in positive mode. HPLC analysis was performed on DAICEL CHIRALCEL® OD-H column.

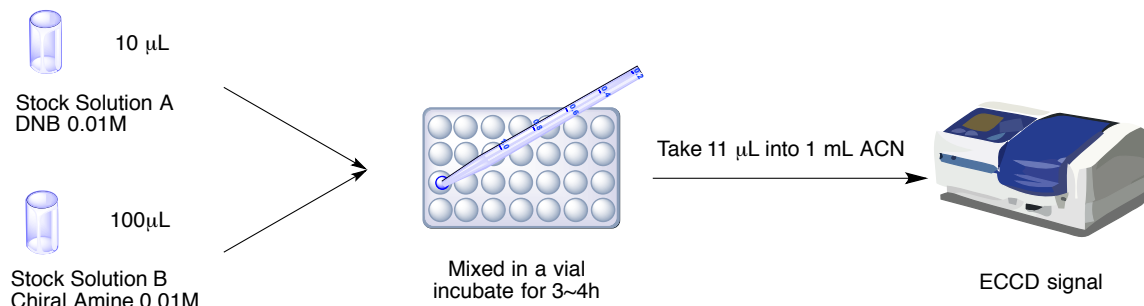
II.9.2 General procedure for analysis of absolute stereochemistry of amines

Primary Amines: Amines were dissolved in anhydrous DCM to obtain a 0.01 M stock solution. Similarly, a 0.01 M stock solution of 1,1'-(bromomethylene)dinaphthalene (**II-1**) in anhydrous DCM was prepared. To initiate the derivatization, **II-1** (1 μL) and 10 μL of the amine stock solution were mixed in acetonitrile (1 mL) and the mixture was incubated at room temperature for 1.5 h (**Scheme II-6**). The solutions were then loaded directly in a CD cuvette and measurements ensued (better signal and faster reaction time can be achieved by increasing the concentration).



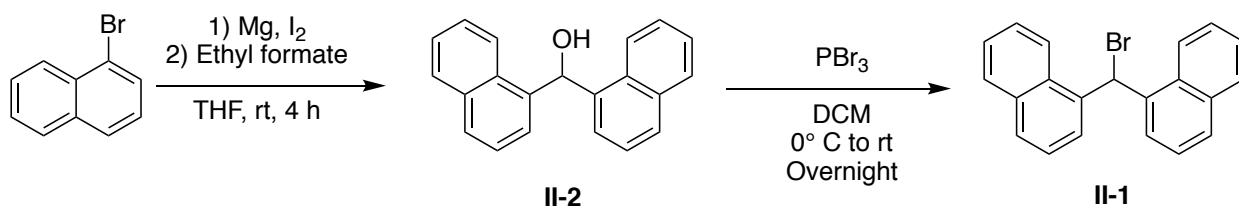
Scheme II-6: General procedure for preparation of samples for CD analysis.

Secondary Amines: The same procedure as above was followed with the following changes; These reactions required a higher final concentration (10^{-2} M) and a longer reaction time. To initiate the reaction, **II-1** (10 μL) and chiral amines (100 μL), each from their respective 0.01 M stock solutions, were incubated for 4 h at room temperature (**Scheme II-7**). For CD analysis, 11 μL of the reaction mixture was added to acetonitrile (1 mL).



Scheme II-7: General procedure to sense chiral secondary benzyl protected amines.

II.9.3 Synthesis of the compounds



1,1'-(bromomethylene)dinaphthalene (**II-1**)⁶⁰⁻⁶¹

To a dried 250 mL round bottom flask was added magnesium turnings (504 mg, 21 mmol, 1.05 equiv) and Iodine (12 mg, 0.05 mmol) in dry THF (100 mL). 1-Bromonaphthalene (4.14 g, 20 mmol) was dissolved in dry THF (10 mL) and was added to the mixture slowly over 15 min. After stirring for 2 h at room temperature, ethyl formate (740 mg, 10 mmol) in dry THF (10 mL) was added to the mixture and stirred for 2 h. The reaction was quenched by addition of cold 1N HCl solution (10 mL) and extracted with ethyl acetate (200 mL), washed with brine, dried over sodium sulfate and concentrated in vacuo to afford the crude product. The product was purified by recrystallization from ethyl acetate and hexane to afford an off white solid product [di(naphthalen-1-yl)methanol] (2.57 g, 90%).

^1H NMR (CDCl_3 , 500 MHz): 8.06 (d, $J = 8.0$ Hz, 2H), 7.91 (d, $J = 8.0$ Hz, 2H), 7.89 (d, $J = 8.0$ Hz, 2H), 7.50–7.38 (m, 9H), 7.33 (d, $J = 4.5$ Hz, 1H), 2.40 (d, $J = 4.5$ Hz, 1H) ppm.

^{13}C NMR (CDCl_3 , 125 MHz): 138.3, 133.9, 131.0, 128.8, 128.6, 126.5, 125.7, 125.4, 125.0, 123.6, 69.7.

To a dried 200 mL round bottom flask was added di(naphthalen-1-yl)methanol (2.57 g, 9.05 mmol) in DCM (70 mL), cooled to 0 °C, and PBr_3 (6 mL, 6 mmol) was added. The reaction was slowly warm up to room temperature and was stirred overnight. The reaction was quenched with the addition of water (40 mL), extracted by DCM (2 x 100 mL), and the combined organics were washed with brine, dried over sodium sulfate and concentrated on vacuo. The product was purified by recrystallized from DCM to afford an

off white solid (2.2 g, 71%). It should be noted that in our hands, exposure to silica gel leads to decomposition.

^1H NMR (CDCl_3 , 500 MHz): 8.06–8.04 (m, 2H), 7.90–7.88 (m, 2H), 7.82 (d, $J = 8.0$ Hz, 2H), 7.79 (s, 1H), 7.72–7.70 (d, $J = 7.5$ Hz, 2H), 7.51–7.48 (m, 4H), 7.42 (t, $J = 8.0$ Hz, 2H)

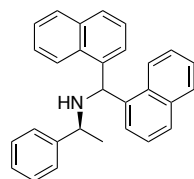
^{13}C NMR (CDCl_3 , 125 MHz): 135.9, 133.8, 130.14, 129.2, 129.0, 128.2, 126.8, 126.0, 125.0, 123.2, 50.0

HRMS (ESI^+) for $\text{C}_{21}\text{H}_{15}$ [$\text{M} - \text{Br}$] $^+$ calculated: 267.1174 found: 267.1177.

II.9.3.1 General procedures for the synthesis of II-1 amine derivatives

As mentioned in the previous text, all free amines are labeled as II-X (X is the number) and its derivative is labeled as II-X-D (D simply refer to derivative).

General Procedure A: To a 5 mL round bottom flask was added chiral amine (0.15 mmol, 1.5 equiv) and 1,1'-(bromomethylene)dinaphthalene (**II-1**) (0.1 mmol, 35 mg) in a 1:1 mixture of acetonitrile and DCM (2 mL overall). K_2CO_3 (0.2 mmol, 2 equiv, 28 mg) was added to the flask and the mixture was stirred under N_2 for 1.5 h. The reaction mixture was concentrated under vacuo and the mixture was directly loaded onto silica gel for purification.



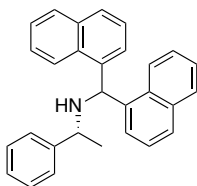
(*S*)-*N*-(di(naphthalen-1-yl)methyl)-1-phenylethan-1-amine (**II-3-D**)

Following the general procedure A, a white solid product was obtained (18.1 mg, 46.8%).

^1H NMR (CDCl_3 , 500 MHz): 8.03 (d, $J = 6.5$ Hz, 1H), 7.87-7.81 (m, 3H), 7.67-7.60 (m, 3H), 7.45-7.42 (m, 2H), 7.39-7.36 (m, 4H), 7.30-7.25 (m, 3H), 7.21-7.18 (m, 2H), 7.10 (d, $J = 5$ Hz, 1 H), 6.21 (s, 1H), 3.92 (q, $J = 6.5$ Hz, 1H), 1.50 (d, $J = 6.5$ Hz, 3H).

^{13}C NMR (CDCl_3 , 125 MHz): 144.9, 139.3, 137.9, 134.1, 133.9, 131.8, 130.9, 128.8, 128.7, 128.4, 127.8, 127.6, 127.4, 127.3, 126.2, 126.0, 125.9, 125.5, 125.4, 125.3, 124.9, 123.4, 122.9, 56.0, 55.0, 23.2.

HRMS (ESI^+) for $\text{C}_{29}\text{H}_{26}\text{N}$ [$\text{M} + \text{H}$] $^+$ calculated: 388.2065 found: 388.2064.



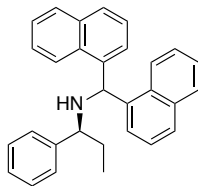
(*R*)-*N*-(di(naphthalen-1-yl)methyl)-1-phenylethan-1-amine (**II-4-D**)

Following the general procedure A, a white solid product was obtained (12 mg, 31%).

^1H NMR (CDCl_3 , 500 MHz): 8.02 (d, $J = 7.0$ Hz, 1H), 7.86-7.80 (m, 3H), 7.66-7.59 (m, 3H), 7.44-7.42 (m, 2H), 7.38-7.35 (m, 4H), 7.30-7.25 (m, 3H), 7.21-7.19 (m, 2H), 7.09-7.07 (m, 1 H), 6.19 (s, 1H), 3.91 (q, $J = 6.5$ Hz, 1H), 1.49 (d, $J = 6.5$ Hz, 3H).

^{13}C NMR (CDCl_3 , 125 MHz): 144.9, 139.3, 137.9, 134.1, 133.9, 131.8, 130.9, 128.8, 128.7, 128.4, 127.8, 127.6, 127.4, 127.3, 126.2, 126.0, 125.9, 125.5, 125.4, 125.3, 124.9, 123.4, 122.9, 56.0, 55.0, 23.2.

HRMS (ESI^+) for $\text{C}_{29}\text{H}_{26}\text{N}$ [$\text{M} + \text{H}$] $^+$ calculated: 388.2065 found: 388.2067.



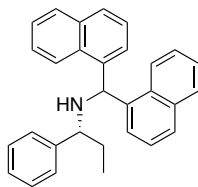
(S)-N-(di(naphthalen-1-yl)methyl)-1-phenylpropan-1-amine (II-5-D)

Following the general procedure A, a white solid product was obtained (35 mg, 88%).

^1H NMR (CDCl_3 , 500 MHz): 8.13 (d, $J = 7.0$ Hz, 1H), 7.86-7.81 (m, 3H), 7.66-7.63 (m, 2H), 7.58 (d, $J = 9$ Hz, 1H), 7.44-7.35 (m, 6H), 7.30-7.27 (m, 1H), 7.22-7.16 (m, 4H), 7.08-7.07 (d, $J = 7.0$ Hz, 1 H), 6.20 (s, 1H), 3.62 (t, $J = 7.0$ Hz, 1H), 1.98-1.96 (m, 1 H), 1.78-1.75 (m, 1H), 0.87 (t, $J = 7.5$ Hz, 3H).

^{13}C NMR (CDCl_3 , 125 MHz): 143.6, 139.5, 138.0, 134.1, 133.9, 131.9, 130.9, 128.8, 128.7, 128.4, 128.1, 127.7, 127.5, 127.3, 126.2, 126.1, 125.9, 125.5, 125.4, 125.3, 125.0, 123.4, 123.0, 62.7, 54.7, 30.0, 11.4.

HRMS (ESI $^+$) for $\text{C}_{30}\text{H}_{28}\text{N}$ [$\text{M} + \text{H}$] $^+$ calculated: 402.2222 found: 402.2223.



(S)-N-(di(naphthalen-1-yl)methyl)-1-phenylpropan-1-amine (II-6-D)

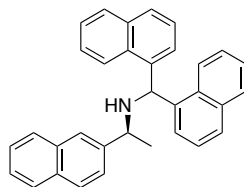
Following the general procedure A, a white solid product was obtained (34 mg, 86%).

^1H NMR (CDCl_3 , 500 MHz): 8.12 (d, $J = 7.0$ Hz, 1H), 7.86-7.80 (m, 3H), 7.67-7.63 (m, 2H), 7.58 (d, $J = 8.5$ Hz, 1H), 7.45-7.35 (m, 6H), 7.30-7.27 (m, 1H), 7.22-7.16 (m, 4H),

7.08-7.07 (d, J = 6.5 Hz, 1 H), 6.20 (s, 1H), 3.63 (t, J = 8.0 Hz, 1H), 1.98-1.96 (m, 1 H), 1.78-1.75 (m, 1H), 0.87 (t, J = 7.5 Hz, 3H).

^{13}C NMR (CDCl_3 , 125 MHz): 143.5, 139.5, 137.9, 134.1, 133.9, 131.9, 130.9, 128.8, 128.7, 128.4, 128.1, 127.7, 127.5, 127.3, 126.2, 126.1, 125.9, 125.5, 125.4, 125.3, 125.0, 123.3, 123.0, 62.7, 54.7, 30.0, 11.4.

HRMS (ESI^+) for $\text{C}_{30}\text{H}_{28}\text{N}$ $[\text{M} + \text{H}]^+$ calculated: 402.2222 found: 402.2231.



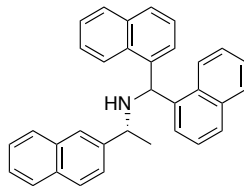
(*S*)-*N*-(di(naphthalen-1-yl)methyl)-1-(naphthalen-2-yl)ethan-1-amine (**II-7-D**)

Following the general procedure A, a white solid product was obtained (41 mg, 93%).

^1H NMR (CDCl_3 , 500 MHz): 7.97 (d, J = 7.5 Hz, 1H), 7.88-7.81 (m, 5H), 7.77 (d, J = 8.0 Hz, 1H), 7.72-7.68 (m, 2H), 7.62-7.58 (m, 2H), 7.53-7.50 (m, 2H), 7.42-7.26 (m, 5H), 7.22-7.19 (m, 1H), 7.14-7.09 (m, 2H), 6.29 (s, 1H), 4.86 (q, J = 7.0 Hz, 1H), 1.62 (d, J = 7.0 Hz, 3H).

^{13}C NMR (CDCl_3 , 125 MHz): 141.6, 139.3, 138.7, 134.0, 133.9, 133.8, 131.8, 131.7, 131.0, 128.8, 128.7, 128.6, 127.8, 127.7, 127.5, 126.1, 125.9, 125.8, 125.7, 125.5, 125.5, 125.4, 125.4, 125.3, 124.9, 123.8, 123.4, 123.2, 123.1, 55.6, 51.2, 23.7.

HRMS (ESI^+) for $\text{C}_{33}\text{H}_{28}\text{N}$ $[\text{M} + \text{H}]^+$ calculated: 438.2222 found: 438.2230.



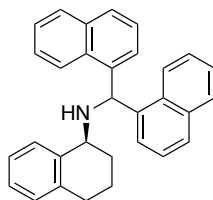
(R)-*N*-(di(naphthalen-1-yl)methyl)-1-(naphthalen-2-yl)ethan-1-amine (**II-8-D**)

Following the general procedure A, a white solid product was obtained (42 mg, 97%).

^1H NMR (CDCl_3 , 500 MHz): 7.99 (m, 1H), 7.89-7.82 (m, 5H), 7.78 (m, 1H), 7.73-7.69 (m, 2H), 7.63-7.60 (m, 2H), 7.55-7.51 (m, 2H), 7.43-7.27 (m, 5H), 7.23-7.20 (m, 1H), 7.15-7.10 (m, 2H), 6.30 (s, 1H), 4.88 (q, $J = 7.0$ Hz, 1H), 1.64 (d, $J = 7.0$ Hz, 3H),

^{13}C NMR (CDCl_3 , 125 MHz): 141.6, 139.3, 138.7, 134.0, 133.9, 133.8, 131.8, 131.7, 131.0, 128.8, 128.7, 128.6, 127.8, 127.7, 127.5, 126.1, 125.9, 125.8, 125.7, 125.5, 125.5, 125.4, 125.4, 125.3, 124.9, 123.8, 123.4, 123.2, 123.1, 55.6, 51.2, 23.7.

HRMS (ESI $^+$) for $\text{C}_{33}\text{H}_{28}\text{N}$ [$\text{M} + \text{H}$] $^+$ calculated: 438.2222 found: 438.2224.



(S)-*N*-(di(naphthalen-1-yl)methyl)-1,2,3,4-tetrahydronaphthalen-1-amine (**II-9-D**)

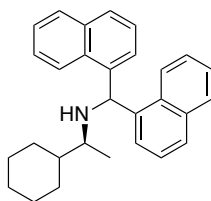
Following the general procedure A, a white solid product was obtained (36 mg, 87%).

^1H NMR (CDCl_3 , 500 MHz): 8.13 (d, $J = 8.5$ Hz, 1 H), 7.92-7.87 (m, 2H), 7.82-7.76 (m, 3H), 7.69 (d, $J = 8.5$ Hz, 1 H), 7.62 (d, $J = 7.5$ Hz, 1 H), 7.50-7.37 (m, 6H), 7.33-7.30

(m, 1H), 7.24-7.21 (m, 1H), 7.17-7.15 (m, 2H), 6.67 (s, 1H), 4.02 (m, 1H), 2.88-2.77 (m, 2H), 2.13-2.03 (m, 2H), 1.79-1.76 (m, 2H).

^{13}C NMR (CDCl_3 , 125 MHz): 138.7, 138.5, 137.3, 134.1, 134.1, 131.5, 131.4, 129.3, 129.0, 129.0, 128.9, 127.8, 127.7, 126.9, 126.2, 126.1, 126.0, 125.6, 125.5, 125.4, 125.4, 123.0, 122.9, 54.7, 53.3, 28.9, 28.5, 18.6.

HRMS (ESI^+) for $\text{C}_{31}\text{H}_{28}\text{N}$ [$\text{M} + \text{H}$] $^+$ calculated: 414.2222 found: 414.2227.



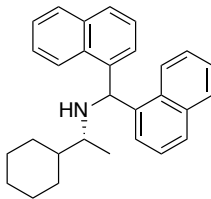
(S)-1-cyclohexyl-N-(di(naphthalen-1-yl)methyl)ethan-1-amine (II-10-D)

Following the general procedure A, a white solid product was obtained (18 mg, 47%).

^1H NMR (CDCl_3 , 500 MHz): 8.20-8.18 (m, 1H), 8.09 (d, $J = 8.0$ Hz, 1H), 7.87-7.85 (m, 2H), 7.76-7.73 (m, 2H), 7.59 (d, $J = .07$ Hz, 1H), 7.50-7.35 (m, 7H), 6.51 (s, 1H), 2.80 (m, 1H), 1.76-1.54 (m, 6H), 1.26-1.21 (m, 2H), 1.11 (d, $J = 7.0$ Hz, 3H), 1.07-1.03 (m, 2H).

^{13}C NMR (CDCl_3 , 125 MHz): 139.6, 138.9, 134.0, 134.0, 131.5, 131.4, 128.9, 128.9, 127.6, 127.5, 126.2, 126.0, 125.9, 125.8, 125.5, 125.5, 125.3, 123.2, 123.1, 56.0, 55.2, 43.2, 30.1, 27.7, 26.8, 26.7, 26.5, 16.5.

HRMS (ESI^+) for $\text{C}_{29}\text{H}_{32}\text{N}$ [$\text{M} + \text{H}$] $^+$ calculated: 394.2535 found: 394.2538.



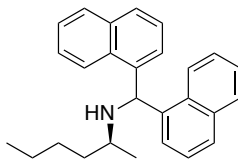
(R)-1-cyclohexyl-*N*-(di(naphthalen-1-yl)methyl)ethan-1-amine (**II-11-D**)

Following the general procedure A, a white solid product was obtained (29 mg, 73%).

^1H NMR (CDCl_3 , 500 MHz): 8.21-8.19 (m, 1H), 8.11 (d, $J = 8.5$ Hz, 1H), 7.88-7.86 (m, 2H), 7.77-7.73 (m, 2H), 7.60 (d, $J = 7.0$ Hz, 1H), 7.51-7.36 (m, 7H), 6.57 (s, 1H), 2.81-2.79 (m, 1H), 1.77-1.55 (m, 6H), 1.26-1.21 (m, 2H), 1.12 (d, $J = 7.0$ Hz, 3H), 1.08-1.03 (m, 2H).

^{13}C NMR (CDCl_3 , 125 MHz): 139.6, 138.9, 134.1, 134.0, 131.6, 131.4, 128.9, 128.9, 127.6, 127.5, 126.2, 126.1, 125.9, 125.8, 125.5, 125.5, 125.3, 123.2, 123.1, 56.0, 55.2, 43.2, 30.1, 27.7, 26.8, 26.7, 26.6, 16.5.

HRMS (ESI $^+$) for $\text{C}_{29}\text{H}_{32}\text{N}$ [$\text{M} + \text{H}$] $^+$ calculated: 394.2535 found: 394.2541.



(S)-*N*-(di(naphthalen-1-yl)methyl)hexan-2-amine (**II-12-D**)

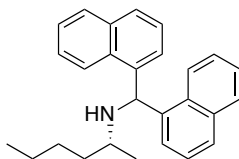
Following the general procedure A, a white solid product was obtained (30 mg, 80%).

^1H NMR (CDCl_3 , 500 MHz): 8.25 (d, $J = 9.0$ Hz, 1H), 8.09 (d, $J = 8.5$ Hz, 1H), 7.88-7.86 (m, 2H), 7.77-7.73 (m, 2H), 7.60 (d, $J = 7.5$ Hz, 1H), 7.49-7.34 (m, 7H), 6.58 (s, 1H),

2.95-2.91 (m, 1H), 1.64-1.58 (m, 1H), 1.44-1.25 (m, 5H), 1.19 (d, J = 6.5 Hz, 3H), 0.89 (t, J = 7.0 Hz, 3H).

^{13}C NMR (CDCl_3 , 125 MHz): 139.4, 138.8, 134.1, 134.1, 131.6, 131.4, 129.0, 128.9, 127.6, 127.6, 126.3, 126.1, 125.8, 125.6, 125.5, 125.4, 125.4, 125.4, 123.1, 123.1, 55.3, 51.6, 37.3, 28.1, 23.0, 20.6, 14.1.

HRMS (ESI $^+$) for $\text{C}_{27}\text{H}_{30}\text{N}$ [$\text{M} + \text{H}$] $^+$ calculated: 368.2378 found: 368.2374.



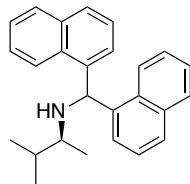
(*R*)-*N*-(di(naphthalen-1-yl)methyl)hexan-2-amine (**II-13-D**)

Following the general procedure A, a white solid product was obtained (28 mg, 76%).

^1H NMR (CDCl_3 , 500 MHz): 8.25 (d, J = 9.0 Hz, 1H), 8.09 (d, J = 8.5 Hz, 1H), 7.88-7.86 (m, 2H), 7.77-7.73 (m, 2H), 7.60 (d, J = 7.5 Hz, 1H), 7.48-7.34 (m, 7H), 6.58 (s, 1H), 2.95-2.91 (m, 1H), 1.64-1.60 (m, 1H), 1.41-1.26 (m, 5H), 1.19 (d, J = 6.5 Hz, 3H), 0.89 (t, J = 7.0 Hz, 3H).

^{13}C NMR (CDCl_3 , 125 MHz): 139.4, 138.8, 134.1, 134.1, 131.6, 131.4, 129.0, 128.9, 127.6, 127.6, 126.3, 126.1, 125.8, 125.6, 125.5, 125.4, 125.4, 125.4, 123.1, 123.1, 55.3, 51.6, 37.3, 28.1, 23.0, 20.6, 14.1.

HRMS (ESI +) for $\text{C}_{27}\text{H}_{30}\text{N}$ [$\text{M} + \text{H}$] $^+$ calculated: 368.2378 found: 368.2369.



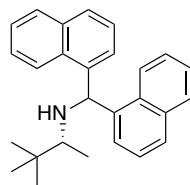
(S)-*N*-(di(naphthalen-1-yl)methyl)-3-methylbutan-2-amine (**II-14-D**)

Following the general procedure A, a white solid product was obtained (30 mg, 86%).

^1H NMR (CDCl_3 , 500 MHz): 8.22-8.20 (m, 1H), 8.10 (d, $J = 8.0$ Hz, 1H), 7.87-7.85 (m, 2H), 7.76-7.73 (m, 2H), 7.61 (d, $J = 7.0$ Hz, 1H), 7.49-7.35 (m, 7H), 6.55 (s, 1H), 2.83-2.81 (m, 1H), 1.92-1.88 (m, 1H), 1.08 (d, $J = 6.5$ Hz, 3H), 0.91 (d, $J = 6.5$ Hz, 3H), 0.89 (d, $J = 6.5$ Hz, 3H).

^{13}C NMR (CDCl_3 , 125 MHz): 139.6, 139.0, 134.0, 134.0, 131.5, 131.4, 128.9, 128.9, 127.6, 127.5, 126.2, 126.1, 125.9, 125.8, 125.5, 125.4, 125.3, 123.1, 56.6, 55.4, 32.5, 19.6, 16.9, 15.5.

HRMS (ESI $^+$) for $\text{C}_{26}\text{H}_{28}\text{N}$ [$\text{M} + \text{H}$] $^+$ calculated: 354.2222 found: 354.2234.



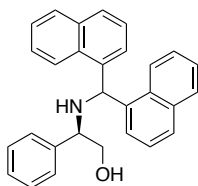
(R)-*N*-(di(naphthalen-1-yl)methyl)-3,3-dimethylbutan-2-amine (**II-15-D**)

Following the general procedure A, a white solid product was obtained (33 mg, 90%).

^1H NMR (CDCl_3 , 500 MHz): 8.37 (d, $J = 8.0$ Hz, 1H), 8.04 (d, $J = 8.5$ Hz, 1H), 7.88-7.85 (m, 2H), 7.78-7.76 (m, 2H), 7.72 (d, $J = 7.5$ Hz, 1H), 7.53-7.30 (m, 7H), 6.54 (s, 1H), 2.68 (q, $J = 6.5$ Hz, 1H), 1.12 (d, $J = 6.5$ Hz, 1H), 0.91 (s, 9H).

^{13}C NMR (CDCl_3 , 125 MHz): 140.4, 138.5, 134.0, 134.0, 131.8, 131.3, 128.9, 128.9, 127.6, 127.4, 126.4, 126.2, 126.0, 125.5, 125.3, 125.3, 125.3, 123.3, 123.2, 60.1, 55.3, 34.6, 26.7, 14.4.

HRMS (ESI^+) for $\text{C}_{27}\text{H}_{30}\text{N}$ [$\text{M} + \text{H}$] $^+$ calculated: 368.2378 found: 368.2378.



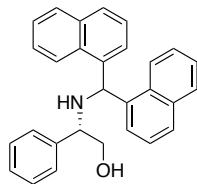
(*R*)-2-((Di(naphthalen-1-yl)methyl)amino)-2-phenylethan-1-ol (**II-16-D**)

Following the general procedure A, a white solid product was obtained (26.9 mg, 66%).

^1H NMR (CDCl_3 , 500 MHz): 8.12 (d, $J = 7.0$ Hz, 1H), 7.88-7.84 (m, 3H), 7.71 (d, $J = 7.5$ Hz, 1H), 7.66-7.61 (m, 2H), 7.54 (d, $J = 8.5$ Hz, 1H), 7.48-7.45 (m, 1H), 7.42-7.37 (m, 4H), 7.34-7.31 (m, 1H), 7.26-7.20 (m, 5H), 6.34 (s, 1H), 4.00 (t, $J = 7$ Hz, 1H), 3.78 (d, $J = 7$ Hz, 2H), 2.45 (s, 1H).

^{13}C NMR (CDCl_3 , 125 MHz): 140.1, 138.7, 136.9, 134.1, 133.9, 131.7, 130.7, 129.0, 128.8, 128.7, 128.2, 128.2, 128.1, 127.9, 126.4, 126.2, 126.1, 125.6, 125.5, 125.4, 125.2, 123.1, 122.6, 66.2, 62.3, 54.4.

HRMS (ESI^+) for $\text{C}_{29}\text{H}_{26}\text{NO}$ [$\text{M} + \text{H}$] $^+$ calculated: 404.2014. found: 404.2003.



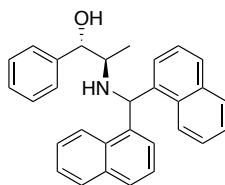
(S)-2-((Di(naphthalen-1-yl)methyl)amino)-2-phenylethan-1-ol (II-17-D)

Following the general procedure A, a white solid product was obtained (22.7 mg, 56%).

^1H NMR (CDCl_3 , 500 MHz): 8.11 (d, $J = 7.0$ Hz, 1H), 7.89-7.85 (m, 3H), 7.71 (d, $J = 8.0$ Hz, 1H), 7.67-7.63(m, 2H), 7.56 (d, $J = 8.5$ Hz, 1H), 7.49-7.46 (m, 1H), 7.43-7.38 (m, 4H), 7.35-7.31 (m, 1H), 7.27-7.21 (m, 5H), 6.34 (s, 1H), 4.01 (t, $J = 7$ Hz, 1H), 3.79 (d, $J = 7$ Hz, 2H), 2.45 (s, 1H).

^{13}C NMR (CDCl_3 , 125 MHz): 140.2, 138.8, 137.0, 134.1, 133.9, 131.8, 130.8, 129.0, 128.8, 128.7, 128.1, 128.0, 127.8, 126.4, 126.1, 126.1, 125.5, 125.5, 125.4, 125.2, 123.1, 122.7, 66.3, 62.2, 54.4.

HRMS (ESI $^+$) for $\text{C}_{29}\text{H}_{26}\text{NO}$ [$\text{M} + \text{H}$] $^+$ calculated: 404.2014 found: 404.2021.



(1S,2R)-2-((Di(naphthalen-1-yl)methyl)amino)-1-phenylpropan-1-ol (II-18-D)

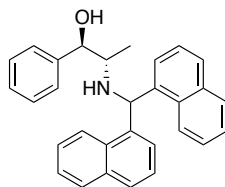
Following the general procedure A, a white solid product was obtained (24.5 mg, 58%).

^1H NMR (CDCl_3 , 500 MHz): 8.33 (d, $J = 8.0$ Hz, 1H), 8.08 (d, $J = 8.5$ Hz, 1H), 7.93 (d, $J = 9.0$ Hz, 2H), 7.84-7.79 (m, 2H), 7.59-7.44 (m, 6H), 7.39-7.38 (m, 2H), 7.30-7.21(m,

5H), 6.76 (s, 1H), 5.04 (d, J = 3.5 Hz, 1H), 3.28 (dt, J = 6.5, 3.5 Hz, 1H), 0.97(d, J = 6.5 Hz, 3H).

^{13}C NMR (CDCl_3 , 125 MHz): 141.0, 134.2, 134.1, 131.5, 131.4, 129.1, 129.0, 128.1, 128.1, 128.0, 127.0, 126.7, 126.6, 125.9, 125.7, 125.7, 125.4, 125.4, 125.3, 124.8, 123.0, 122.7, 73.4, 57.4, 55.4, 13.9.

HRMS (ESI^+) for $\text{C}_{30}\text{H}_{28}\text{NO}$ [$\text{M} + \text{H}$] $^+$ calculated: 418.2171. found:418.2177.



(1*R*,2*S*)-2-((Di(naphthalen-1-yl)methyl)amino)-1-phenylpropan-1-ol (**II-19-D**)

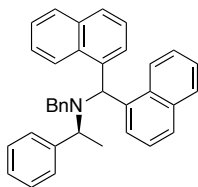
Following the general procedure A, a white solid product was obtained (21.9 mg, 52%).

^1H NMR (CDCl_3 , 500 MHz): 8.32 (d, J = 9.0 Hz, 1H), 8.07 (d, J = 8.5 Hz, 1H), 7.92 (d, J = 8.0 Hz, 2H), 7.83-7.78 (m, 2H), 7.58-7.43 (m, 6H), 7.38-7.37 (m, 2H), 7.29-7.21(m, 5H), 6.75 (s, 1H), 5.03 (d, J = 3.0 Hz, 1H), 3.26 (dt, J = 7.0, 3.0 Hz, 1H), 0.96(d, J = 7.0 Hz, 3H).

^{13}C NMR (CDCl_3 , 125 MHz): 141.0, 134.1, 134.1, 131.5, 131.3, 129.1, 129.0, 128.8, 128.1, 128.1, 128.0, 127.0, 126.7, 126.5, 125.9, 125.7, 125.7, 125.4, 125.3, 124.8, 123.0, 122.7, 73.4, 57.3, 55.4, 13.9.

HRMS (ESI^+) for $\text{C}_{30}\text{H}_{28}\text{NO}$ [$\text{M} + \text{H}$] $^+$ calculated: 418.2171. found: 418.2175.

General Procedure B: To a 5 mL round bottom flask was added chiral Bn protected amine (0.12 mmol, 1.2 equiv) and 1,1'-(bromomethylene)dinaphthalene (**II-1**) (0.1 mmol, 35 mg) in a 1:1 mixture of acetonitrile and DCM (2 mL). K₂CO₃ (0.2 mmol, 2 equiv, 28 mg) was added to the flask and the mixture was stirred under N₂ for 4 h. The reaction mixture was concentrated under vacuo and the mixture was directly loaded onto silica gel for purification.



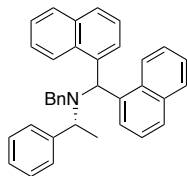
(*S*)-*N*-benzyl-*N*-(di(naphthalen-1-yl)methyl)-1-phenylethan-1-amine (**II-20-D**)

Following the general procedure B, a white solid product was obtained (27 mg, 57%).

¹H NMR (CDCl₃, 500 MHz): 8.00 (d, *J* = 7.0 Hz, 1H), 7.82-7.74 (m, 3H), 7.62 (d, *J* = 9.0 Hz, 1H), 7.57 (d, *J* = 8.5 Hz, 2H), 7.48-7.40 (m, 2H), 7.38-7.25 (m, 6H), 7.21-7.17 (m, 2H), 7.03-6.96 (m, 4H), 6.73-6.70 (m, 3H), 4.31 (q, *J* = 7.0 Hz, 1H), 4.21 (d, *J* = 16.0 Hz, 1H), 3.77 (d, *J* = 16.0 Hz, 1H), 1.48 (d, *J* = 7.0 Hz, 3H).

¹³C NMR (CDCl₃, 125 MHz): 143.5, 142.3, 138.6, 137.7, 134.1, 133.8, 132.3, 132.0, 128.8, 128.8, 128.7, 128.6, 128.1, 127.6, 127.5, 127.2, 127.2, 126.5, 126.0, 125.9, 125.5, 125.2, 125.1, 124.9, 123.5, 123.5, 60.3, 59.5, 50.4, 19.5.

HRMS (ESI⁺) for C₃₆H₃₂N [M + H]⁺ calculated: 478.2529 found: 478.2534.



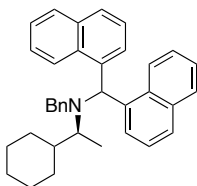
(R)-*N*-benzyl-*N*-(di(naphthalen-1-yl)methyl)-1-phenylethan-1-amine (**II-21-D**)

Following the general procedure B, a white solid product was obtained (25 mg, 52%).

^1H NMR (CDCl_3 , 500 MHz): 7.97 (d, $J = 7.5$ Hz, 1H), 7.81-7.76 (m, 3H), 7.60 (d, $J = 8.5$ Hz, 1H), 7.56-7.53 (m, 2H), 7.46-7.39 (m, 2H), 7.36-7.22 (m, 6H), 7.19-7.14 (m, 2H), 7.01-6.94 (m, 4H), 6.70-6.67 (m, 3H), 4.29 (q, $J = 7.5$ Hz, 1H), 4.18 (d, $J = 15.0$ Hz, 1H), 3.74 (d, $J = 15.0$ Hz, 1H), 1.46 (d, $J = 7.5$ Hz, 3H).

^{13}C NMR (CDCl_3 , 125 MHz): 143.5, 142.3, 138.6, 137.7, 134.0, 133.7, 132.3, 132.0, 128.8, 128.8, 128.7, 128.6, 128.1, 127.6, 127.5, 127.2, 127.2, 126.5, 126.0, 125.9, 125.5, 125.2, 125.1, 124.9, 123.5, 123.5, 60.3, 59.5, 50.4, 19.5.

HRMS (ESI $^+$) for $\text{C}_{36}\text{H}_{32}\text{N}$ [$\text{M} + \text{H}$] $^+$ calculated: 478.2529 found: 478.2530.



(S)-*N*-benzyl-1-cyclohexyl-*N*-(di(naphthalen-1-yl)methyl)ethan-1-amine (**II-22-D**)

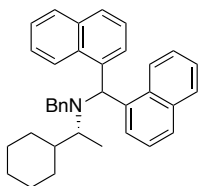
Following the general procedure B, a white solid product was obtained (30 mg, 61%).

^1H NMR (CDCl_3 , 500 MHz): 8.47 (d, $J = 8.5$ Hz, 1H), 8.08 (d, $J = 7.5$ Hz, 1H), 7.94 (d, $J = 9$ Hz, 1H), 7.81 (d, $J = 8.0$ Hz, 2H), 7.73 (d, $J = 8$ Hz, 1H), 7.58-7.46 (m, 4H), 7.37-

7.32 (m, 2H), 7.29-7.26 (m, 1H), 7.01-6.95 (m, 4H), 6.80-6.77 (m, 3H), 4.03 (d, J = 16.0 Hz, 1H), 3.78 (d, J = 16.0 Hz, 1H), 2.90-2.88 (m, 1H), 2.06-2.04 (m, 1H), 1.70-1.52 (m, 4H), 1.36-1.34 (m, 1H), 1.21 (d, J = 6.5 Hz, 3H), 1.03-0.88 (m, 4H), 0.79-0.76 (m, 1H).

¹³C NMR (CDCl₃, 125 MHz): 143.1, 139.1, 137.8, 134.0, 133.8, 132.4, 131.9, 129.0, 129.0, 128.8, 127.5, 127.5, 127.4, 127.3, 126.8, 126.0, 125.9, 125.4, 125.1, 125.1, 125.0, 124.9, 123.4, 123.4, 61.4, 59.8, 51.8, 42.6, 32.0, 29.4, 26.7, 26.6, 26.5, 12.7.

HRMS (ESI⁺) for C₃₆H₃₈N [M + H]⁺ calculated: 484.2999 found: 484.3006.



(*R*)-*N*-benzyl-1-cyclohexyl-*N*-(di(naphthalen-1-yl)methyl)ethan-1-amine (**II-23-D**)

Following the general procedure B, a white solid product was obtained (28 mg, 58%).

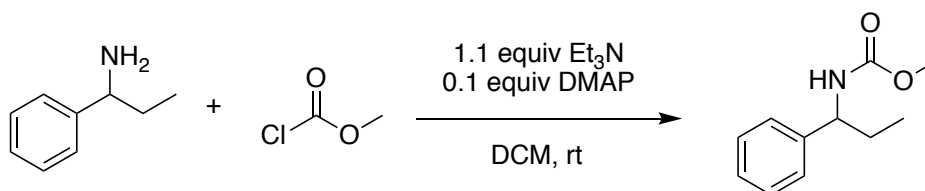
¹H NMR (CDCl₃, 500 MHz): 8.47 (d, J = 9.0 Hz, 1H), 8.09 (d, J = 6.5 Hz, 1H), 7.95 (d, J = 8.5 Hz, 1H), 7.81 (d, J = 7.5 Hz, 2H), 7.74 (d, J = 8.5 Hz, 1H), 7.58-7.46 (m, 4H), 7.38-7.33 (m, 2H), 7.30-7.27 (m, 1H), 7.01-6.95 (m, 4H), 6.80-6.77 (m, 3H), 4.04 (d, J = 16.0 Hz, 1H), 3.78 (d, J = 16.0 Hz, 1H), 2.90-2.88 (m, 1H), 2.07-2.04 (m, 1H), 1.71-1.50 (m, 4H), 1.36-1.35 (m, 1H), 1.21 (d, J = 6.5 Hz, 3H), 1.04-0.86 (m, 4H), 0.79-0.76 (m, 1H).

¹³C NMR (CDCl₃, 125 MHz): 143.1, 139.1, 137.9, 134.0, 133.8, 132.5, 131.9, 129.0, 129.0, 128.8, 127.5, 127.5, 127.4, 127.3, 126.8, 126.0, 125.9, 125.5, 125.1, 125.1, 125.0, 124.9, 123.4, 123.4, 61.4, 59.8, 51.8, 42.6, 32.0, 29.4, 26.7, 26.6, 26.5, 12.8.

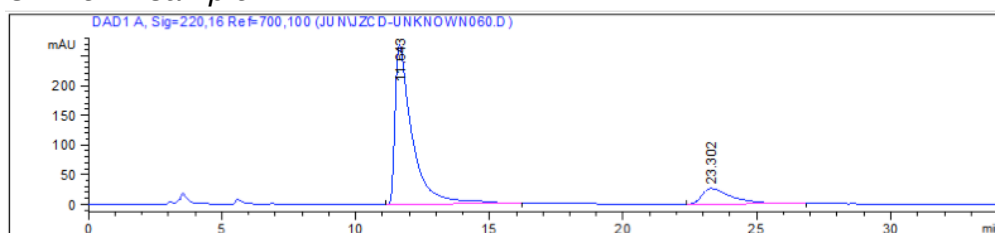
HRMS (ESI⁺) for C₃₆H₃₈N [M + H]⁺ calculated: 484.2999 found: 484.3003.

II.9.4 HPLC data for chiral amines

All chiral amines were derivatized as their corresponding methyl carbamate for HPLC analysis as shown below for ethyl benzyl amine. HPLC analysis was performed with an analytical DAICEL CHIRALCEL® OD-H column, operating with a flow rate of 0.7 mL/min, with 99:1 hexanes: isopropyl alcohol as eluent. The 4*S*-enantiomer elutes at 11 min, while the 4*R*-enantiomer appears at 23 min.



Unknown sample 1:

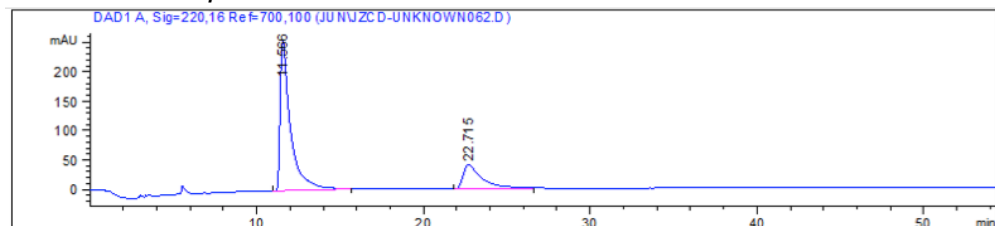


Signal 1: DAD1 A, Sig=220,16 Ref=700,100

Peak #	RetTime [min]	Type	Width [min]	Area [mAU*s]	Height [mAU]	Area %
1	11.643	BB	0.6261	1.18589e4	268.07932	85.5590
2	23.302	BB	1.0944	2001.59460	25.99415	14.4410

Totals : 1.38605e4 294.07346

Unknown sample 2



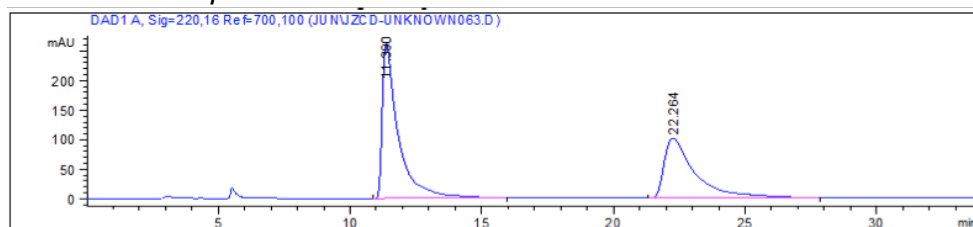
Signal 1: DAD1 A, Sig=220,16 Ref=700,100

Peak #	RetTime [min]	Type	Width [min]	Area [mAU*s]	Height [mAU]	Area %
1	11.566	BB	0.6054	1.09350e4	254.43579	77.7263
2	22.715	BB	1.0926	3133.58008	40.77359	22.2737

Totals : 1.40685e4 295.20938

Figure II-17. HPLC data for chiral amines.

Figure II-17 (cont'd)
Unknown sample 3

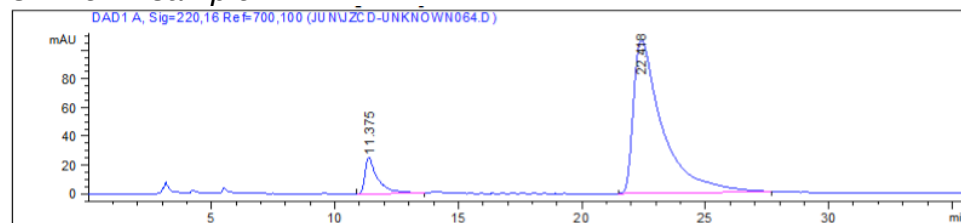


Signal 1: DAD1 A, Sig=220,16 Ref=700,100

Peak #	RetTime [min]	Type	Width [min]	Area [mAU*s]	Height [mAU]	Area %
1	11.390	BB	0.5895	1.10237e4	262.71075	57.2081
2	22.264	BB	1.1458	8245.74707	101.71544	42.7919

Totals : 1.92694e4 364.42619

Unknown sample 4

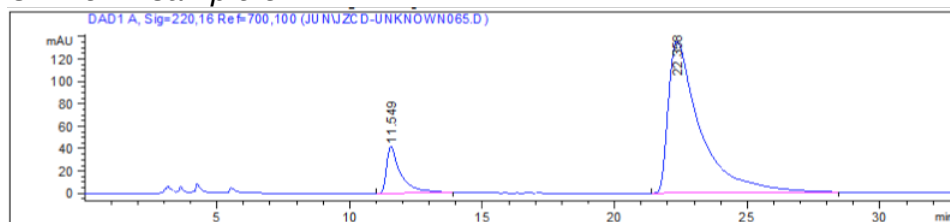


Signal 1: DAD1 A, Sig=220,16 Ref=700,100

Peak #	RetTime [min]	Type	Width [min]	Area [mAU*s]	Height [mAU]	Area %
1	11.375	BB	0.5007	905.53143	25.35308	9.3949
2	22.418	BB	1.1742	8732.98828	106.55245	90.6051

Totals : 9638.51971 131.90554

Unknown sample 5



Signal 1: DAD1 A, Sig=220,16 Ref=700,100

Peak #	RetTime [min]	Type	Width [min]	Area [mAU*s]	Height [mAU]	Area %
1	11.549	MM	0.6176	1560.76135	42.11751	12.1399
2	22.358	BB	1.1893	1.12956e4	135.40125	87.8601

Totals : 1.28564e4 177.51875

II.9.5 Crystal structure of II-3-D

Single colourless needle-shaped crystals of **(II-3-D)** were used as received. A suitable crystal (0.43×0.19×0.12) was selected and mounted on a nylon loop with paratone oil on a Bruker APEX-II CCD diffractometer. The crystal was kept at $T = 173(2)$ K during data collection. Using Olex2, the structure was solved with the ShelXS structure solution program, using the Direct Methods solution method. The model was refined with version 2014/6 of ShelXL using Least Squares minimisation. Crystal structure of compound **II-3-D** is shown in **Figure II-18**.

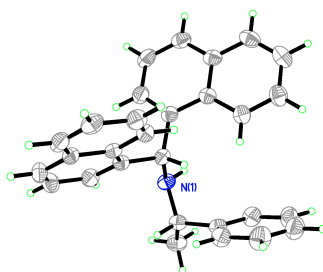


Figure II-18. Crystal structure of **II-3-D**.

Compound	II-3-D
Formula	C ₂₉ H ₂₅ N
$D_{calc.}/g\text{ cm}^{-3}$	1.207
μ/mm^{-1}	0.069
Formula Weight	387.50
Colour	colourless
Shape	needle
Max Size/mm	0.43
Mid Size/mm	0.19
Min Size/mm	0.12
T/K	173(2)
Crystal System	orthorhombic
Flack Parameter	-1.8(10)
Hooft Parameter	-2(2)
Space Group	P2 ₁ 2 ₁ 2 ₁
$a/\text{\AA}$	9.9737(8)
$b/\text{\AA}$	14.2237(11)
$c/\text{\AA}$	15.0374(12)
$\alpha/^\circ$	90
$\beta/^\circ$	90
$\gamma/^\circ$	90
$V/\text{\AA}^3$	2133.2(3)
Z	4
Z'	1
$\Theta_{min}/^\circ$	1.971
$\Theta_{max}/^\circ$	25.379
Measured Refl.	17845
Independent Refl.	3907
Reflections Used	3379
R_{int}	0.0414
Parameters	276
Restraints	0
Largest Peak	0.115
Deepest Hole	-0.143
GooF	1.048
wR_2 (all data)	0.0926
wR_2	0.0859
R_1 (all data)	0.0470
R_1	0.0378

Table II-8. Crystal data and structure refinement for **II-3-D**.

Atom	x	y	z	U_{eq}
N1	7287(2)	5937.4(16)	7034.2(14)	33.7(5)
C1	7632(2)	5574.1(16)	6142.9(15)	30.1(5)
C2	7747(2)	6374.0(16)	5473.6(16)	30.1(5)
C3	7141(2)	7221.3(17)	5620.6(18)	36.5(6)
C4	7215(3)	7958.6(18)	4997.2(19)	42.0(6)
C5	7904(3)	7842.8(17)	4225.5(18)	39.4(6)
C6	8548(2)	6982.1(16)	4038.6(16)	31.5(5)
C7	9243(2)	6841.2(19)	3224.6(17)	37.1(6)
C8	9863(2)	6012.5(19)	3038.9(17)	38.3(6)
C9	9810(3)	5275.0(18)	3659.3(17)	37.2(6)
C10	9142(2)	5379.3(17)	4443.0(17)	32.2(6)
C11	8479(2)	6232.0(16)	4663.7(15)	28.2(5)
C12	6574(2)	4853.4(16)	5878.5(15)	31.4(5)
C13	5356(2)	5149.9(19)	5569.5(18)	38.0(6)
C14	4326(3)	4512(2)	5360.9(18)	43.5(7)
C15	4526(3)	3570.8(19)	5461.4(17)	40.8(7)
C16	5767(3)	3222.5(18)	5774.6(16)	35.2(6)
C17	5986(3)	2241.1(18)	5881.9(18)	43.1(7)
C18	7160(3)	1914.1(18)	6219(2)	46.2(7)
C19	8171(3)	2547.2(18)	6464.9(19)	42.6(7)
C20	8012(3)	3491.2(17)	6353.2(17)	36.5(6)
C21	6805(2)	3868.2(16)	5998.4(15)	30.7(5)
C22	7934(3)	6725.5(19)	8399.1(18)	43.2(7)
C23	8447(2)	6289.9(17)	7540.2(16)	33.3(6)
C24	9510(2)	5536.5(18)	7682.2(16)	32.4(6)
C25	10683(3)	5543(2)	7190.0(19)	40.8(6)
C26	11621(3)	4829(2)	7273(2)	51.9(8)
C27	11403(3)	4096(2)	7850(2)	51.7(7)
C28	10240(3)	4077(2)	8343.0(19)	49.0(7)
C29	9305(3)	4788.5(19)	8258.9(18)	40.9(6)

Table II-9. Fractional atomic coordinates ($\times 10^4$) and equivalent isotropic displacement parameters ($\text{\AA}^2 \times 10^3$) for **II-3-D**. U_{eq} is defined as 1/3 of the trace of the orthogonalised U_{ij} .

II.9.6 ECCD spectra of II-1 derivatized chiral amines

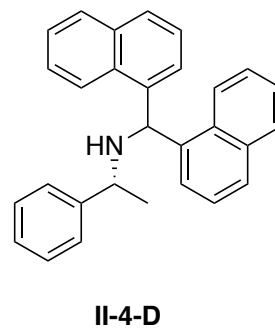
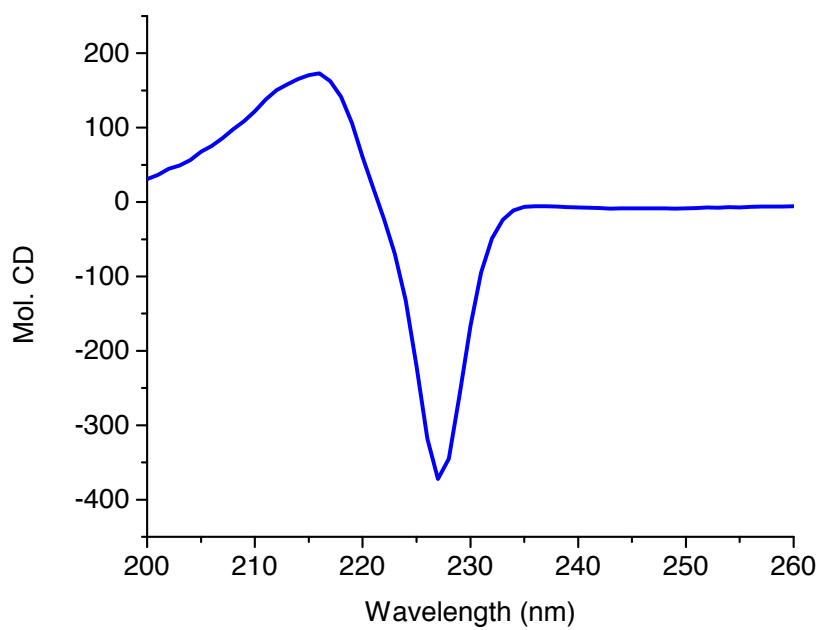
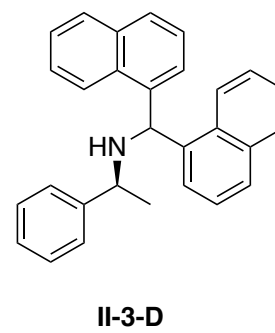
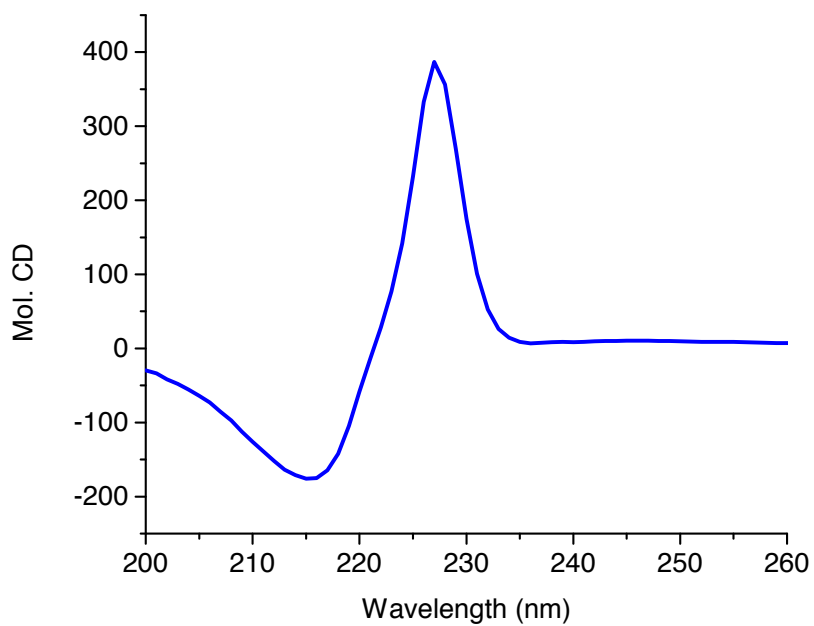
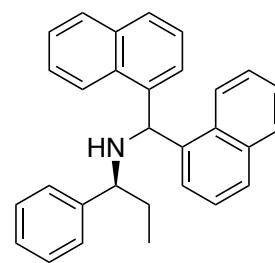
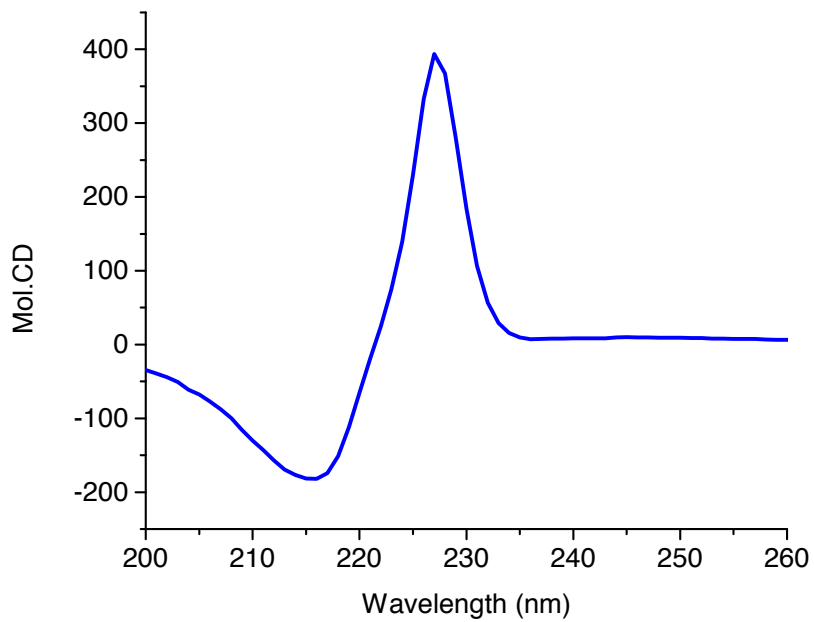
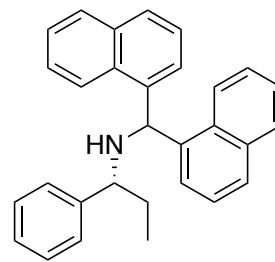
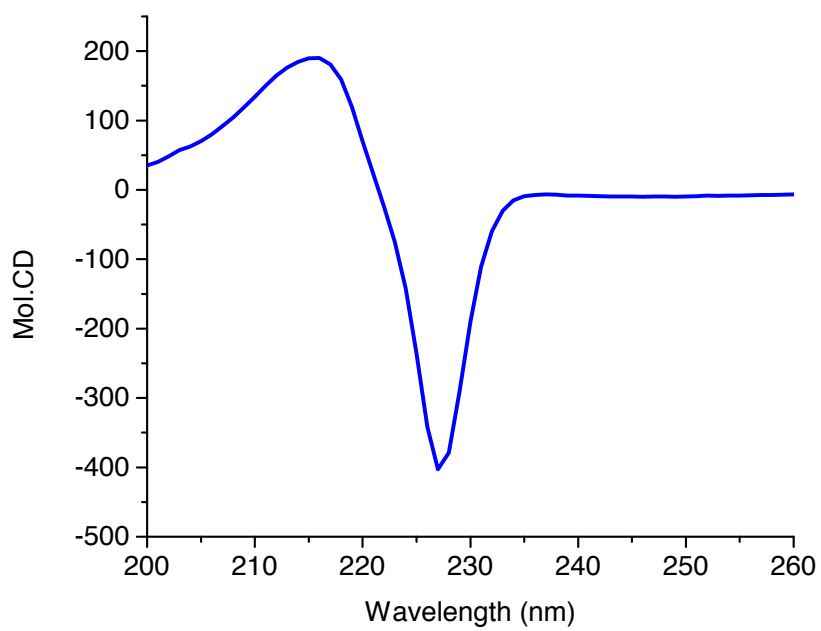


Figure II-19. ECCD spectra of II-1 derivatized chiral amines.

Figure II-19 (cont'd)



II-5-D



II-6-D

Figure II-19 (cont'd)

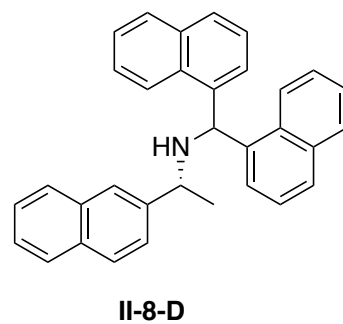
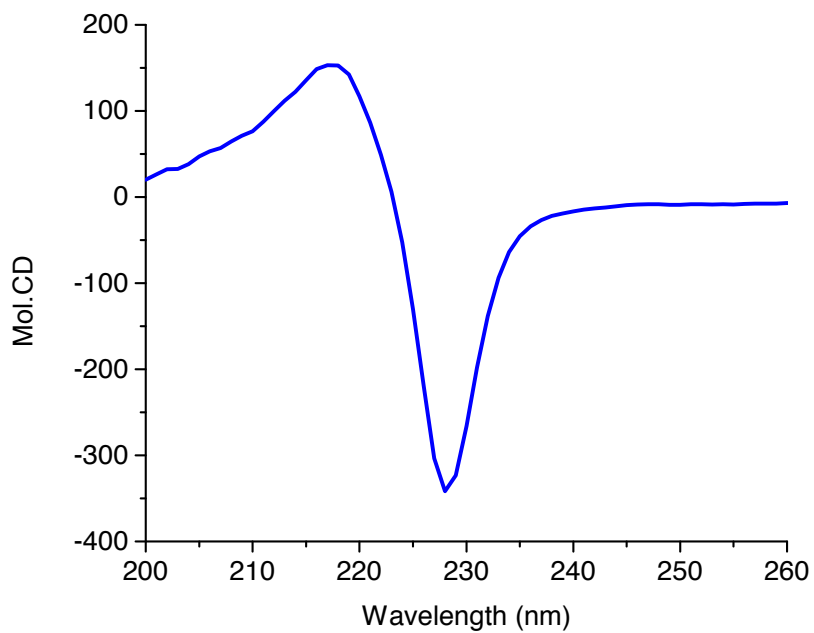
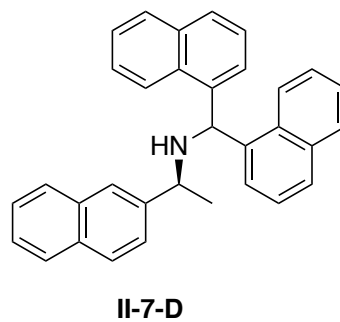
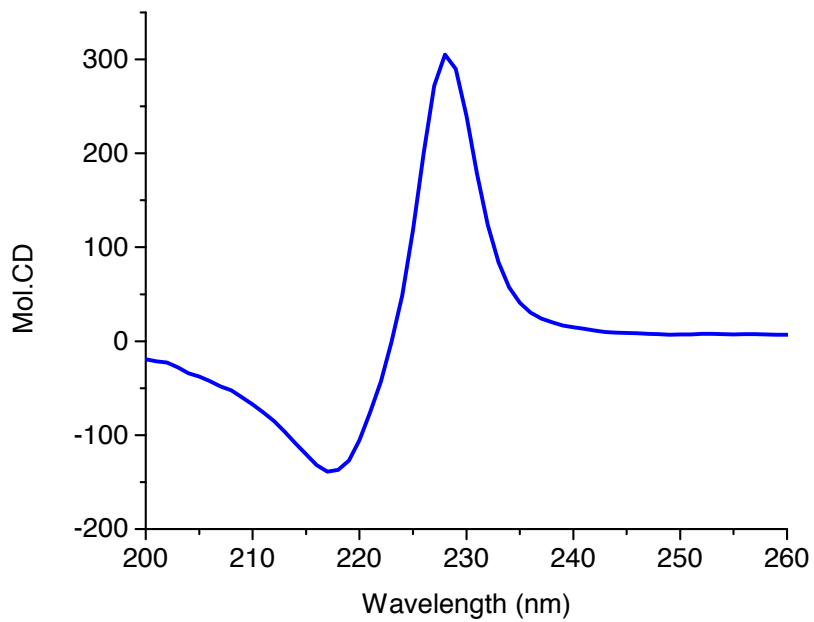
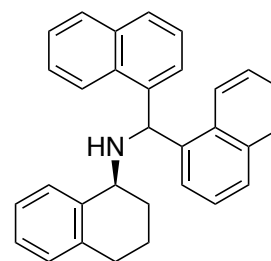
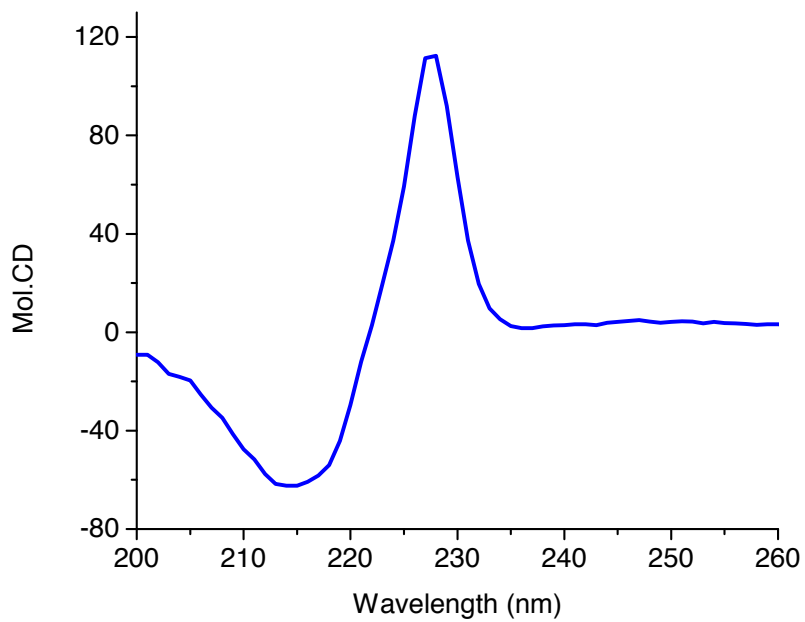
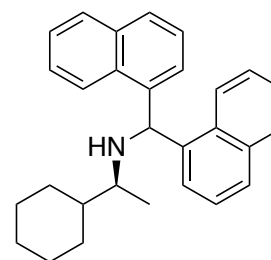
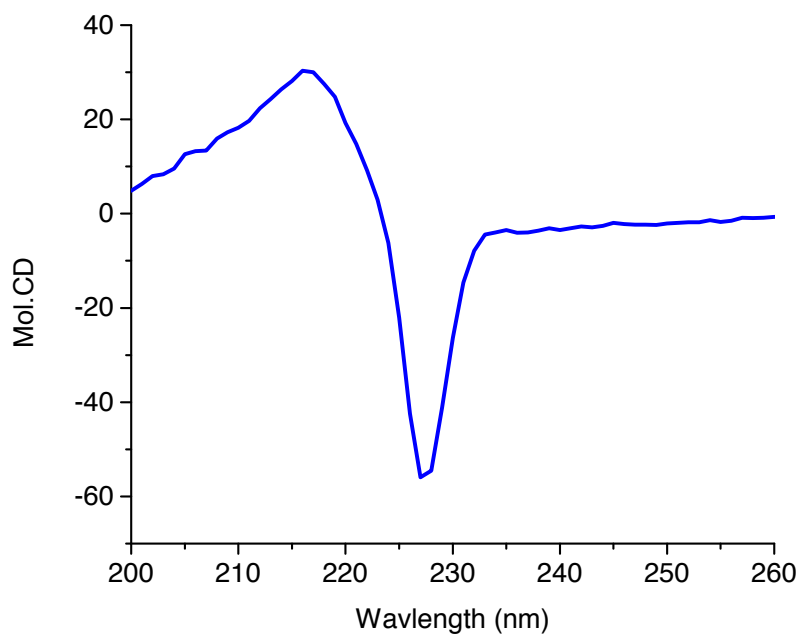


Figure II-19 (cont'd)

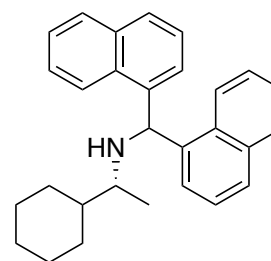
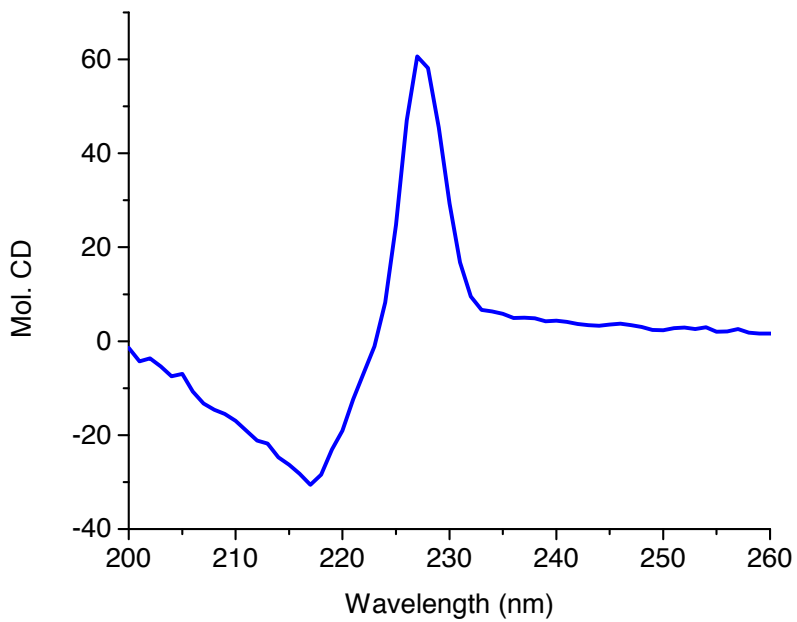


II-9-D

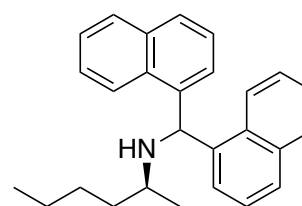
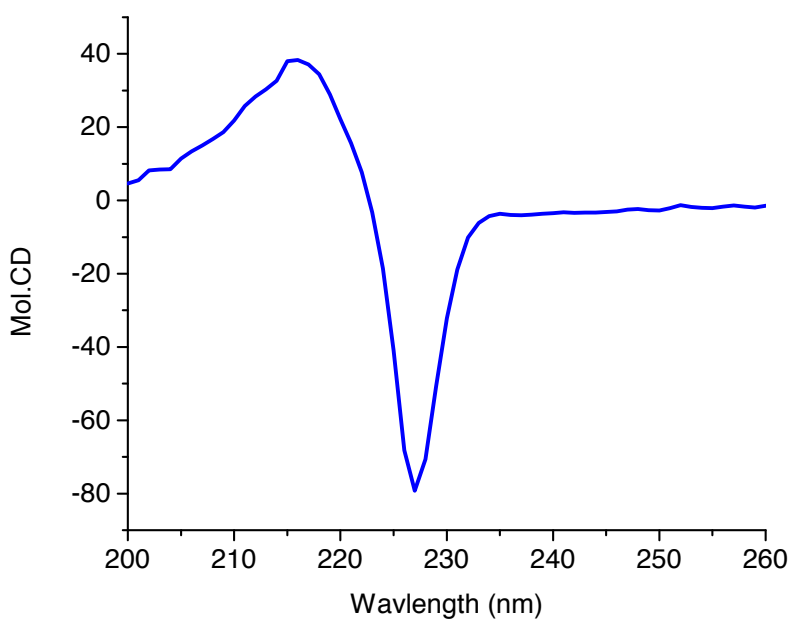


II-10-D

Figure II-19 (cont'd)

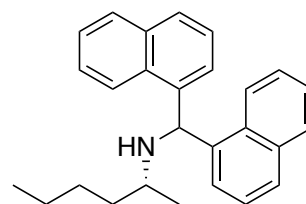
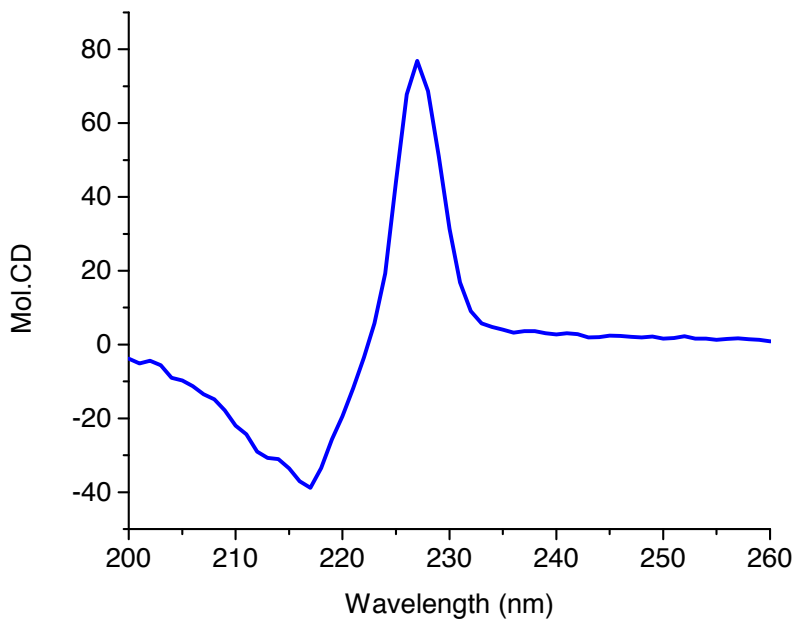


II-11-D

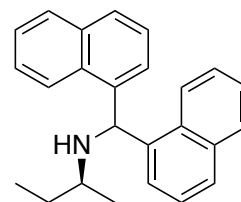
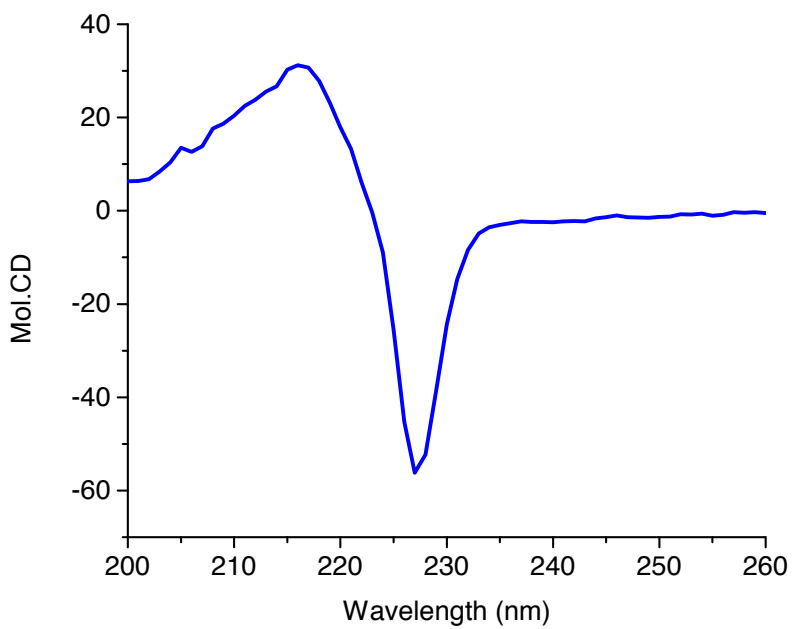


II-12-D

Figure II-19 (cont'd)



II-13-D



II-14-D

Figure II-19 (cont'd)

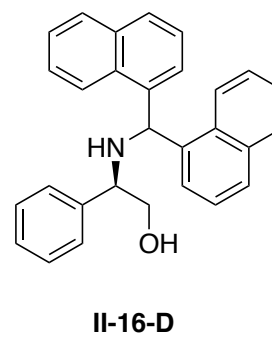
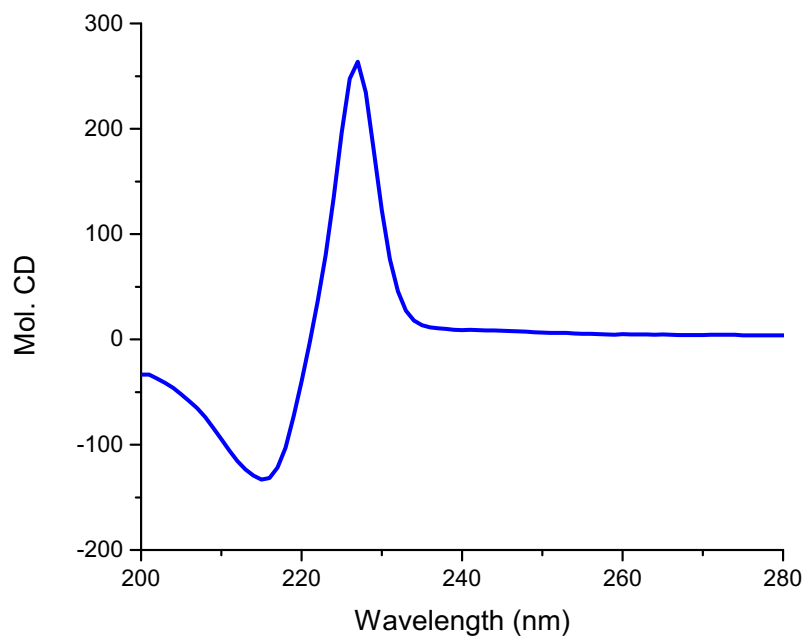
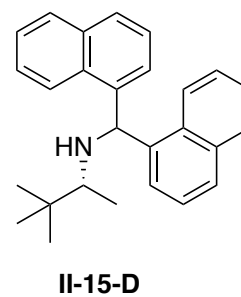
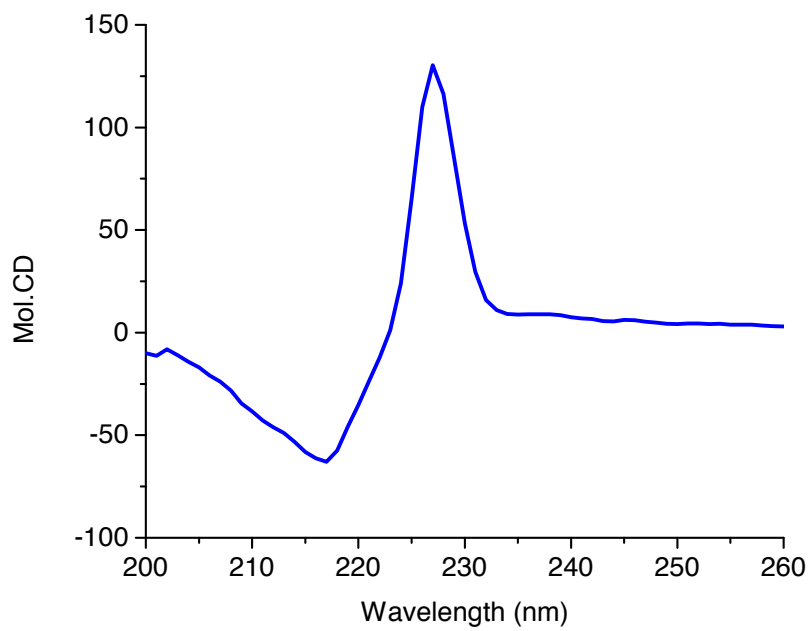
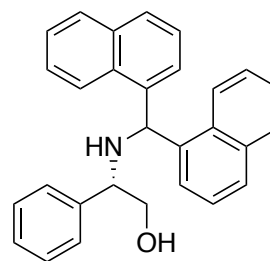
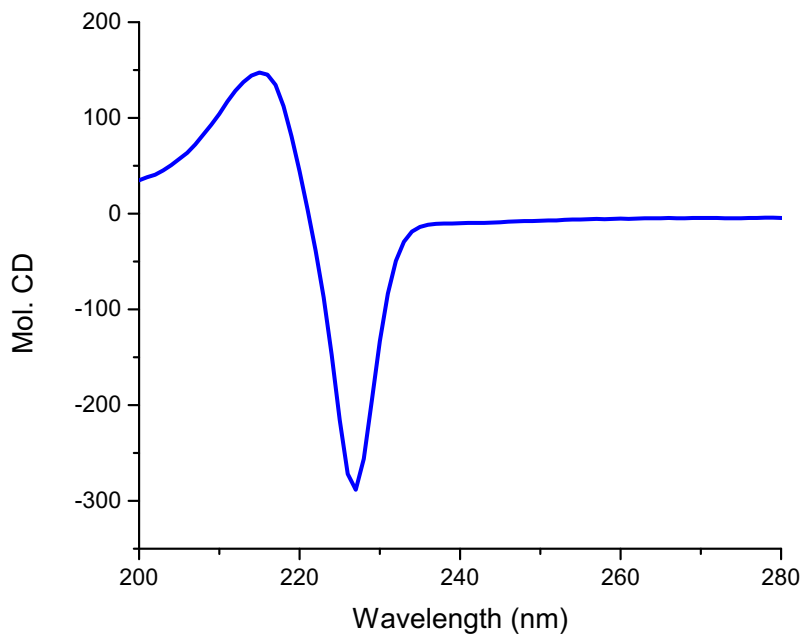
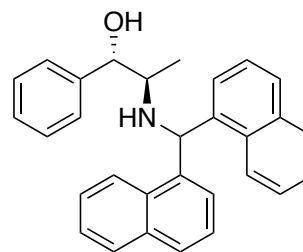
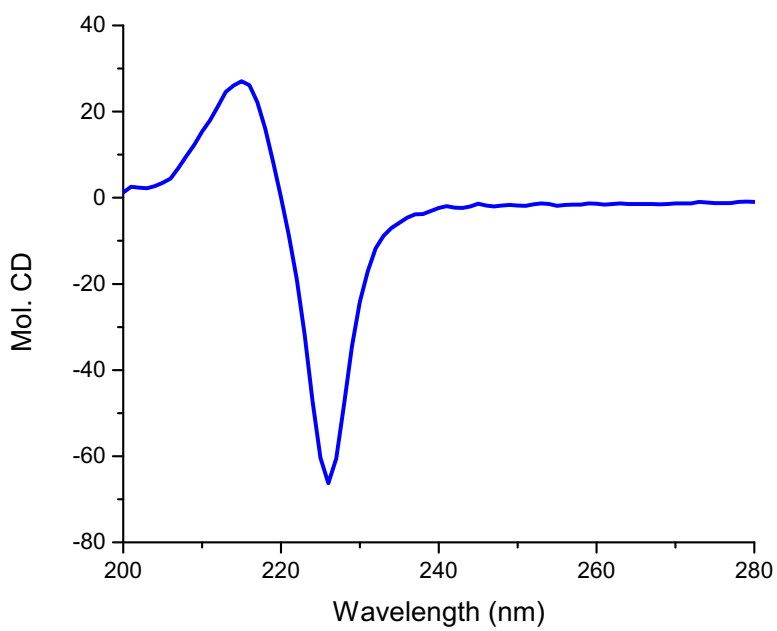


Figure II-19 (cont'd)

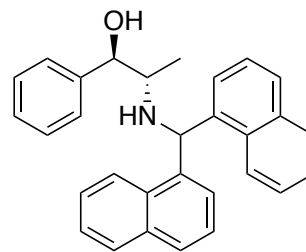
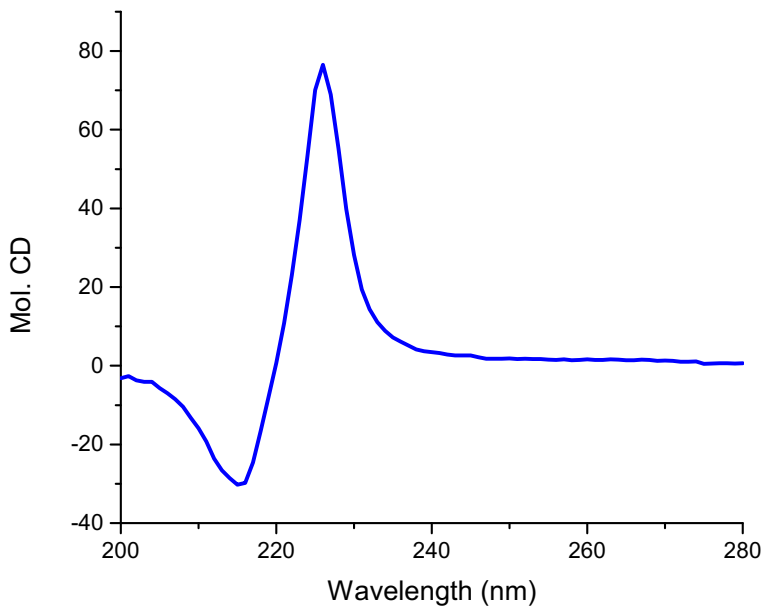


II-17-D

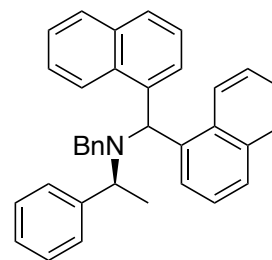
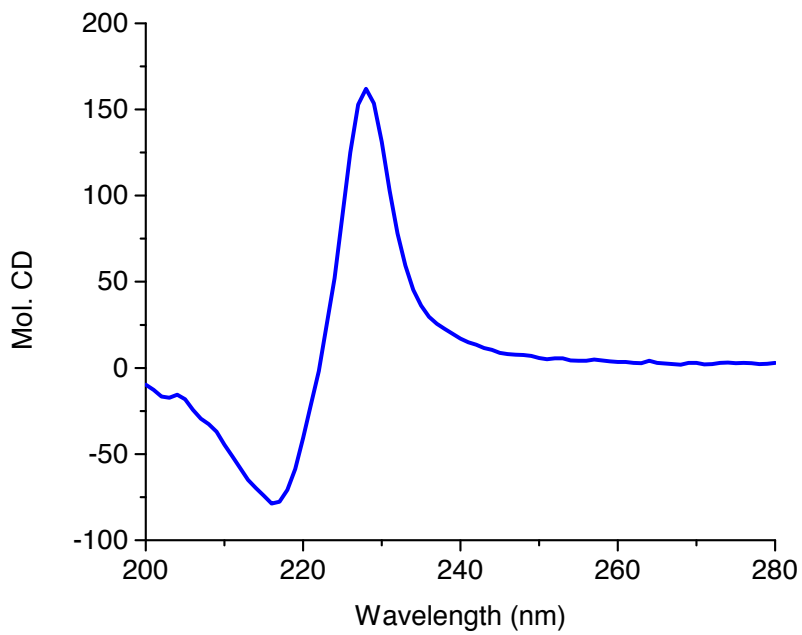


II-18-D

Figure II-19 (cont'd)



II-19-D



II-20-D

Figure II-19 (cont'd)

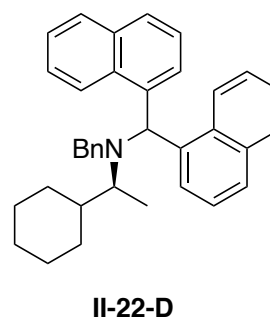
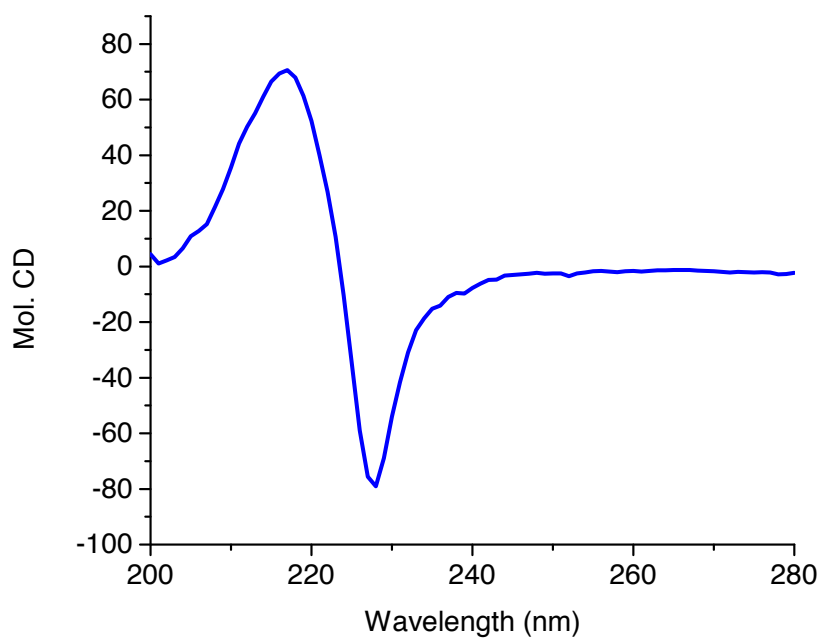
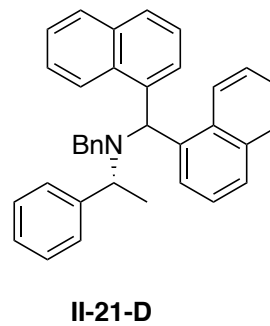
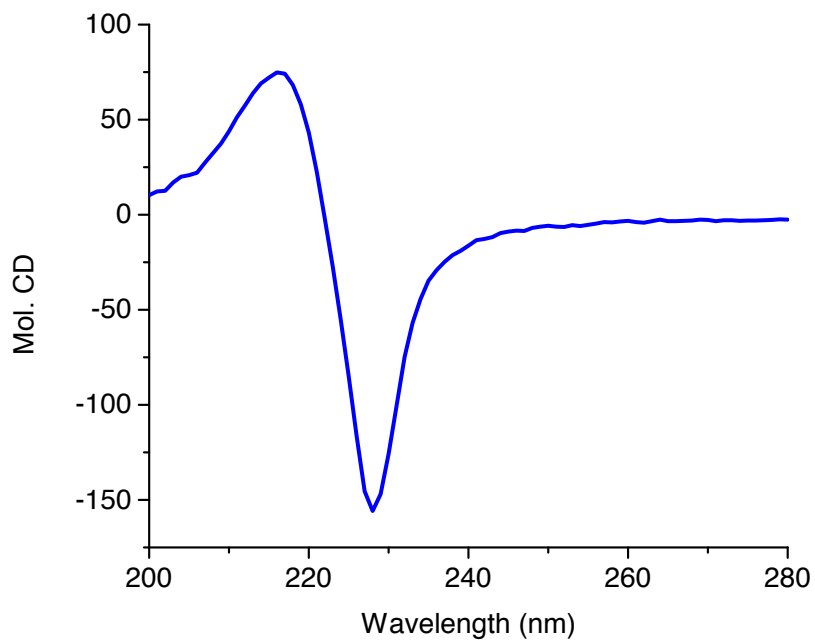
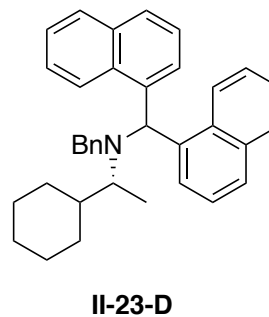
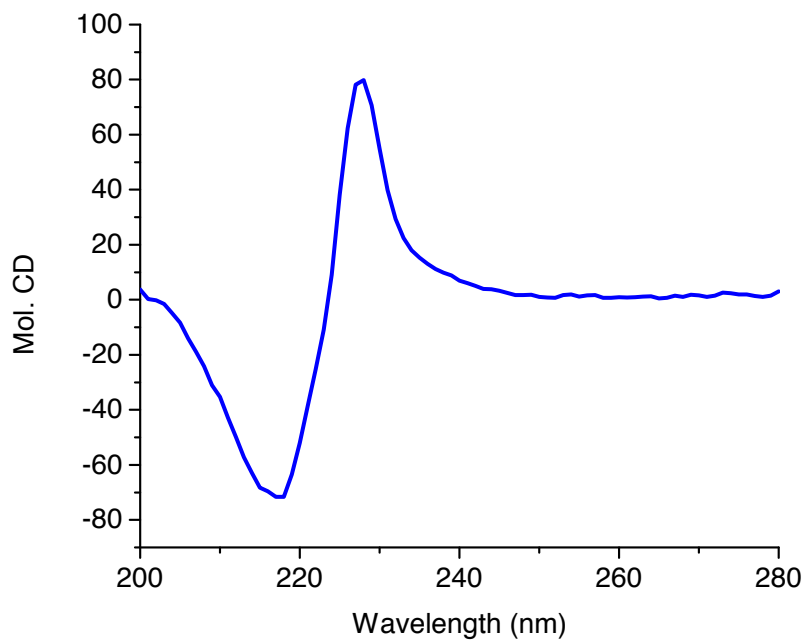


Figure II-19 (cont'd)



REFERENCES

REFERENCES

1. Lu, H.; Kobayashi, N., Optically active porphyrin and phthalocyanine systems. *Chem Rev* **2016**, *116* (10), 6184-6261.
2. Bentley, K. W.; Zhang, P.; Wolf, C., Miniature high-throughput chemosensing of yield, *ee*, and absolute configuration from crude reaction mixtures. *Sci Adv* **2016**, *2* (2).
3. Mei, X.; Wolf, C., Enantioselective sensing of chiral carboxylic acids. *J Am Chem Soc* **2004**, *126* (45), 14736-14737.
4. Zahn, S.; Canary, J. W., Electron-induced inversion of helical chirality in copper complexes of N, N-dialkylmethionines. *Science* **2000**, *288* (5470), 1404-1407.
5. Yashima, E.; Nimura, T.; Matsushima, T.; Okamoto, Y., Poly ((4-dihydroxyborophenyl) acetylene) as a novel probe for chirality and structural assignments of various kinds of molecules including carbohydrates and steroids by circular dichroism. *J Am Chem Soc* **1996**, *118* (40), 9800-9801.
6. Kuwahara, S.; Nakamura, M.; Yamaguchi, A.; Ikeda, M.; Habata, Y., Combination of a new chiroptical probe and theoretical calculations for chirality detection of primary amines. *Org Lett* **2013**, *15* (22), 5738-5741.
7. Zhang, P.; Wolf, C., Sensing of the concentration and enantiomeric excess of chiral compounds with tropos ligand derived metal complexes. *Chem Commun* **2013**, *49* (62), 7010-7012.
8. Seo, M. S.; Lee, A.; Kim, H., 2,2'-Dihydroxybenzil: A Stereodynamic Probe for Primary Amines Controlled by Steric Strain. *Org Lett* **2014**, *16* (11), 2950-2953.
9. You, L.; Zha, D.; Anslyn, E. V., Recent Advances in Supramolecular Analytical Chemistry Using Optical Sensing. *Chem Rev* **2015**, *115* (15), 7840-7892.
10. AkritopoulouZanze, I.; Nakanishi, K.; Stepowska, H.; Grzeszczyk, B.; Zamojski, A.; Berova, N., Configuration of heptopyranoside and heptofuranoside side chains: 2-Anthroate, a powerful chromophore for exciton coupled CD. *Chirality* **1997**, *9* (7), 699-712.
11. Berova, N.; Pescitelli, G.; Petrovic, A. G.; Proni, G., Probing molecular chirality by CD-sensitive dimeric metalloporphyrin hosts. *Chem Commun* **2009**, (40), 5958-5980.

12. Degenbeck, H.; Felten, A. S.; Escudero-Adan, E. C.; Benet-Buchholz, J.; Di Bari, L.; Pescitelli, G.; Vidal-Ferran, A., New Chiral Zinc Complexes: Synthesis, Structure, and Induction of Axial Chirality. *Inorg Chem* **2012**, *51* (16), 8643-8645.
13. Eelkema, R.; Feringa, B. L., Macroscopic expression of the chirality of amino alcohols by a double amplification mechanism in liquid crystalline media. *J Am Chem Soc* **2005**, *127* (39), 13480-13481.
14. Goto, H.; Furusho, Y.; Yashima, E., Helicity induction on water-soluble oligoresorcinols in alkaline water and their application to chirality sensing. *Chem Commun* **2009**, (13), 1650-1652.
15. Wezenberg, S. J.; Salassa, G.; Escudero-Adan, E. C.; Benet-Buchholz, J.; Kleij, A. W., Effective Chirogenesis in a Bis(metallosalphen) Complex through Host-Guest Binding with Carboxylic Acids. *Angew Chem Int Edit* **2011**, *50* (3), 713-716.
16. Wolf, C.; Bentley, K. W., Chirality sensing using stereodynamic probes with distinct electronic circular dichroism output. *Chem Soc Rev* **2013**, *42* (12), 5408-5424.
17. Zhao, Y. C.; Swager, T. M., Simultaneous Chirality Sensing of Multiple Amines by F-19 NMR. *J Am Chem Soc* **2015**, *137* (9), 3221-3224.
18. Yang, L.; Wenzel, T.; Williamson, R. T.; Christensen, M.; Schafer, W.; Welch, C. J., Expedited Selection of NMR Chiral Solvating Agents for Determination of Enantiopurity. *Acs Central Sci* **2016**, *2* (5), 332-340.
19. Berova, N.; Polavarapu, P. L.; Nakanishi, K.; Woody, R. W., Comprehensive Chiroptical Spectroscopy, Applications in Stereochemical Analysis of Synthetic Compounds, Natural Products, and Biomolecules. Volume 2. Wiley, 2012.
20. Harada, N.; Nakanishi, K. j., *Circular dichroic spectroscopy : exciton coupling in organic stereochemistry*. University Science Books: Mill Valley, CA, 1983.
21. Yang, Q.; Olmsted, C.; Borhan, B., Absolute stereochemical determination of chiral carboxylic acids. *Org Lett* **2002**, *4* (20), 3423-3426.
22. Proni, G.; Pescitelli, G.; Huang, X.; Quraishi, N. Q.; Nakanishi, K.; Berova, N., Configurational assignment of α -chiral carboxylic acids by complexation to dimeric Zn-porphyrin: host-guest structure, chiral recognition and circular dichroism. *Chem Commun* **2002**, (15), 1590-1591.
23. Tanasova, M.; Borhan, B., Conformational Preference in Bis(porphyrin) Tweezer Complexes: A Versatile Chirality Sensor for α -Chiral Carboxylic Acids. *Eur J Org Chem* **2012**, *2012* (17), 3261-3269.

24. Joyce, L. A.; Maynor, M. S.; Dragna, J. M.; da Cruz, G. M.; Lynch, V. M.; Canary, J. W.; Anslyn, E. V., A simple method for the determination of enantiomeric excess and identity of chiral carboxylic acids. *J Am Chem Soc* **2011**, *133* (34), 13746-13752.
25. Huang, X.; Rickman, B. H.; Borhan, B.; Berova, N.; Nakanishi, K., Zinc porphyrin tweezer in host-guest complexation: determination of absolute configurations of diamines, amino acids, and amino alcohols by circular dichroism. *J Am Chem Soc* **1998**, *120* (24), 6185-6186.
26. Li, X.; Burrell, C. E.; Staples, R. J.; Borhan, B., Absolute configuration for 1, n-glycols: A nonempirical approach to long-range stereochemical determination. *J Am Chem Soc* **2012**, *134* (22), 9026-9029.
27. Anyika, M.; Gholami, H.; Ashtekar, K. D.; Acho, R.; Borhan, B., Point-to-Axial Chirality Transfer A New Probe for "Sensing" the Absolute Configurations of Monoamines. *J Am Chem Soc* **2014**, *136* (2), 550-553.
28. Tanasova, M.; Anyika, M.; Borhan, B., Sensing Remote Chirality: Stereochemical Determination of beta-, gamma-, and delta-Chiral Carboxylic Acids. *Angew Chem Int Edit* **2015**, *54* (14), 4274-4278.
29. Gholami, H.; Anyika, M.; Zhang, J.; Vasileiou, C.; Borhan, B., Host-Guest Assembly of a Molecular Reporter with Chiral Cyanohydrins for Assignment of Absolute Stereochemistry. *Chem. - Eur. J.* **2016**, *22* (27), 9235-9.
30. Aimi, J.; Oya, K.; Tsuda, A.; Aida, T., Chiroptical sensing of asymmetric hydrocarbons using a homochiral supramolecular Box from a bismetalloporphyrin rotamer. *Angew Chem Int Edit* **2007**, *46* (12), 2031-2035.
31. Ikbal, S. A.; Dhamija, A.; Brahma, S.; Rath, S. P., A Nonempirical Approach for Direct Determination of the Absolute Configuration of 1,2-Diols and Amino Alcohols Using Mg(II)bisporphyrin. *J Org Chem* **2016**, *81* (13), 5440-9.
32. Hayashi, S.; Yotsukura, M.; Noji, M.; Takanami, T., Bis(zinc porphyrin) as a CD-sensitive bidentate host molecule: direct determination of absolute configuration of mono-alcohols. *Chem Commun* **2015**, *51* (55), 11068-11071.
33. Hayashi, T.; Aya, T.; Nonoguchi, M.; Mizutani, T.; Hisaeda, Y.; Kitagawa, S.; Ogoshi, H., Chiral recognition and chiral sensing using zinc porphyrin dimers. *Tetrahedron* **2002**, *58* (14), 2803-2811.
34. Ishii, Y.; Onda, Y.; Kubo, Y., 2,2'-Biphenyldiol-bridged bis(free base porphyrin): synthesis and chiroptical probing of asymmetric amino alcohols. *Tetrahedron Lett* **2006**, *47* (47), 8221-8225.

35. Lintuluoto, J. M.; Borovkov, V. V.; Inoue, Y., Direct determination of absolute configuration of monoalcohols by bis(magnesium porphyrin). *J Am Chem Soc* **2002**, *124* (46), 13676-13677.
36. Redl, F. X.; Lutz, M.; Daub, J., Chemistry of porphyrin-appended cellulose strands with a helical structure: Spectroscopy, electrochemistry, and in situ circular dichroism spectroelectrochemistry. *Chem. -Eur J* **2001**, *7* (24), 5350-5358.
37. Zhang, J.; Holmes, A. E.; Sharma, A.; Brooks, N. R.; Rarig, R. S.; Zubieta, J.; Canary, J. W., Derivatization, complexation, and absolute configurational assignment of chiral primary amines: Application of exciton-coupled circular dichroism. *Chirality* **2003**, *15* (2), 180-189.
38. Dale, J. A.; Mosher, H. S., Nuclear magnetic resonance enantiomer reagents. Configurational correlations via nuclear magnetic resonance chemical shifts of diastereomeric mandelate, O-methylmandelate, and alpha-methoxy-alpha-trifluoromethylphenylacetate (MTPA) esters. *J Am Chem Soc* **1973**, *95* (2), 512-519.
39. Fukui, H.; Fukushi, Y., NMR Determinations of the Absolute Configuration of alpha-Chiral Primary Amines. *Org Lett* **2010**, *12* (12), 2856-2859.
40. Hoye, T. R.; Erickson, S. E.; Erickson-Birkedahl, S. L.; Hale, C. R. H.; Izgu, E. C.; Mayer, M. J.; Notz, P. K.; Renner, M. K., Long-Range Shielding Effects in the H-1 NMR Spectra of Mosher-like Ester Derivatives. *Org Lett* **2010**, *12* (8), 1768-1771.
41. Porto, S.; Quinoa, E.; Riguera, R., Designing chiral derivatizing agents (CDA) for the NMR assignment of the absolute configuration: a theoretical and experimental approach with thiols as a case study. *Tetrahedron* **2014**, *70* (20), 3276-3283.
42. Takeuchi, Y.; Segawa, M.; Fujisawa, H.; Omata, K.; Ludwig, S. N.; Unkefer, C. J., The CFTA method: A reliable procedure for the determination of the absolute configuration of chiral primary amines by H-1 NMR spectroscopic analysis. *Angew Chem Int Edit* **2006**, *45* (28), 4617-4619.
43. Wenzel, T. J.; Wilcox, J. D., Chiral reagents for the determination of enantiomeric excess and absolute configuration using NMR spectroscopy. *Chirality* **2003**, *15* (3), 256-270.
44. Seco, J. M.; Quinoá, E.; Riguera, R., The assignment of absolute configuration by NMR. *Chem Rev* **2004**, *104* (1), 17-118.
45. You, L.; Berman, J. S.; Anslyn, E. V., Dynamic multi-component covalent assembly for the reversible binding of secondary alcohols and chirality sensing. *Nature chemistry* **2011**, *3* (12), 943-948.

46. Jo, H. H.; Edupuganti, R.; You, L.; Dalby, K. N.; Anslyn, E. V., Mechanistic studies on covalent assemblies of metal-mediated hemi-aminal ethers. *Chem Sci* **2015**, *6* (1), 158-164.
47. You, L.; Berman, J. S.; Lucksanawichien, A.; Anslyn, E. V., Correlating Sterics Parameters and Diastereomeric Ratio Values for a Multicomponent Assembly To Predict Exciton-Coupled Circular Dichroism Intensity and Thereby Enantiomeric Excess of Chiral Secondary Alcohols. *J Am Chem Soc* **2012**, *134* (16), 7126-7134.
48. Sciebura, J.; Skowronek, P.; Gawronski, J., Trityl Ethers: Molecular Bevel Gears Reporting Chirality through Circular Dichroism Spectra. *Angew Chem Int Edit* **2009**, *48* (38), 7069-7072.
49. Dai, Z. H.; Xu, X. D.; Canary, J. W., Rigidified tripodal chiral ligands in the asymmetric recognition of amino compounds. *Chirality* **2005**, *17*, 227-233.
50. Telfer, S. G.; McLean, T. M.; Waterland, M. R., Exciton coupling in coordination compounds. *Dalton T* **2011**, *40* (13), 3097-3108.
51. Tartaglia, S.; Pace, F.; Scafato, P.; Rosini, C., A New Case of Induced Helical Chirality in a Bichromophoric System: Absolute Configuration of Transparent and Flexible Diols from the Analysis of the Electronic Circular Dichroism Spectra of the Corresponding Di(1-naphthyl)ketals. *Org Lett* **2008**, *10* (16), 3421-3424.
52. Hosoi, S.; Kamiya, M.; Ohta, T., Novel development of exciton-coupled circular dichroism based on induced axial chirality. *Org Lett* **2001**, *3* (23), 3659-3662.
53. Bachrach, S. M., Computational organic chemistry. Wiley-Interscience, Hoboken, N.J., 2007.
54. Shao, Y. H.; Gan, Z. T.; Epifanovsky, E.; Gilbert, A. T. B.; Wormit, M.; Kussmann, J.; Lange, A. W.; Behn, A.; Deng, J.; Feng, X. T.; Ghosh, D.; Goldey, M.; Horn, P. R.; Jacobson, L. D.; Kaliman, I.; Khaliullin, R. Z.; Kus, T.; Landau, A.; Liu, J.; Proynov, E. I.; Rhee, Y. M.; Richard, R. M.; Rohrdanz, M. A.; Steele, R. P.; Sundstrom, E. J.; Woodcock, H. L.; Zimmerman, P. M.; Zuev, D.; Albrecht, B.; Alguire, E.; Austin, B.; Beran, G. J. O.; Bernard, Y. A.; Berquist, E.; Brandhorst, K.; Bravaya, K. B.; Brown, S. T.; Casanova, D.; Chang, C. M.; Chen, Y. Q.; Chien, S. H.; Closser, K. D.; Crittenden, D. L.; Diedenhofen, M.; DiStasio, R. A.; Do, H.; Dutoi, A. D.; Edgar, R. G.; Fatehi, S.; Fusti-Molnar, L.; Ghysels, A.; Golubeva-Zadorozhnaya, A.; Gomes, J.; Hanson-Heine, M. W. D.; Harbach, P. H. P.; Hauser, A. W.; Hohenstein, E. G.; Holden, Z. C.; Jagau, T. C.; Ji, H. J.; Kaduk, B.; Khistyayev, K.; Kim, J.; Kim, J.; King, R. A.; Klunzinger, P.; Kosenkov, D.; Kowalczyk, T.; Krauter, C. M.; Lao, K. U.; Laurent, A. D.; Lawler, K. V.; Levchenko, S. V.; Lin, C. Y.; Liu, F.; Livshits, E.; Lochan, R. C.; Luenser, A.; Manohar, P.; Manzer, S. F.; Mao, S. P.; Mardirossian, N.; Marenich, A. V.; Maurer, S. A.; Mayhall, N. J.; Neuscamman, E.; Oana, C. M.; Olivares-Amaya, R.; O'Neill, D. P.; Parkhill, J. A.;

- Perrine, T. M.; Peverati, R.; Prociuk, A.; Rehn, D. R.; Rosta, E.; Russ, N. J.; Sharada, S. M.; Sharma, S.; Small, D. W.; Sodt, A.; Stein, T.; Stuck, D.; Su, Y. C.; Thom, A. J. W.; Tsuchimochi, T.; Vanovschi, V.; Vogt, L.; Vydrov, O.; Wang, T.; Watson, M. A.; Wenzel, J.; White, A.; Williams, C. F.; Yang, J.; Yeganeh, S.; Yost, S. R.; You, Z. Q.; Zhang, I. Y.; Zhang, X.; Zhao, Y.; Brooks, B. R.; Chan, G. K. L.; Chipman, D. M.; Cramer, C. J.; Goddard, W. A.; Gordon, M. S.; Hehre, W. J.; Klamt, A.; Schaefer, H. F.; Schmidt, M. W.; Sherrill, C. D.; Truhlar, D. G.; Warshel, A.; Xu, X.; Aspuru-Guzik, A.; Baer, R.; Bell, A. T.; Besley, N. A.; Chai, J. D.; Dreuw, A.; Dunietz, B. D.; Furlani, T. R.; Gwaltney, S. R.; Hsu, C. P.; Jung, Y. S.; Kong, J.; Lambrecht, D. S.; Liang, W. Z.; Ochsenfeld, C.; Rassolov, V. A.; Slipchenko, L. V.; Subotnik, J. E.; Van Voorhis, T.; Herbert, J. M.; Krylov, A. I.; Gill, P. M. W.; Head-Gordon, M., Advances in molecular quantum chemistry contained in the Q-Chem 4 program package. *Mol Phys* **2015**, *113* (2), 184-215.
55. Winstein, S.; Holness, N. J., Neighboring Carbon and Hydrogen .19. Tert-Butylcyclohexyl Derivatives - Quantitative Conformational Analysis. *J Am Chem Soc* **1955**, *77* (21), 5562-5578.
56. Charton, M., Steric Effects .1. Esterification and Acid-Catalyzed Hydrolysis of Esters. *J Am Chem Soc* **1975**, *97* (6), 1552-1556.
57. Verloop, A. T., J., *In Biological Activity and Chemical Structure*. 1977.
58. Zhou, Y. T.; Ren, Y. L.; Zhang, L.; You, L.; Yuan, Y. F.; Anslyn, E. V., Dynamic covalent binding and chirality sensing of mono secondary amines with a metal-templated assembly. *Tetrahedron* **2015**, *71* (21), 3515-3521.
59. Traverse, J. F.; Snapper, M. L., High-throughput methods for the development of new catalytic asymmetric reactions. *Drug Discov Today* **2002**, *7* (19), 1002-1012.
60. Bassas, O.; Huuskonen, J.; Rissanen, K.; Koskinen, A. M. P., A Simple Organocatalytic Enantioselective Synthesis of Pregabalin. *Eur J Org Chem* **2009**, (9), 1340-1351.
61. Holtz-Mulholland, M.; Collins, S. K., Synthesis of Chiral C-1-Symmetric N-Heterocyclic Carbene Ligands: Application toward Copper-Catalyzed Homocoupling of 2-Naphthols. *Synthesis-Stuttgart* **2014**, *46* (3), 375-380.

Chapter III: Di(1-Naphthyl) Methanol Ester of Carboxylic Acids for Absolute Stereochemical Determination

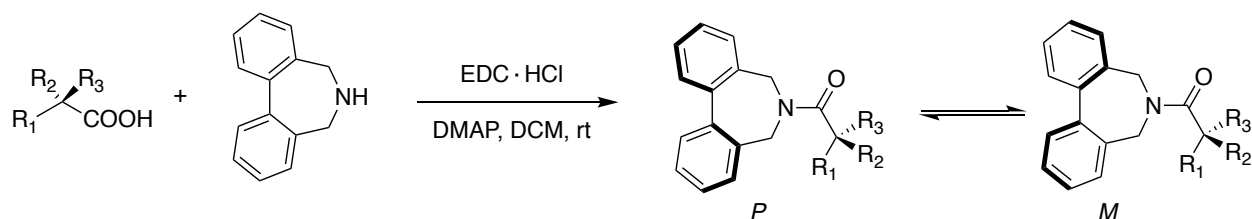
III.1. Introduction

Carboxylic acids are important building blocks in organic chemistry. Due in part to the abundance of enantio-enriched carboxylic acids: i.e. amino acids, versatile methodologies for their use have been developed in recent years. To name a few, Baran's lab has developed a series of decarboxylative alkynylation/alkenylation/borylation methodologies of the carboxylic acids.¹⁻³ Nicewicz's lab developed an anti-Markovnikov addition of the carboxylic acids to alkenes.⁴ Buchwald's lab introduced a simple Cu-H catalyzed asymmetric reduction of α,β unsaturated carboxylic acids methodology.⁵ Parallel to synthetic efforts, there is a continual need for developing simple methods to determine the absolute stereochemistry of the carboxylic acids.

Over the past four decades, chiroptical spectroscopy, and in particular circular dichroism (CD), has played a pivotal role in the absolute stereochemical determination of organic molecules.⁶⁻¹⁴ Numerous strategies have been brought to bear to address this important issue; nonetheless, it is clear that a unified solution to the problem is not forthcoming. The best solution for a particular functional group, or a sub-family of molecules is not necessarily the best choice for another, and thus the continual optimization of old methods and new creative approaches are needed. In the past few years, many groups have developed elegant sensors for the carboxylic acids chiral sensing, including: Rosini, Canary, Anslyn, Borhan, Wolf and others.¹⁵⁻¹⁹

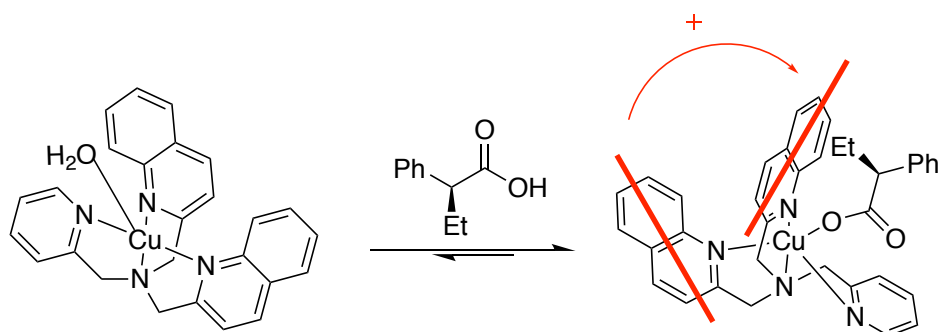
In 2006, Rosini's lab developed a biphenyl chromophore sensor to determine the absolute stereochemistry of carboxylic acids (**Scheme III-1**).¹⁵ Biphenyl amine can be

easily coupled with chiral carboxylic acids through a DMAP catalyzed EDC coupling reaction. The chiral amide product can either adopt *P* or *M* helicity, depending on the chirality of the carboxylic acids. Active CD signal can be recorded and correlated to the absolute stereochemistry of the acids.



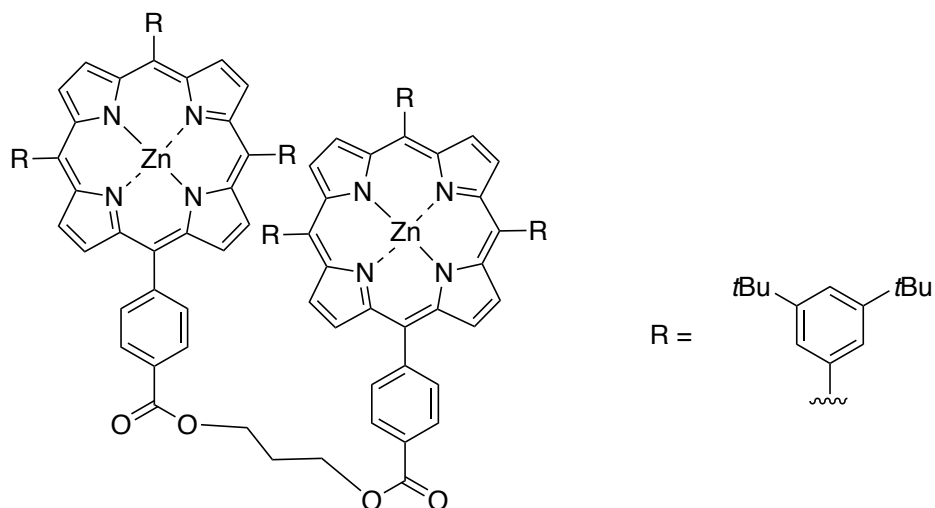
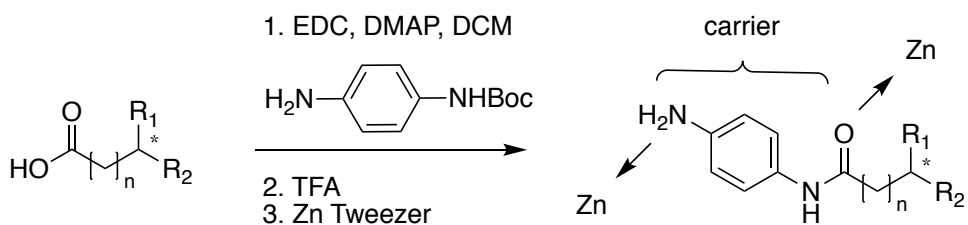
Scheme III-1. Biphenyl chromophore probe for carboxylic acids absolute stereochemistry assignment. EDC = 1-ethyl-3-(3-dimethylaminopropyl)carbodiimide. DMAP = 4-dimethylaminopyridine.

An achiral copper host for absolute stereochemical determination of chiral carboxylic acids and also *ee* measurement was developed by Canary's and Anslyn's groups.¹⁶ In this report, Cu (II) metal coordinates with quinolines and pyridine to yield an achiral pocket (**Scheme III-2**). Upon addition of chiral carboxylic acids, water is exchanged with the carboxylic acid to bind with copper inside the pocket. A helical twist is induced due to the steric repulsion between the substituents on the asymmetric center and the chromophores. For example, (*S*)-2-phenylbutanoic acid forces two quinoline chromophores to adopt a clockwise twist, thus, a positive ECCD signal was observed.



Scheme III-2. Anslyn's host for carboxylic acids absolute stereochemistry determination.

Our group has also developed a powerful porphyrin tweezer methodology for sensing remote stereochemistry in carboxylic acids.¹⁷ Most methods for absolute stereochemical determination of chiral carboxylic acids are limited to asymmetry at the α position. Determining the absolute stereochemistry on β or even γ and δ positions remains challenging. Our group successfully tackled this problem by using chemical derivatization assisted ECCD sensing via a bulky porphyrin tweezer (**Scheme III-3**). Carboxylic acids which contain chiral centers on β , γ or δ positions were derivatized with the diamine carrier first and the resulting chiral amides were subjected to the porphyrin tweezer for ECCD analysis. During the course of the study, a variety of porphyrin based tweezers were screened. Different numbers of the carbon linker and the substituents on the porphyrin rings were tested. The optimal tweezer is shown in **Scheme III-3**, containing 3 carbons in the linker to connect two porphyrins and the bulky 3,5-di-*t*-butylphenyl as the substituent on both porphyrins.



Scheme III-3. Bis(porphyrin) tweezers for remote chirality sensing. TFA = trifluoroacetic acid.

III.1.1 Strategies towards the chiral carboxylic acids sensing

In **Chapter II**, we disclosed the marriage of the chemical derivatization and the CD study, combining the stability in structure of the derivatized sample, with the routine determination of helicity via the ECCD method in determining the absolute stereochemistry of asymmetric amines. Herein, we apply this approach to the absolute stereochemical determination of chiral carboxylic acids.

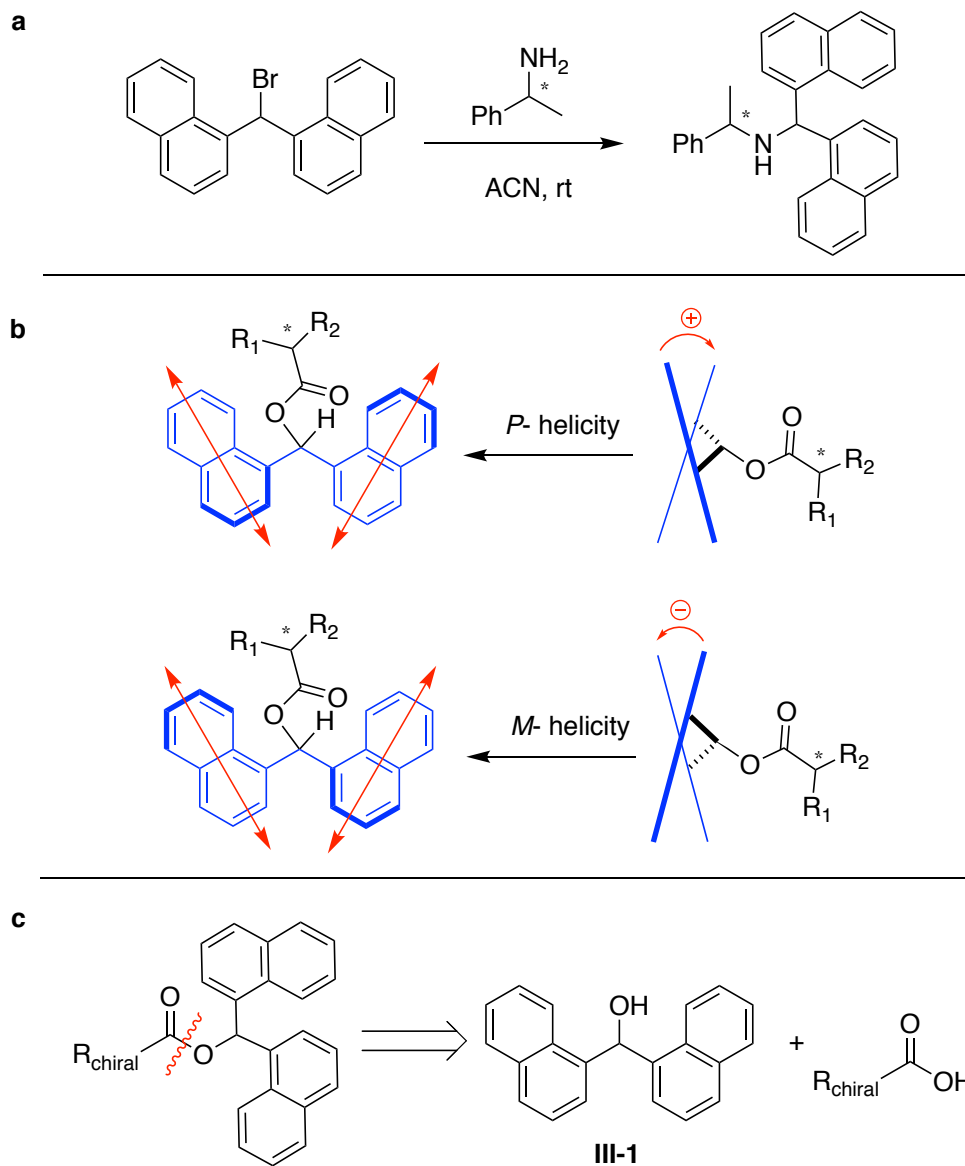


Figure III-1. (a) Chiral amine sensing. (b) Working models for the carboxylic acids sensing. *P* and *M* helical conformations of the chiral ester. (c) Breaking down the chiral ester.

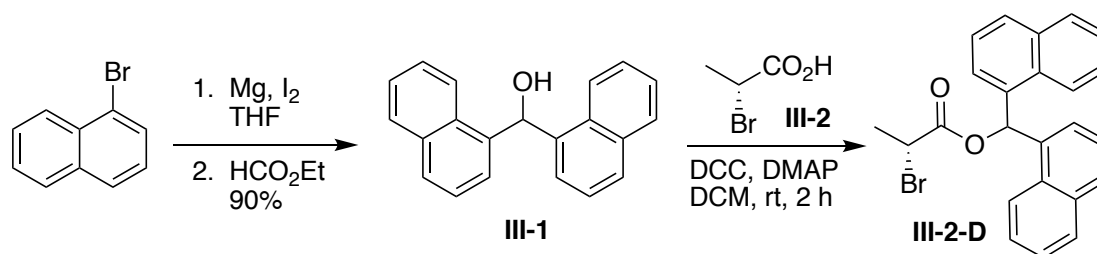
We demonstrated that 1,1'-(bromomethylene)dinaphthalene can easily alkylate an asymmetric amine (**Figure III-1, a**). The naphthyl rings of the derivatized molecule adopt a preponderance of either the *P* or *M* helicity as a consequence of intramolecular interactions, yielding either a positive or negative ECCD signal. Low cost computational analysis provides a theoretical population distribution of conformers. Statistical analysis

of the helicity of the computed structures that predict an excess population of either *P* or *M* helicity leads to the prediction of an ECCD signal for the chirality of the computed derivatized compound. Comparison with experimental ECCD data leads to the absolute stereochemical determination of the derivatized amines. In a similar fashion, this methodology is transferred for use with chiral carboxylic acids. Esterification of the chiral carboxylic acids with bisnaphthalene chromophores generate the preponderance of one helicity (*P* or *M*) (**Figure III-1, b**). Obtaining the ECCD spectra of the chiral esters in conjunction with computational prediction leads to the absolute stereochemistry determination of carboxylic acids.

Following a similar strategy as with amines, di(1-naphthyl)methanol **III-1** (**Figure III-1, c**) was chosen as the reagent for esterification with chiral carboxylic acids. ECCD signals require coupling of the electric transition dipole moments of two or more independently conjugated chromophores. The structure of **III-1**, with its two naphthyl rings, has the prerequisites for generating an ECCD signal, given that the two aryl groups adopt a non-racemic helical population. The methine group that separates the two rings not only provides a handle for derivatization,²⁰⁻²³ but also aids in reducing the rotational barrier for the two aryl groups, thus enabling them to adopt a preferred conformation as dictated by the chirality of the derivatized carboxylic acid. At the onset, we would predict that upon esterification of **III-1** with a chiral carboxylic acid, either the *P* or *M* helicity of the bisnaphthyl group would be favored, resulting in an ECCD signal that can be directly correlated to the chirality of the carboxylic acid.

III.2 Absolute stereochemical determination of chiral aliphatic carboxylic acids

Although compound **III-1** is commercially available, it can be easily synthesized and purified by recrystallization in gram scale from the Grignard reaction of 1-bromonaphthalene with ethyl formate in 90% overall yield. The DCC mediated derivatization of compound **III-1** with chiral carboxylic acids requires less than 2 h for completion. A short silica plug purification is all that is needed for preparation of the sample for CD analysis (**Scheme III-4**).



Scheme III-4. Synthesis of compound **III-1** and simple esterification of the carboxylic acids for the ECCD study. DCC = N,N'-Dicyclohexylcarbodiimide. DMAP = 4-dimethylaminopyridine.

Derivatization of carboxylic acid **III-2** with compound **III-1** yields ester **III-2-D** that generates a positive ECCD spectrum. As expected, its enantiomer **III-3-D** exhibits the opposite ECCD signal (see **Figure III-2**). The observed spectra is the result of induced helicity of the coupling naphthyl groups, adopting specific conformations as a result of their interaction with the nearby groups attached to the asymmetric center. The asymmetry observed in the ECCD spectra resulting from the coupling of naphthyl groups has been observed before.²⁴ The asymmetrical shape of the couplet is closely related to the relevant electric transition moment, one of the factors responsible for the Cotton effects.²⁵ Namely, the transition fall-offs from the vibrational bands reflect the flatness of the longer wavelength. The shape also seems to be deformed by the strong absorption

of solvents and/or minute impurities close to 200 nm, which diminishes the signal due to reduce signal/noise ratio. The spectra remained virtually identical as the temperature was reduced to 0 °C. It should be noted that although naphthyl groups have two main transitions (1L_a ~270 nm and 1B_b ~220 nm), we observe the coupling from the more intense 1B_b band (long axis transition), and see no evidence of the short axis 1L_a transition in the ECCD spectra.

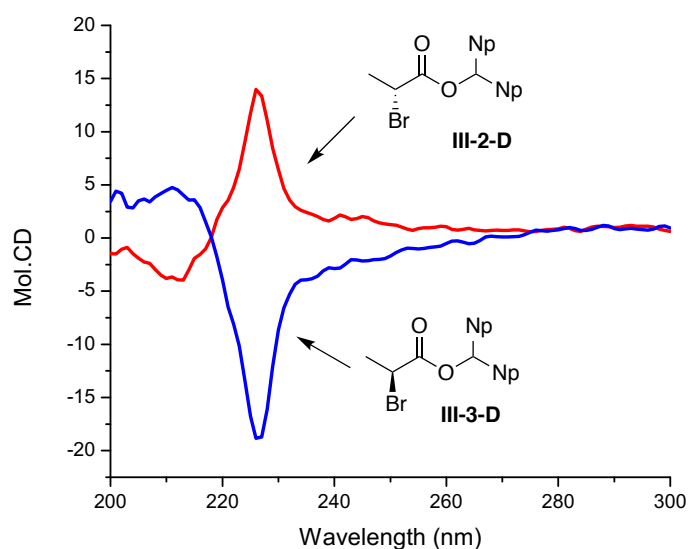


Figure III-2. A CD spectra of chiral aliphatic carboxylic esters **III-2-D** and **III-3-D** show the opposite ECCD signals. Np = 1-naphthyl.

Signals obtained from the chiral carboxylic acids are much weaker than the signals from the chiral amines in **Chapter II** (Mol. CD for acids are less than 100 whereas Mol. CD for amines are greater than 100). This phenomenon can be explained in **Figure III-3**. The distances between the chiral center and the bisnaphthalene chromophores are different between the two systems. We speculated that closer the chiral center to the chromophores, the stronger their interaction, leading to a higher ECCD amplitude.

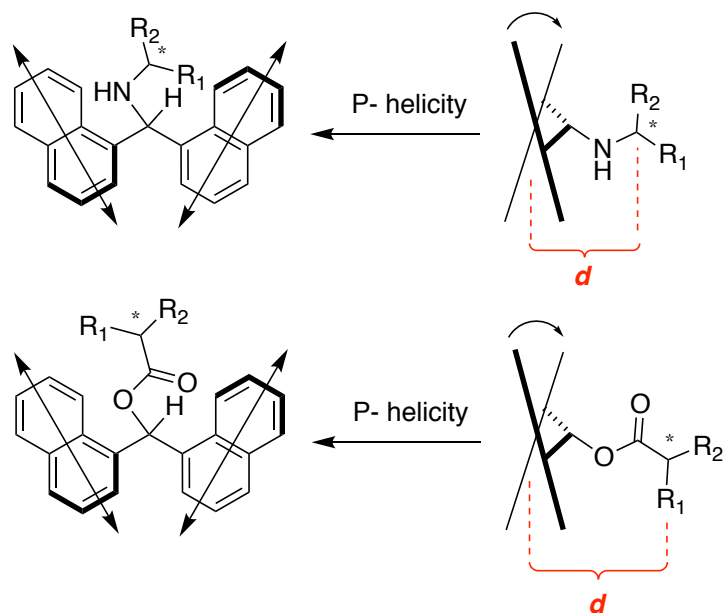


Figure III-3. Distance differences between the chiral amines and chiral carboxylic acids. *d* refers to distance.

During the course of the study, we found that using DFT/B3LYP/6-31GD calculation method to compute the *P:M* ratio for the carboxylic acids is time-consuming. Amines have a much smaller number of conformers as compared to carboxylic acids. This limits the use of DFT for the carboxylic acids, as the prolonged calculation time is in contrary to our goal. In order to find a fast and reliable way to get a relative accurate *P:M* ratio for our analysis, we collaborated with Prof. Tatsuo Nehira (Hiroshima University, Japan) to develop a simple computational method to predict the ECCD signals.

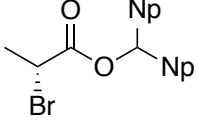
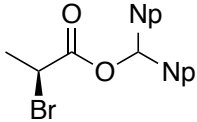
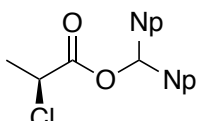
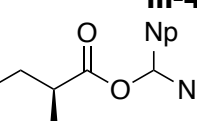
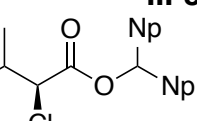
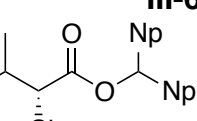
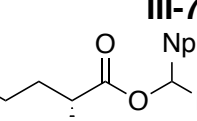
Entry	Amine ^a	Predicted Sign <i>P/M</i> ratio ^b	$\lambda(\text{nm}), \Delta\epsilon$	A
1	 III-2-D	Pos (54.7/38.8)	226, +14	+18
2	 III-3-D	Neg (38.8/54.7)	226, -19	-24
3	 III-4-D	Neg (36.5/56.3)	227, -11	-16
4	 III-5-D	Neg (44.1/46.4)	226, -10	-16
5	 III-6-D	Neg (40.7/49.8)	227, -8	-13
6	 III-7-D	Pos (49.8/40.7)	227, +5	+6
7	 III-8-D	Pos (51.1/39.3)	226, +8	+10

Table III-1. ^aAll CD measurements were recorded with 10 μM ester derivative in acetonitrile at rt. ^bCalculated populations of *P* and *M* helical conformers were obtained via tabulating the population of conformations that yield positive and negative helicity.

Our approach to the prediction of ECCD relies on evaluating conformational distribution of populations that adopt either the *P* (leading to positive ECCD) or the *M* (leading to negative ECCD) helicity. After several trials, we were able to use a routine and expeditious conformational modeling method (MMFF94S force field on CONFLEX7) to

estimate the *P:M* ratios. The estimate for the percentage of *P* and *M* populations for conformers with over 90% abundance (spanning 2.3 Kcal/mol from the most stable conformer) were calculated, leading to a predicted helicity. For example, molecular modeling of ester **III-2-D** (**Table III-1**, entry 1) leads to a set of conformers, of which 93.5% reside within 1.12 Kcal/mol. Conformational analysis of this group of molecules shows a *P:M* calculated ratio of 54.7:38.8. The dominance of the *P* helical population would predict a positive ECCD spectrum, which in fact is in agreement with the experimentally observed data ($A = +18$).

By using this method, we were able to determine the absolute stereochemistry of a variety of chiral aliphatic carboxylic acids. **Table III-1** illustrates a set of diverse chiral alkyl carboxylic acids derivatized with compound **III-1** (**III-2-D** to **III-8-D**) that produce ECCD active species. Notably, the system is sensitive to discrimination of substituents with similar size such as a methyl vs. ethyl group (**Table III-1**, **III-5-D**). The same analysis for molecules listed in **Table III-1** yields predictions that are in line with the ECCDs obtained for each molecule.

III.3 Absolute stereochemical determination of chiral aromatic carboxylic acids

After the screening of the chiral aliphatic carboxylic acids, we turned our attention to the enantio-enriched aromatic carboxylic acids. Our journey began with the 2-methoxy-2-phenylacetic acid. To our delight, (*R*)-2-methoxy-2-phenylacetic acid derivative **III-9-D** yields a negative sign whereas the (*S*)-2-methoxy-2-phenylacetic acid derivative **III-10-D** yields a positive sign (**Figure III-4**).

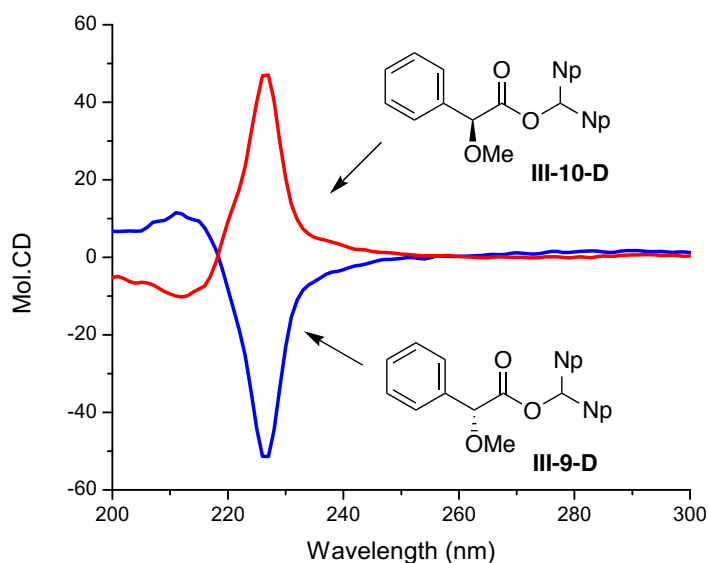


Figure III-4. CD spectra of chiral aromatic carboxylic esters **III-9-D** and **III-10-D** show the opposite ECCD signals. Np = 1-naphthyl.

Table III-2 summarizes the extension of the same principles and analysis to chiral carboxylic systems that are aryl substituted. In general, the derivatized aryl substituted carboxylic acids exhibit stronger ECCD signals as compared to the aliphatic substituted carboxylic acid derivatives listed in **Table III-1**. This is presumably the result of stronger interactions of the binaphthyl group with the aryl substituents. Similar to that discussed with aliphatic substrates, computational studies also predict the correct *P:M* ratio, matching the observed ECCD signals. It is interesting to point out that derivative **III-12-D** and **III-14-D** share similar structures, the difference is the substituent on the *para* position on the phenyl ring. With a *sec*-butyl group on compound **III-14-D**, it yields a much larger amplitude than compound **III-12-D**. We believe phenyl and binaphthalenes are closer in distance to each other. Thus, the *sec*-butyl group has a pronounced steric effect to increase the ECCD amplitude (see crystal structure of compound **III-11-D**, **Figure III-7**).

Of note, the benzyl substituted derivatives **III-15-D** and **III-16-D** (**Table III-2**, entries 7 and 8) do lead to observable ECCD spectra, albeit weaker in strength as compared to other aryl-substituted examples. This is presumably the result of having the phenyl group further away from the dinaphthyl moiety, thus lessening its influence on dictating the *P:M* population difference.

In **Chapter II**, we discussed aromatic and aliphatic amines of the same psuedo chirality yield opposite ECCD signals. Indeed, the same phenomenon was also observed for chiral carboxylic acids. The aryl substituted esters yield the opposite ECCD in comparison to their alkyl carboxylic acid derivatives. For example, ester **III-6-D**, with its medium sized chloride and large sized isopropyl substituent, yields a negative ECCD signal. Ester **III-12-D**, having the same disposition of substituents based on size as determined by A_{value} steric parameters (medium sized methyl group and large sized aryl group), produces a positive ECCD. Importantly, the conformational analysis for both leads to the correct prediction, thus providing an operationally expedient system that considers all mechanical interactions that lead to a preferred helicity.

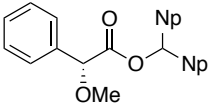
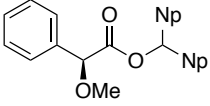
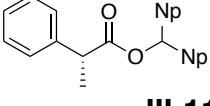
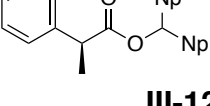
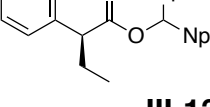
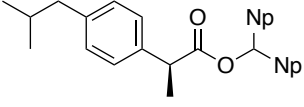
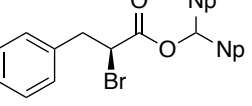
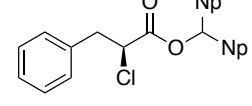
Entry	Amine ^a	Predicted Sign <i>P/M</i> ratio ^b	$\lambda(\text{nm}), \Delta\epsilon$	A
1	 III-9-D	Neg (8.1/83.1)	226, -52	-63
2	 III-10-D	Pos (83.1/8.1)	227, +48	+58
3	 III-11-D	Neg (32.8/57.5)	227, -30	-48
4	 III-12-D	Pos (57.5/32.8)	227, +31	+43
5	 III-13-D	Pos (56.9/33.8)	225, +31	+42
6	 III-14-D	Pos (51.9/38.3)	227, +70	+92
7	 III-15-D	Pos (49.6/43.1)	228, +11	+25
8	 III-16-D	Pos (48.1/41.1)	228, +8	+15

Table III-2. ^aAll CD measurement were recorded with 10 μM ester derivative in acetonitrile at rt. ^bCalculated populations of *P* and *M* helical conformers were obtained via tabulating the population of conformations that yield positive and negative helicity.

During the ECCD studies of the enantio-enriched carboxylic acids, we found that a greater difference in helical population translate to higher ECCD amplitudes. As depicted in **Figure III-5**, a trend was observed between the *P* and *M* populations for esters

III-2-D to III-16-D (alkyl and aryl systems), plotted as a function of the observed amplitude. It clearly suggested that a higher $P:M$ ratio can translate into a higher ECCD signal.

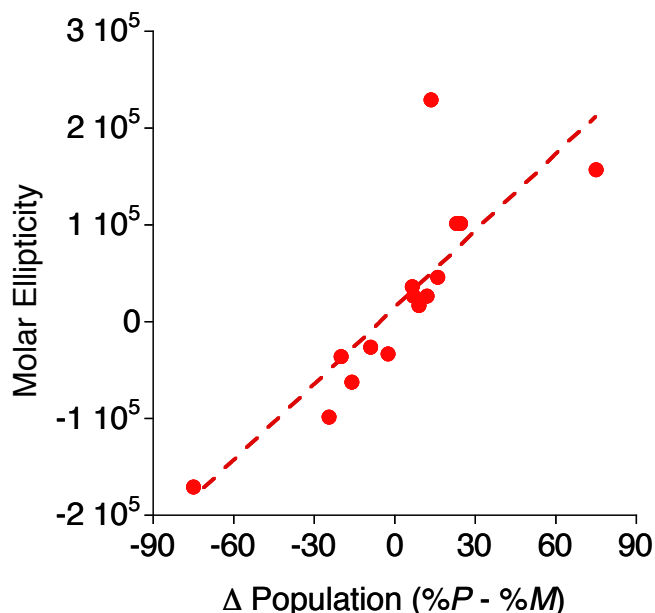


Figure III-5. A correlation is observed between the strength of the ECCD spectra ($\Delta\epsilon$ of the high wavelength Cotton effect) and the population difference calculated for P and M helicities.

III.4 High level computation and crystal structure study

Although we find that a simple conformational analysis (MMFF94S), requiring less than a few hours per substrate, is sufficient to yield predictable populations for absolute stereochemical determinations, a higher-level calculation was also carried out for substrate III-11-D. For this purpose, all conformers (> 1% population) obtained from MMFF minimization, were further optimized by DFT calculation (hybrid functional B3LYP, double-zeta basis set 6-31G(d) in gas phase). The energetically most stable conformers, accounting for 91.0% of the population (4 conformers) were then subject to TDDFT calculation with a hybrid functional B3LYP and a double-zeta basis set cc-pVDZ. The calculated ECCD spectra were integrated by considering their population, resulting in a

theoretical ECCD spectrum for substrate **III-11-D** as shown in **Figure III-6**. As anticipated, the calculated ECCD matches the Cotton effects observed experimentally for **III-11-D**, thus confirming that the calculated *P:M* ratio results in the observed sign for the ECCD spectra.

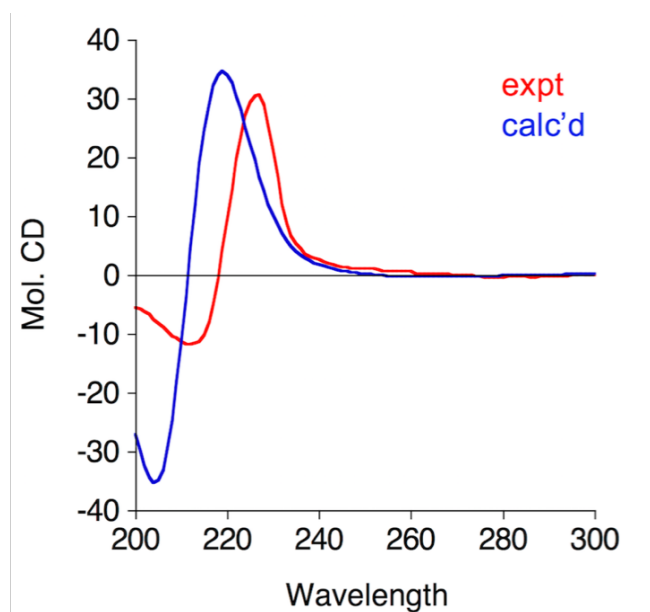


Figure III-6. Theoretical calculation of ECCD for **III-11-D** overlapped with the experimentally observed spectrum.

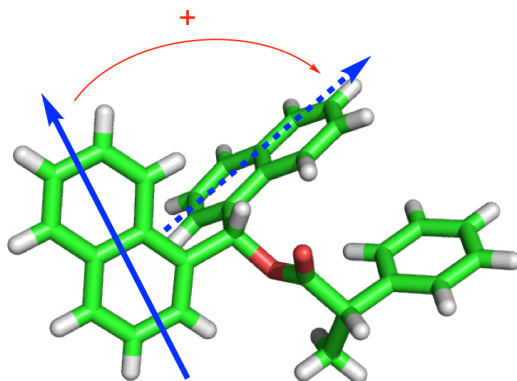


Figure III-7. Crystal structure of compound **III-11-D** exhibits the *P* helicity that would yield a positive ECCD signal.

To investigate the validity of the *P:M* ratio argument, we crystalized the carboxylic acid derivative **III-11-D** to examine its preferred helicity. Fortuitously, ester **III-11-D** succumbed to crystallization, exhibiting the *P* helical conformation, matching the predicted dominant population by modeling (66.8% *P* helicity, **Figure III-7**).

III.5 Use of a standard curve for ee determination

Due to the fact that ECCD signals generated from the carboxylic acids are much weaker and the derivatization reaction can not proceed at micro-molar conditions, this method can not be applied for High Throughput Screening (HTS) process. Nonetheless, a standard curve for the carboxylic acids was obtained to validate *ee* analysis.

We chose 2-phenylpropanoic acid for the standard curve study. Six different concentrations of the mixtures were prepared (-100, -60, -40, 40, 60, 100, from pure *R* to pure *S*). Exact *ee* value for each standard stock solution was verified by HPLC. Each stock solution was subjected to the standard reaction conditions to afford the carboxylic acid derivatives. ECCD spectra were recorded for the purified derivatives (**Figure III-8**). Linear correlation between the exact *ee* values and the ECCD Cotton effects at 227 nm are shown in **Figure III-9**. The regression line fits well with the experimentally observed ECCD signals ($R^2 = 0.995$).

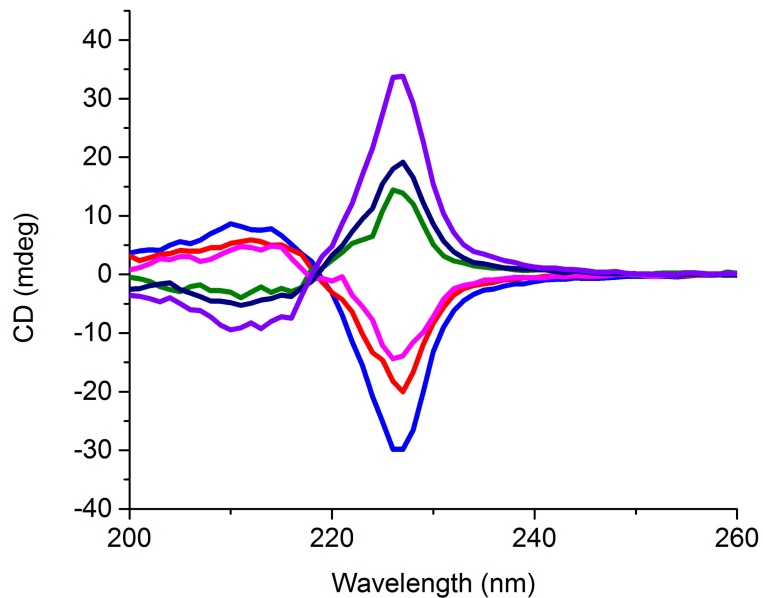


Figure III-8. ECCD spectra of chiral carboxylic acids **III-11-D** and **III-12-D** at various ees.

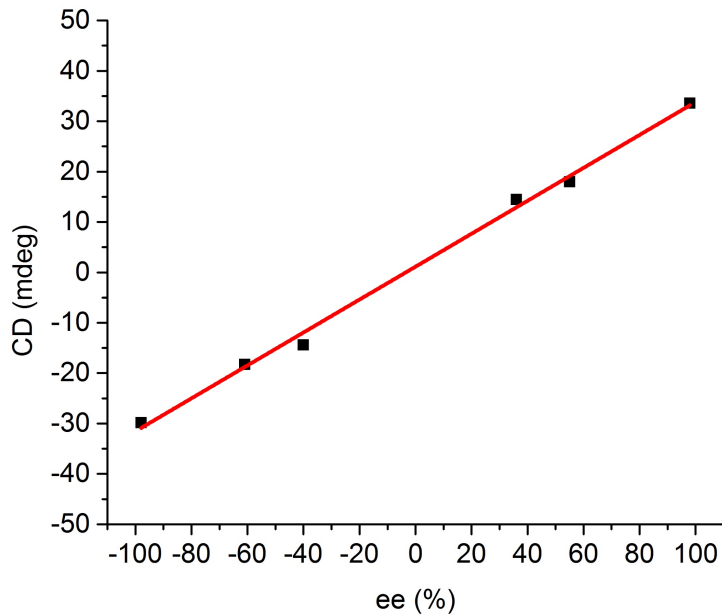


Figure III-9. Linear correlation of the ECCD signals at 227 nm with exact ee values of chiral carboxylic acids.

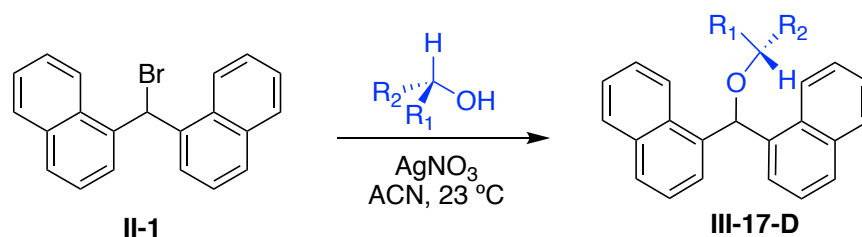
III.6 Future work

The work in this and the previous chapter highlight a new method to determine the absolute stereochemistry of enantio-enriched carboxylic acids and amines. The compounds required for such analysis can be easily prepared in gram scale and the reaction conditions are mild. As for the computational studies, we chose commercially available software such as SPARTAN and CONFLEX, which have user friendly interfaces. Step by step procedures for computational analysis are demonstrated in **Chapter II**. We believe this new method for chiral sensing can be applied to other functional groups as well.

III.6.1 Absolute stereochemical determination of chiral alcohols

After the successful determination of enantio-enriched carboxylic acids and amines, we questioned whether the absolute stereochemistry of chiral alcohols can be determined in a similar fashion. Although there were several elegant hosts that have already been designed to sense the absolute stereochemistry of chiral alcohols. New methodologies that complement previous strategies are desired. The major challenge with alcohols is their weaker binding towards a variety of metals. Thus, using non-covalent bonding hosts to sense chiral alcohols can be difficult. For example, our lab was able to use porphyrin tweezers to sense chiral diols, but mono-alcohols do not bind to the porphyrin tweezers to yield an observable ECCD signal. In order to solve this problem, we are currently working on improving the binding affinity of the MAPOL system for such analysis. On the other hand, covalently derivatized systems such as the Mosher ester analysis produce stable conformers for analysis.

We believe that mono-alcohols can be attached to the bisnaphthalenes host through a silver catalyzed reaction (**Scheme III-5**). In this way, we can borrow from the idea related to the absolute stereochemical determination of amines (**Chapter II**). Indeed, compound **II-1** can yield a new ether bond with chiral mono-alcohols in presence of the silver nitrate catalyst.



Scheme III-5. Chiral mono-alcohol sensing method.

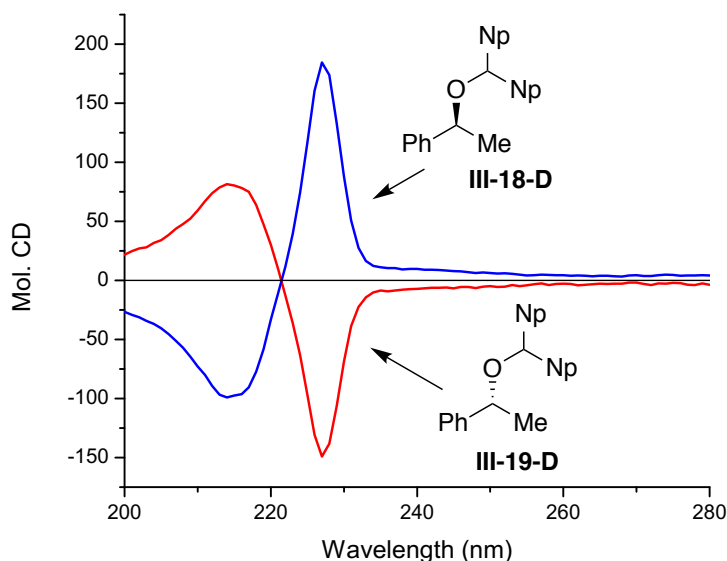


Figure III-10. CD spectra of chiral mono alcohol ethers **III-18-D** and **III-19-D** show the opposite ECCD signals. Np = 1-naphthyl.

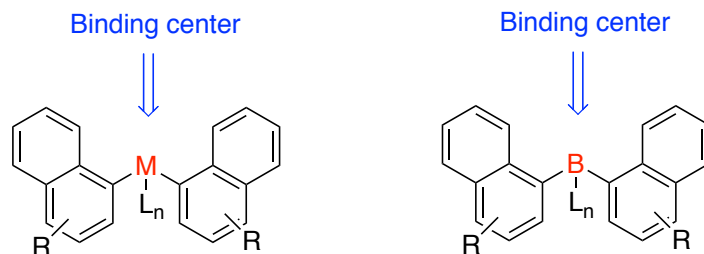
Our initial studies began with chiral 1-phenylethanol. To our delight, two enantiomers **III-18-D** and **III-19-D** yielded opposite ECCD signals (**Figure III-10**). This demonstrates our method can be used to tackle the challenging mono-alcohol chirality

sensing problem in a simple way. This project can be completed in short order with a series of chiral alcohols and the necessary calculations.

III.6.2 A non-derivatizing host for absolute stereochemical determinations

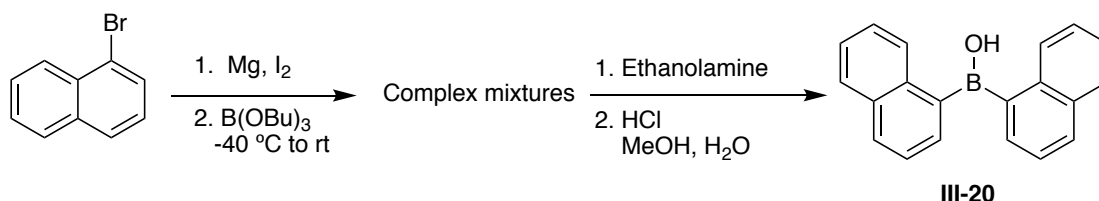
The absolute stereochemical determinations discussed in **Chapter II** and **Chapter III** utilize covalent bonds for new complex formation. Formation of covalent bonds have advantages such as stability and restricted conformational flexibility. However, using non-covalent bonds can potentially expand our unique methods for different types of chiral analytes while being operationally less complicated and quicker.

In order to build a host capable of non-covalent bonding for our system, we need to find a replacement for the methine between the two naphthalene chromophores. That can provide an empty orbital to accept analytes (**Scheme III-6**). Transition or post transition metals can be a powerful choice since a variety of elegant hosts utilize these metals to provide the required binding center. On the other hand, using a host with a metal center could lead to ligand to metal charge transfer absorption band that redshifts the CD signal. A challenging problem for this approach is that di-alkylated metals are generally strong nucleophiles and not very stable under air conditions.



Scheme III-6. Design of new hosts. M refers to metal, B refers to boron, R refers to the substituents that can red shift the chromophores, L is the ligand.

Another approach is using metalloids, especially boron. Boron can provide an empty orbital to accept ligands and is relatively more stable than the di-alkylated metals. In order to examine our proposal, we have synthesized a simple boron host with bisnaphthalenes as chromophores (**III-20**, **Scheme III-7**).



Scheme III-7. Synthesis of the new host.

Compound **III-20** can be synthesized through 4 steps. Complex mixtures were formed after the addition of tributyl borate. The desired product can not be isolated by flash column purification. However, in presence of excess amount of ethanolamine, the amino borate can be precipitated, followed by the HCl hydrolysis to yield pure **III-20**.

During the purification of compound **III-20**, I realized that the crystal formation upon adding the ethanolamine is fast even at room temperature. Instead of the ethanolamine, chiral amino alcohols should be able to bind to compound **III-20** and yield observable ECCD signal. To test this hypothesis, chiral (*R*)-(-)-2-phenylglycinol was tested. To our delight, upon adding 5 equivalents of the chiral amino alcohol to the host **III-20** in acetonitrile at room temperature (10^{-5} M concentration), positive ECCD signal was observed (**Figure III-11**). Prolonging the time to 1 h, the ECCD signal becomes much stronger. Cooling the temperature to 0 °C also increases the ECCD amplitude. This exciting result demonstrates our new boron host can be used to sense dual binding guests.

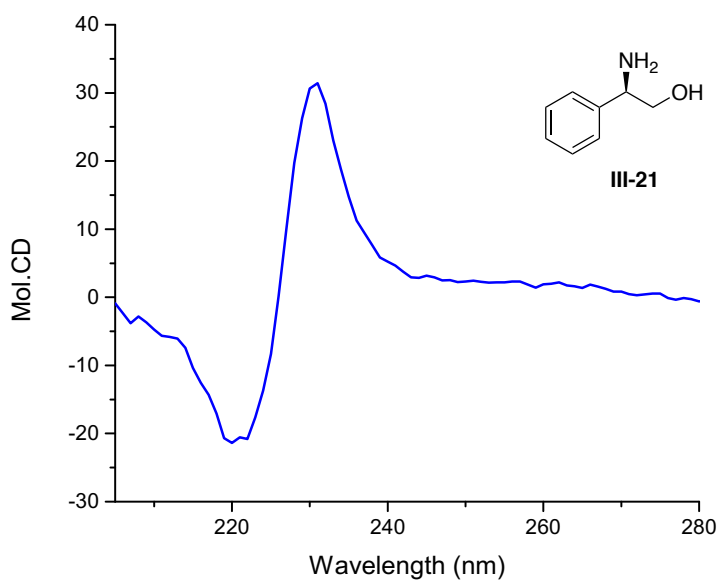
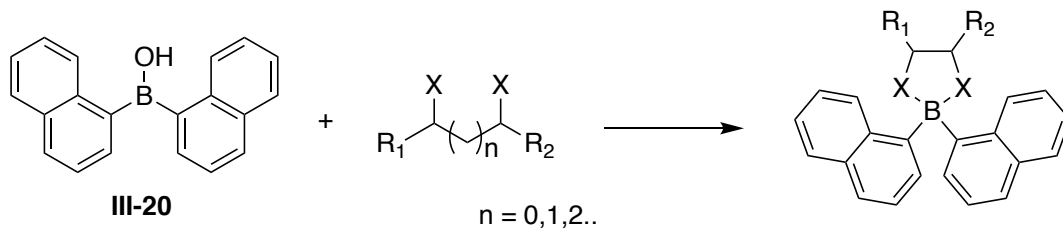
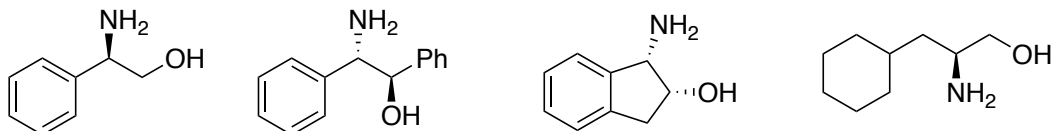


Figure III-11. ECCD spectrum of enantio-enriched amino alcohol **III-21** with new host **III-20** in acetonitrile at 0 °C.

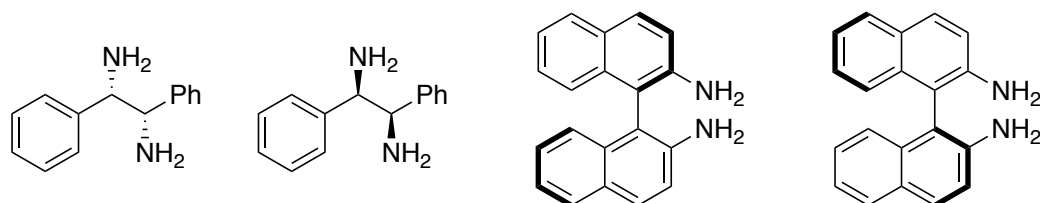
Our binding model is shown in **Figure III-12**. Based on our preliminary result, we propose that more chiral analytes can be analyzed with this new host system. Chiral guests such as amino alcohols, diamines, diols, amino acids and α hydroxyl ketone or esters can bind to our host molecule to yield active ECCD signal (**Figure III-12**).



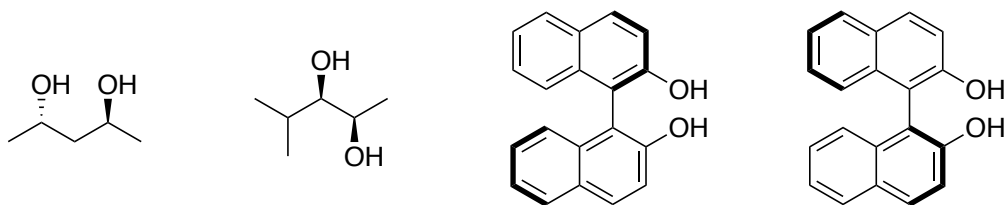
Amino alcohols:



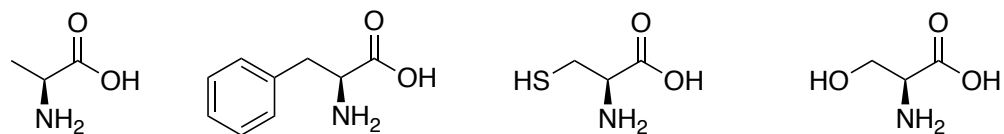
Diamines:



Diols:



Amino Acids:



Hydroxyl ketones/esters:

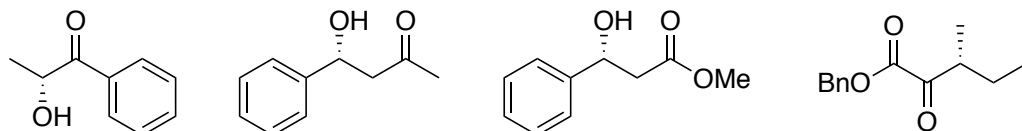
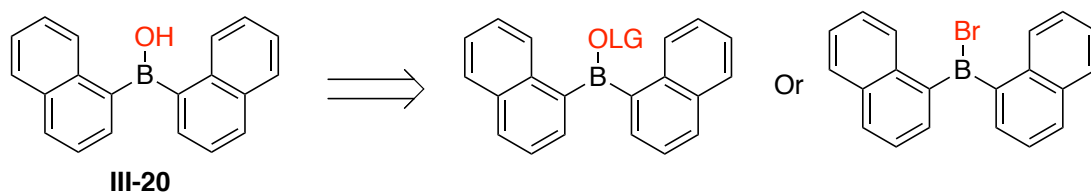


Figure III-12. Potential chiral guests for ECCD study.

Attempts to use our system for chiral mono-binding analytes, such as mono-alcohols and amines was not successful. However, we did observe a weak ECCD signal by mixing 10 equivalent of alcohol **III-18** with boron host **III-20** after incubating overnight (10^{-5} M concentration). This reaction rate is too slow at low concentrations. Thus, we propose that the reaction can be accelerated by adding a leaving group (OMs, OTs or bromide) to the borinic acid, thus making the mono-binding chiral sensing feasible (**Scheme III-8**).



Scheme III-8. Improve the reactivity of the new boron host. LG = leaving group.

III.6.3 More red-shifted chromophores

One drawback for our bisnaphthalene systems is the low ECCD wavelength (< 300 nm). Alternation of the naphthalenes to redshifted chromophores can not only reduce the noise from the analytes but also give us more choice of solvents with higher UV cutoffs.

Currently, two approaches can yield a red-shifted CD signal: 1) Ligand to metal charge transfer. 2) Chromophores with red shifted absorption. In **Chapter III.6.1**, we mentioned that using ligand to metal charge transfer is a potential way to yield redshifted CD signals. Here, we want to introduce two chromophores that can potentially yield redshifted CD signals.

One important thing that needs to be addressed here is that the red-shifted CD signal may not be generated through the ECCD mechanism. But opposite signs are expected for the enantiomers in the CD spectra. After careful screening of the

chromophores and computational modeling, we arrive at two chromophores to redshift our signals. These chromophores are fluorene and biphenylene (**Scheme III-9**). Fluorenes exhibit UV-absorptions up to 310 nm, but these chromophores can be easily engineered to even redder absorption. Another choice of the chromophores is biphenylene, it exhibits the UV absorption as high as 400 nm.



Scheme III-9. Two chromophores that can yield a redshifted CD signals.

III.7 Experimental section

III.7.1 Materials and general instruments

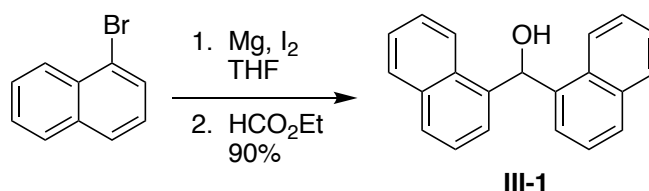
Anhydrous spectra grade solvents used for CD measurements were purchased from Sigma Aldrich. THF was dried over sodium. Column chromatography was performed using SiliCycle silica gel (230-400 mesh). $^1\text{H-NMR}$ and $^{13}\text{C-NMR}$ spectra were obtained on Varian 500 MHz instrument and are reported in parts per million (ppm) relative to the solvent resonances (δ), with coupling constants (J) in Hertz (Hz). CD spectra were recorded on a JASCO J-810 spectropolarimeter, equipped with a temperature controller (Neslab 111) and are reported as λ [nm] ($\Delta\epsilon_{\text{max}}$ [$\text{mol}^{-1} \text{cm}^{-1}$]). Chiral carboxylic acids not synthesized in the experimental section were purchased from commercial sources and were used without further purification. HRMS analysis was performed on a Q-TOF Ultima system using electrospray ionization in negative mode. GC analysis was performed on HP 6890 series equipped with Agilent GC autosample controller G1512A. Enantiomeric excess was measured by Gamma-Dex 225 fused silica capillary column (30 m * 0.25 mm * 0.25 μm) on GC.

III.7.2 General procedure for CD measurements

Chiral carboxylic acids derivatized with **III-1** were dissolved in acetonitrile to make a 0.01 M stock solution. From the stock solution 1 μL was dissolved in acetonitrile (1 mL) solution yielding a 10 μM final solution ready for CD measurement. Background spectra of acetonitrile was recorded from 350 nm to 200 nm with a scan rate of 100 nm/min at room temperature. CD spectra of ester samples measured with 10 accumulations, was

subtracted from background and normalized based on the concentration to obtain the molecular CD (Mol. CD).

III.7.3 Synthesis of the starting materials



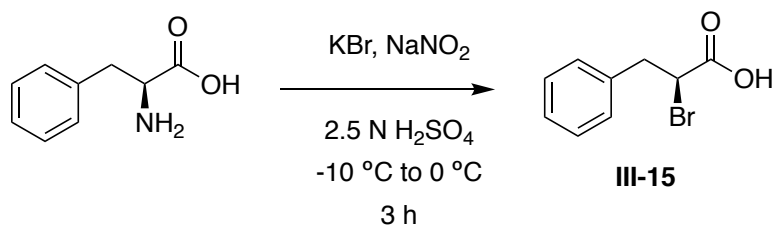
Di(naphthalen-1-yl)methanol (**III-1**)²⁶

To a dried 250 mL round bottom flask was added magnesium turnings (504 mg, 21 mmol) and iodide (12 mg, 0.05 mmol) in dry THF (100 mL), 1-Bromonaphthalene (4.14 g, 20 mmol) was dissolved in dry THF (10 mL) and was added to the mixture slowly over 15 minutes. After stirring for 2 h at room temperature, ethyl formate (740 mg, 10 mmol) in dry THF (10 mL) was added to the mixture and stirred for 2 h. The reaction was quenched by addition of cold HCl (1N) solution and extracted with ethyl acetate (200 mL), washed with brine, dried over sodium sulfate and concentrated in vacuo to afford the crude product. The product was purified by recrystallization from ethyl acetate and hexane to afford an off white solid product (2.57 g, 90 %).

¹H NMR (CDCl₃, 500 MHz): 8.06 (d, J = 8.0 Hz, 2H), 7.91 (d, J = 8.0 Hz, 2H), 7.89 (d, J = 8.0 Hz, 2H), 7.50–7.38 (m, 9H), 7.33 (d, J = 4.5 Hz, 1H), 2.40 (d, J = 4.5 Hz, 1H).

¹³C NMR (CDCl₃, 125 MHz): 138.3, 133.9, 131.0, 128.8, 128.6, 126.5, 125.7, 125.4, 125.0, 123.6, 69.7.

Synthesis of chiral α -bromo carboxylic acid



(S)-2-Bromo-3-phenylpropanoic acid (**III-15**)

To a solution of L-phenylalanine (1.65 g, 10 mmol) and potassium bromide (3.6 g, 30 mmol) in 2.5 N sulfuric acid (25 mL) was added sodium nitrite (2.1 g, 30 mmol) in water (5 mL) at -10 °C slowly. The reaction mixture was then stirred for 3 h at 0 °C and extracted with CH₂Cl₂ (3 × 30 mL). The combined organic layers were dried over anhydrous sodium sulfate and concentrated in vacuo. The crude carboxylic acid was obtained as a yellow oil in 45% (1.02 g) yield and was used without further purification.

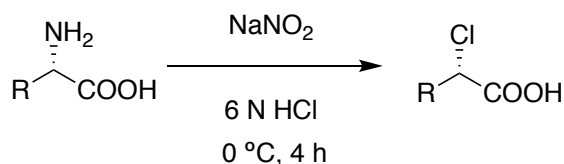
¹H-NMR (CDCl₃, 500 MHz): 7.32-7.20 (m, 5H), 4.42-4.39 (m, 1H), 3.47-3.43 (m, 1H), 3.26-3.21 (m, 1H).

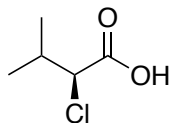
¹³C-NMR (CDCl₃, 125 MHz): 174.8, 136.3, 129.2, 128.8, 127.5, 44.7, 40.7.

HRMS (Q-TOF MS (ESI⁻)): calc'd for C₉H₈BrO₂ [M-H]⁻ m/z =226.9708, obs'd 226.9706.

[α]_D²⁰ = -12.6 (c, 10 mg/ml in DCM).

Synthesis of chiral α -chloro carboxylic acids





(S)-2-Chloro-3-methylbutyric acid (III-6)

To a solution of L-valine (1.17 g, 10 mmol) in 6 N sulfuric acid (20 mL) was added sodium nitrite (2.1 g, 30 mmol) in water (5 mL) at 0 °C slowly. The reaction mixture was stirred for 4 h at 0 °C and then extracted with CH₂Cl₂ (3 × 30 mL). The combined organic layers were dried over anhydrous sodium sulfate and concentrated in vacuo. The crude carboxylic acid was obtained as a light yellow oil in 42% (575 mg) yield and was used without further purification.

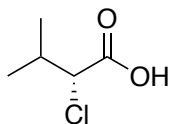
¹H-NMR (CDCl₃, 500 MHz): 4.20 (d, J = 6.0 Hz, 1H), 2.37-2.33 (m, 1H), 1.08-1.05 (m, 6H).

¹³C-NMR (CDCl₃, 125 MHz): 174.8, 63.9, 32.5, 19.6, 17.8.

HRMS (Q-TOF MS (ESI-)): calc'd for C₅H₈ClO₂ [M-H]⁻ m/z =135.0213, obs'd 135.0215;

[α]_D²⁰ = -4.1 (c, 10 mg/ml in DCM).

Chiral GC: performed on Gamma-Dex 225 column, starting temperature 90 °C, increased by 3 °C/min to 220 °C, then hold at this temperature for 20 mins. t_R (major) = 18.2 min, t_R (minor) = 17.2 min; 99%ee.



(R)-2-Chloro-3-methylbutyric acid (III-7)

To a solution of D-valine (1.17 g, 10 mmol) in 6 N sulfuric acid (20 mL) was added sodium nitrite (2.1 g, 30 mmol) in water (5 mL) at 0 °C slowly. The reaction mixture was stirred for 4 h at 0 °C and then extracted with CH₂Cl₂ (3 × 30 mL). The combined organic layers were dried over anhydrous sodium sulfate and concentrated in vacuo. The crude carboxylic acid was obtained as a light yellow oil in 48% (656 mg) yield and was used without further purification.

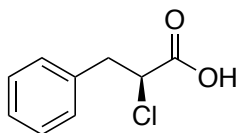
¹H-NMR (CDCl₃, 500 MHz): 4.20 (d, J = 6.0 Hz, 1H), 2.37-2.33 (m, 1H), 1.08-1.05 (m, 6H).

¹³C-NMR (CDCl₃, 125 MHz): 174.8, 63.9, 32.5, 19.6, 17.8.

HRMS (Q-TOF MS (ESI-)): calc'd for C₅H₈ClO₂ [M-H]⁻ m/z =135.0213, obs'd 135.0215.

[α]_D²⁰ = +2.6 (c, 10 mg/ml in DCM).

Chiral GC: performed on Gamma-Dex 225 column, starting temperature 90 °C, increased by 3 °C/min to 220 °C, then hold at this temperature for 20 mins. t_R (major) = 17.2 min, t_R (minor) = 18.2 min; 99% ee.



(S)-2-Chloro-3-phenylpropanoic acid (**III-16**)

To a solution of L-phenylalanine (1.65 g, 10 mmol) and potassium bromide (3.6 g, 30 mmol) in 2.5 N sulfuric acid (25 mL) was added sodium nitrite (2.1 g, 30 mmol) in water (5 mL) at 0 °C slowly. The reaction mixture was stirred for 3 h at 0 °C and then extracted

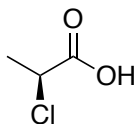
with CH₂Cl₂ (3 × 30 mL). The combined organic layers were dried over anhydrous sodium sulfate and concentrated in vacuo. The crude carboxylic acid was obtained as a yellow oil in 81% (1.49 g) yield and was used without further purification.

¹H-NMR (CDCl₃, 500 MHz): 10.9 (br, 1H), 7.34-7.23 (m, 5H), 4.50-4.47 (m, 1H), 3.41-3.37 (m, 1H), 3.20-3.16 (m, 1H).

¹³C-NMR (CDCl₃, 125 MHz): 175.0, 135.4, 129.3, 128.7, 127.5, 57.2, 40.8.

HRMS (Q-TOF MS (ESI-)): calc'd for C₉H₈ClO₂ [M-H]⁻ m/z =183.0213, obs'd 183.0211.

[α]_D²⁰ = -1.4 (c, 10 mg/ml in DCM).



(S)-2-Chloropropanoic acid (III-4)

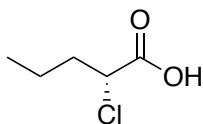
To a solution of L-alanine (890 mg, 10 mmol) in 6 N sulfuric acid (20 mL) was added sodium nitrite (2.1 g, 30 mmol) in water (5 mL) at 0 °C slowly. The reaction mixture was stirred for 4 h at 0 °C and then extracted with CH₂Cl₂ (3 × 30 mL). The combined organic layers were dried over anhydrous sodium sulfate and concentrated in vacuo. The crude carboxylic acid was obtained as colorless oil in 17% (186 mg) yield and was used without further purification.

¹H-NMR (CDCl₃, 500 MHz): 4.59 (q, J = 7.0 Hz, 1H), 1.73 (d, J = 7.0 Hz, 1H).

¹³C-NMR (CDCl₃, 125 MHz): 175.6, 52.1, 21.4.

HRMS (Q-TOF MS (ESI-)): calc'd for C₃H₄ClO₂ [M-H]⁻ m/z =106.9900, obs'd 106.9905.

[α]_D²⁰ = -15.4 (c, 10 mg/ml in DCM).



(*R*)-2-Chloropentanoic acid (**III-8**)

To a solution of D-norvaline (590 mg, 5 mmol) and potassium bromide (1.8 g, 15 mmol) in 2.5 N sulfuric acid (15 mL) was added sodium nitrite (1.05 g, 15 mmol) in water (3 mL) at 0 °C slowly. The reaction mixture was stirred for 4 h at 0 °C and then extracted with CH₂Cl₂ (3 × 15 mL). The combined organic layers were dried over anhydrous sodium sulfate and concentrated in vacuo. The crude carboxylic acid was obtained as a colorless oil in 68% (461 mg) yield and was used without further purification.

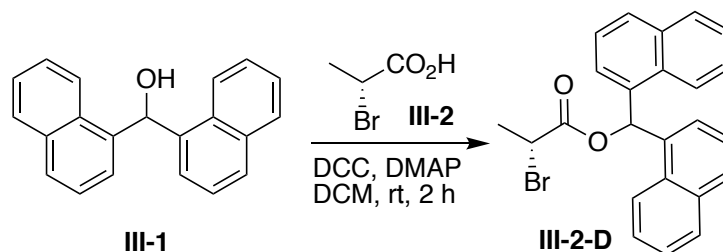
¹H-NMR (CDCl₃, 500 MHz): 4.33-4.30 (m, 1H) 2.04-1.90 (m, 2H), 1.55-1.49 (m, 2H), 0.97-0.94 (m, 3H).

¹³C-NMR (CDCl₃, 125 MHz): 175.5, 56.8, 36.6, 19.2, 13.3.

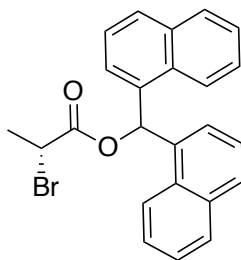
HRMS (Q-TOF MS (ESI-)): calc'd for C₅H₈ClO₂ [M-H]⁻ m/z =135.0213, obs'd 135.0214.

[α]_D²⁰ = +25.4 (c, 10 mg/ml in DCM).

III.7.4 General synthesis of esters for absolute stereochemical determination



General procedure: To the chiral carboxylic acid (0.1 mmol), di(naphthalen-1-yl)methanol (0.11 mmol, 31.3 mg) in DCM, dicyclohexylcarbodiimide (0.12 mmol, 25 mg) and DMAP (1 mg) were added at room temperature. After a few minutes, a white precipitate formed and the solution turned cloudy. The reaction was stirred for 100 min, the solution was concentrated under reduced pressure, and the crude product was passed through a short silica pad with 2.5% EtOAc/ Hexane to afford the pure product for CD experiments.

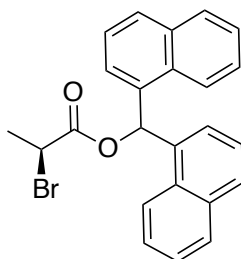


Di(naphthalen-1-yl)methyl (*R*)-2-bromopropanoate (**III-2-D**)

Prepared according to the general procedure, product was isolated as an off white solid (39 mg, 93%).

$^1\text{H-NMR}$ (CDCl_3 , 500 MHz): 8.43 (s, 1H), 7.85-7.19 (m, 6H), 7.52-7.38 (m, 8H), 4.50 (q, $J = 6.5$ Hz, 1H), 1.84 (d, $J = 6.5$ Hz, 3H).

^{13}C -NMR (CDCl_3 , 125 MHz): 169.3, 134.2, 134.0, 133.9, 133.8, 131.0, 130.9, 129.4, 129.3, 129.0, 128.9, 126.9, 126.7, 126.1, 126.0, 125.9, 125.8, 125.3, 125.3, 123.4, 123.2, 72.4, 40.1, 21.7.

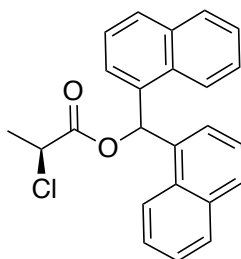


Di(naphthalen-1-yl)methyl (*S*)-2-bromopropanoate (**III-3-D**)

Prepared according to the general procedure, product was isolated as an off white solid (38 mg, 91%).

^1H -NMR (CDCl_3 , 500 MHz): 8.43 (s, 1H), 8.00-7.84 (m, 6H), 7.52-7.38 (m, 8H), 4.69 (q, $J = 6.5$ Hz, 1H), 1.84 (d, $J = 6.5$ Hz, 3H).

^{13}C -NMR (CDCl_3 , 125 MHz): 169.3, 134.2, 134.0, 133.9, 133.8, 131.1, 131.0, 129.4, 129.3, 129.0, 128.9, 126.9, 126.7, 126.1, 126.0, 125.9, 125.8, 125.3, 125.3, 123.4, 123.2, 72.4, 40.1, 21.7.

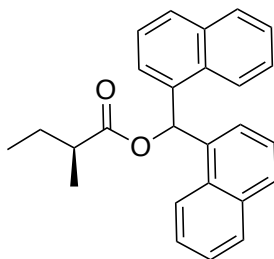


Di(naphthalen-1-yl)methyl (*S*)-2-chloropropanoate (**III-4-D**)

Prepared according to the general procedure, product was isolated as an off white solid (36 mg, 89%).

$^1\text{H-NMR}$ (CDCl_3 , 500 MHz): 8.44 (s, 1H), 7.98-7.85 (m, 6H), 7.51-7.39 (m, 8H), 4.53 (q, $J = 8.0$ Hz, 1H), 1.70 (d, $J = 8.0$ Hz, 3H).

$^{13}\text{C-NMR}$ (CDCl_3 , 125 MHz): 169.2, 134.1, 134.0, 133.9, 133.8, 131.0, 130.9, 129.4, 129.3, 129.0, 128.9, 126.9, 126.8, 126.1, 126.0, 125.9, 125.8, 125.3, 125.3, 123.3, 123.2, 72.5, 52.6, 21.5.

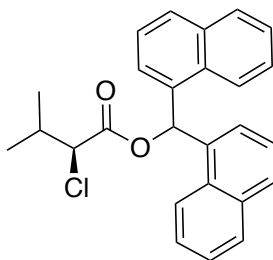


Di(naphthalen-1-yl)methyl (*S*)-2-methylbutanoate (**III-5-D**)

Prepared according to the general procedure, product was isolated as an off white solid (12 mg, 33%).

$^1\text{H-NMR}$ (CDCl_3 , 500 MHz): 8.41 (s, 1H), 7.97 (d, $J = 8.0$ Hz, 2H), 7.89 (d, $J = 8.0$ Hz, 2H), 7.84 (d, 7.5 Hz, 2H), 7.48-7.34 (m, 8H), 2.52 (m, 1H), 1.56 (m, 1H), 1.49 (m, 1H), 1.17 (d, $J = 7.0$ Hz, 3H), 0.86 (t, $J = 7.0$ Hz, 3H).

$^{13}\text{C-NMR}$ (CDCl_3 , 125 MHz): 175.9, 135.1, 133.8, 133.8, 131.1, 131.1, 123.0, 128.8, 126.6, 126.6, 125.8, 125.8, 125.7, 125.2, 125.2, 125.2, 123.5, 123.5, 70.5, 41.4, 26.7, 16.7, 11.7.

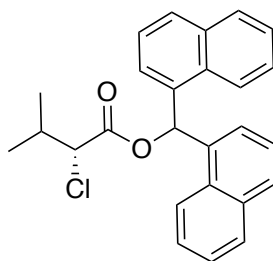


Di(naphthalen-1-yl)methyl (*S*)-2-chloro-3-methylbutanoate (**III-6-D**)

Prepared according to the general procedure, product was isolated as an off white solid (36 mg, 89%).

$^1\text{H-NMR}$ (CDCl_3 , 500 MHz): 8.48 (s, 1H), 8.00-7.85 (m, 6H), 7.52-7.38 (m, 8H), 4.22 (d, $J = 7.0$ Hz, 1H), 2.32-2.30 (m, 1H), 0.98 (d, $J = 7.5$ Hz, 6H).

$^{13}\text{C-NMR}$ (CDCl_3 , 125 MHz): 168.6, 134.2, 134.1, 133.8, 131.0, 130.9, 129.3, 129.3, 128.9, 126.8, 126.7, 126.0, 126.0, 126.0, 125.3, 125.2, 123.3, 72.3, 64.3, 32.4, 19.7, 18.0.

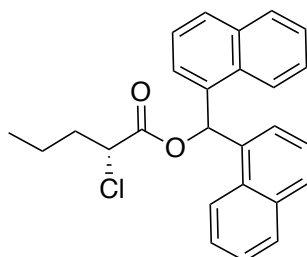


Di(naphthalen-1-yl)methyl (*R*)-2-chloro-3-methylbutanoate (**III-7-D**)

Prepared according to the general procedure, product was isolated as an off white solid (35 mg, 87%).

$^1\text{H-NMR}$ (CDCl_3 , 500 MHz): 8.48 (s, 1H), 8.00-7.85 (m, 6H), 7.52-7.38 (m, 8H), 4.22 (d, $J = 7.0$ Hz, 1H), 2.34-2.30 (m, 1H), 0.98 (d, $J = 7.5$ Hz, 6H).

$^{13}\text{C-NMR}$ (CDCl_3 , 125 MHz): 168.6, 134.2, 134.1, 133.8, 131.0, 130.9, 129.3, 129.3, 128.9, 126.8, 126.7, 126.0, 126.0, 125.9, 125.3, 125.2, 123.3, 72.3, 64.3, 32.4, 19.7, 18.0.

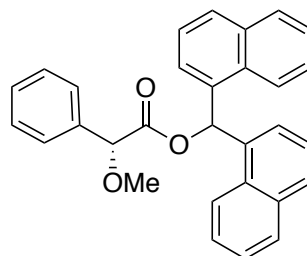


Di(naphthalen-1-yl)methyl (*R*)-2-chloropentanoate (**III-8-D**)

Prepared according to the general procedure, product was isolated as an off white solid (36 mg, 89%).

$^1\text{H-NMR}$ (CDCl_3 , 500 MHz): 8.44 (s, 1H), 7.96-7.85 (m, 6H), 7.51-7.40 (m, 8H), 4.38 (m, 1H), 2.02-1.89 (m, 2H), 1.46-1.35 (m, 2H), 0.87-0.84 (m, 3H).

$^{13}\text{C-NMR}$ (CDCl_3 , 125 MHz): 168.9, 134.1, 134.0, 133.8, 131.0, 129.4, 129.3, 128.7, 128.9, 126.8, 126.0, 125.9, 125.2, 123.3, 123.3, 72.4, 57.2, 36.6, 19.2, 13.2.

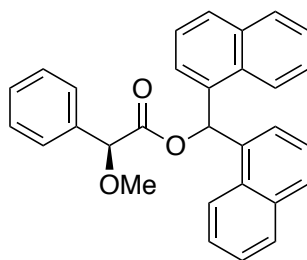


Di(naphthalen-1-yl)methyl (*R*)-2-methoxy-2-phenylacetate (**III-9-D**)

Prepared according to the general procedure, product was isolated as an off white solid (28 mg, 65%).

$^1\text{H-NMR}$ (CDCl_3 , 500 MHz): 8.43 (s, 1H), 8.06 (d, $J = 8.0$ Hz, 1H), 7.91-7.89 (m, 1H), 7.82-7.80 (m, 2H), 7.74 (d, $J = 8.5$ Hz, 1H), 7.61 (d, $J = 8.5$ Hz, 1H), 7.52-7.20 (m, 10H), 7.13-7.09 (m, 2H), 6.84 (d, $J = 7.5$ Hz, 1H), 4.89 (s, 1H), 3.38 (s, 3H).

$^{13}\text{C-NMR}$ (CDCl_3 , 125 MHz): 169.8, 135.8, 134.4, 134.0, 133.8, 133.6, 131.2, 130.7, 129.3, 128.9, 128.9, 129.8, 128.7, 128.6, 127.6, 126.9, 126.5, 126.4, 126.0, 125.7, 125.2, 125.0, 125.0, 123.4, 123.2, 82.6, 71.5, 57.3.

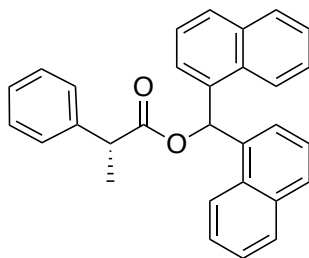


Di(naphthalen-1-yl)methyl (*S*)-2-methoxy-2-phenylacetate (**III-10-D**)

Prepared according to the general procedure, product was isolated as an off white solid (31 mg, 72%).

$^1\text{H-NMR}$ (CDCl_3 , 500 MHz): 8.40 (s, 1H), 8.06 (d, $J = 8.0$ Hz, 1H), 7.91-7.89 (m, 1H), 7.82-7.80 (m, 2H), 7.74 (d, $J = 8.5$ Hz, 1H), 7.61 (d, $J = 8.5$ Hz, 1H), 7.52-7.20 (m, 10H), 7.13-7.09 (m, 2H), 6.84 (d, $J = 7.5$ Hz, 1H), 4.87 (s, 1H), 3.38 (s, 3H).

$^{13}\text{C-NMR}$ (CDCl_3 , 125 MHz): 169.8, 135.8, 134.4, 134.0, 133.8, 133.6, 131.2, 130.7, 129.3, 128.9, 128.9, 129.8, 128.7, 128.6, 127.6, 126.9, 126.5, 126.4, 126.0, 125.7, 125.2, 125.0, 125.0, 123.4, 123.2, 82.6, 71.5, 57.3.

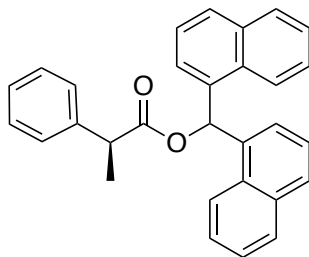


Di(naphthalen-1-yl)methyl (*R*)-2-phenylpropanoate (**III-11-D**)

Prepared according to the general procedure, product was isolated as an off white solid (34 mg, 82%).

$^1\text{H-NMR}$ (CDCl_3 , 500 MHz): 8.36 (s, 1H), 8.04 (d, $J = 7.5$ Hz, 1H), 7.91-7.89 (m, 1H), 7.83-7.81 (m, 2H), 7.76 (d, $J = 8.0$ Hz, 1H), 7.71 (d, $J = 8.5$ Hz, 1H), 7.53-7.38 (m, 2H), 7.42-7.39 (m, 3H), 7.30-7.24 (m, 6H), 7.20-7.17 (m, 1H), 7.14 (d, $J = 6.5$ Hz, 1H), 6.97 (d, $J = 7.5$ Hz, 1H), 3.85-3.84 (m, 1H), 1.53-1.52 (m, 3H).

$^{13}\text{C-NMR}$ (CDCl_3 , 125 MHz): 173.5, 140.0, 134.8, 134.5, 133.8, 133.7, 131.2, 130.8, 129.1, 128.9, 128.7, 129.6, 128.6, 128.6, 127.8, 127.2, 126.8, 126.4, 126.3, 125.9, 125.7, 125.2, 125.2, 125.1, 123.5, 123.3, 71.1, 45.6, 18.2.

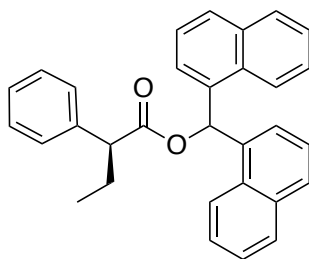


Di(naphthalen-1-yl)methyl (*S*)-2-phenylpropanoate (**III-12-D**)

Prepared according to the general procedure, product was isolated as an off white solid (36 mg, 86%).

$^1\text{H-NMR}$ (CDCl_3 , 500 MHz): 8.36 (s, 1H), 8.04 (d, $J = 7.5$ Hz, 1H), 7.91-7.89 (m, 1H), 7.83-7.81 (m, 2H), 7.76 (d, $J = 8.0$ Hz, 1H), 7.71 (d, $J = 8.5$ Hz, 1H), 7.53-7.38 (m, 2H), 7.42-7.39 (m, 3H), 7.30-7.24 (m, 6H), 7.20-7.17 (m, 1H), 7.14 (d, $J = 6.5$ Hz, 1H), 6.97 (d, $J = 7.5$ Hz, 1H), 3.86-3.83 (m, 1H), 1.54-1.53 (m, 3H).

$^{13}\text{C-NMR}$ (CDCl_3 , 125 MHz): 173.5, 140.0, 134.8, 134.6, 133.8, 133.7, 131.2, 130.8, 129.1, 128.9, 128.7, 128.7, 128.6, 127.8, 127.2, 126.8, 126.4, 126.3, 125.9, 125.7, 125.2, 125.2, 125.1, 123.5, 123.3, 71.1, 45.6, 18.2.

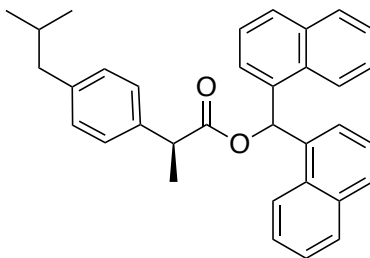


Di(naphthalen-1-yl)methyl (*S*)-2-phenylbutanoate (**III-13-D**)

Prepared according to the general procedure, product was isolated as an off white solid (35 mg, 81%).

$^1\text{H-NMR}$ (CDCl_3 , 500 MHz): 8.35 (s, 1H), 8.03 (d, $J = 8.0$ Hz, 1H), 7.91-7.89 (m, 1H), 7.83-7.81 (m, 2H), 7.76 (d, $J = 8.0$ Hz, 1H), 7.70 (d, $J = 8.0$ Hz, 1H), 7.53-7.46 (m, 2H), 7.42-7.39 (m, 3H), 7.30-7.24 (m, 6H), 7.18-7.12 (m, 2H), 6.97 (d, $J = 7.0$ Hz, 1H), 3.61 (t, $J = 7.5$ Hz, 1H), 2.20-2.14 (m, 1H), 1.85-1.79 (m, 1H), 0.92 (t, $J = 7$ Hz, 3H).

$^{13}\text{C-NMR}$ (CDCl_3 , 125 MHz): 173.1, 138.6, 134.9, 134.5, 133.8, 133.7, 131.2, 130.9, 129.1, 128.9, 128.7, 128.6, 128.6, 128.2, 127.3, 126.7, 126.4, 126.2, 125.9, 125.7, 125.2, 125.1, 123.5, 123.4, 71.0, 53.6, 26.2, 12.2.

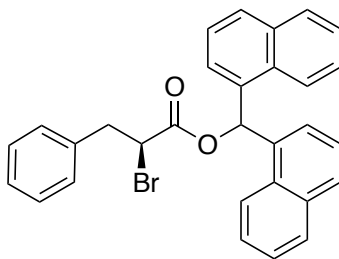


Di(naphthalen-1-yl)methyl (*S*)-2-(4-isobutylphenyl)propanoate (**III-14-D**)

Prepared according to the general procedure, product was isolated as an off white solid (36 mg, 76%).

$^1\text{H-NMR}$ (CDCl_3 , 500 MHz): 8.36 (s, 1H), 8.04 (d, $J = 8.0$ Hz, 1H), 7.91-7.89 (m, 1H), 7.83-7.80 (m, 2H), 7.76 (d, $J = 8.0$ Hz, 1H), 7.71 (d, $J = 8.5$ Hz, 1H), 7.52-7.47 (m, 2H), 7.42-7.39 (m, 1H), 7.29-7.26 (m, 2H), 7.18-7.12 (m, 4H), 7.05 (d, $J = 7.5$ Hz, 2H), 6.99 (d, $J = 6.5$ Hz, 1H), 3.84 (q, $J = 7.5$ Hz, 1H), 2.47 (d, $J = 6.5$ Hz, 2H), 1.88-1.83 (m, 1H), 1.52 (d, $J = 6.5$ Hz, 3H), 0.93 (d, $J = 6.5$ Hz, 6H).

$^{13}\text{C-NMR}$ (CDCl_3 , 125 MHz): 173.7, 140.7, 137.2, 134.9, 134.6, 133.8, 133.7, 131.2, 130.9, 129.3, 129.1, 128.9, 128.7, 128.6, 127.5, 126.7, 126.4, 126.3, 125.9, 125.7, 125.2, 125.2, 125.0, 123.5, 123.4, 70.9, 45.3, 45.1, 30.3, 22.4, 22.4, 18.2.

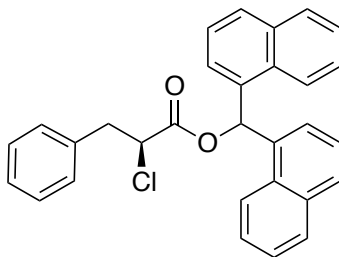


Di(naphthalen-1-yl)methyl (*S*)-2-bromo-3-phenylpropanoate (**III-15-D**)

Prepared according to the general procedure, product was isolated as an off white solid (30 mg, 61%).

$^1\text{H-NMR}$ (CDCl_3 , 500 MHz): 8.33 (s, 1H), 7.92-7.89 (m, 2H), 7.87-7.84 (m, 2H), 7.81 (d, $J = 7.5$ Hz, 1H), 7.68 (d, $J = 8$ Hz, 1H), 7.51-7.44 (m, 3H), 7.38-7.23 (m, 5H), 7.21-7.18 (m, 2H), 7.10-7.09 (m, 3H), 4.55-4.51 (m, 1 H), 3.52- 3.47 (m, 1H), 3.26-3.22 (m, 1H).

$^{13}\text{C-NMR}$ (CDCl_3 , 125 MHz): 168.5, 136.5, 133.9, 133.8, 133.8, 133.7, 131.0, 130.8, 129.3, 129.3, 129.1, 128.9, 128.8, 128.7, 127.3, 126.8, 126.7, 126.5, 125.9, 125.8, 125.6, 125.3, 125.2, 123.4, 123.2, 72.5, 44.7, 41.0.



Di(naphthalen-1-yl)methyl (*S*)-2-chloro-3-phenylpropanoate (**III-16-D**)

Prepared according to the general procedure, product was isolated as an off white solid (31 mg, 69%).

$^1\text{H-NMR}$ (CDCl_3 , 500 MHz): 8.38 (s, 1H), 7.93-7.81 (m, 5H), 7.76 (d, $J = 8.5$ Hz, 1H), 7.50-7.45 (m, 3H), 7.38-7.29 (m, 4H), 7.24-7.16 (m, 3H), 7.10- 7.09(m, 2H), 4.57-4.54 (m, 1 H), 3.41-3.37 (m, 1H), 3.18-3.14 (m, 1H).

$^{13}\text{C-NMR}$ (CDCl_3 , 125 MHz): 168.4, 135.6, 133.9, 133.8, 133.7, 131.0, 130.8, 129.4, 129.3, 129.2, 128.9, 128.9, 128.6, 127.3, 126.9, 126.7, 126.0, 126.0, 125.9, 125.7, 125.3, 125.2, 123.3, 123.2, 72.6, 57.0 40.9.

III.7.5 Molecular modeling and CD calculations (represented with III-12-D)

Conformational searches of the derivatized carboxylic acids were performed with CONFLEX7 (Ver. 7.A.0910 by CONFLEX, Tokyo)²⁷⁻²⁸ using a commercially available PC (operating system: Windows7 Professional SP1 64-bit, CPU: QuadCore Xeon E3-1225 processor 3.10 GHz, RAM 8 GB). DFT calculations were conducted with Gaussian09 (Revision D.01 by Gaussian, Wallingford, CT)²⁹ with a PC (operating system: CentOS a Linux, CPU: Intel Xeon E5-2643 v3 processors 3.4 GHz, 6-Core, RAM 32 GB).

Theoretical CD spectrum of **III-12-D** was obtained from a typical calculation procedure described as follows.³⁰⁻³¹ The initial structure was constructed on a graphical user interface considering the absolute configurations of interest and subjected to a conformational search with CONFLEX7 using MMFF94S (2010-12-04HG) as the force field, where initial stable conformers were generated for up to 50 kcal/mol. Of the 76 stable conformers obtained, the best 9 (all with >1% of abundance (conformer codes in table below were named as c01-09) were further optimized by DFT (hybrid B3LYP functional and the double-zeta 6-31G(d) basis set). Boltzmann distribution of populations at 298 K was calculated based on internal energies and vibrational corrections (see the table below). The energies and dipole moments of the optimized conformers were carefully examined leading to the convergence of some (c05 and c08) into one. The 4 stable conformers (c01, c02, c04, and c09), yielding total abundance >90%, were subject to time-dependent simulations at the double-zeta approximation level using the cc-pVDZ basis set and hybrid functional B3LYP. For each conformer, the resultant rotational strengths were converted into Gaussian curves (bandwidth sigma = 3000 cm⁻¹) and

summed to give the CD spectrum (**Figure III-13**). The theoretical CD spectra for the substrate were integrated based on the Boltzmann distribution to give the final theoretical CD spectrum (**Figure III-5**).

Code	Stability Order	Energy in Hartree	(Relative)	Energy in kcal/mol	$\exp(-\Delta G_i/RT)$	Population (%)	Dipole Moment (Debye)	Helicity
c01	1	-1307.740478	0.000000	0.000	1.0000	66.8	1.58	P
c02	2	-1307.738654	0.001824	1.145	0.1449	9.7	1.53	P
c03		-1307.737679	0.002799	1.756	0.0516	3.4	1.93	M
c04	3	-1307.738653	0.001825	1.145	0.1447	9.7	1.53	M
c05		-1307.737090	0.003388	2.126	0.0276	1.8	1.78	P
c06		-1307.737481	0.002997	1.881	0.0418	2.8	1.51	P
c07		-1307.736503	0.003975	2.494	0.0148	1.0	1.65	M
c09	4	-1307.733423	0.007055	4.427	0.0718	4.8	1.75	M
					1.4973	100.0		

Table III-3. Summarized calculation data.

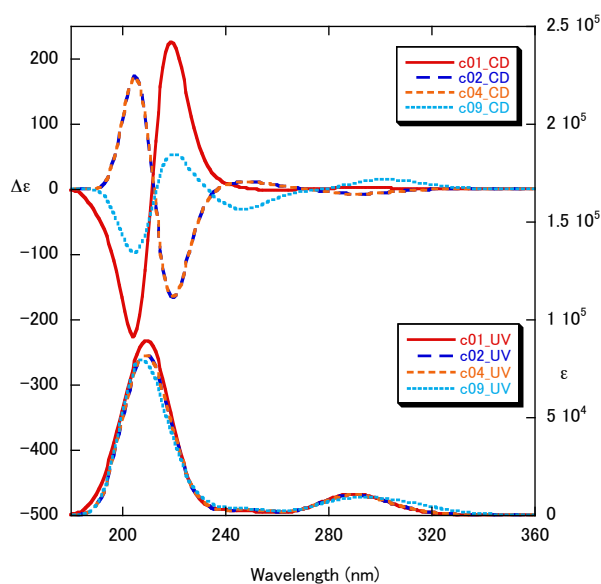


Figure III-13. Theoretical CD spectra of **III-12-D** conformers calculated at B3LYP/cc-pVDZ level.

III.7.6 Crystal structure

Single colourless needle-shaped crystals of **III-12-D** were used. A suitable crystal (0.33×0.15×0.12) was selected and mounted on a nylon loop with paratone oil on a Bruker APEX-II CCD diffractometer. The crystal was kept at $T = 173(2)$ K during data collection.

Using Olex2 (Dolomanov et al., 2009), the structure was solved with the ShelXS (Sheldrick, 2008) structure solution program, using the Direct Methods solution method. The model was refined with version 2014/6 of XL (Sheldrick, 2008) using Least Squares minimisation.

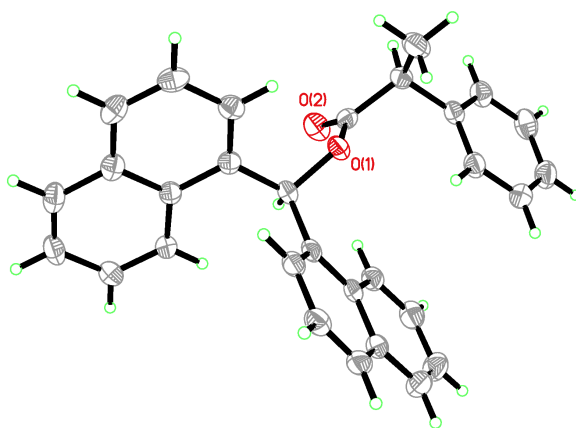


Figure III-14. Crystal structure of III-12-D.

Compound	III-12-D
Formula	C ₃₀ H ₂₄ O ₂
$D_{calc.}/g\text{ cm}^{-3}$	1.263
$/\text{mm}^{-1}$	0.606
Formula Weight	416.49
Colour	colourless
Shape	needle
Max Size/mm	0.33
Mid Size/mm	0.15
Min Size/mm	0.12
T/K	173(2)
Crystal System	orthorhombic
Flack Parameter	0.20(9)
Hooft Parameter	0.22(9)
Space Group	P2 ₁ 2 ₁ 2 ₁
$a/\text{\AA}$	7.05970(10)
$b/\text{\AA}$	17.2231(2)
$c/\text{\AA}$	18.0131(2)
α°	90
β°	90
γ°	90
$V/\text{\AA}^3$	2190.21(5)
Z	4
Z'	1
Θ_{min}°	3.550
Θ_{max}°	72.159
Measured Refl.	17383
Independent Refl.	4230
Reflections Used	4044
R_{int}	0.0356
Parameters	290
Restraints	0
Largest Peak	0.147
Deepest Hole	-0.168
GooF	1.053
wR_2 (all data)	0.0771
wR_2	0.0758
R_1 (all data)	0.0314
R_1	0.0297

Table III-4. Crystal data and structure refinement for **III-12-D**.

Atom	x	y	z	U_{eq}
O1	2011.3(18)	453.7(7)	6150.1(6)	26.5(3)
O2	-24(2)	245.3(8)	7091.1(7)	37.6(3)
C1	3544(3)	1742.7(12)	6819.4(12)	38.0(5)
C2	1524(3)	1488.8(10)	7003.5(10)	28.9(4)
C3	1073(3)	659.3(10)	6774.1(9)	25.5(4)
C4	1631(2)	-320.3(9)	5852.1(9)	23.5(3)
C5	46(3)	2029.7(10)	6662.1(9)	26.1(3)
C6	-1076(3)	2496.1(11)	7111.5(11)	33.0(4)
C7	-2413(3)	2987.8(12)	6801.3(12)	38.3(4)
C8	-2669(3)	3005.1(12)	6041.2(12)	39.2(5)
C9	-1559(3)	2542.7(11)	5589.9(11)	38.1(5)
C10	-201(3)	2061.7(10)	5896.6(10)	31.0(4)
C11	1509(2)	-226.4(9)	5012.4(9)	23.9(3)
C12	2995(3)	-440.7(10)	4569.2(10)	26.8(4)
C13	2932(3)	-344.9(10)	3790.6(10)	30.4(4)
C14	1364(3)	-37.5(10)	3467(1)	32.3(4)
C15	-204(3)	201.1(10)	3900.3(10)	29.5(4)
C16	-1813(3)	556.6(12)	3574.2(11)	38.8(5)
C17	-3270(3)	819.9(13)	3994.6(13)	42.3(5)
C18	-3233(3)	726.1(12)	4769.2(12)	36.9(4)
C19	-1720(3)	374.4(10)	5107.4(10)	29.2(4)
C20	-143(3)	109.3(9)	4688.6(9)	24.9(3)
C21	3153(2)	-880.4(10)	6104.4(9)	24.3(3)
C22	4864(3)	-627.9(10)	6367.9(9)	28.1(4)
C23	6312(3)	-1158.9(12)	6558.5(10)	31.9(4)
C24	6028(3)	-1938.6(12)	6484.6(11)	32.8(4)
C25	4269(3)	-2227.9(11)	6223.4(9)	27.7(4)
C26	3946(3)	-3036.0(11)	6141.6(11)	34.5(4)
C27	2260(3)	-3308.7(11)	5878.5(11)	36.3(4)
C28	814(3)	-2786.4(11)	5680.1(11)	32.6(4)
C29	1078(3)	-2001.8(10)	5750.1(10)	27.3(4)
C30	2807(2)	-1696.8(10)	6027.7(9)	23.7(3)

Table III-5. Fractional atomic coordinates ($\times 10^4$) and equivalent isotropic displacement parameters ($\text{\AA}^2 \times 10^3$) for **III-12-D**. U_{eq} is defined as 1/3 of the trace of the orthogonalised U_{ij} .

III.7.7 ECCD spectra of III-1 derivatized chiral carboxylic acids

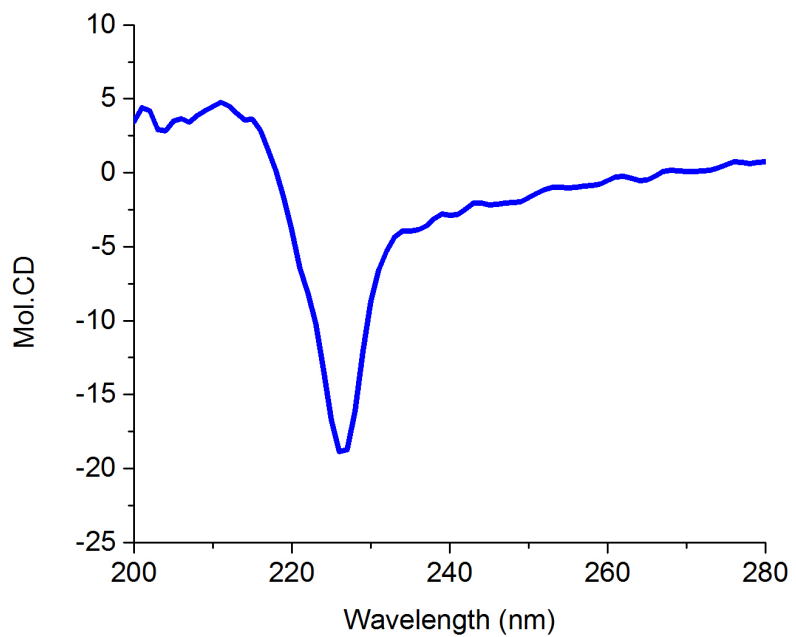
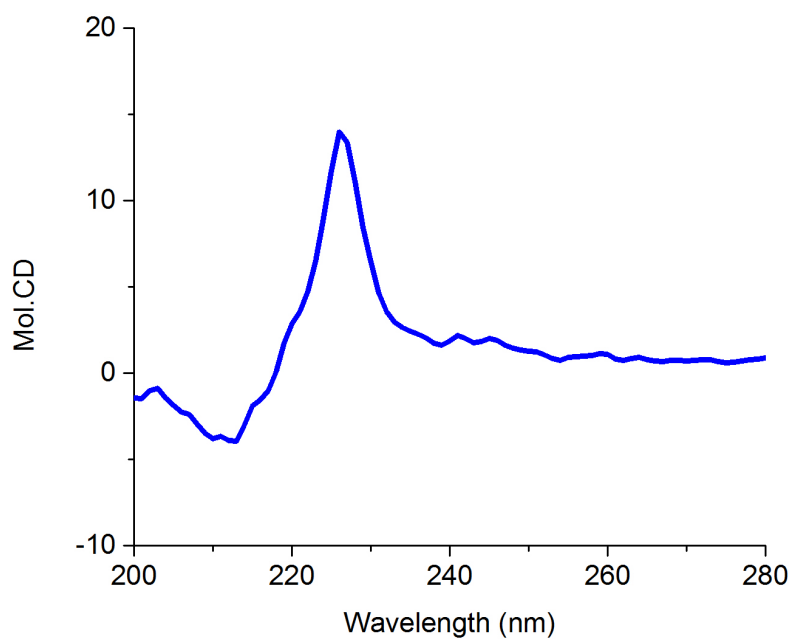


Figure III-15. ECCD spectra of III-1 derivatized chiral carboxylic acids.

Figure III-15 (cont'd)

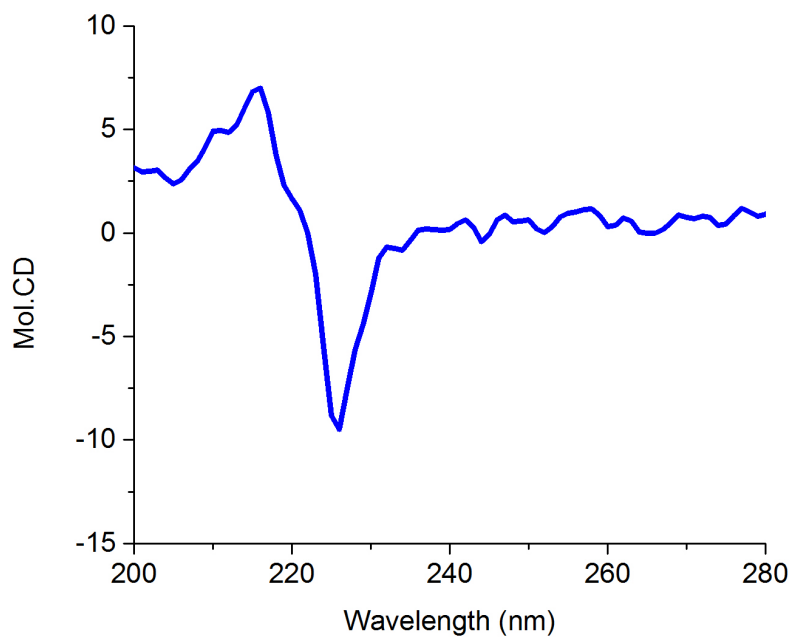
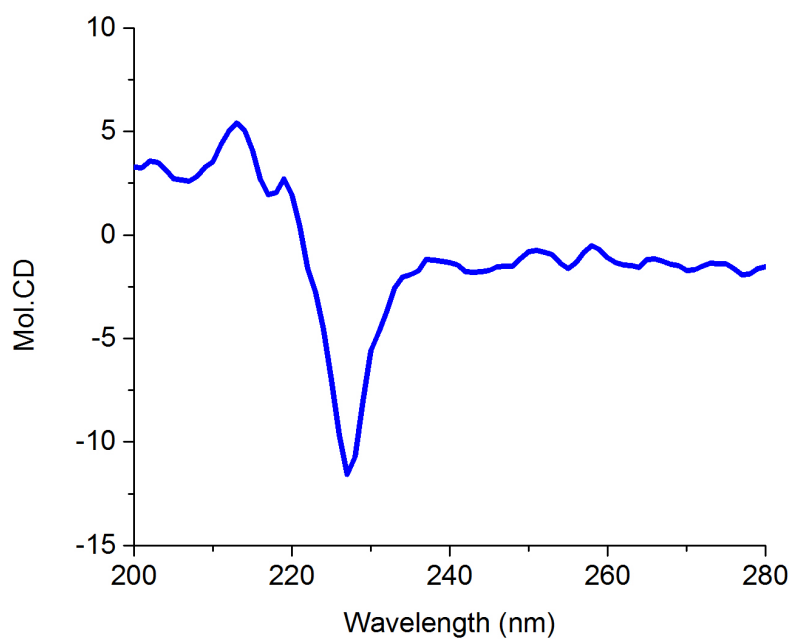


Figure III-15 (cont'd)

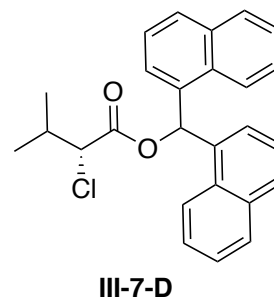
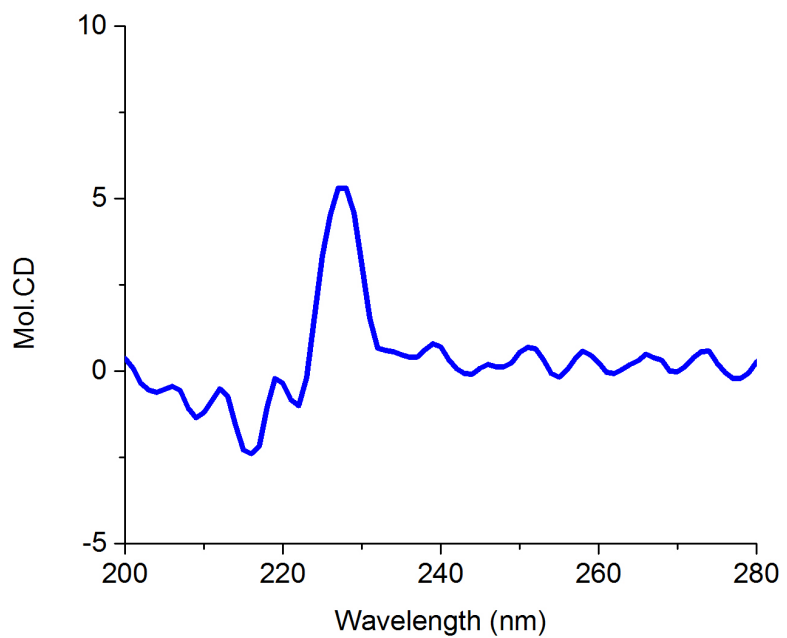
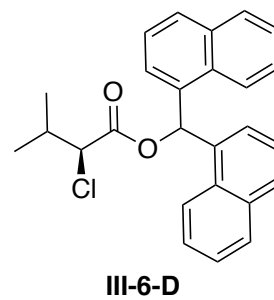
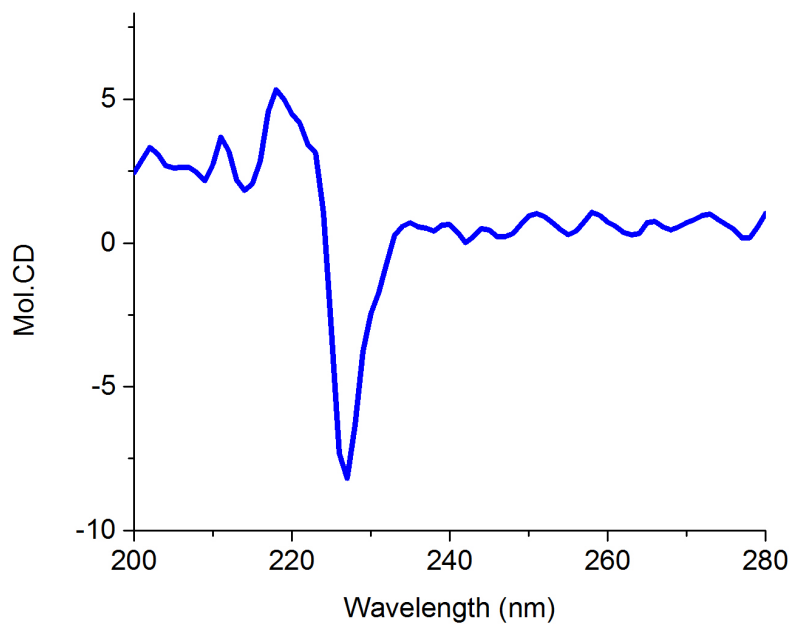


Figure III-15 (cont'd)

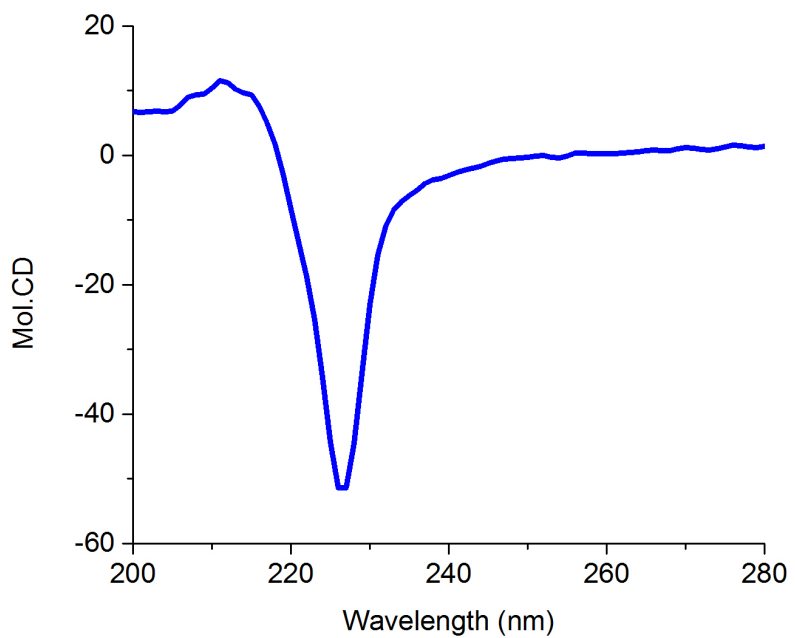
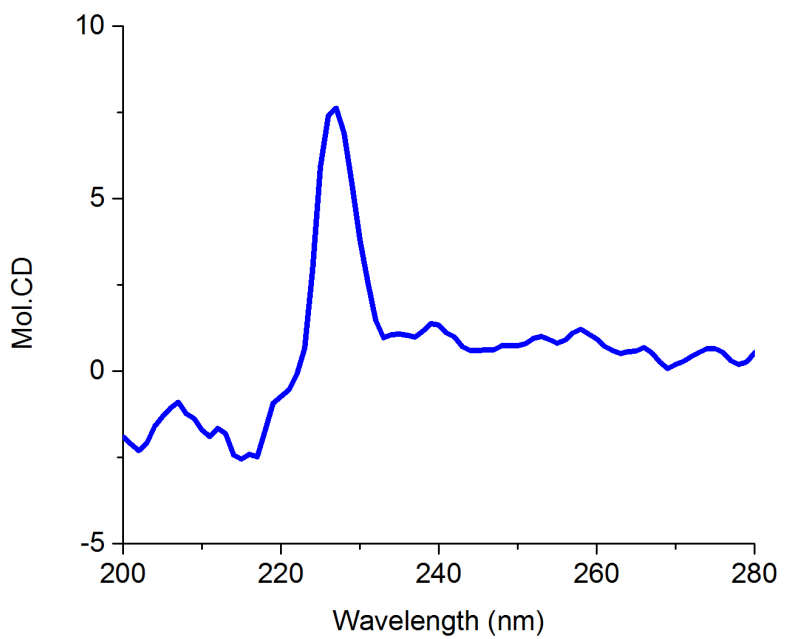


Figure III-15 (cont'd)

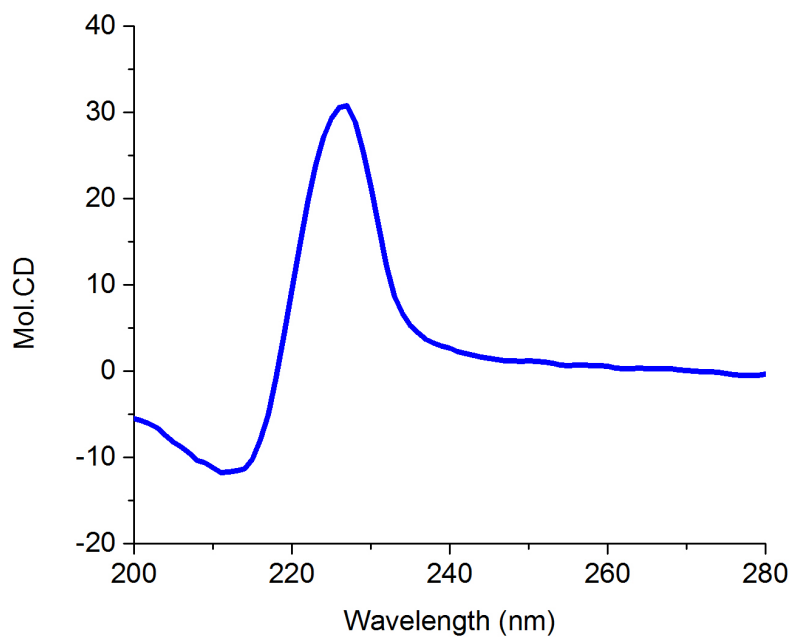
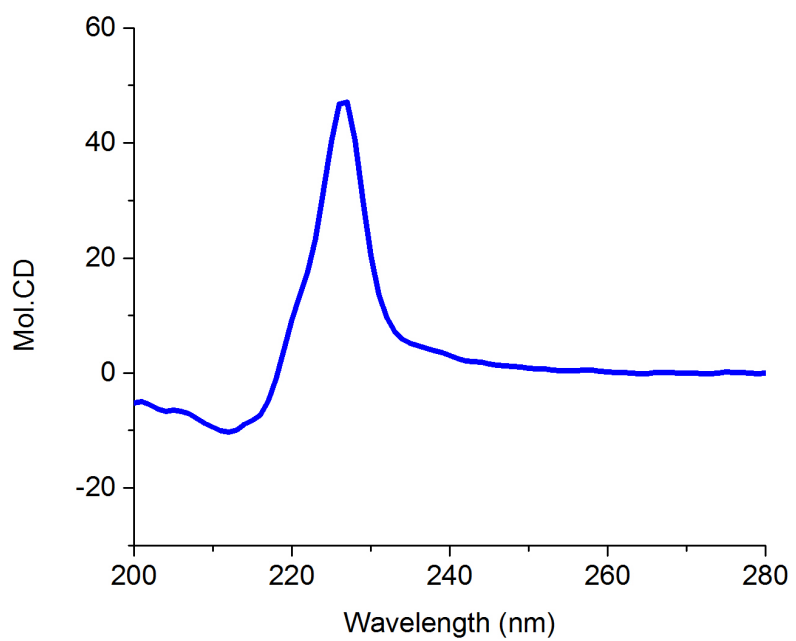


Figure III-15 (cont'd)

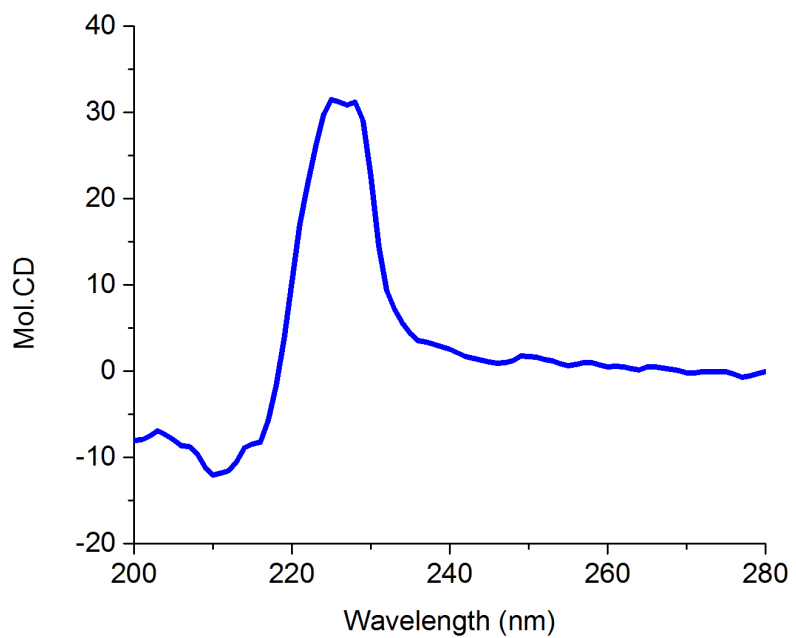
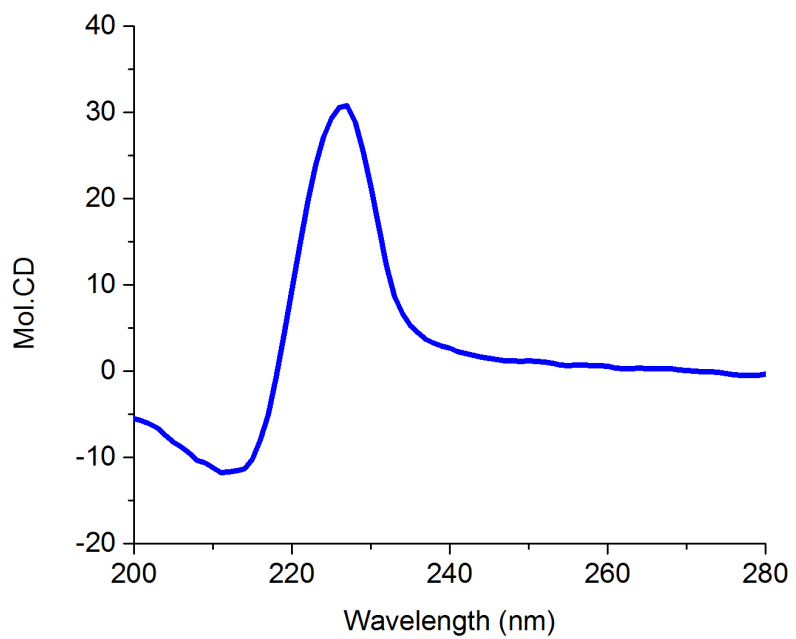


Figure III-15 (cont'd)

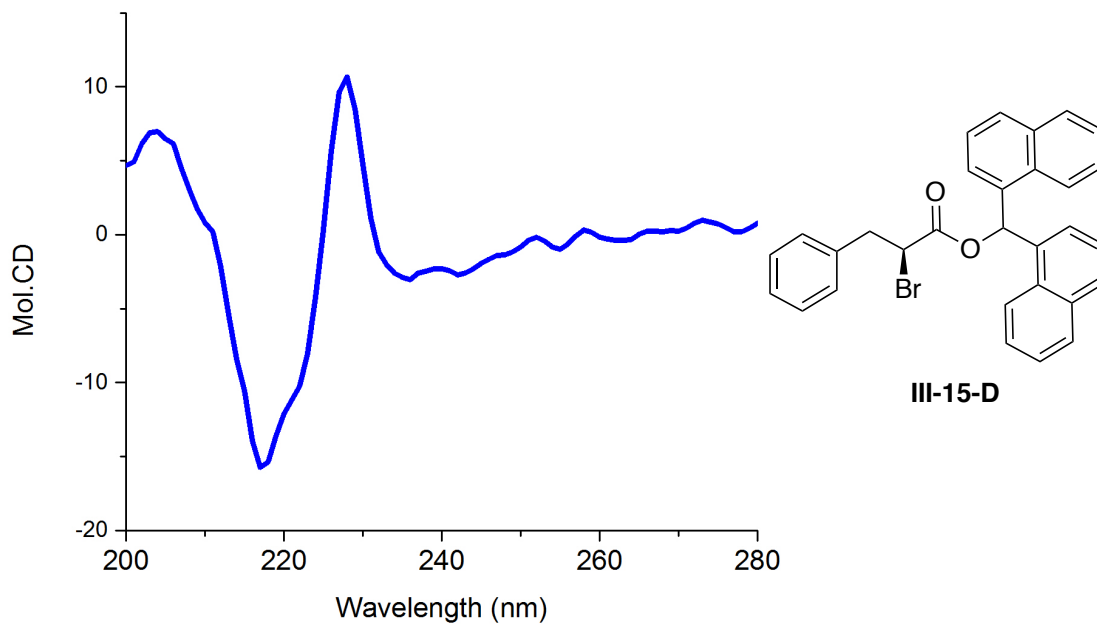
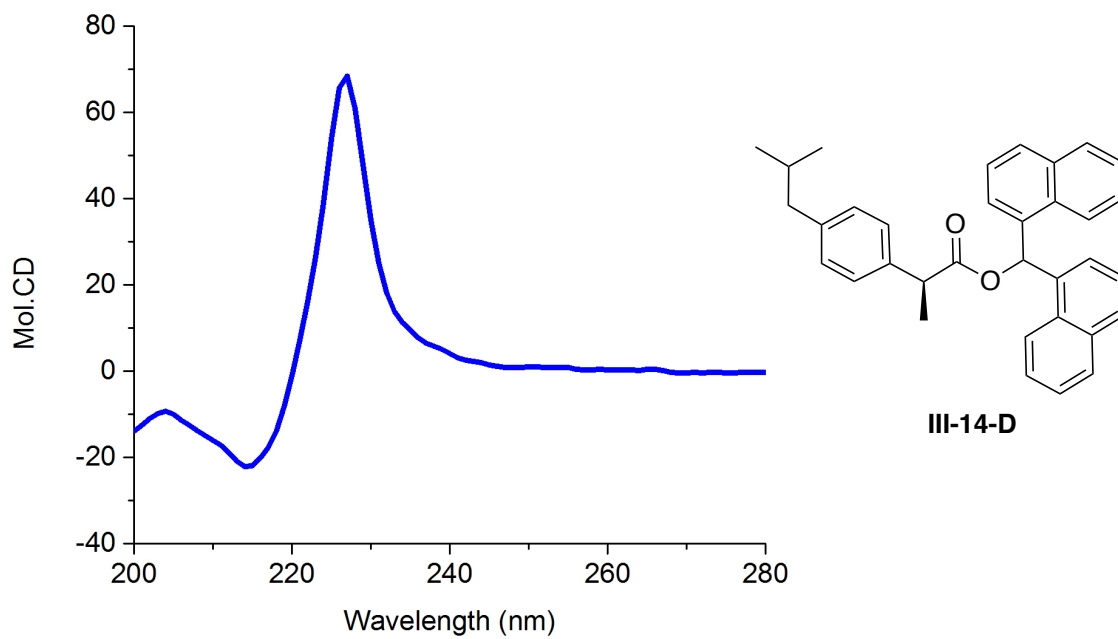
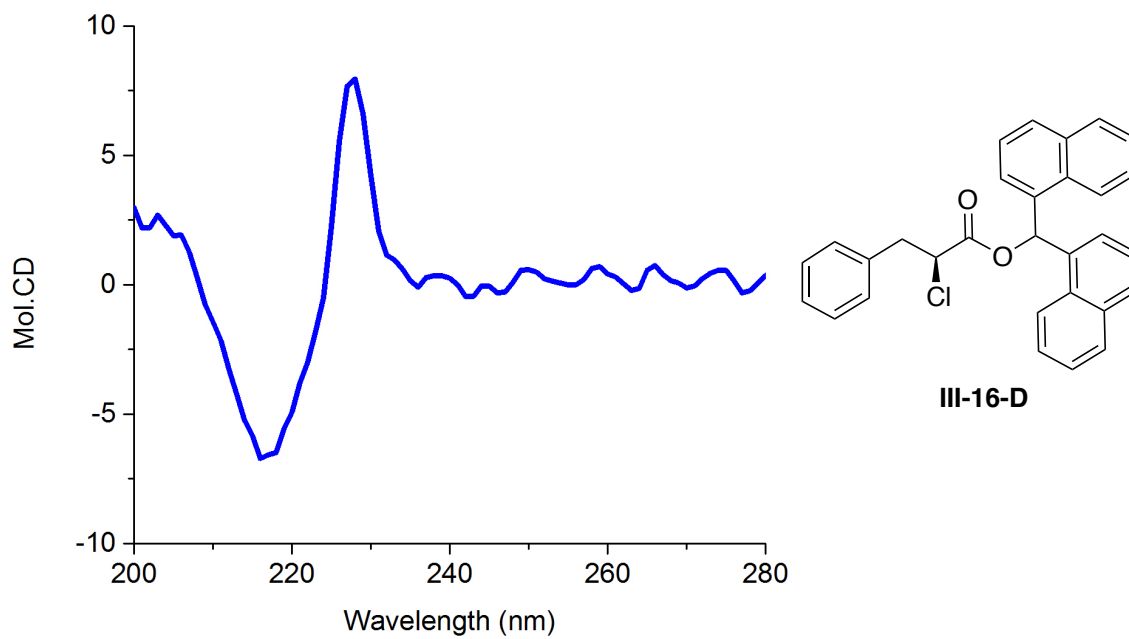


Figure III-15 (cont'd)



REFERENCES

REFERENCES

1. Smith, J. M.; Qin, T.; Merchant, R. R.; Edwards, J. T.; Malins, L. R.; Liu, Z. Q.; Che, G. D.; Shen, Z. C.; Shaw, S. A.; Eastgate, M. D.; Baran, P. S., Decarboxylative Alkynylation. *Angew Chem Int Edit* **2017**, *56* (39), 11906-11910.
2. Edwards, J. T.; Merchant, R. R.; McClymont, K. S.; Knouse, K. W.; Qin, T.; Malins, L. R.; Vokits, B.; Shaw, S. A.; Bao, D. H.; Wei, F. L.; Zhou, T.; Eastgate, M. D.; Baran, P. S., Decarboxylative alkenylation. *Nature* **2017**, *545* (7653), 213-218.
3. Li, C.; Wang, J.; Barton, L. M.; Yu, S.; Tian, M. Q.; Peters, D. S.; Kumar, M.; Yu, A. W.; Johnson, K. A.; Chatterjee, A. K.; Yan, M.; Baran, P. S., Decarboxylative borylation. *Science* **2017**, *356* (6342), aam7355.
4. Perkowski, A. J.; Nicewicz, D. A., Direct Catalytic Anti-Markovnikov Addition of Carboxylic Acids to Alkenes. *J Am Chem Soc* **2013**, *135* (28), 10334-10337.
5. Zhou, Y. J.; Bandar, J. S.; Buchwald, S. L., Enantioselective CuH-Catalyzed Hydroacylation Employing Unsaturated Carboxylic Acids as Aldehyde Surrogates. *J Am Chem Soc* **2017**, *139* (24), 8126-8129.
6. You, L.; Zha, D. J.; Anslyn, E. V., Recent Advances in Supramolecular Analytical Chemistry Using Optical Sensing. *Chem Rev* **2015**, *115* (15), 7840-7892.
7. Yashima, E.; Nimura, T.; Matsushima, T.; Okamoto, Y., Poly ((4-dihydroxyborophenyl) acetylene) as a novel probe for chirality and structural assignments of various kinds of molecules including carbohydrates and steroids by circular dichroism. *J Am Chem Soc* **1996**, *118* (40), 9800-9801.
8. Zahn, S.; Canary, J. W., Electron-induced inversion of helical chirality in copper complexes of N, N-dialkylmethionines. *Science* **2000**, *288*, 1404-1407.
9. Mazaleyrat, J.-P.; Wright, K.; Gaucher, A.; Toulemonde, N.; Wakselman, M.; Oancea, S.; Peggion, C.; Formaggio, F.; Setnicka, V.; Keiderling, T. A., Induced axial chirality in the biphenyl core of the Ca-tetrasubstituted α -amino acid residue Bip and subsequent propagation of chirality in (Bip) n/Val oligopeptides. *J Am Chem Soc* **2004**, *126* (40), 12874-12879.
10. Pira, S. L.; Wallace, T. W.; Graham, J. P., Enantioselective Route to 5-Methyl-and 5, 7-Dimethyl-6, 7-dihydro-5 H-dibenz [c, e] azepine: Secondary Amines with Switchable Axial Chirality. *Org Lett* **2009**, *11* (7), 1663-1666.
11. Yu, S.; Pu, L., Pseudoenantiomeric fluorescent sensors in a chiral assay. *J Am Chem Soc* **2010**, *132* (50), 17698-17700.

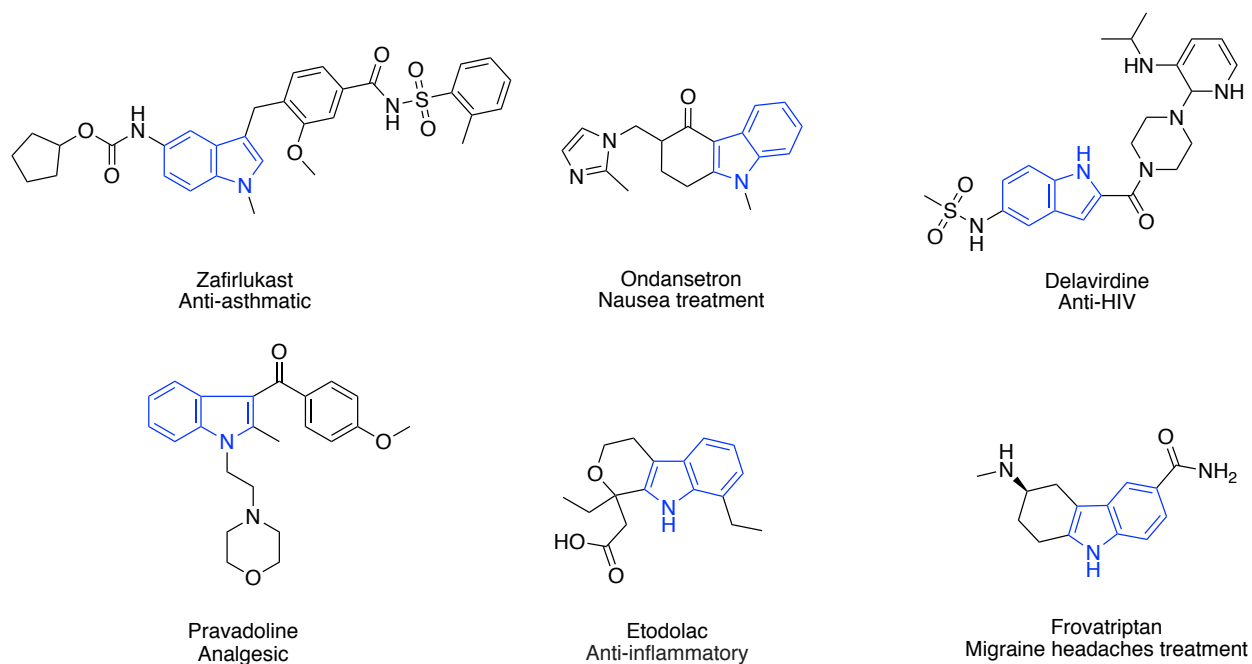
12. Kuwahara, S.; Nakamura, M.; Yamaguchi, A.; Ikeda, M.; Habata, Y., Combination of a new chiroptical probe and theoretical calculations for chirality detection of primary amines. *Org Lett* **2013**, *15* (22), 5738-5741.
13. Seo, M.-S.; Lee, A.; Kim, H., 2, 2'-Dihydroxybenzil: A Stereodynamic Probe for Primary Amines Controlled by Steric Strain. *Org Lett* **2014**, *16* (11), 2950-2953.
14. Zhang, P.; Wolf, C., Sensing of the concentration and enantiomeric excess of chiral compounds with tropos ligand derived metal complexes. *Chem Comm* **2013**, *49* (62), 7010-7012.
15. Superchi, S.; Bisaccia, R.; Casarini, D.; Laurita, A.; Rosini, C., Flexible biphenyl chromophore as a circular dichroism probe for assignment of the absolute configuration of carboxylic acids. *J Am Chem Soc* **2006**, *128* (21), 6893-6902.
16. Joyce, L. A.; Maynor, M. S.; Dragna, J. M.; da Cruz, G. M.; Lynch, V. M.; Canary, J. W.; Anslyn, E. V., A simple method for the determination of enantiomeric excess and identity of chiral carboxylic acids. *J Am Chem Soc* **2011**, *133* (34), 13746-13752.
17. Tanasova, M.; Anyika, M.; Borhan, B., Sensing Remote Chirality: Stereochemical Determination of beta-, gamma-, and delta-Chiral Carboxylic Acids. *Angew Chem Int Edit* **2015**, *54* (14), 4274-4278.
18. Mei, X.; Wolf, C., Enantioselective sensing of chiral carboxylic acids. *J Am Chem Soc* **2004**, *126* (45), 14736-14737.
19. Akdeniz, A.; Mosca, L.; Minami, T.; Anzenbacher, P., Sensing of enantiomeric excess in chiral carboxylic acids. *Chem Comm* **2015**, *51* (26), 5770-5773.
20. Yang, X.; Birman, V. B., Homobenzotetramisole-Catalyzed Kinetic Resolution of α -Aryl-, α -Aryloxy-, and α -Arylthioalkanoic Acids. *Adv Syn Cat* **2009**, *351* (14), 2301.
21. Shiina, I.; Nakata, K.; Ono, K.; Onda, Y.-s.; Itagaki, M., Kinetic resolution of racemic α -arylalkanoic acids with achiral alcohols via the asymmetric esterification using carboxylic anhydrides and acyl-transfer catalysts. *J Am Chem Soc* **2010**, *132* (33), 11629-11641.
22. Yang, X.; Birman, V. B., Kinetic Resolution of α -Substituted Alkanoic Acids Promoted by Homobenzotetramisole. *Chem Euro J* **2011**, *17* (40), 11296-11304.
23. Nakata, K.; Gotoh, K.; Ono, K.; Futami, K.; Shiina, I., Kinetic resolution of racemic 2-hydroxy- γ -butyrolactones by asymmetric esterification using diphenylacetic acid with pivalic anhydride and a chiral acyl-transfer catalyst. *Org Lett* **2013**, *15* (6), 1170-1173.

24. Tartaglia, S.; Pace, F.; Scafato, P.; Rosini, C., A New Case of Induced Helical Chirality in a Bichromophoric System: Absolute Configuration of Transparent and Flexible Diols from the Analysis of the Electronic Circular Dichroism Spectra of the Corresponding Di(1-naphthyl)ketals. *Org Lett* **2008**, *10* (16), 3421-3424.
25. Harada, N.; Nakanishi, K. j., *Circular dichroic spectroscopy : exciton coupling in organic stereochemistry*. University Science Books: Mill Valley, CA, 1983.
26. Bassas, O.; Huuskonen, J.; Rissanen, K.; Koskinen, A. M. P., A Simple Organocatalytic Enantioselective Synthesis of Pregabalin. *Euro J Org Chem* **2009**, (9), 1340-1351.
27. Goto, H.; Osawa, E., Corner Flapping - a Simple and Fast Algorithm for Exhaustive Generation of Ring Conformations. *J Am Chem Soc* **1989**, *111* (24), 8950-8951.
28. Goto, H.; Osawa, E., An Efficient Algorithm for Searching Low-Energy Conformers of Cyclic and Acyclic Molecules. *J Chem Soc Perk T 2* **1993**, (2), 187-198.
29. M. J. Frisch, G. W. T., H. B. Schlegel, G. E. Scuseria, M. A. Robb, J. R. Cheeseman, G. Scalmani, V. Barone, B. Mennucci, G. A. Petersson, H. Nakatsuji, M. Caricato, X. Li, H. P. Hratchian, A. F. Izmaylov, J. Bloino, G. Zheng, J. L. Sonnenberg, M. Hada, M. Ehara, K. Toyota, R. Fukuda, J. Hasegawa, M. Ishida, T. Nakajima, Y. Honda, O. Kitao, H. Nakai, T. Vreven, J. A. Montgomery, Jr., J. E. Peralta, F. Ogliaro, M. Bearpark, J. J. Heyd, E. Brothers, K. N. Kudin, V. N. Staroverov, T. Keith, R. Kobayashi, J. Normand, K. Raghavachari, A. Rendell, J. C. Burant, S. S. Iyengar, J. Tomasi, M. Cossi, N. Rega, J. M. Millam, M. Klene, J. E. Knox, J. B. Cross, V. Bakken, C. Adamo, J. Jaramillo, R. Gomperts, R. E. Stratmann, O. Yazyev, A. J. Austin, R. Cammi, C. Pomelli, J. W. Ochterski, R. L. Martin, K. Morokuma, V. G. Zakrzewski, G. A. Voth, P. Salvador, J. J. Dannenberg, S. Dapprich, A. D. Daniels, O. Farkas, J. B. Foresman, J. V. Ortiz, J. Cioslowski, and D. J. Fox, Gaussian 09, Revision D.01. Gaussian, Inc., Wallingford CT, : 2013.
30. Bringmann, G.; Bruhn, T.; Maksimenka, K.; Hemberger, Y., The Assignment of Absolute Stereostructures through Quantum Chemical Circular Dichroism Calculations. *Euro J Org Chem* **2009**, (17), 2717-2727.
31. Matsumoto, K.; Inagaki, T.; Nehira, T.; Kannami, M.; Inokuchi, D.; Kurata, H.; Kawase, T.; Pescitelli, G.; Oda, M., Phenyl-(2-pyridyl)-(3-pyridyl)-(4-pyridyl)methane: Synthesis, chiroptical properties, and theoretical calculation of its absolute configuration. *Chem-Asian J* **2007**, *2* (8), 1031-1036.

Chapter IV: Tuning Indole Oxidation by Copper Catalyst

IV.1. Introduction

Indole alkaloids, one of the most important natural product families, exhibit unique biological activities and have therefore attracted significant attention. The construction of highly functionalized indoles is prevalent among the pharmaceutical industry and medicinal chemistry. Due in part to the fact that the indole core is presented in several marketed drugs (**Scheme IV-1**), exploring organic methodologies to functionalize indoles is highly desired.¹⁻²



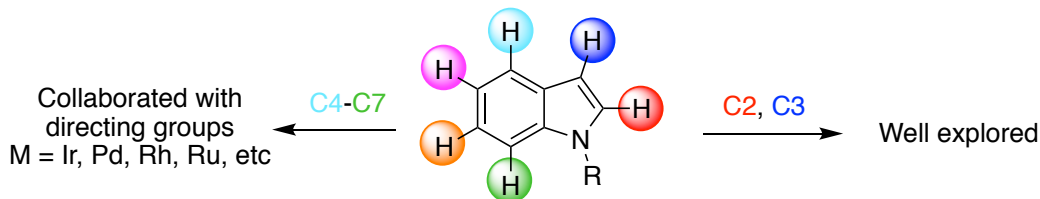
Scheme IV-1. Selected marketed drugs with indole core.

Over the years, extensive effort has been directed towards functionalizing the indole core via C-H activation on different positions via metal catalyst, nucleophilic C2 functionalization, indole core construction, indole natural product synthesis and others.³⁻

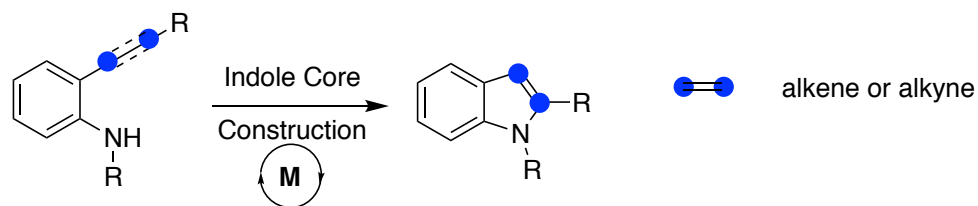
¹⁰ As shown in **Scheme IV-2**, various positions on the indole have been explored. C2 and

C3 indole chemistry has been well developed while the functionalization of the less reactive C4 to C7 indole positions remains more challenging. In recent years, this problem was tackled via directing group assisted metal catalyzed C-H functionalization reactions.¹¹ Directing groups located on either N or C3 positions can coordinate with the metal, approaching the specific positions on the indole backbone. Another area of the emphasis has been the indole core construction. A number of new methodologies via metal catalyzed cyclization reactions were developed in recent years.

Indole functionalization at various positions:



Indole core construction:



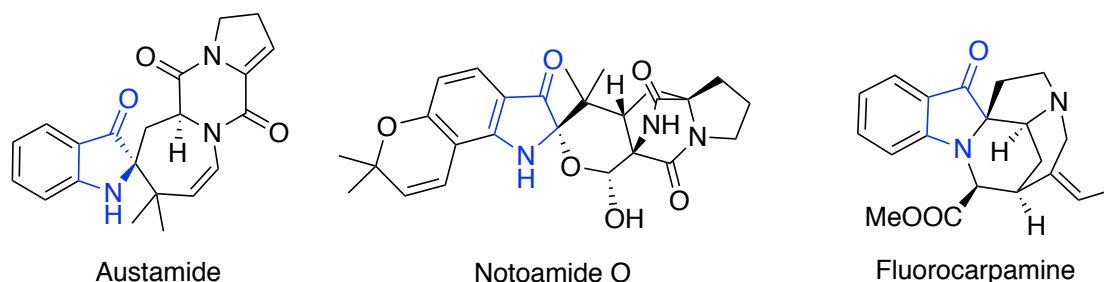
Scheme IV-2. Selected indole functionalization reactions.

Some of the less explored areas of indole chemistry involve the direct dearomatization of indole to oxindole and allylic C2 functionalization reaction.¹²⁻¹⁴ In this chapter, we will focus on an unanticipated discovery that leads to the development of an indole dearomatization reaction and selective C-H functionalization reaction.

IV.1.1. Intramolecular oxindole core construction

Oxindole is one of the dearomatized forms of indole. Substituted carbonyls can be located either on 2 or 3 positions. Some of the oxindoles also exhibit biological activity

that have attracted the attention of synthetic chemists (**Scheme IV-3**).¹⁵⁻¹⁶ However, there are not many recent methodologies to synthesize oxindole through the dearomatization pathway.¹⁷⁻¹⁹ Both intramolecular and intermolecular approaches to synthesize 3-oxindole will be discussed below.



Scheme IV-3. Biologically active compounds which contain 3-oxindole moiety.

Visible light induced aerobic oxidation to synthesize 3-oxindole intramolecularly was reported by Zhu's group.²⁰ The reaction and proposed mechanism are shown in **Figure IV-1**. In presence of 2 mol % $\text{Ru}(\text{bpy})_3\text{Cl}_2$ photo catalyst and light, indole can be dearomatized into 3-oxindole. The mechanism begins with the excited state of the photocatalyst inducing a single electron oxidation of the indole **IV-1** to yield the indoyl radical **IV-1-a**. Meanwhile, a superoxide anion generated from molecular oxygen reacts with the indoyl radical **IV-1-a** to afford intermediate **IV-1-b**. Intramolecular nucleophilic attack from the hydroxyl group on the indole leads to the intermediate **IV-1-c**. After dehydration, final product **IV-2** can be obtained.

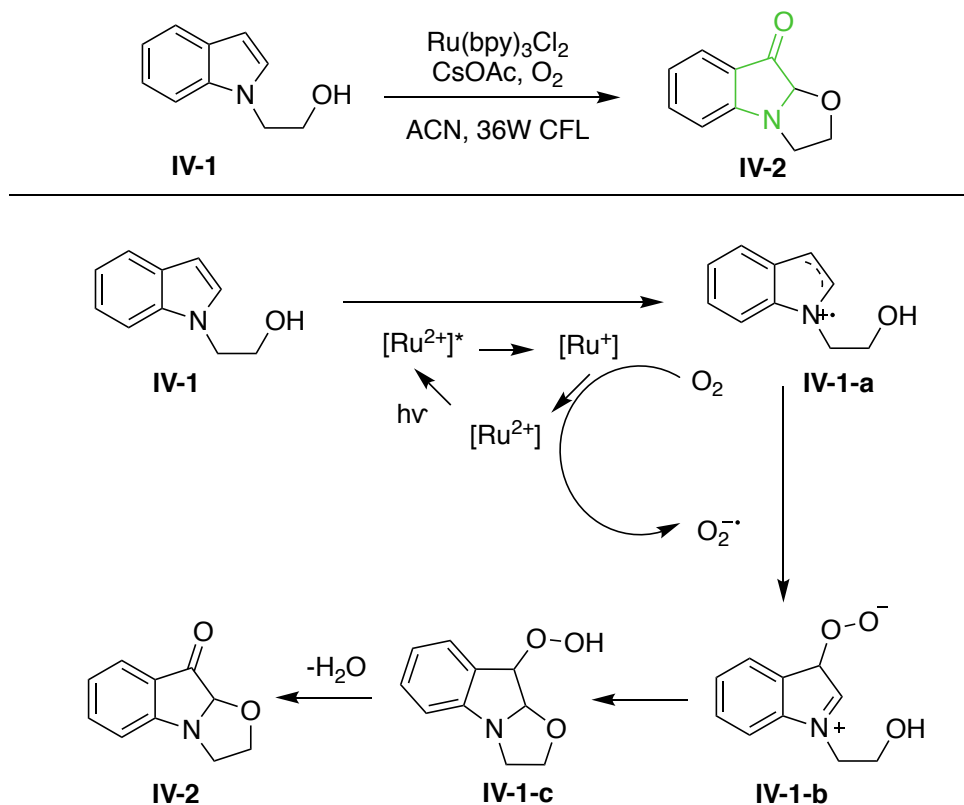


Figure IV-1. Visible light induced aerobic dearomatization of indole.

Another method for the copper catalyzed oxidative dearomatization of indoles was developed by Li's group (**Figure IV-2**).²¹ It features a dearomatization and spirocyclization of the indole-2-carboxamides. *Tert*-butyl hydroperoxide (TBHP) is used as the oxidant. In this report, 2 possible mechanisms are proposed. One involves $\text{Cu}(\text{I})/\text{Cu}(\text{II})$ oxidation states, the other involves $\text{Cu}(\text{II})/\text{Cu}(\text{III})$ oxidation states. The mechanism involving $\text{Cu}(\text{I})/\text{Cu}(\text{II})$ is shown here since the $\text{Cu}(\text{III})$ oxidation state is generally considered difficult to access. As shown in **Figure IV-2**, indole radical **IV-3-a** is generated in presence of $\text{Cu}(\text{OTf})_2$ and TBHP, which can be coupled with the *tert*-butylperoxy radical to form **IV-3-b**. Excess *tert*-butylperoxy radical abstracts the hydrogen and then cleaves the peroxy bond from **IV-3-c** to yield **IV-3-d**. Intermediate **IV-3-d** undergoes aromatic spirocyclization to yield the final product **IV-4**.

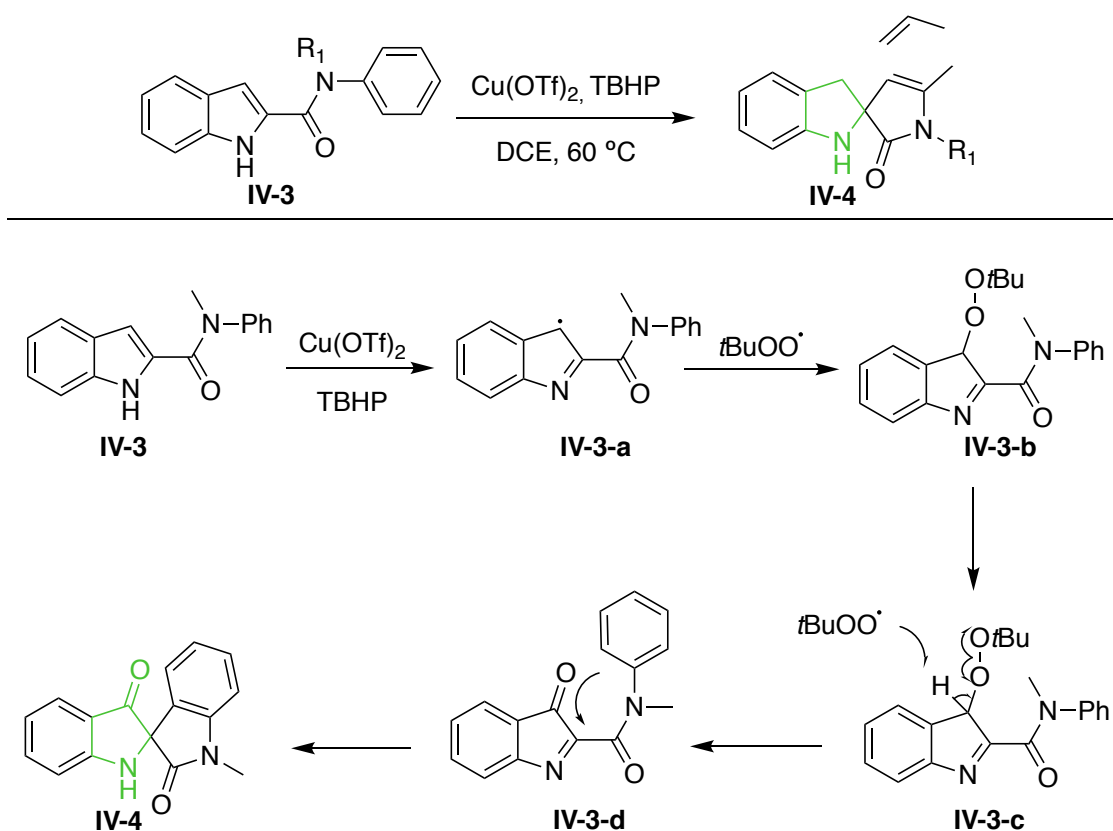


Figure IV-2. Copper catalyzed oxidative dearomatization/spirocyclization of indole.

IV.1.2. Intermolecular oxindole core construction

A Pd catalyzed oxindole formation was reported by Guchhait's group.²² They introduced an oxidative dearomatization of indole via a Pd catalyzed C-H peroxygenation reaction.

The reaction and proposed mechanism are shown in **Figure IV-3**. Indole **IV-5** reacts with Pd(II) catalyst to yield intermediate **IV-5-a**, which undergoes ligand exchange with TBHP to form **IV-5-b**. Reductive elimination of **IV-5-b** constructs the peroxide bond on the indole (**IV-5-c**). Meanwhile Pd(0) can be regenerated by the excess amount of MnO_2 . A Kornblum-DeLaMare type reaction occurs to produce the key intermediate **IV-5-d**, which can easily trap excess amount of nucleophilic indoles to form **IV-5-e**.

Dehydrogenation of **IV-5-f** followed by trapping excess amount of the starting material (**IV-5**) leads to the final product (**IV-6**).

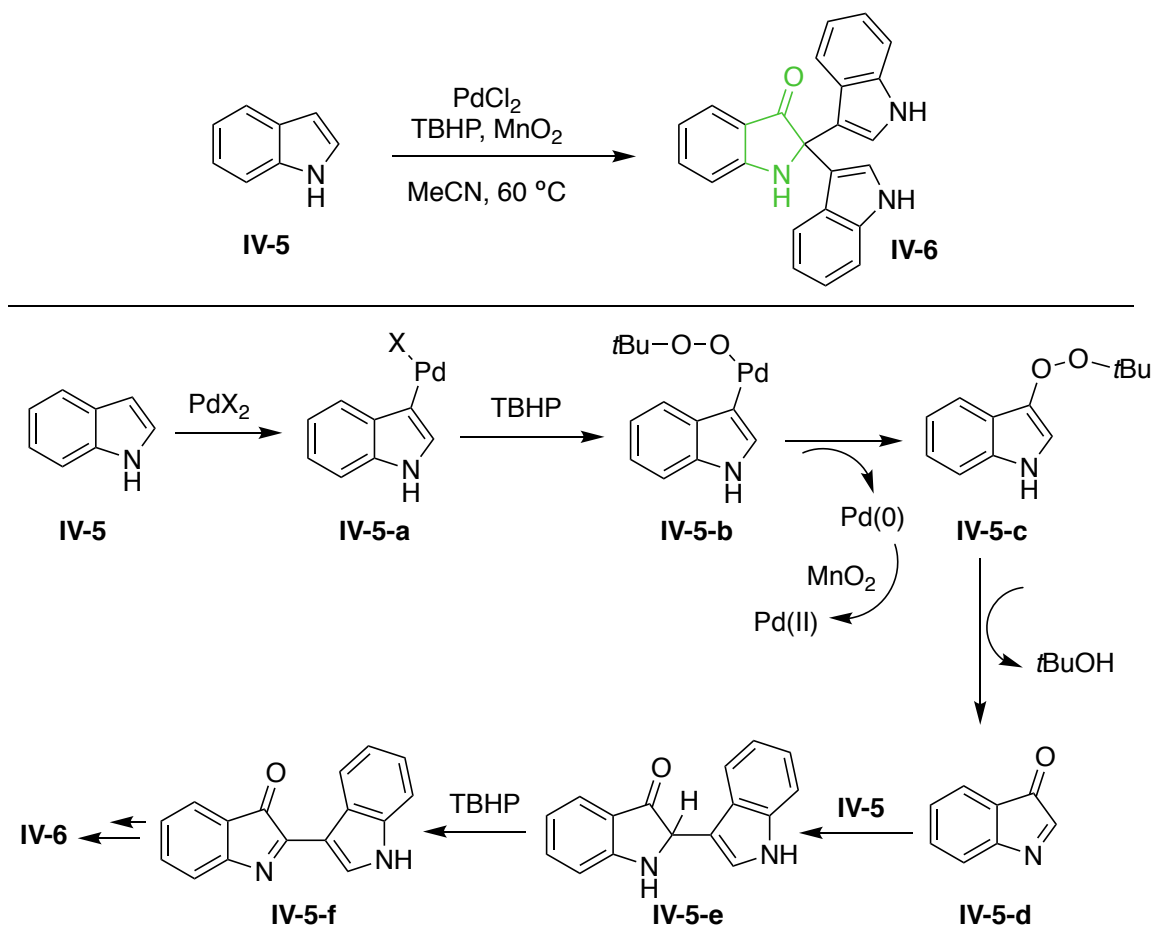


Figure IV-3. Oxidative dearomatization of indole by Pd catalyst.

Another indole oxidation and cyclization reaction was developed by Deng's group.²³ In this report, aerobic oxygenation between indole and oxime was triggered by the copper catalyst. The reaction and proposed mechanism are shown in **Figure IV-4**. Reduction of ketonoxime **IV-8** by Cu(II) catalyst yields a Cu(III) imine species (**IV-8-a**), which simultaneously releases an acetoxy radical upon contacting with molecular oxygen. The resulting nitrene intermediate **IV-8-b** may convert into azirine **IV-8-c**. On the other hand, starting material **IV-7** reacts with the acetoxy radical to form intermediate **IV-7-a**,

which can isomerize into **IV-7-b**. Peroxyl radical reacts with **IV-7-b** to afford **IV-7-c**, which can cyclize with azirine **IV-8-c** to afford **IV-7-d**. Under the Cu(II)/Cu(III) oxidation cycle, final product **IV-9** can be formed.

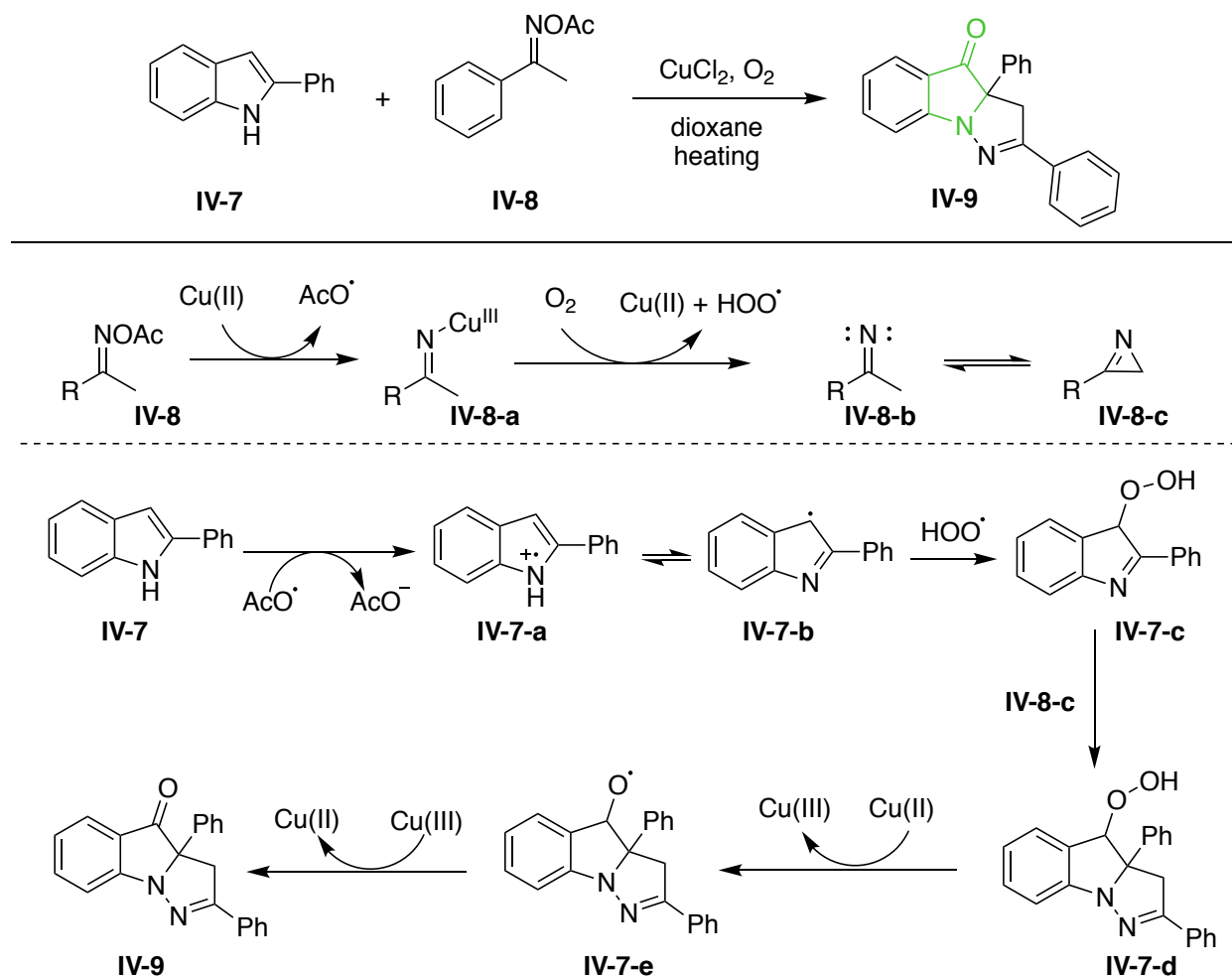


Figure IV-4. Copper catalyzed aerobic oxidation of indole.

To date, most of the methods require a strong oxidant (such as TBHP) and heating conditions to initiate the indole dearomatization reaction. Among these reactions, unknown radicals can be formed and contribute to the overall reaction. Thus, determining the real reaction mechanism is difficult and challenging.

IV.1.3. Indole selective C-H functionalization

Another less explored area for indole methodologies is the selective allylic functionalization of C2 and C3 dialkylated indoles or ring fused indoles.²⁴ Kawasaki's lab developed several different methods to functionalize the C2 allylic position.²⁵⁻²⁶ **Figure IV-5** illustrates one these methods which utilizes an active thionium species. Different nucleophiles such as alcohol, amines, Grignard reagents and azides can be used for this reaction. The mechanism for this transformation starts with the active thionium species, which is generated by DMSO and TFAA, and can be trapped by the electron rich indoles (**IV-10**) to form intermediate **IV-10-a**. Deprotonation at the allylic C2 position leads to the formation of intermediate **IV-10-b**, which subsequently trap different nucleophiles to yield the final product **IV-11**.

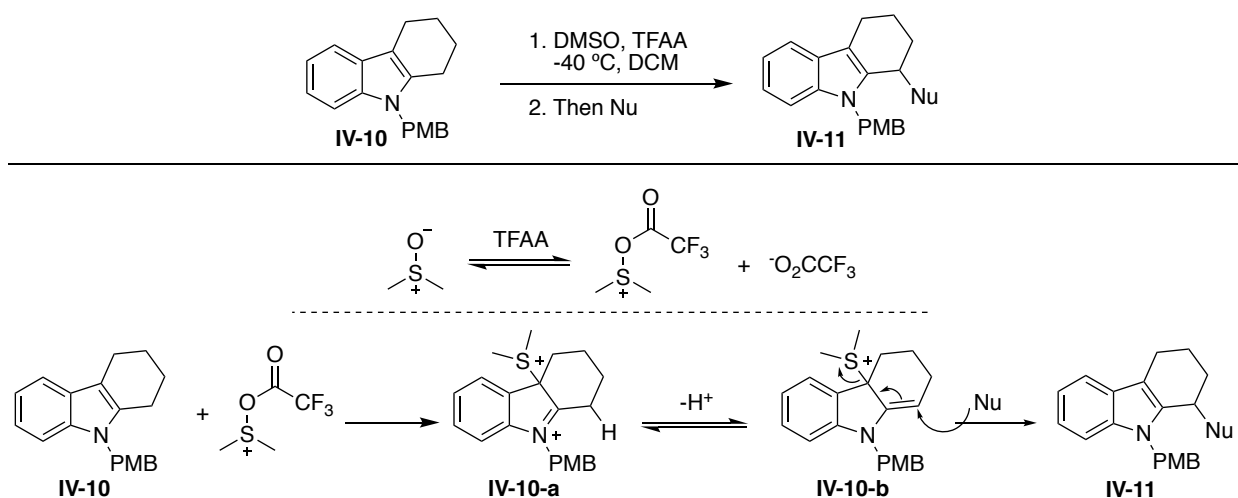
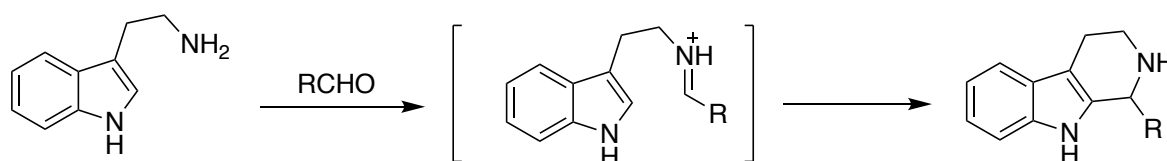


Figure IV-5. Thionium mediated indole functionalization.

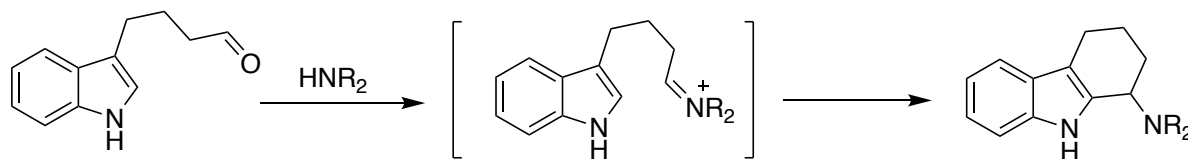
There are also some other transformations which share similar reaction mechanisms. For example, *tert*-butyl hypochlorite and singlet oxygen activated by photosensitizer can be used to form a **IV-10-a** like intermediate and followed by the nucleophilic attacked to complete the reaction.²⁷⁻²⁸

Other alternative way to achieve allylic functionalization of indoles is the Pictet-Spengler type reaction (**Scheme IV-4**). The classical Pictet-Spengler reaction constructs the cyclic rings, meanwhile leaving the allylic position altered by different aldehydes. The modified of the classical Pictet-Spengler reaction, the exocyclic variant leads to the tetrahydrocarbazole motif via a similar mechanism, instead of delivering the piperidine ring.²⁹

Classical Pictet-Spengler:



Exocyclic Pictet-Spengler:



Scheme IV-4. Different types of the Pictet-Spengler reactions.

Overall, both dearomatization of indole to oxindole and selective indole allylic C-H functionalization are less explored areas. Our unexpected reaction discovery described below contributes to both areas.

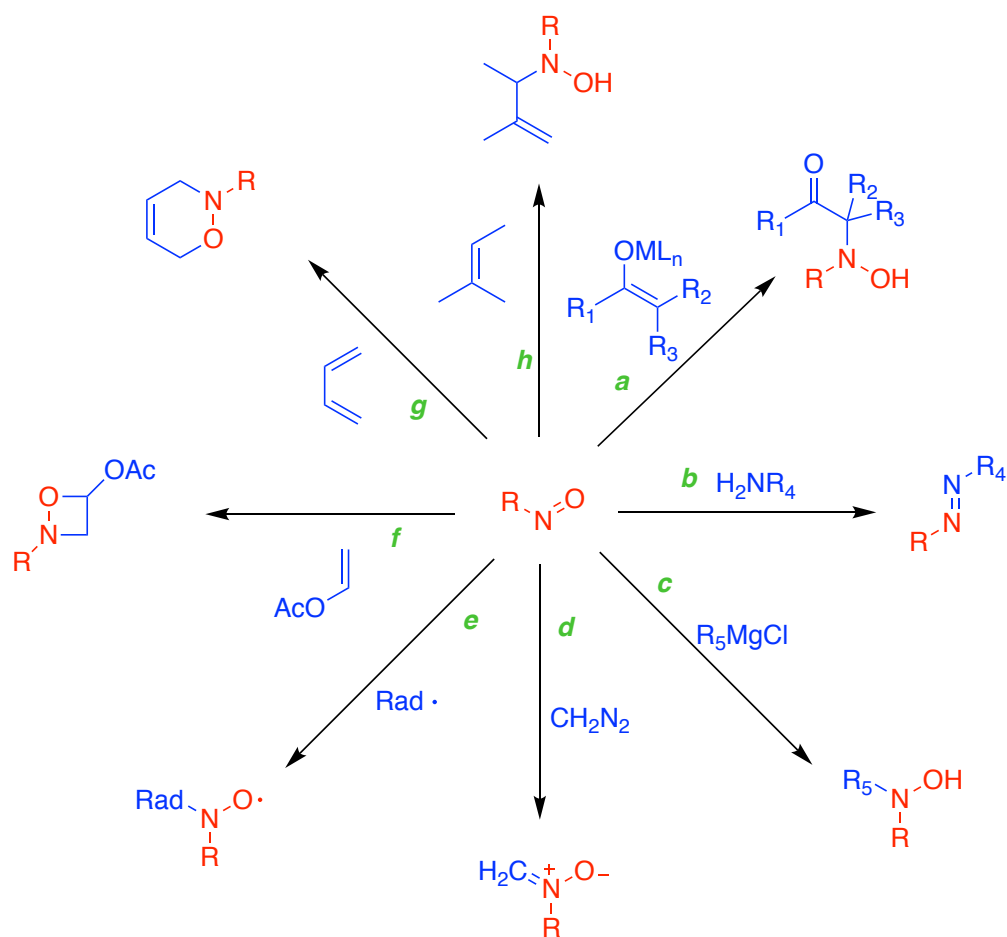
IV.2. Discovery of the new reaction

IV.2.1. Brief introduction to the reactions

Nitroso compounds are one of the most versatile reagents for organic chemists. These compounds act as double edged sword in the organic synthesis: they can provide a variety of different reactions but meanwhile may lead to many undesired side

reactions.³⁰⁻³¹ Selected transformations of the nitroso compounds are shown in **Scheme IV-5**.

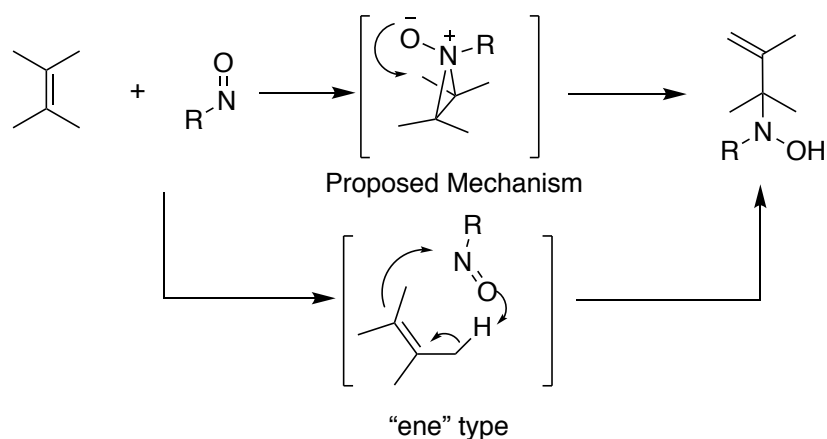
Different nucleophiles can be trapped by nitroso compounds, such as enolates, primary amines and Grignard reagents (Pathway *a* to *c*, **Scheme IV-5**). In presence of the diazomethane, nitroso moiety can be converted into nitrones (Pathway *d*). Nitroso compounds can also trap various radicals. Sometimes they can be used as radical scavengers (Pathway *e*). Nitroso compound also participated in [2+2] and [4+2] cyclizations (Pathway *g* and *f*). Last but not least, nitroso ene reactions can be used to functionalize allylic position of alkenes (Pathway *h*).



Scheme IV-5. Versatile applications of the nitroso compound.

IV.2.2. The initial proposed reaction

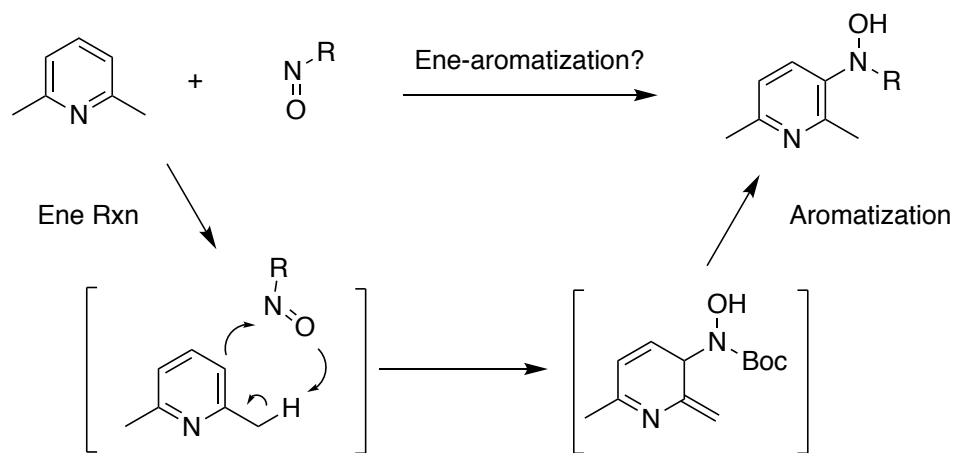
In the past few years, many elegant reactions involving nitroso compounds have been developed.³²⁻³⁷ Among these reactions, nitroso ene reaction features regioselective and stereoselective functionalization of the alkenes. However, the mechanism for the nitroso ene reaction is still debated.³⁸⁻³⁹ A likely mechanism was proposed by Greene and coworkers, and was supported by a detailed kinetic isotope effect (KIE) study.⁴⁰ The proposed mechanism includes an aziridine oxide intermediate formation, followed by allylic hydrogen abstraction to yield the final product (**Scheme IV-6**). However, some still prefer a simplified “ene” type mechanism.



Scheme IV-6. Mechanism for nitroso ene reaction.

After a comprehensive literature search of the nitroso ene reactions, we were surprised that this transformation is only used for aliphatic systems and has not been used to dearomatize organic compounds.⁴¹ Thus, we were curious whether the “ene-aromatization” process can be triggered by the nitroso compounds (**Scheme IV-7**). We hypothesized the ene reaction to first dearomatize the 2,6-dimethylpyridine, followed by

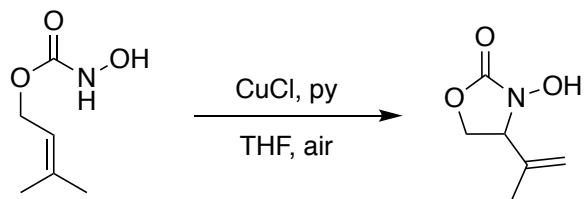
aromatization of the unstable intermediate to afford the final product. If the reaction proceeds as planned, it can be used to functionalize a variety of aromatic compounds.



Scheme IV-7. Initial proposed reaction.

Commonly, commercially available nitroso compounds are less reactive. In order to generate more reactive nitroso compounds, periodate salts are used to oxidize hydroxamic acids into the corresponding nitroso compounds. High reactivity of these compounds originates from the electron withdrawing groups (ketone or ester) that are attached to the nitroso functional group. The lifetime of these reactive compounds is short.⁴²⁻⁴³ We planned to avoid using periodate conditions since the proposed final product structure also contains a hydroxyl amine functional group, which can be oxidized again by the periodate salts. Thus, mild conditions to generate the desired nitroso was key for our initial proposal.

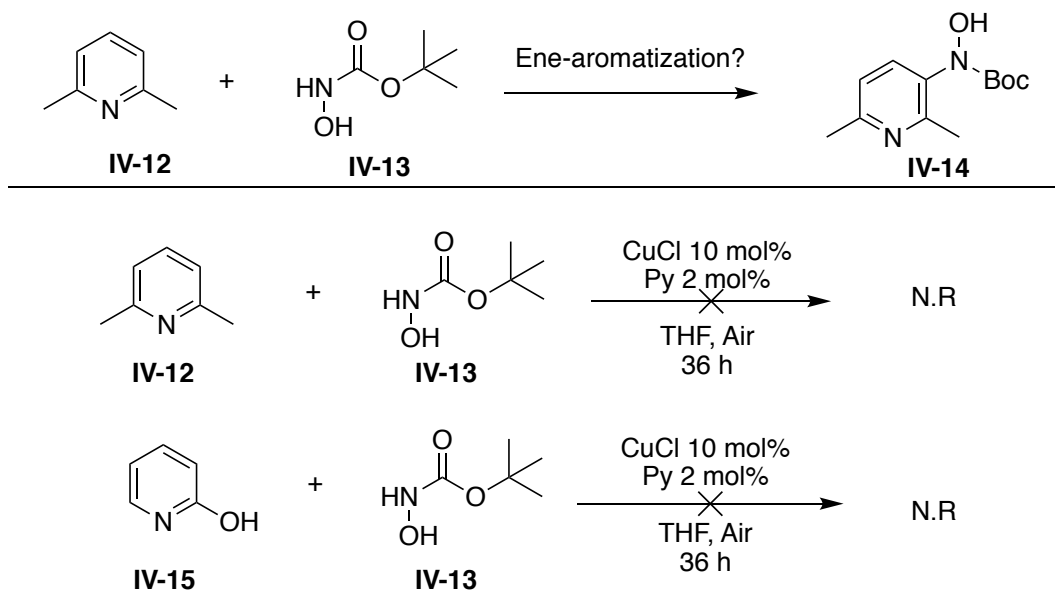
Upon extensive literature search, a set of milder reaction conditions reported by Alaniz's group attracted our attention.⁴⁴ In his report, CuCl and air were used to oxidize the hydroxamic acids into the nitroso compounds and an intramolecular nitroso ene type reaction was initiated (**Scheme IV-8**).



Scheme IV-8. Mild nitroso generation. Py = pyridine.

IV.2.3. Initial reaction discovery

We began our investigation with 2,6-dimethylpyridine (**IV-12**) and 2-hydroxypyridine (**IV-15**) for the ene or hetero-ene reactions. However, under the reported nitroso generation conditions (CuCl 10 mol%, pyridine 2 mol%), there was no reaction for both entries (**Scheme IV-9**).



Scheme IV-9. Initial test reactions to validate the nitroso ene-aromatization proposal.

We reasoned that compound **IV-15** can be tautomerized to its 2-pyridone form, and thus making the hetero-ene reaction difficult. As for compound **IV-12**, the activation barrier for the pyridine dearomatization process may be too high to overcome under the mild reaction condition. We focused our attention to indoles with a lower dearomatization

energy barrier as compared with pyridine. For this purpose, indoles **IV-15** and **IV-16** were proposed (**Figure IV-6**).

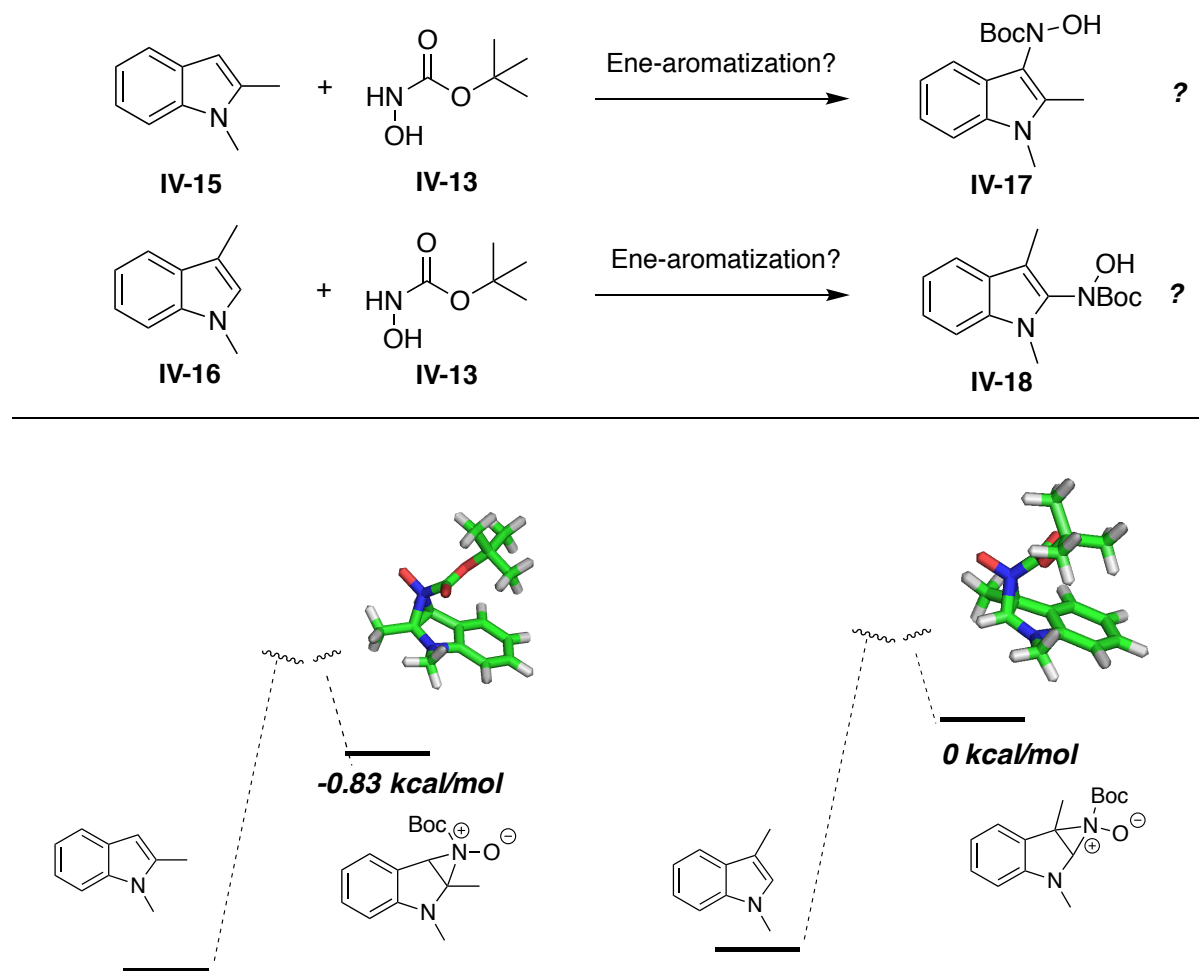
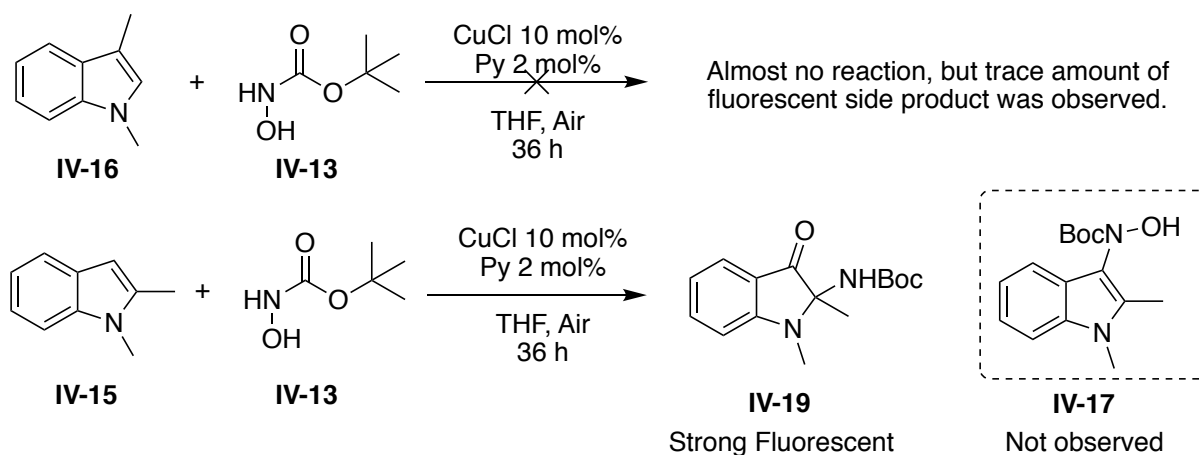


Figure IV-6. Proposed indole substrates **IV-15** and **IV-16**. Reaction intermediates were computed at DFT/B3LYP 6-31+G* level (vacuum), with relative energies shown in the figure.

A quick computational study to analyze which indole yields a more stable aziridine oxide intermediate with the nitroso compound was also carried out prior to the experiments. However, the calculated difference between the two reaction intermediates was only 0.83 Kcal/mol (**Figure IV-6**). Although the intermediate of **IV-15** is slightly favored, this energy difference is too small to suggest this with high confidence.

To satisfy our curiosity, we carried out both reactions (**IV-15** and **IV-16**). Compound **IV-16** did not yield the desired product, but we did observe trace amount of fluorescent side products under UV irradiation. These side products were formed in trace amounts and could not be separated and characterized.

To our surprise, when the reaction with 1,2 dimethylindole (**IV-15**) was performed, a strong yellow-greenish side product was formed and isolated. Initially, we did have a difficult time to confirm the structure of compound **IV-19** due to the limited information available from 2-D NMR studies. Luckily, this compound was crystallized and analyzed by X-ray crystallography. As a result, structure **IV-19** was confirmed instead of the proposed **IV-17** (**Scheme IV-10**).



Scheme IV-10. Unexpected results of the indole test reactions.

Interestingly, product **IV-19** can not be formed through the proposed mechanism. To the best of our knowledge, similar oxindoles have not formed in a similar fashion previously. This unexpected result motivated us to further explore this reaction and initiated a new project in our lab.

IV.3 Reaction screening

IV.3.1 Indole alkyl position screening

We began our screening this reaction with alkyls at different positions on the indole ring. Preliminary results (**Scheme IV-10**) showed oxindole product was only formed with 1,2-dialkyl indole (**IV-15**). In fact and no reaction was observed for the 1,3-dialkyl indole (**IV-16**). Thus, we carried out a series of indole substrate reactions, the results of which are shown in **Figure IV-7**.

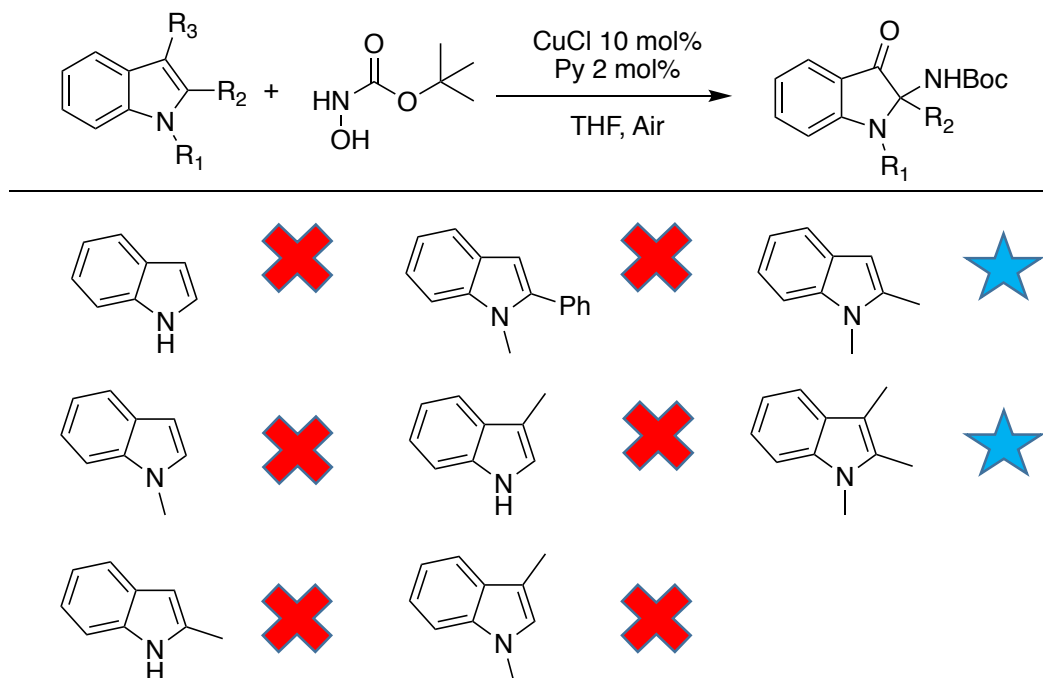


Figure IV-7. Screening of the alkyl positions on indole. Substrates marked as “X” indicate no reaction. Substrates marked as “star” indicate there was a reaction.

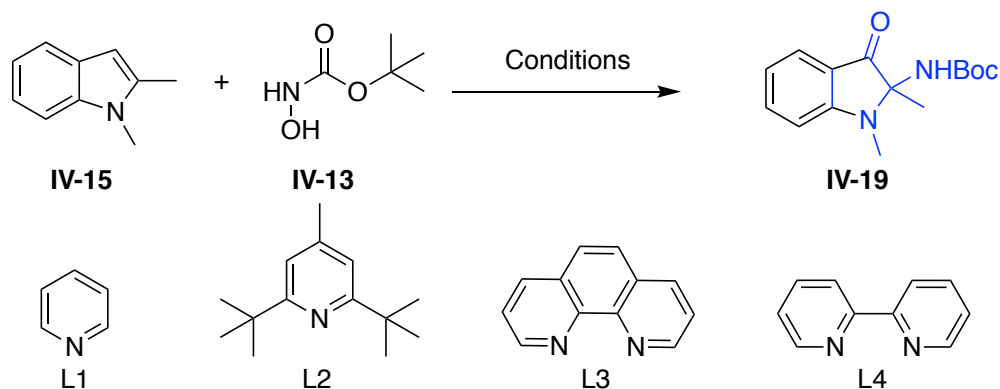
A variety of alkylated indoles were subjected to the standard reaction condition (10 mol% CuCl with 2 mol% pyridine). Interestingly, the presence of the methyl in the 1,2-dimethyl indole was obligatory for the success of the reaction. Attempts to replace the methyl group on the C2 position with a bulky phenyl group also led to no reaction. Nonetheless, subjecting the 1,2,3-trimethyl indole to the reaction led to a surprising result.

Two completely different allylic C-H oxidized and aminated products were formed instead of the dearomatization product.

IV.3.2 Oxindole reaction condition screening

Excited by the initial results, we set to screen and optimize our reaction conditions. In a Pyrex test tube (12 * 75 mm), 1,2-dimethyl indole (**IV-15**) (0.01 mmol, 1 mL in THF), *tert*-butyl hydroxycarbamate (**IV-13**), ligands and copper catalyst in 1 mL THF was added. The reaction was stirred at rt open to air. After 24 h, the mixture was concentrated and then passed through a short celite pad to remove the copper catalyst. The crude product was concentrated under vacuum and subjected to NMR analysis to measure the yield with methyl *tert* butyl ether (MTBE) as the internal standard.

The optimization results are summarized in **Table IV-1**. Using 10 mol% CuCl as the catalyst, 2 mol% pyridine as the ligand, and 1 equivalent of **IV-13**, product oxindole **IV-19** was obtained in 54% yield (entry 1). Switching the catalyst to CuCl₂ or Cu(ACN)₄PF₆ affords slightly lower yield (entry 3, 42% yield; entry 8, 16% yield). However, other copper catalysts such as CuI, Cu(OAc)₂ or Cu₂O did not give the desired product. Next, different ligands for this reaction were tested. Pyridine based ligands such as bipyridine, 1,10-phenanthroline, etc. resulted in lower yields (< 40%, entry 12-14). Increasing the pyridine loading to 10 mol% also lowered the reaction yield (entry 8, 19% yield). Interestingly, without the pyridine, the reaction can proceed to afford a slightly lower yield (entry 6). We speculated that pyridine can improve the solubility of the copper species during the reaction. However, excess amount of the ligand may change the basicity of the solution and lead to a lower yield.



Entry	Catalyst 10 mol%	IV-13 equiv	Ligand (mol %)	Solvent	Conversion ^a	Yield ^a
1	CuCl	1	L1 (2)	THF	77	54
2	CuI	1	L1 (2)	THF	12	0
3	CuCl ₂	1	L1 (2)	THF	91	42
4	Cu(OAc) ₂	1	L1 (2)	THF	11	0
5	Cu ₂ O	1	L1 (2)	THF	0	0
6	CuCl	1	L1 (0)	THF	78	45
7	CuCl	2	L1 (2)	THF	89	88
8	CuCl	1	L1 (10)	THF	33	19
9	Cu(ACN) ₄ PF ₆	1	L1 (2)	THF	55	16
10	CuCl	2	L1 (2)	DCE	81	26
11	CuCl	2	L1 (2)	ACN	77	3
12	CuCl	2	L2 (2)	THF	99	33
13	CuCl	2	L3 (2)	THF	81	20
14	CuCl	2	L4 (2)	THF	87	28
15	CuBr	2	L1 (2)	THF	69	35

Table IV-1. Oxindole formation optimization. ^aDetermined by ¹H-NMR using MTBE as an internal standard. All reactions were performed at 0.1 mmol scale.

We were delighted to find that by increasing the *tert*-butyl hydroxycarbamate **IV-13** loading to 2 equivalent, formation of oxindole **IV-19** was improved to 88% yield (entry 7). However, when the reaction was run in other solvents such as acetonitrile or dichloroethane, **IV-19** was obtained in poor yields (entry 10 and 11). In this regard, we speculated that the combination of CuCl, pyridine and THF promotes the formation of the transient active nitroso intermediate to avoid self-decomposition. Indeed, the optimal

conditions were found to be CuCl (10 mol%), pyridine (2 mol%) and 2 equivalent of **IV-13** in THF under air (entry 7, **Table IV-1**).

IV.4 Indole dearomatization reaction

IV.4.1 Reaction substrate scope

With the optimal indole oxidation conditions established, a range of indole substrates were screened. Substitution on positions C4 to C7 of the indole were found to be well tolerated to afford the desired oxindole in good yield (**Figure IV-8**). Generally, electron donating substituents led to a faster reaction and higher yield while electron withdrawing substrates provided the product in lower yields (**IV-37**, 17%). Presumably, electron withdrawing groups lower the HOMO orbital energy of the indole. Thus, such substrates have lower reactivity towards the nitroso intermediate and lead to lower yield. Notably, less hindered alkyl groups such as ethyl and benzyl on the indole N are also tolerated in this reaction (**IV-34** and **IV-35**, yield 60% and 37% respectively). Other small allyl group besides methyl, such as an ethyl group on the C-2 position also were tolerated, yielding the corresponding product in moderate yield (49%, **IV-36**).

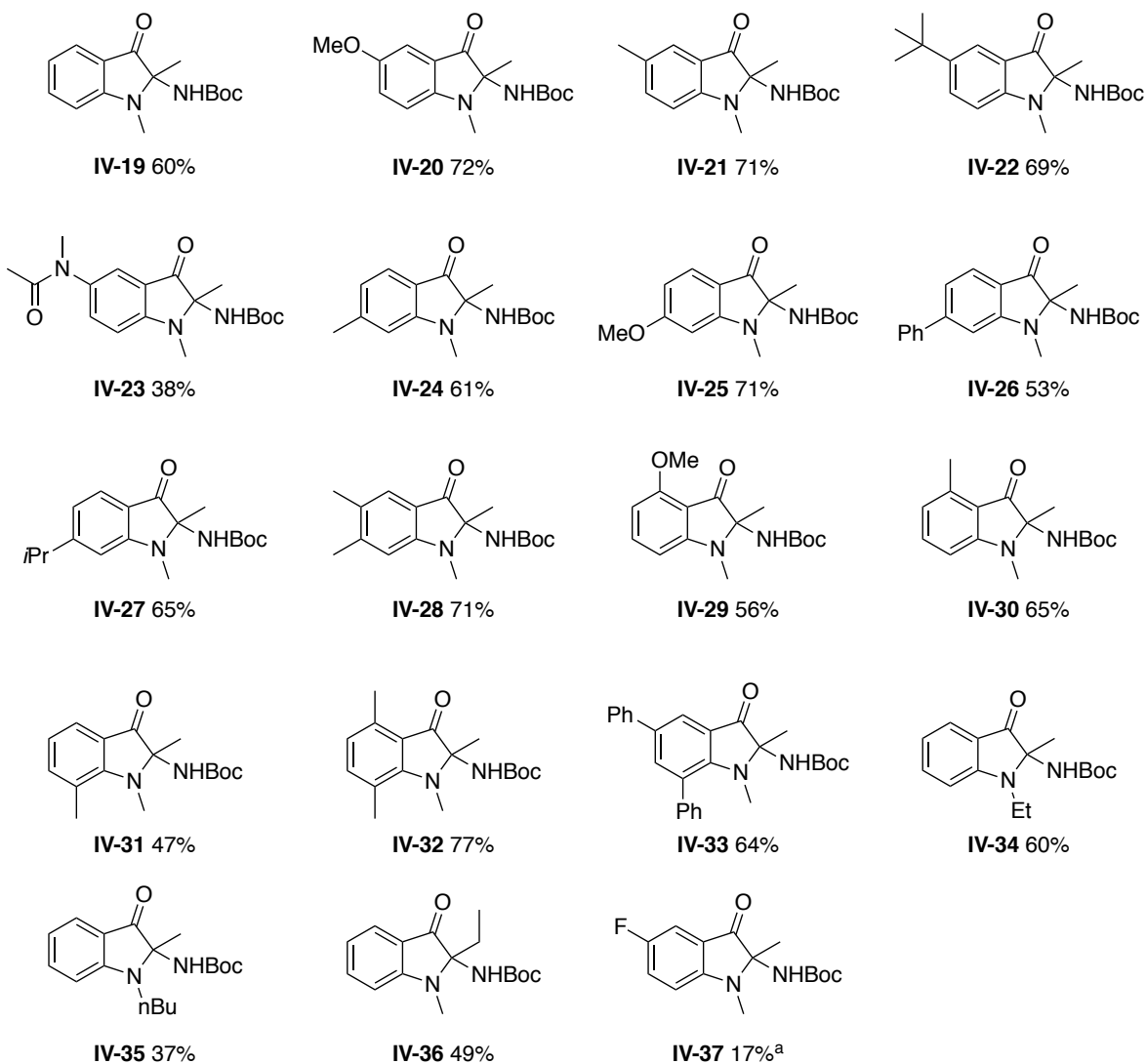
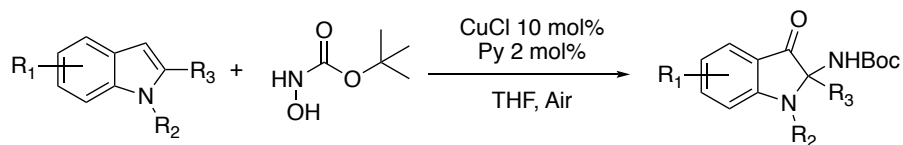


Figure IV-8. Indole dearomatization substrate scope. Reactions were conducted on 0.1 mmol scale and isolated by Prep-TLC. ^a1 equiv CuCl and 4 equiv of **IV-19** were used.

IV.4.2 Important note regarding the reaction

Obtaining most of the starting materials require multiple synthetic steps, as detailed in the experimental section of this chapter. As for purification of the oxindole products, prep-TLC separation is highly recommended due to the various side products

formed during this reaction. A bright yellow band on the prep-TLC contains the desired product. In some cases, extra HPLC separation is needed to obtain the product in pure form.

Another important note is the solvent for NMR studies. Oxindole product **IV-19** can be stable in solid form for months at lower temperature. However, this compound is not stable in CDCl_3 and we do observe a color change from bright yellow to green within an hour. Even with the pre-dried and acid neutralized CDCl_3 , we still observe the slow decomposition of the oxindole compound. Thus, methanol- d_4 and CD_2Cl_2 are recommended for NMR studies.

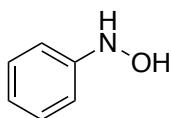
IV.4.3 Substrates that do not work

During the course of the substrate study, we found this reaction works exclusively with electron rich 1,2-dialkylated indoles with *tert*-butyl hydroxycarbamate **IV-13** as a pre-nitroso source. Herein, the following lists all the failed reactions or those that have extremely low yield.

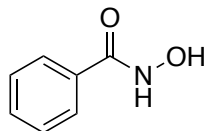
First, we attempted to use different hydroxylamines instead of **IV-13** for this reaction. However, all the listed hydroxylamines (**IV-38-A** to **IV-38-D**, **Figure IV-9**) did not initiate the indole dearomatization reaction leading only to slow decomposition of these hydroxylamines. On the other hand, we examined a variety of indoles and other similar heterocycles. Surprisingly, compound **IV-39-A** did not work under dearomatization conditions. Substrate **IV-39-C** also did not work; we reasoned that the MOM protecting group might bind to the copper catalyst to stop the reaction. Sterically bulky substrates on N or C2 positions also prevents the reaction to occur (**IV-39-B**, **IV-39-E** and **IV-39-F**).

Indoles which have electron withdrawing groups on either N or indole ring also afforded no reaction (**IV-39-D**) or trace amount of the product (**IV-39-H**).

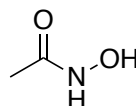
Hydroxylamines:



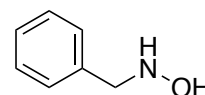
IV-38-A



IV-38-B

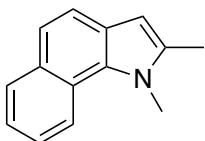


IV-38-C

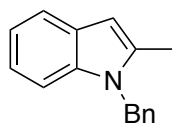


IV-38-D

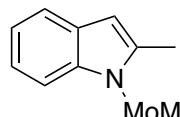
Substrates:



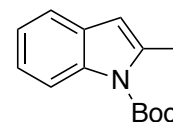
IV-39-A
NR



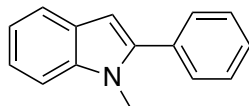
IV-39-B
Low yield



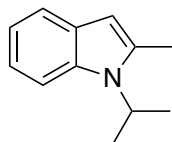
IV-39-C
Low yield



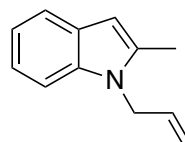
IV-39-D
NR



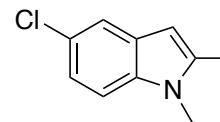
IV-39-E
NR



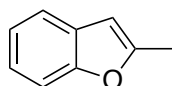
IV-39-F
Low yield



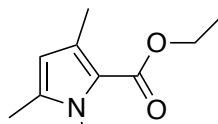
IV-39-G
Low yield



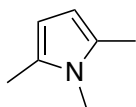
IV-39-H
Low yield



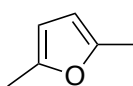
IV-39-I
NR



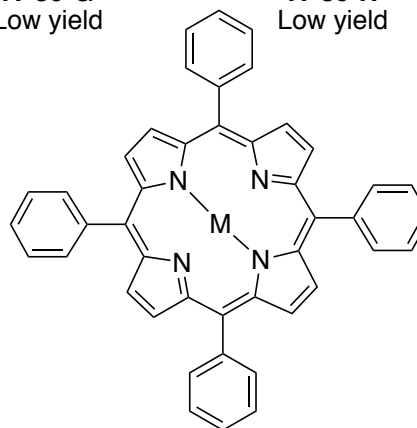
IV-39-J
NR



IV-39-K
(not isolable)



IV-39-L
(not isolable)



IV-39-M M = Zn, NR
IV-39-N M = H₂, NR

Figure IV-9. Hydroxylamines or indole substrates that did not work under the optimal conditions. NR stands for no reaction.

Heterocycles **IV-39-I**, **IV-39-J**, **IV-39-M** and **IV-39-N** were also tested, but no reaction was observed. Interestingly, under the optimal indole dearomatization conditions,

compounds **IV-39-K** and **IV-39-L** were consumed within a short time period. A large number of products were formed, however, we were not able to isolate and characterize them.

IV.4.4 Photo physical properties of the oxindole product

Oxindole product **IV-19** exhibits interesting photophysical properties. When irradiated by UV light, a strong green fluorescence can be observed. 3-Oxindole cores are found in indigo or hemiindigo compounds, having unique photo properties.⁴⁵⁻⁴⁶ Recently, Matsumoto's group demonstrated similar core structures can be engineered to emit up to 640 nm near-IR fluorescence.⁴⁷ As a matter of curiosity, we tested the UV-absorption and fluorescent of compound **IV-19**. UV spectra showed a low absorption peak at 407 nm and a strong absorption peak at 232 nm in acetonitrile (**Figure IV-10**). Interestingly, we also observed compound **IV-19** has solvatochromic properties, as shown in **Figure IV-11**. In various solvents, fluorescence emission of structure **IV-19** ranges from 450 nm to 530 nm.

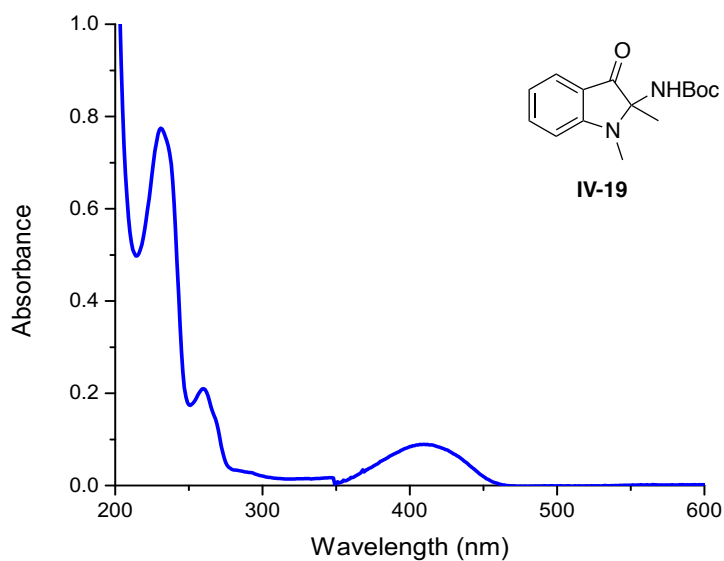


Figure IV-10. UV-Vis spectra of compound **IV-19**, 30 μM in acetonitrile at rt.

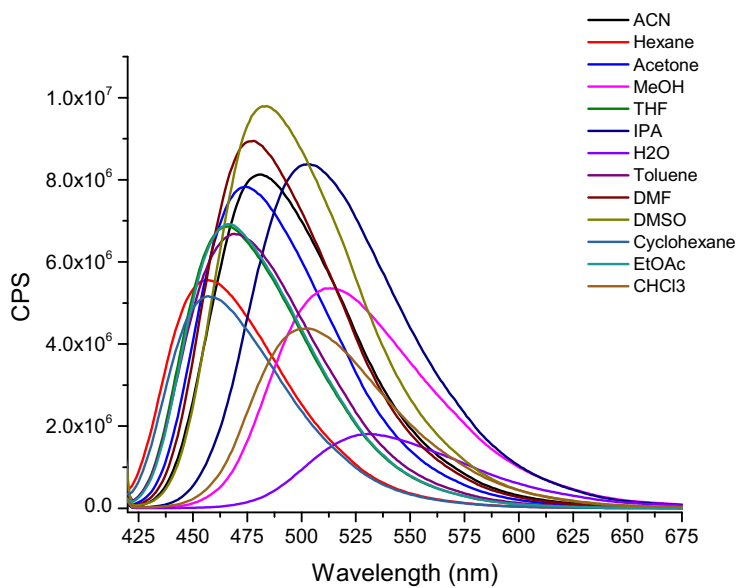
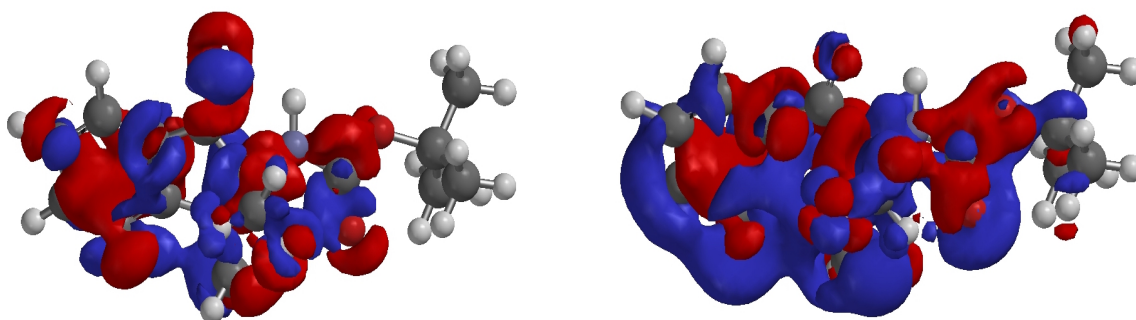


Figure IV-11. Fluorescent spectra of compound **IV-19** in various solutions at rt. Excited at 407 nm.

IV.4.5 Photophysical calculations



Excitation:

$$E(S_0): -918.049977$$

$$E(S_1'): -917.920602$$

$$E(\text{excitation}) = E(S_1') - E(S_0) = 0.128275 \text{ hartree} = 355 \text{ nm}$$

Emission:

$$E(S_1): -917.933385$$

$$E(S_0'): -918.022958$$

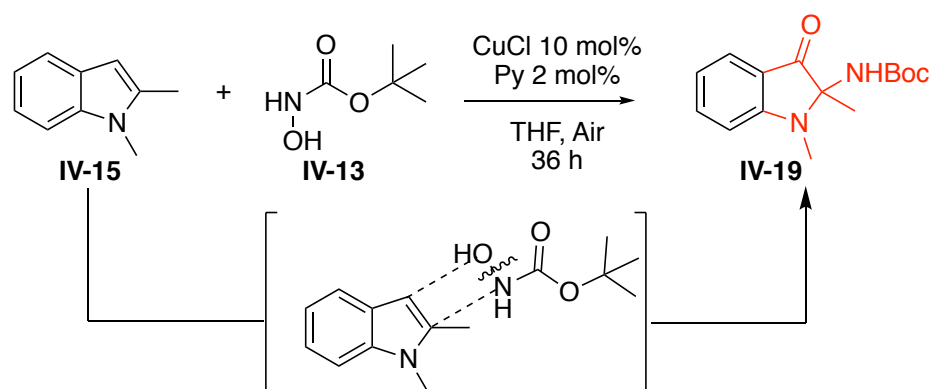
$$E(\text{excitation}) = E(S_1) - E(S_0') = 0.089573 \text{ hartree} = 509 \text{ nm}$$

Figure IV-12. HOMO and LUMO of compound **IV-19**. Left is HOMO, right is LUMO. Calculated results are shown below at PBE0-6-311+G** level. S₀ is the ground state, S₁ is the first excited state.

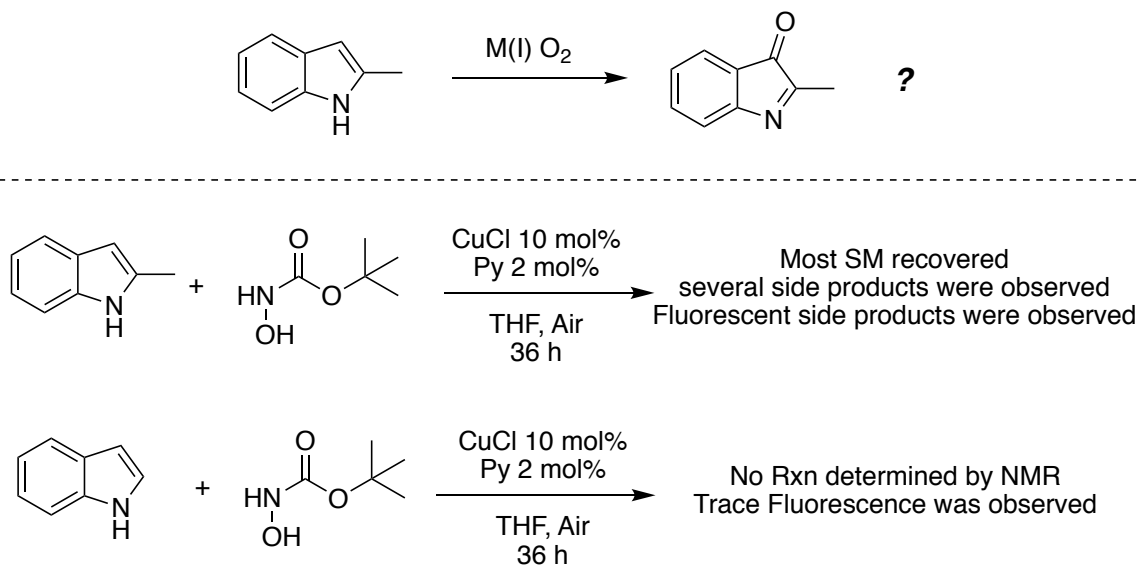
Due in part to the interesting photophysical properties of **IV-19**, we carried out theoretical calculation of this compound. Computational analysis was carried out on a Dell Precision Tower 5810 equipped with Intel Xeon E5-1660 v3 CPU and 64 G memory. System was built on Kernel Linux, version: 2.6.32-642.13.1 el6 x84_64, with Spartan 16 calculation package.⁴⁸ Conformers search was first carried out at MMFF level, followed by HF-6-31G level optimization. The minimal energy conformer obtained from the HF-6-31GD level was subjected to a higher PBE0-6-311+G**/vacuum level to get the final optimized geometry. Ground state HOMO and LUMO of compound **IV-19** are shown in **Figure IV-12**. We also carried out the excited state geometry by TDDFT study. Vertical

excitation energy and direct fluorescent emission were calculated at PBE0-6-311+G** level, considering the two lowest singlet states ($S_0 \rightarrow S_1$). Excitation was calculated to be 355 nm at this level (experimental result is 407 nm). At the B3LYP/CC-PVQZ level, a closer absorption was achieved (378 nm). Direct fluorescence was computed to be 509 nm at PBE0-6-311+G** level, which was in agreement with the experimental result (407 nm).

IV.4.6 Mechanistic studies

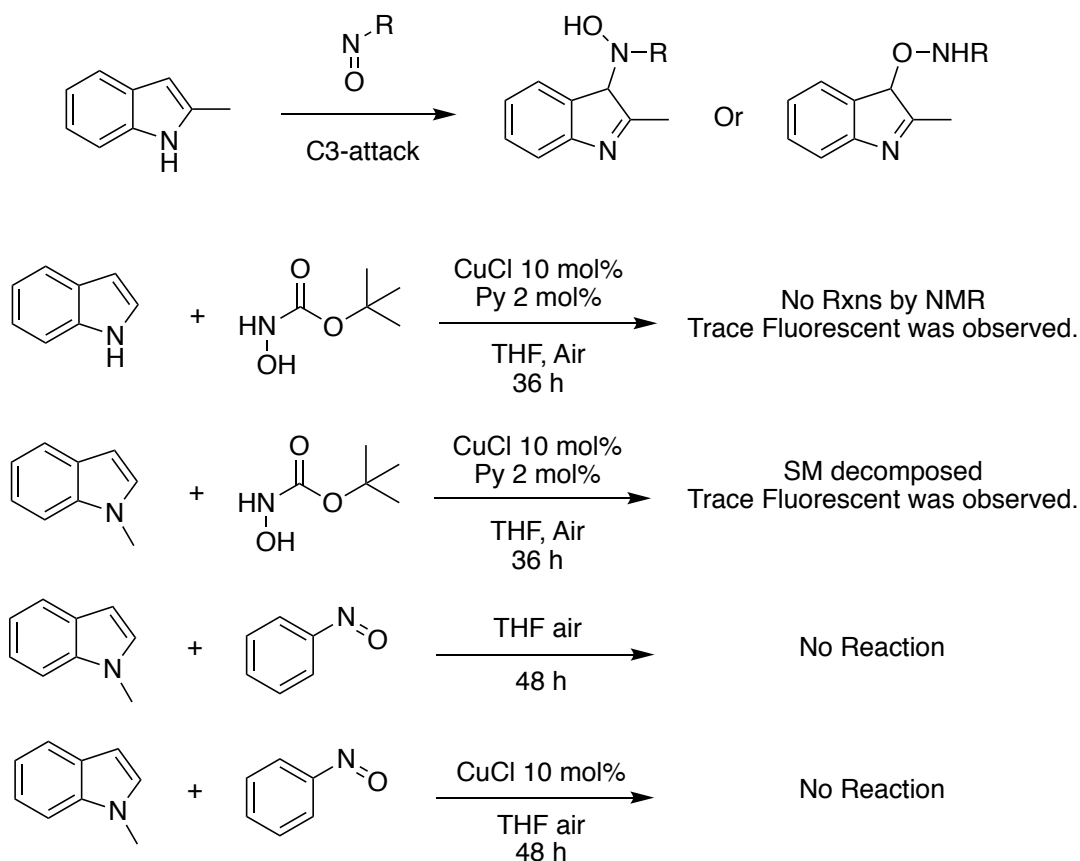


Scheme IV-11. Indole dearomatization reaction.



Scheme IV-12. Control experiments for copper and air oxidation pathway.

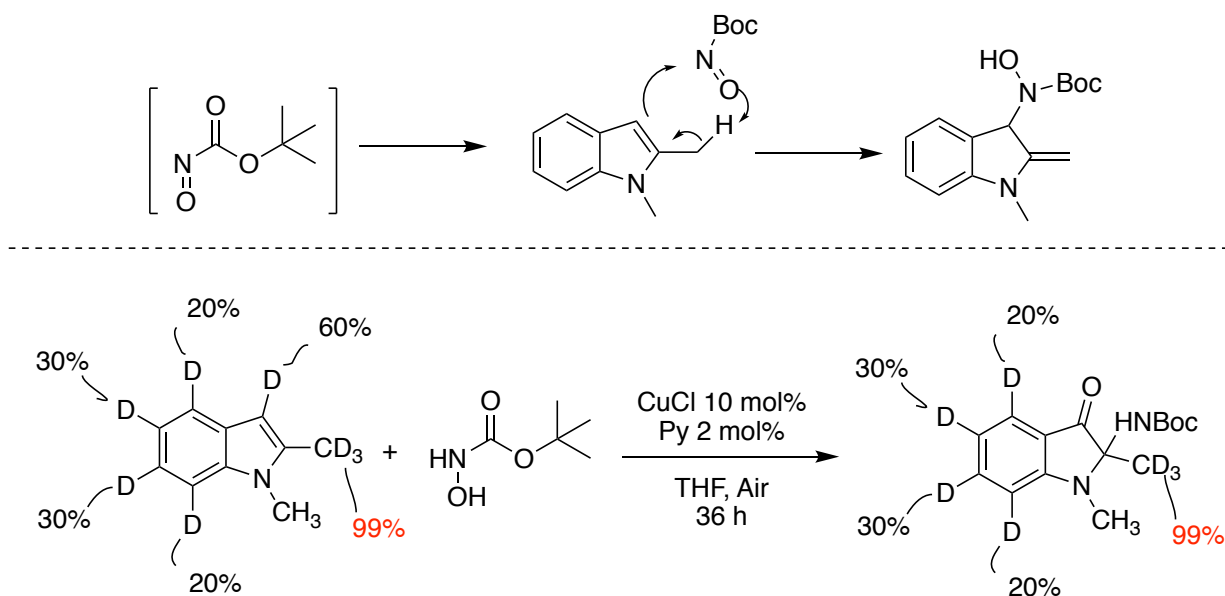
To explore the mechanism of this reaction (**Scheme IV-11**), we carried out a set of control experiments. First, we examined the possibility of the indole oxidation with only O₂ and copper at ambient conditions (**Scheme IV-12**). Under the optimal reaction condition, neither indole nor 2-methyl indole led to the desired product. However, we did observe some fluorescent side products after the reaction was complete, but their amount was too small to isolate. The majority of the starting materials can be recovered. This experimental result is in agreement with the literature reports that strong heating and oxidative environment is required for indole oxidation.⁴⁹⁻⁵² Thus, we can exclude this reaction follows the copper and air oxidation pathway.



Scheme IV-13. Nitroso trapping experiments.

Next, we carried out experiments to trap the putative nitroso intermediate (**Scheme IV-13**). Different indole substrates were tested. Under the standard conditions, there was no reaction for 1H-indole and 1-methyl indole (determined by H-NMR), but we did observe some decomposition of 1-methyl indole. We also tried the commercially available nitrosobenzene as nitroso source. Similar to 1,2-dimethyl indole (**IV-15**) that failed to react with the nitrosobenzene, 1-methyl indole also was not reactive under these conditions.

From these control experiments, we did observe different reactivities between the nitroso sources. Indeed, nitroso generated by *tert*-butyl hydroxycarbamate (**IV-13**) is more reactive. Perhaps this more reactive *tert*-butyl nitrosoformate can react with electron rich 1,2-dialkylated indoles.



Scheme IV-14. Deuterium labeling experiment was carried out to exclude an ene type reaction mechanism.

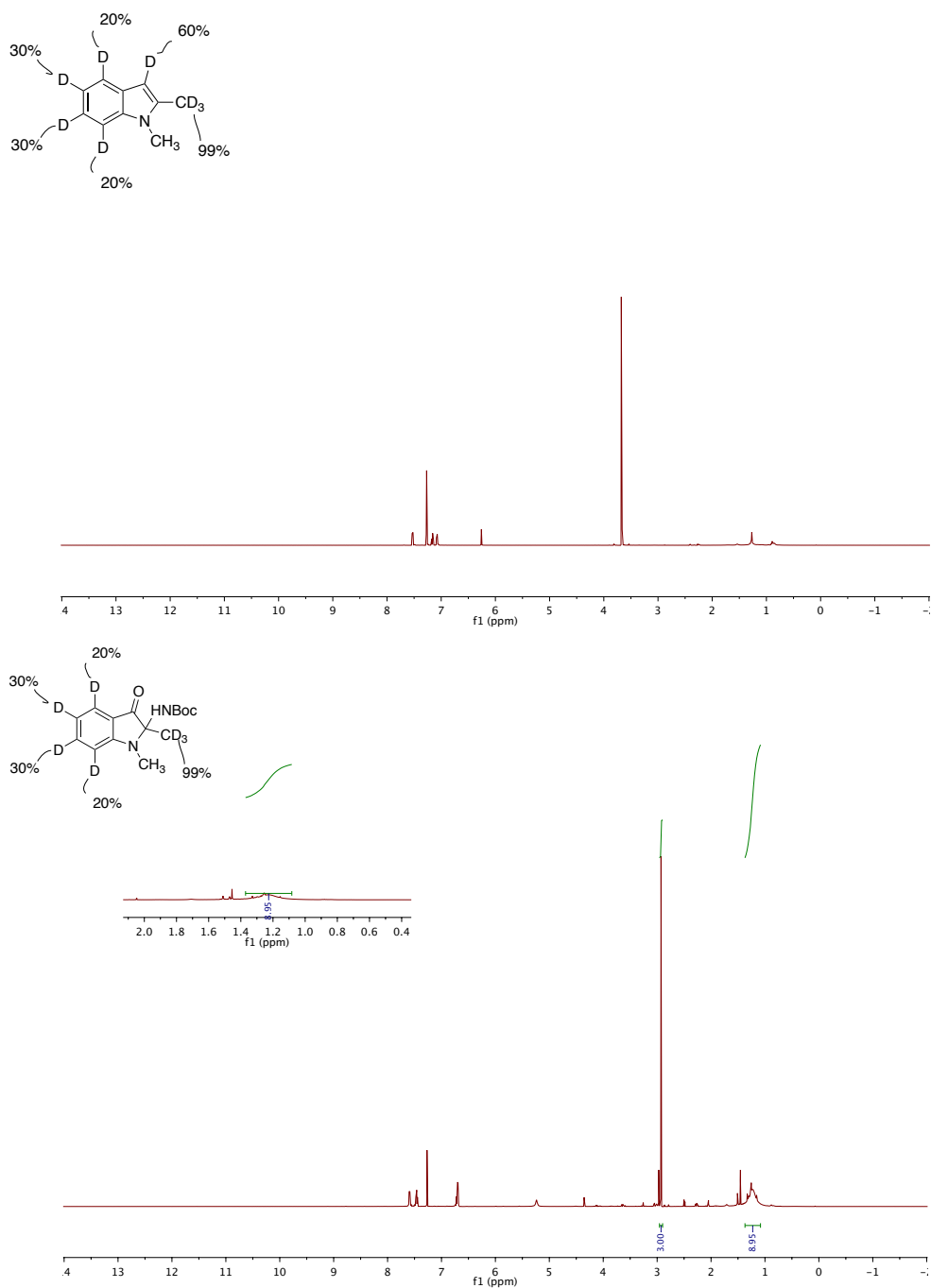


Figure IV-13. C2 position CD₃ remained unchanged after the reaction. Top picture: starting material with deuterated C2 position. Bottom picture: After the reaction, product was analyzed by ¹H-NMR, integration of the area only indicated the Boc group.

We also investigated whether an ene-type reaction is involved in this mechanism (Scheme IV-14). To test this possibility, deuterated starting material was prepared

according to the literature.⁵³ If the reaction proceeds via an ene mechanism, we should expect to see deuterium loss from the C2 methyl position on the indole. However, no loss of the deuterium loss from C2 methyl group was evident based on ¹H-NMR integration (Figure IV-13).

IV.4.7 Proposed mechanism

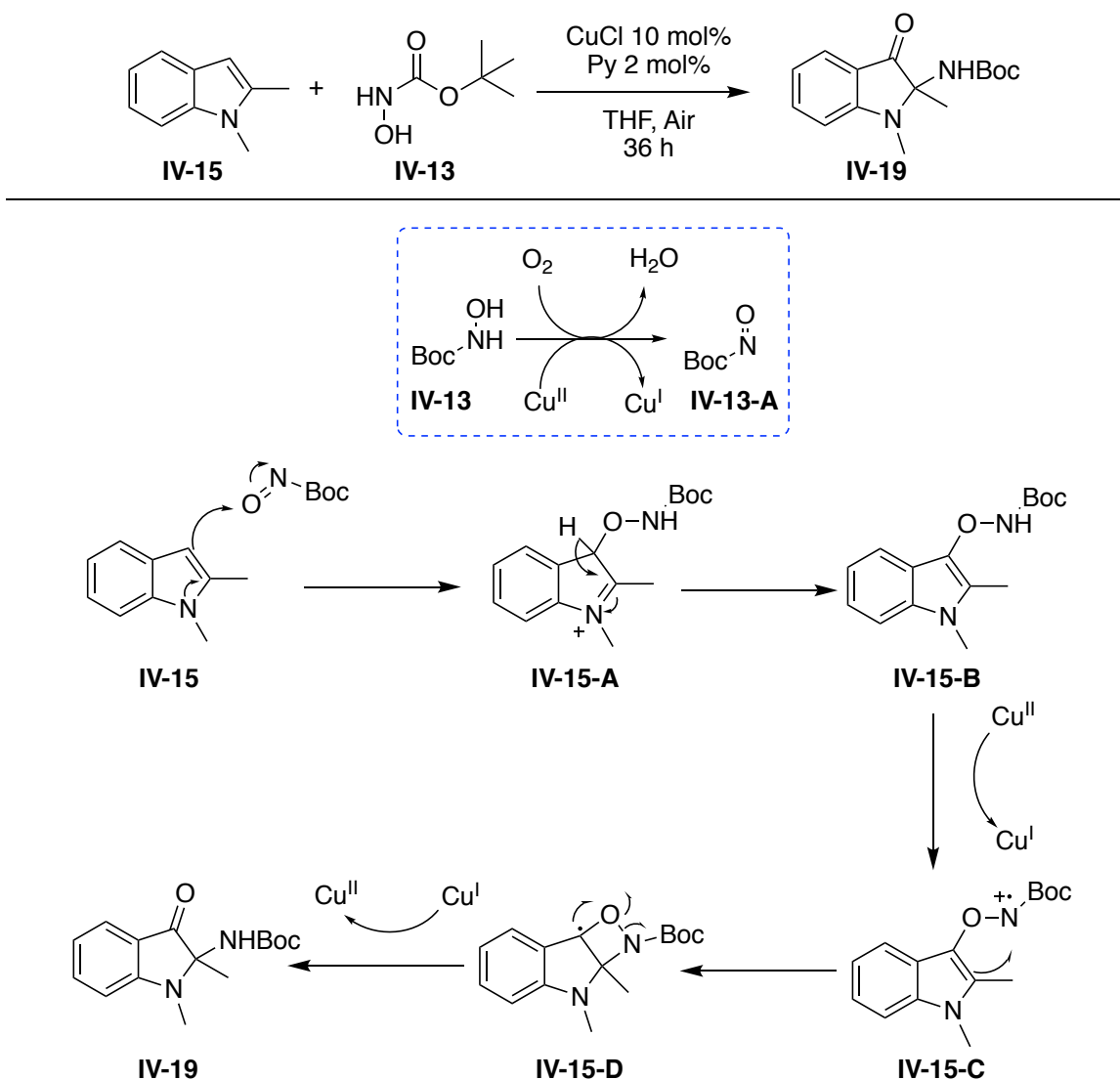


Figure IV-14. Proposed mechanism for indole dearomatization reaction.

Based on the above experiments, we proposed a plausible mechanism for the oxindole formation in **Figure IV-14**. Cu(I) is first oxidized by air to Cu(II). Meanwhile the

tert-butyl hydroxycarbamate (**IV-13**) is oxidized into the *tert*-butyl nitrosoformate (**IV-13-A**). Highly reactive **IV-13-A** is trapped by 1,2-dimethylindole **IV-15** to form intermediate **IV-15-A**. Subsequent loss of H⁺ forms intermediate **IV-15-B**. Oxidation of intermediate **IV-15-B** mediated through Cu(II) to Cu(I) yields intermediate **IV-15-C**, which undergoes a cyclobutane formation to form intermediate **IV-15-D**. Fragmentation of the intermediate **IV-15-D** yields the final oxindole product **IV-19**.

IV.5 Selective C-H functionalization

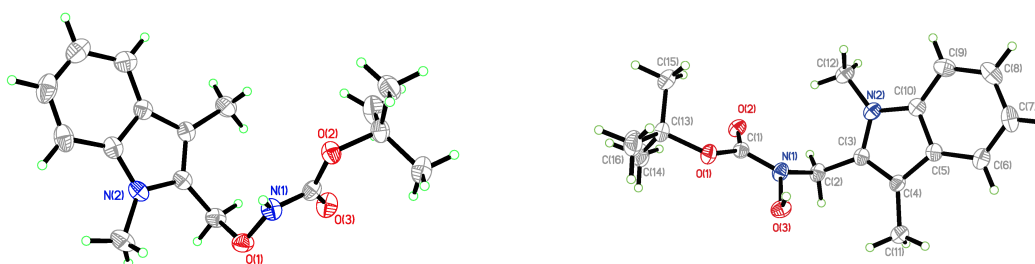
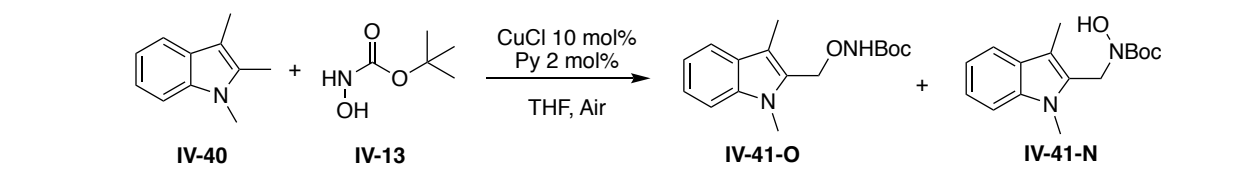
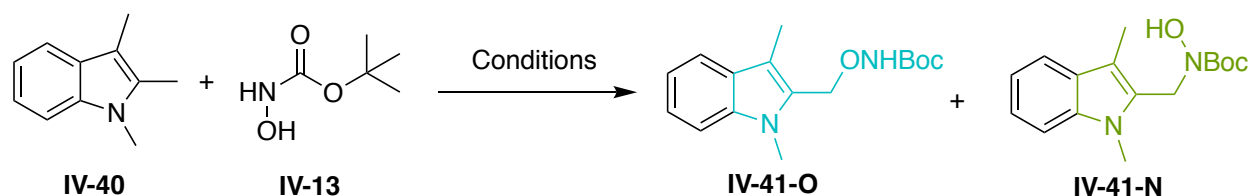


Figure IV-15. Unexpected indole allylic functionalization reaction. Crystal structures of compound **IV-41-O** is on the left and **IV-41-N** is on the right.

During the initial indole substrates screening (**Figure IV-7**), we were surprised to find that when 1,2,3-trialkylindole **IV-40** was subjected to the optimal oxindole reaction conditions, two different regioisomeric products were obtained: C-H oxidation product **IV-41-O** and C-H amination product **IV-41-N**. The oxidation product **IV-41-O** has a slightly higher yield over the amination product **IV-41-N**. Crystal structures to confirm both of

these two products were obtained (**Figure IV-15**). Notably, this interesting indole allylic functionalization happens exclusively on C2 position ($rr_{C2:C3} > 19:1$).

IV.5.1 Reaction optimization



Entry	CuCl X mol %	IV-13 equiv	Pyridine X mol %	Additive (X mol %)	THF volumn	IV-41-O yield ^a	IV-41-N yield ^a
1	20	4	0	--	2	57	20
2	20	4	2	--	2	55	25
3	50	4	2	--	2	50	20
4	20	4	12	--	2	14	53
5	20	4	12	--	4	34	41
6	20	4	12	--	1	32	<5
7	20	4	2	H ₂ O (5)	2	45	16
8	20	4	2	H ₂ O (10)	2	46	15
9	20	4	2	H ₂ O (15)	2	45	25
10	20	4	2	H ₂ O (20)	2	20	46
11	20	4	2	H ₂ O (30)	2	20	69
12	20	4	2	H₂O (20)	1	63	9
13	20	4	2	Cs ₂ CO ₃ (100)	2	N/A	N/A
14	20	4	2	K ₂ CO ₃ (100)	2	N/A	N/A

Table IV-2. Reaction optimization. ^aDetermined by ¹H-NMR using MTBE as an internal standard, all reactions were performed at 0.1 mmol scale.

We have taken the liberty to define *ar* as the amphireactive-selectivity ratio, denoting the distribution of products obtained from reaction at the oxygen atom relative to the nitrogen atom of the nitroso group. Intrigued by this different reaction, we examined the possibility to obtain either form in a higher amphireactive-selectivity ratio (**Table IV-2**). After trying different additives, it was found that water can suppress the amination product,

thus favoring the oxidation product **IV-41-O**. We first tested water as an additive, however increasing its concentration only leads to a worse $ar_{O:N}$ ratio at 1 mL THF (0.05M concentration), (entry 7-11, **Table IV-2**). Surprisingly, when the reaction was conducted at 0.1M concentration with 20 equivalent water as an additive, a higher amphireactive-selectivity for oxidation was achieved ($ar_{O:N} = 6.7:1$, entry 12).

Next, the effect of base was examined. Gratifyingly, when the pyridine loading was increased to 12 mol%, the selectivity was reversed from the C-H oxidation to the C-H amination product ($ar_{O:N} = 1:3.8$, entry 4). However, adding more pyridine leads to overall suppression of the reaction, while replacing the pyridine to other base shuts down the reaction (entry 13, 14). Overall, we can selectively tune this reaction either towards the amination or oxidation pathway by simply altering the reaction conditions.

IV.5.2 Reaction substrate scope

Using the optimized conditions for oxidation and amination, the substrate scope of this reaction was investigated. Replacing the methyl group on the nitrogen atom to benzyl or ethyl group leads to a lower ar ratio for both oxidation and amination reactions (**IV-42**, **IV-43**). For electron rich indoles, $ar_{O:N}$ is much higher as compared with electron poor indole substrates. Substrates **IV-44** to **IV-48** have a much lower C-H amination selectivity ($ar_{O:N} < 1:3$) even under the amination conditions. However, with the electron withdrawing groups on the indole, C-H amination is highly favored (**IV-49-N**, **IV-50-N**, $ar_{O:N} < 1:10$). For these two entries, less amount of pyridine was used, since 12 mol% loading leads to the suppression of these two reactions. Another interesting observation is that the selectivity for C-H oxidation was higher when C2 is ethyl group instead of methyl group

(IV-52-O, 53%, $ar_{O:N} = 13:1$), even under the conditions that favor amination, there is no clear preference for amination vs oxidation. However, if C3 is an ethyl group, this preference is not observed.

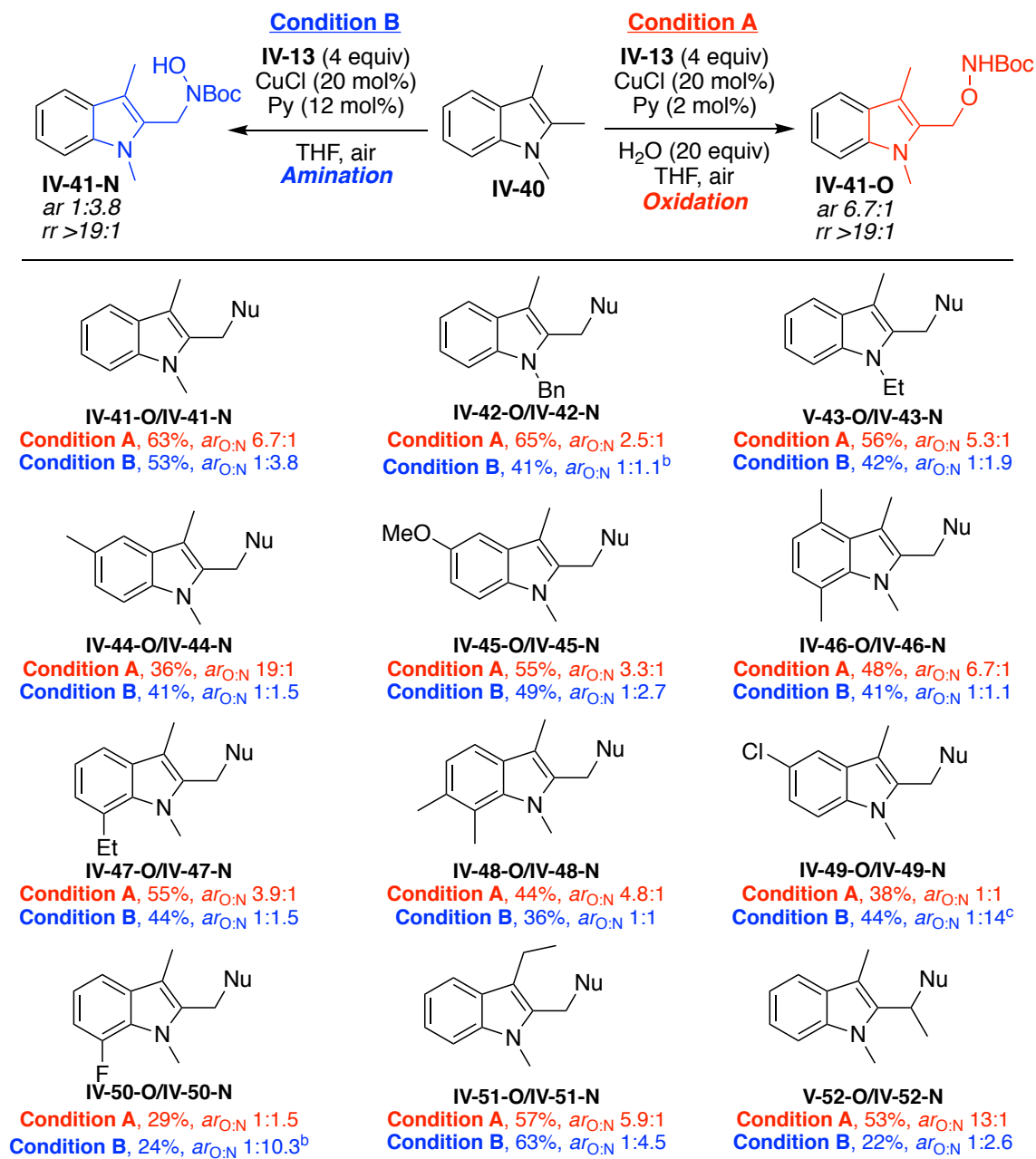


Figure IV-16. Indole selective C-H functionalization scope. a) Reactions were conducted on a 0.1 mmol scale in 1 mL THF (with 20 equiv H₂O) and yield was measured by NMR with internal standard MTBE. $ar_{O:N}$ defined as the oxidation to amination product ratio. b) 6 mol% pyridine was used. c) 4 mol% pyridine was used.

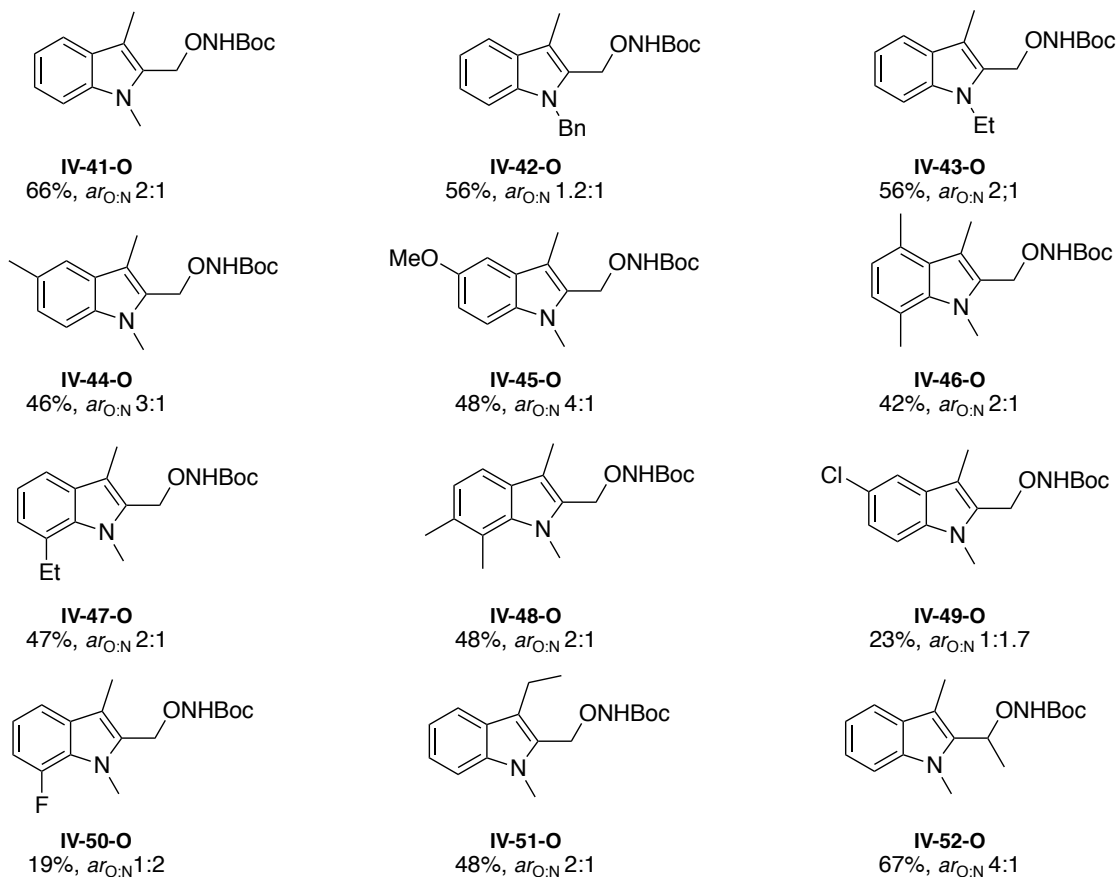
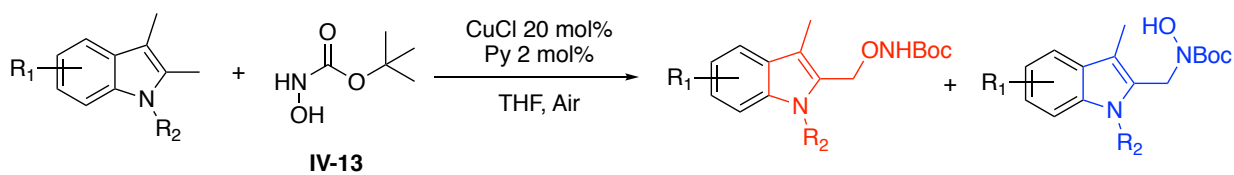
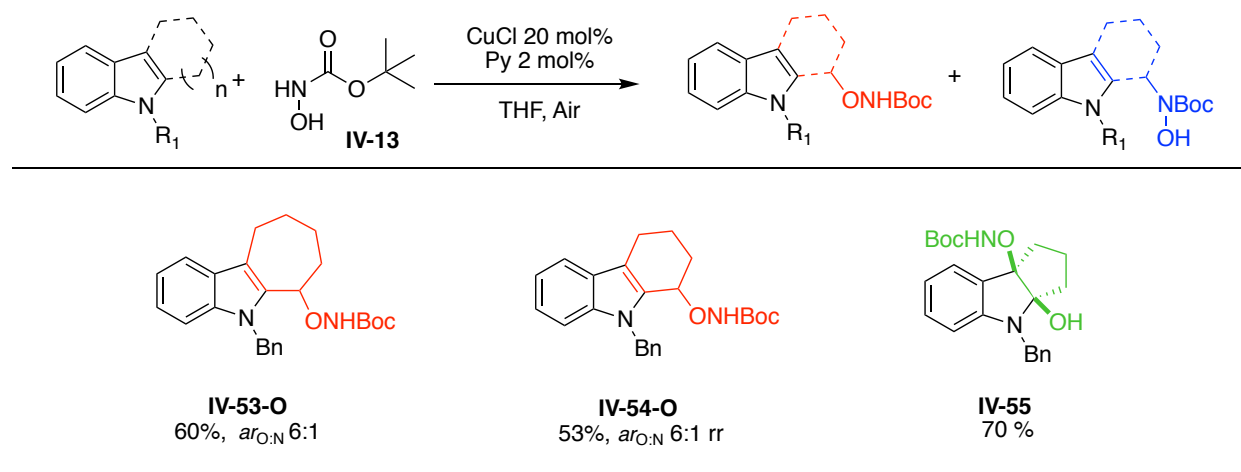


Figure IV-17. Obtaining both products in decent amount of yield. Reaction were conducted on a 0.2 mmol scale with 4 equivalent **IV-13** in 4 mL THF open to air.

Next, we explored the possibility for a one pot reaction condition (with 20 mol% CuCl, 2 mol% pyridine in 4 mL THF) that can afford both C-H oxidation and amination products in decent yields (**Figure IV-17**). Under these reaction conditions, C-H oxidation product is favored for the electron rich and neutral substrates (**IV-41** to **IV-48**) whereas amination product is favored for the electron withdrawing substrates (**IV-49**, **IV-50**). Both products can be isolated in decent amount yields.

IV.5.3 Exploring ring fused indoles



Crystal Structure of **IV-55**:

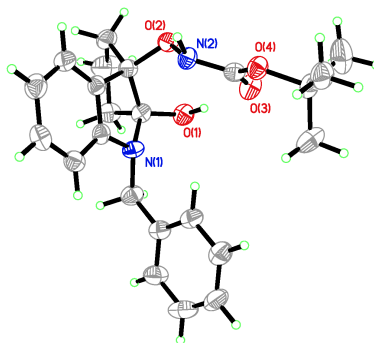


Figure IV-18. Ring fused indoles substrate scope. Reactions were conducted on a 0.2 mmol scale with 4 equivalent **IV-13** open to air. Crystal structure of **IV-55** was confirmed by X-Ray and crystal structure is shown above.

The ability to selectively functionalize indole allylic positions provides a useful method for the total synthesis of indole alkaloids. Efforts towards expansion of this reaction to ring fused indoles by our approach is listed in **Figure IV-18**. Both 6 and 7 member fused ring substrates afforded good yield (60% and 53% yield for **IV-53-O** and **IV-54-O** respectively) and amphoteric-selectivity ratio ($ar_{O:N} = 6:1$). However, in an

attempt to get the 5-member fused indole structure, a 5-member ring fused indoline was formed (**IV-55**) instead in 70% yield. Instead of going through an allylic functionalization, the indole ring undergoes dearomatization leading to a hydroxylated indoline. This transformation suggests that trapping of the *tert*-butyl nitrosoformate is involved in this reaction (**Figure IV-19**). It is believed that the 5-member ring strain restricts the allylic H elimination, thus only affords **IV-55** as the product.

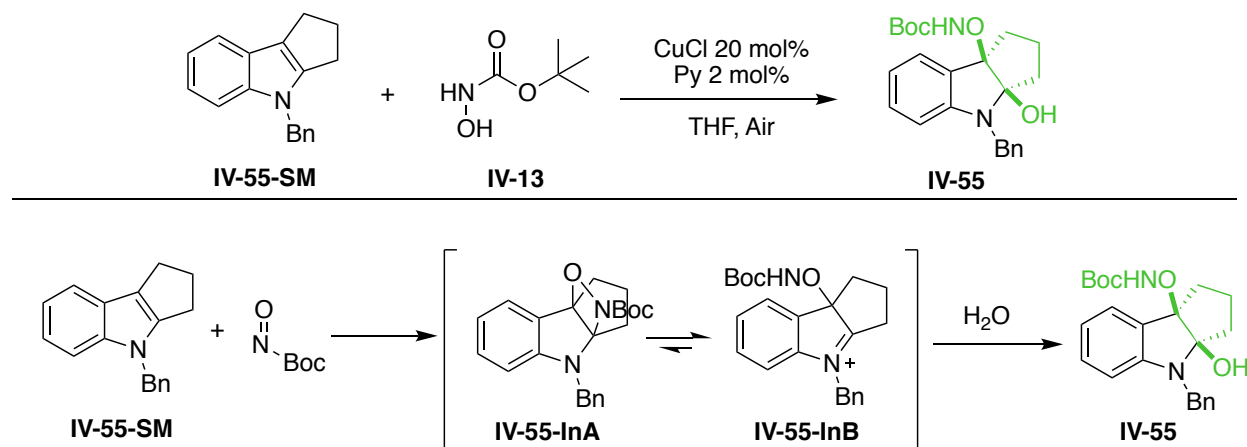


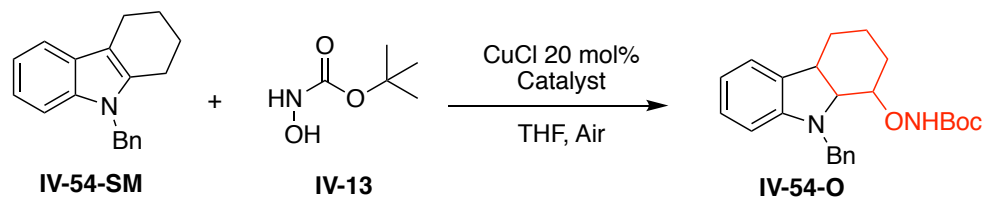
Figure IV-19. Possible reaction mechanism to yield **IV-55**. Intermediates **IV-55-InA** and **IV-55-InB** are possible intermediates which can trap water to yield final product.

IV.5.4. Attempts towards enantioselective C-H functionalization

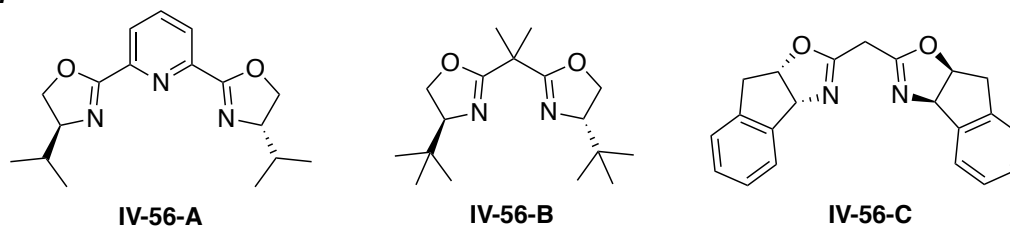
Next, we attempted to functionalize the indole allylic position in an enantioselective manner by using chiral box ligands, which have been widely used for the enantioselective copper catalyzed reactions.⁵⁴⁻⁵⁵ We chose 3 different box ligands **IV-56-A**, **IV-56-B** and **IV-56-C**. We began our investigation with the reaction yielding compound **IV-54-O**, which can be analyzed for enantio-enriched products by chiral OD-H column.

With 4 mol% chiral box ligand loading, reactions were suppressed and low conversion and racemic product were obtained (entry 1-3, **Figure IV-20**). However, when the loading was reduced to 2 mol%, we did observe an increased reaction conversion for

all 3 entries, however the products obtained were still racemic. Unfortunately, we were not able to optimize this reaction to occur in an enantioselective manner.



Catalyst:



Entry	Catalyst	Catalyst loading mol %	Conversion (%) ^a	Product yield (%) ^a	<i>ee</i> (%) ^b
1	IV-56-A	4	37	36	0
2	IV-56-B	4	37	30	0
3	IV-56-C	4	52	42	0
4	IV-56-A	2	88	84	0
5	IV-56-B	2	69	57	0
6	IV-56-C	2	84	69	0

Figure IV-20. Attempts to the enantioselective allylic indole functionalization. 4 equivalent of **IV-13** were used. ^a Reaction conversion and product yield were measured by ¹H-NMR. ^b *ee* value was measured by chiral HPLC equipped with OD-H column.

IV.5.5. Reaction mechanism

Regarding the C-H functionalization mechanism, we believe the oxidation cycle of hydroxylamine remains the same (**Figure IV-21**). After trapping the *tert*-butyl nitrosoformate by the trialkylindole, intermediate **IV-41-A** undergoes isomerization to form indoline **IV-41-B**. This active indoline can be attacked by either O or N from the free form of the hydroxylamine **IV-13** to yield either **IV-41-N** or **IV-41-O**. O or N attack can also be

altered by switching the reaction conditions to yield the final product, presumably as result of the change on acidity of NH and OH in the presence or absence of water.

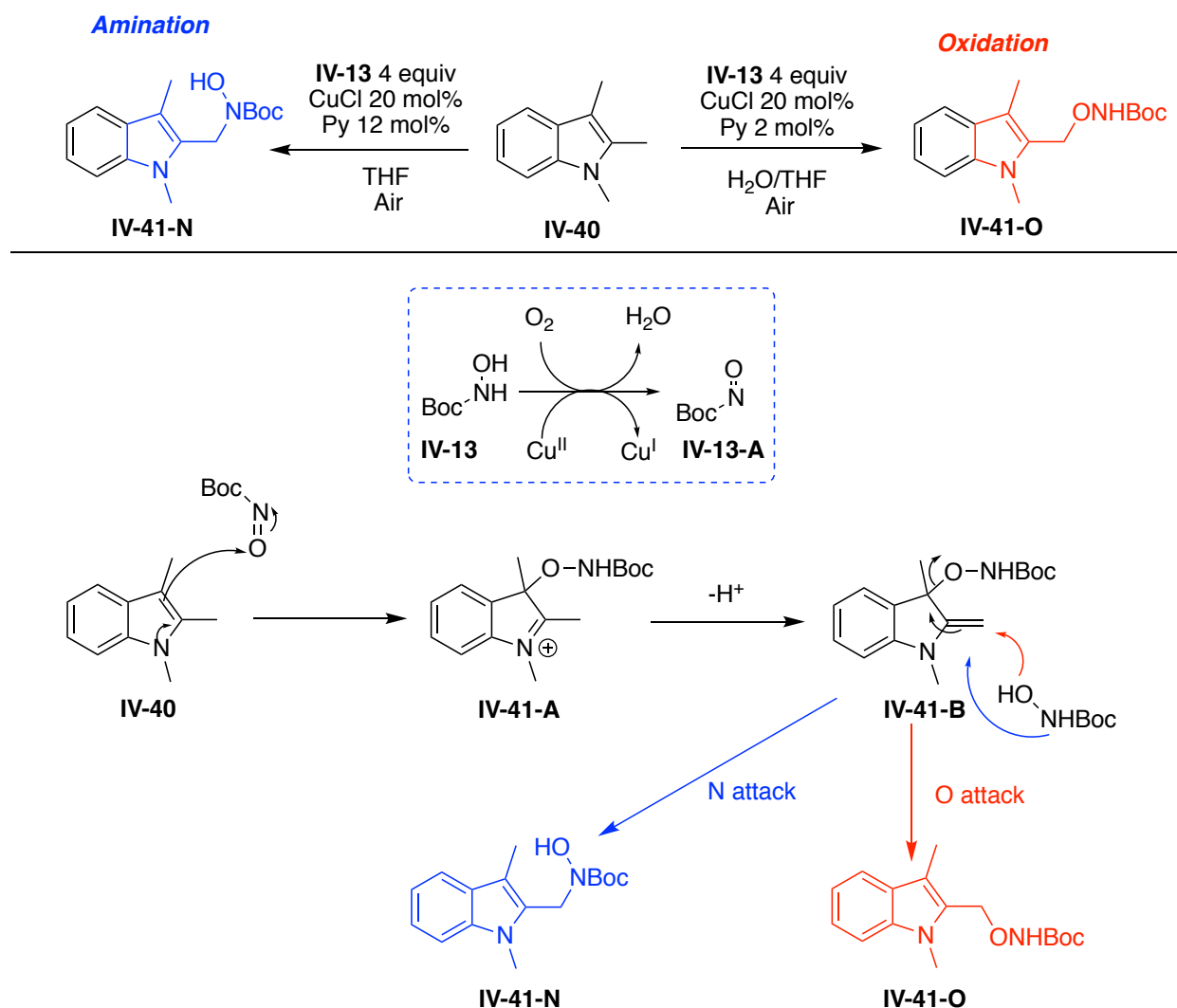
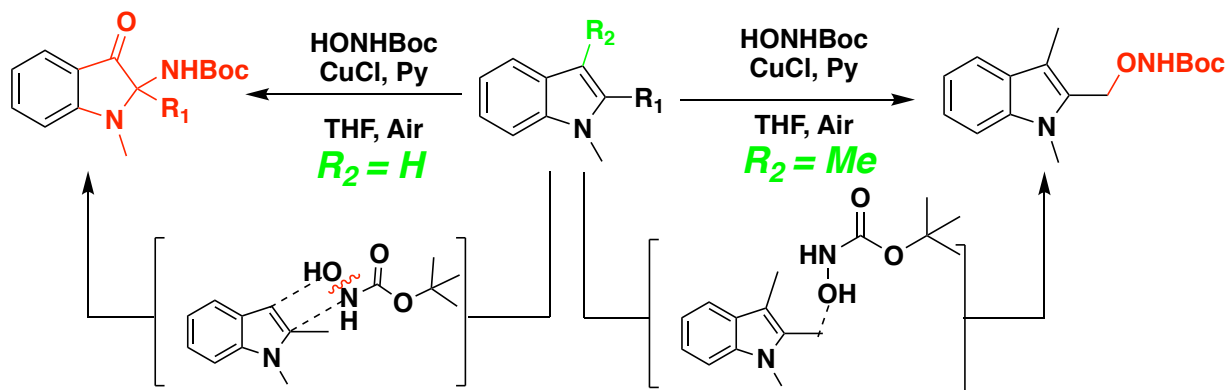


Figure IV-21. Indole C-H functionalization mechanism.

IV.6 Summary and conclusion

In conclusion, we have developed a mild tunable copper (I) catalyzed indole oxidation and a selective C-H functionalization method (**Scheme IV-15**). It features a new way to oxidize 1,2-dialkyl indoles to form oxindole frameworks. Meanwhile it also provides a new approach for the selective C-H functionalization of 1,2,3-trialkyl indoles or cyclic

indoles. This project started from an unexpected reaction and I am very grateful for all the support to continue and finish this project.



Scheme IV-15. Overall reaction scheme.

IV.7 Experimental section

IV.7.1 Materials and general instrumentations

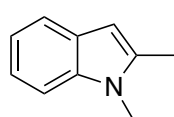
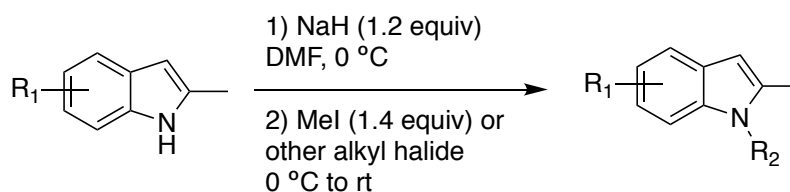
Solvents and reagents used for reactions were purchased from commercial sources. Tetrahydrofuran (THF) and diethyl ether (Et₂O) were dried over sodium whereas toluene and dichloromethane (DCM) were dried over calcium hydride (CaH₂) before use. N,N-dimethylformamide (DMF) was dried over 3Å molecule sieves. THF for copper catalyzed reactions was HPLC grade from Sigma-Aldrich. CuCl was reagent plus grade from Sigma-Aldrich and was used directly.

Column chromatography was performed on SiliCycle silica gel (230-400 mesh). Prep-TLC (1000 micros) and thin layer chromatography (TLC) with fluorescent indicator was purchased from Analtech. Oxindole formation reactions were performed in Pyrex 12 * 75 mm or 13 * 100 mm size test tubes based on the solvent volume.

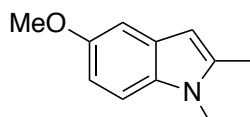
¹H-NMR and ¹³C-NMR spectra were obtained on Agilent Direct Drive2 500 MHz and Varian Inova 500 MHz instruments and were reported in parts per million (ppm) relative to the solvent resonances (δ), with coupling constants (J) in Hertz (Hz). HRMS analysis was performed on a Q-TOF Ultima system using electrospray ionization in positive mode. UV-Vis was performed on Agilent Cary 100 series machine and PL was recorded on Fluorolog by ISA instrument. HPLC purification was performed on Rainin HPXL solvent delivery system equipped with Rainin Dynamax absorbance detector. Low temperature reaction was carried out in Operon Ultra-low temperature freezer with accurate temperature control. X-Ray crystallography was performed on Apex II CCD instrument in Michigan State University crystallography center.

IV.7.2 Preparation of starting materials

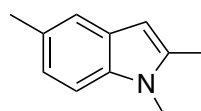
IV.7.2.1 Procedure 1



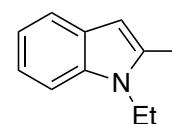
IV-15
99%



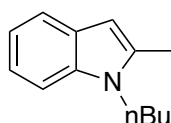
IV-20-SM
70%



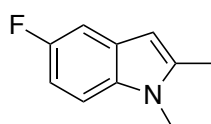
IV-21-SM
67%



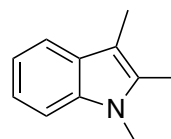
IV-34-SM
99%



IV-35-SM
99%



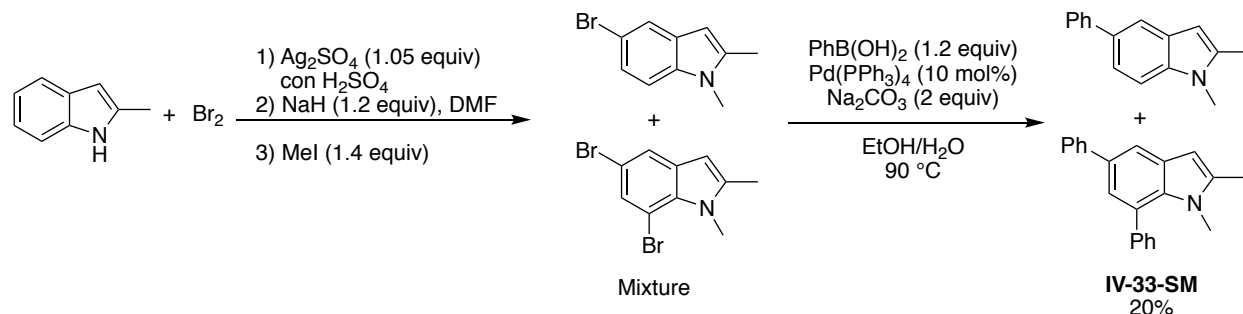
IV-37-SM
63%



IV-40
99%

To a solution of commercially available unprotected indole (2 mmol) in N,N-dimethylformamide (5 mL, DMF) was added 60% NaH in mineral oil (96 mg, 2.4 mmol, 1,2 equiv) at 0 °C. The reaction was slowly warm up to rt. After stirring for 30 min, the reaction was cooled back to 0 °C and the appropriated alkyl halide (2.4 mmol, 1.2 equiv) was added dropwise. The mixture was allowed to warm up to rt and the reaction was monitored by TLC. After the reaction was complete, it was quenched with water (5 mL) and extracted with ethyl acetate (3*20 mL). The organic layer was washed with water (3*10 mL) and brine (10 mL), dried over sodium sulfate and concentrated in vacuum. In most of cases, the crude product could be used without further purification. If necessary, the crude was purified by flash column with ethyl acetate and hexanes.

IV.7.2.2 Procedure 2



1,2-Dimethyl-5,7-diphenylindole (IV-33-SM):

2-Methyl indole (1.31g, 10 mmol) was slowly dissolved in conc. H₂SO₄ (20 mL), followed by slow addition of Ag₂SO₄ (3.27 g, 1.05 equiv) at 0 °C and stirred for 0.5 h. To the mixture was added Br₂ (0.54 mL, 1.05 equiv) slowly (~40 min) at the same temperature. The reaction was allowed to warm up to rt and stirred for 4 h, quenched by cold water (20 mL), extracted by DCM (3*70 mL), washed with water and brine. The organic layer was passed through a celite pad to remove the silver and then dried over sodium sulfate and concentrated in vacuo to afford the crude product. The mixture was taken to the next step without purification. The crude was dissolved in DMF (15 mL) and *procedure 1* was followed to synthesize the methylated indole. However, at this stage, the mixtures were not able to be separated by flash column and thus were directly injected to the next step.

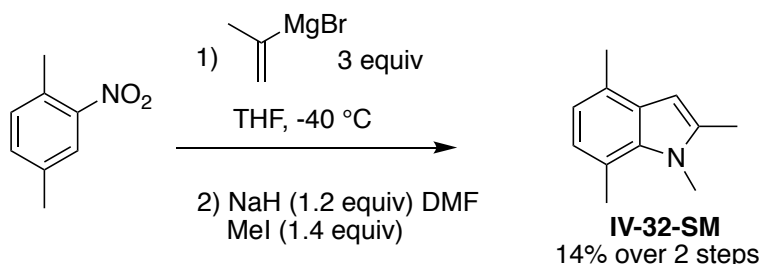
To the mixed products (~2.5 mmol) in toluene (10 mL) was added Pd(PPh₃)₄ (289 mg, 10 mol%), Na₂CO₃ (530 mg, 5 mmol, 2 equiv), PhB(OH)₂ (366 mg, 3 mmol), EtOH (1 mL) and H₂O (2 mL). The reaction was heated in a sealed tube at 90 °C for 24 h. The mixture was poured into the water, extracted with EtOAc (3*50 mL), washed with water and brine, passed through a celite pad to remove the catalyst and then dried over sodium

sulfate and concentrated in vacuo. The desired product was purified by flash column with 5% EtOAc/Hexanes and further purified by recrystallization in DCM/Hexanes to yield a white solid product **IV-33-SM** (150 mg, 20 %).

$^1\text{H-NMR}$ (500 MHz, CDCl_3): δ 7.54 (s, 1H), 7.27 (s, 1H), 7.20 – 7.11 (m, 10H), 6.28 (s, 1H), 3.68 (s, 3H), 2.44 (s, 3H).

$^{13}\text{C-NMR}$ (126 MHz, CDCl_3): δ 143.11, 142.96, 138.05, 136.90, 133.84, 132.71, 130.39, 130.32, 127.63, 127.55, 127.33, 125.75, 125.53, 121.45, 110.63, 99.56, 29.53, 12.87.

IV.7.2.3 Procedure 3



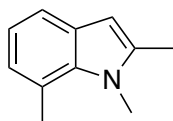
1,2,4,7-Tetramethylindole (**IV-32-SM**)

Bartoli Indole synthesis was used to prepare the following indoles.⁵⁶ To 1,4-dimethyl-2-nitrobenzene (453 mg, 3 mmol) in anhydrous THF (10 mL) was added isopropenyl magnesium bromide solution (0.5 M in THF, 18 mL, 3 equiv) in one portion at $-40\text{ }^\circ\text{C}$. The mixture was stirred at this temperature for 1 h, quenched with saturated NH_4Cl (10 mL) at $-40\text{ }^\circ\text{C}$, extracted with EtOAc (3*20 mL), washed with water and brine, dried over sodium sulfate and concentrated in vacuo. The crude product was purified by flash column with 5% EtOAc/Hexanes to yield a brown oil (100 mg, 21%). *Procedure 1*

was followed to yield the methylated yellow solid product **IV-32-SM** (74 mg, 14% over 2 steps).

$^1\text{H-NMR}$ (500 MHz, CDCl_3): δ 6.78 – 6.68 (m, 2H), 6.21 (s, 1H), 3.90 (s, 3H), 2.72 (s, 3H), 2.43 (s, 3H), 2.39 (s, 3H).

$^{13}\text{C-NMR}$ (126 MHz, CDCl_3): δ 136.50, 135.60, 128.24, 126.87, 123.65, 123.62, 119.38, 117.97, 98.70, 32.43, 20.02, 18.36, 13.33.



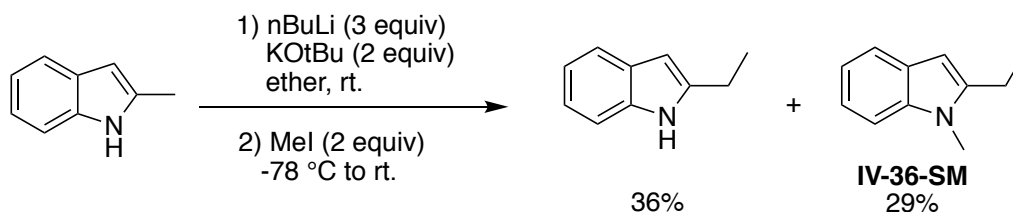
1,2,7-Trimethylindole (**IV-31-SM**)

The title compound was prepared according to *procedure 3* using 2-nitrotoluene (411 mg, 3 mmol) with isopropenyl magnesium bromide solution (0.5 M in THF, 18 mL, 3 equiv) in THF (10 mL). The crude product was purified by flash column to yield a red oil (121 mg, 28%). Methylation following *procedure 1* yields the final product **IV-31-SM** (130 mg, 27% over 2 steps).

$^1\text{H-NMR}$ (500 MHz, CDCl_3): δ 7.38 (d, $J = 7.6$ Hz, 1H), 6.95 (t, $J = 7.4$ Hz, 1H), 6.86 (m, 1H), 6.24 (s, 1H), 3.93 (s, 3H), 2.79 (s, 3H), 2.41 (s, 3H).

$^{13}\text{C-NMR}$ (126 MHz, CDCl_3): δ 137.18, 136.10, 128.65, 123.69, 120.48, 119.32, 117.86, 100.28, 32.53, 20.29, 13.31.

IV.7.2.4 Procedure 4



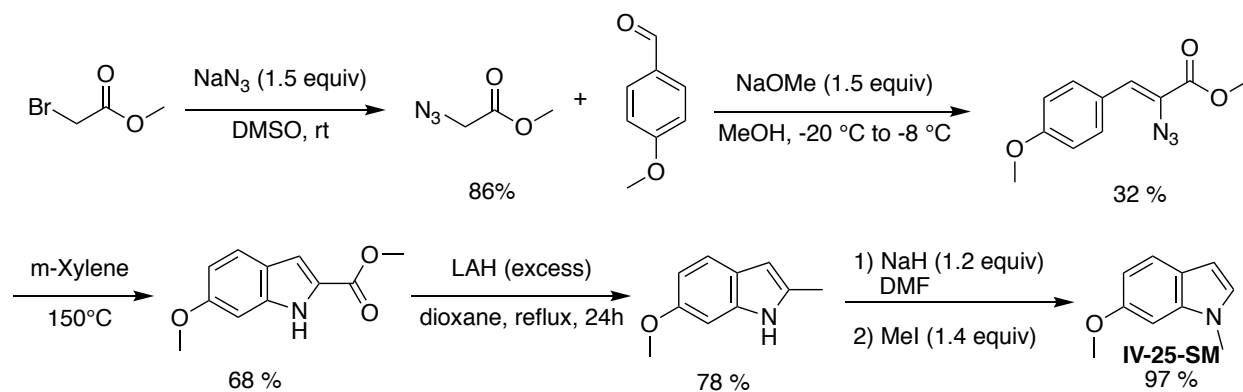
2-Ethyl-1-methylindole (IV-36-SM)

The title compound was prepared according to literature procedure.⁵⁷ To 2-methylindole (262 mg, 2 mmol) in anhydrous ether (20 mL) was added *n*BuLi (2.4 mL, 6 mmol, 3 equiv) at rt, followed by addition of KOtBu (450 mg, 2 equiv). The mixture was stirred at rt for 0.5 h, then cooled to -78 °C, MeI (0.25 mL, 2 equiv) was added at this temperature and stirred for 2 h. The reaction was quenched with H₂O (5 mL), extracted with EtOAc (3*20 mL), washed with water and brine, dried over sodium sulfate and concentrated in vacuo. The crude was purified by flash column with 5% EtOAc/Hexanes to yield product **IV-36-SM** (91 mg, 29%).

¹H-NMR (500 MHz, CDCl₃): δ 7.53 (d, *J* = 7.8 Hz, 1H), 7.24 (d, *J* = 7.8 Hz, 1H), 7.14 (t, *J* = 7.6 Hz, 1H), 7.05 (t, *J* = 7.4 Hz, 1H), 6.24 (s, 1H), 3.65 (s, 3H), 2.75 (q, *J* = 7.5 Hz, 2H), 1.34 (t, *J* = 7.5 Hz, 3H).

¹³C-NMR (126 MHz, CDCl₃): δ 142.89, 137.35, 127.85, 120.48, 119.74, 119.15, 108.63, 97.75, 29.31, 20.09, 12.75.

IV.7.2.5 Procedure 5



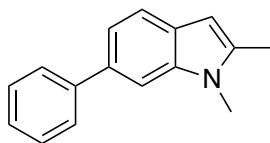
6-Methoxy-1,2-dimethylindole (IV-25-SM)⁵⁸⁻⁵⁹

To a NaOMe/MeOH solution (3 mmol) in MeOH (1 mL) was added 4-methoxy benzaldehyde (272 mg, 2 mmol) and methyl 2-azidoacetate (690 mg, 6 mmol, 3 equiv) at $-20\text{ }^\circ\text{C}$ (strong exothermic reaction, slow addition). The mixture was stirred at $-8\text{ }^\circ\text{C}$ for 7 h. The reaction was quenched by addition of water (10 mL), extracted with EtOAc (3*20 mL), washed with water and brine, dried over sodium sulfate and concentrated in vacuo. The crude was purified by flash column with 15% EtOAc/Hexanes to yield methyl (Z)-2-azido-3-(4-methoxyphenyl)acrylate product (149 mg, 32%). The product was dissolved in dry m-xylene (3 mL) and refluxed for 3 h in a sealed tube. Solvent was removed under nitrogen flow to yield the methyl 6-methoxy-indole-2-carboxylate as an off white solid product (89 mg, 68%). The crude was taken to the next step without purification. To LiAlH_4 (160 mg, 10 equiv) in anhydrous dioxane (3 mL) was added the crude indole product from the previous step. The mixture was heated to reflux for 24 h. The reaction was cooled down to $0\text{ }^\circ\text{C}$ and quenched with water, extracted with EtOAc (3*20 mL), passed through a celite pad, washed with water and brine, dried over sodium sulfate and concentrated in vacuo. The crude product was purified by flash column to yield the 6-

methoxy-2-methyl-1*H*-indole as a white solid product (52 mg, 78%). *Procedure 1* was followed to yield 6-methoxy-1,2-dimethyl-indole **IV-25-SM** as an off white solid (55 mg, 97%).

¹H-NMR (500 MHz, CDCl₃): δ 7.41 – 7.31 (m, 1H), 6.80 – 6.62 (m, 2H), 6.11 (s, 1H), 3.85 (s, 3H), 3.59 (s, 3H), 2.37 (s, 3H).

¹³C-NMR (126 MHz, CDCl₃): δ 155.48, 137.93, 135.64, 122.16, 120.09, 108.52, 99.16, 93.10, 55.82, 29.42, 12.79.



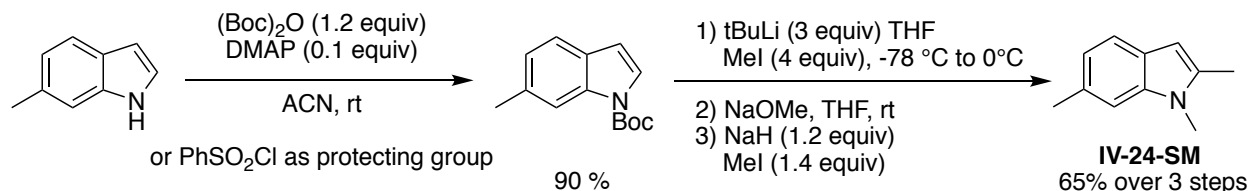
1,2-Dimethyl-6-phenylindole (**IV-26-SM**)

The title compound was prepared according to *procedure 5* starting from *p*-phenyl benzaldehyde (546 mg, 3 mmol), methyl 2-azidoacetate (690 mg, 6 mmol, 3 equiv) and NaOMe/MeOH solution (3 mmol). The first step yielded 754 mg of product (90% yield). Step 2: Product from previous step (1 mmol) was dissolved in xylene (3 mL) and refluxed, yielding 233 mg product (93% yield). Step 3: product from previous step (0.5 mmol) was reacted with 10 equiv of LAH to yield 42 mg of the indole product (40% yield). Final methylation step (*procedure 1*) yielded **IV-26-SM** as an off white solid (44 mg, 99%).

¹H-NMR (500 MHz, CDCl₃): δ 7.68 – 7.63 (m, 2H), 7.54 (dd, *J* = 8.2, 0.6 Hz, 1H), 7.45 – 7.39 (m, 3H), 7.33 – 7.26 (m, 2H), 6.23 (s, 1H), 3.69 (s, 3H), 2.43 (s, 3H).

¹³C-NMR (126 MHz, CDCl₃): δ 142.77, 137.82, 137.61, 134.01, 128.62, 127.36, 127.29, 126.33, 119.73, 119.12, 107.38, 99.45, 29.43, 12.88

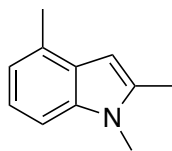
IV.7.2.6 Procedure 6



To the 6-methyl indole (196 mg, 1.5 mmol) in acetonitrile (5 mL) was added (Boc)₂O (392 mg, 1.8 mmol, 1.2 equiv) and DMAP (18 mg, 0.15 mmol, 0.1 equiv) at rt. After stirring for 1 h, the reaction was quenched with addition of water, the mixture was subjected to the general workup protocol and purified by flash chromatography with 5% EtOAc/Hexanes to yield an oil (313 mg, 90%). *Step 2:* To the Boc protected indole (310 mg, 1.34 mmol) was added tBuLi (4 mmol, 3 equiv) in anhydrous THF (15 mL) at -78 °C, the mixture was stirred for 1 h, MeI (767 mg, 5.4 mmol, 4 equiv) was then added. The reaction was slowly warm up to 0 °C and stirred for 1.5 h. After the reaction was complete, it was quenched by saturated NH₄Cl, subjected to the workup protocol and purified by flash chromatography to yield a brown solid product (316 mg, 96 %). *Step 3:* Compound from previous step was dissolved in THF (2 mL), followed by addition of NaOMe in MeOH (4.7 M solution, 1 mL) at rt. The reaction was stirred for 50 min and subjected to the workup protocol, the crude product was taken to the next step without purification. *Step 4: Procedure 1* was followed to methylate the crude product to yield an off white solid product **IV-24-SM** (54 mg, 65 % over 3 steps).

¹H-NMR (500 MHz, CDCl₃): δ 7.37 (d, *J* = 7.9 Hz, 1H), 7.03 (dd, *J* = 1.7, 0.8 Hz, 1H), 6.88 (dd, *J* = 7.9, 1.4 Hz, 1H), 6.16 (s, 1H), 3.61 (s, 3H), 2.46 (s, 3H), 2.38 (s, 3H).

^{13}C -NMR (126 MHz, CDCl_3): δ 137.69, 136.09, 130.09, 125.67, 120.84, 119.22, 108.84, 99.21, 29.29, 21.86, 12.77.

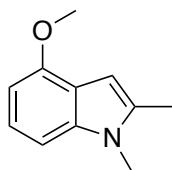


1,2,4-Trimethylindole (**IV-30-SM**)

The title compound was prepared according to *procedure 6* starting from 4-methyl indole (262 mg, 2 mmol) and PhSO_2Cl (424mg, 2.4 mmol) to yield protected indole (340 mg, 63 %). *Step 2*: Subjected 1 mmol of the previous product for alkylation to yield the second product (159 mg, 56%). *Step 3 and 4*: Deprotection yielded 82 mg of the product, which was directly subjected to the *procedure 1* alkylation to yield the final product **IV-30-SM** as a yellow solid (90 mg, 99%).

^1H -NMR (500 MHz, CDCl_3): δ 7.13 – 6.98 (m, 2H), 6.85 (d, $J = 6.9$ Hz, 1H), 6.22 (s, 1H), 3.64 (s, 3H), 2.49 (s, 3H), 2.42 (s, 3H).

^{13}C -NMR (126 MHz, CDCl_3): δ 136.96, 136.12, 129.04, 127.63, 120.56, 119.48, 106.37, 98.06, 29.53, 18.68, 12.81.



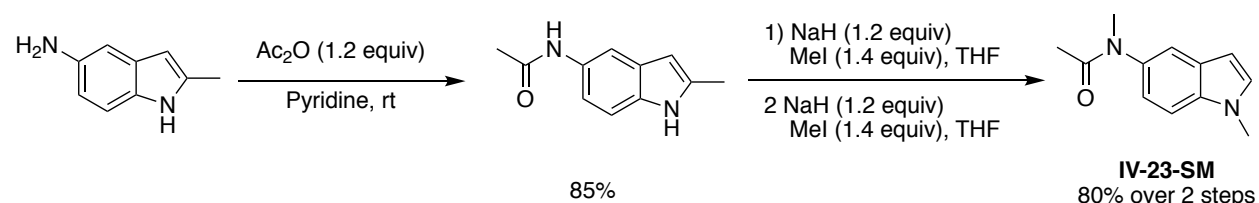
4-Methoxy-1,2-dimethylindole (**IV-29-SM**)

The title compound was prepared according to *procedure 6* starting from 4-methoxy indole (220 mg, 1.5 mmol) and (Boc)₂O (392 mg, 1.8 mmol) to yield Boc protected indole (367 mg, 99%). *Step 2*: procedure 6 was followed to yield *t*-butyl 4-methoxy-2-methyl-1*H*-indole-1-carboxylate (335 mg, 86%). *Step 3*: Deprotection yielded a light yellow product (156 mg, 76%). *Step 4*: Unprotected indole (0.6 mmol) was subjected to *procedure 1* methylation to yield a white solid product **IV-29-SM** (102 mg, 97%).

¹H-NMR (500 MHz, CDCl₃): δ 7.06 (t, *J* = 8.0 Hz, 1H), 6.89 (dd, *J* = 8.2, 0.7 Hz, 1H), 6.50 (dd, *J* = 7.8, 0.6 Hz, 1H), 6.32 (s, 1H), 3.93 (s, 3H), 3.63 (s, 3H), 2.40 (s, 3H).

¹³C-NMR (126 MHz, CDCl₃): δ 152.56, 138.74, 121.14, 118.13, 102.45, 99.49, 96.67, 55.35, 29.72, 12.75.

IV.7.2.7 Procedure 7



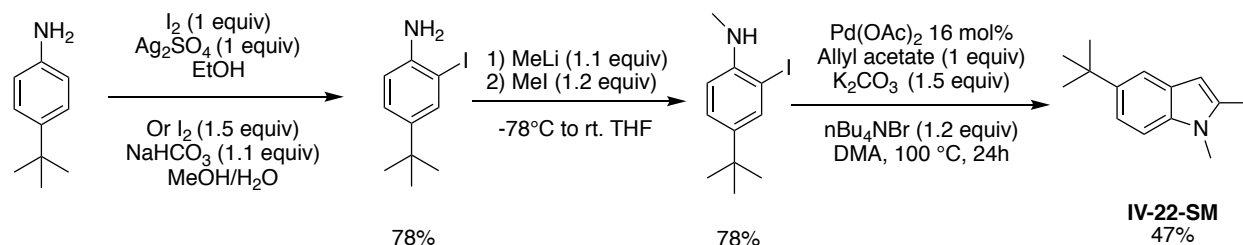
N-(1,2-dimethylindol-5-yl)-*N*-methylacetamide (**IV-23-SM**)

To the 2-methyl-1*H*-indol-5-amine (146 mg, 1 mmol) in pyridine (5 mL) was added acetic anhydride (114 μL, 1.2 mmol, 1.2 equiv), the mixture was stirred overnight and quenched with water, subjected to the work up protocol followed by flash column purification to yield a grey solid product (160 mg, 85%). Double methylation following *procedure 1* yielded the final product **IV-23-SM** (86 mg, 80%).

$^1\text{H-NMR}$ (500 MHz, CDCl_3): δ 7.29 (dd, $J = 2.1, 0.6$ Hz, 1H), 7.22 (d, $J = 8.5$ Hz, 1H), 6.92 (dd, $J = 8.5, 2.1$ Hz, 1H), 6.24 (s, 1H), 3.67 (s, 3H), 3.28 (s, 3H), 2.42 (s, 3H), 1.84 (s, 3H).

$^{13}\text{C-NMR}$ (126 MHz, CDCl_3): δ 171.40, 138.60, 136.86, 136.22, 128.27, 119.43, 117.91, 109.52, 99.86, 37.75, 29.62, 22.42, 12.83.

IV.7.2.8 Procedure 8



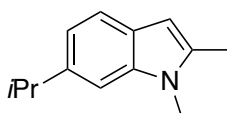
5-(*Tert*-butyl)-1,2-dimethylindole (**IV-22-SM**)

The title compound was prepared according to a modified literature procedure.⁶⁰ To the 4-*tert*-butyl aniline (447 mg, 3 mmol), Ag_2SO_4 (954 mg, 3 mmol) in ethanol (10 mL) was added I_2 (762 mg, 3 mmol) in ethanol (10 mL) dropwise at rt. After stirring 4 h at rt, the reaction was dried under vacuum and dissolved in DCM (100 mL), washed with NaHSO_3 and brine, concentrated on vacuum and purified by flash column to yield a brown oil product 4-(*tert*-butyl)-2-iodoaniline (644 mg, 78%). To the 4-(*tert*-butyl)-2-iodoaniline (412 mg, 1.5 mmol) in anhydrous THF (5 mL) was added MeLi (1.05 mL, 1.65 mmol) at -78°C . After stirring 1 h at this temperature, MeI (256 mg, 1.8 mmol) was added dropwise, the reaction was allowed to warm up to rt and stirred for overnight. The reaction was quenched by saturated NH_4Cl and subjected to the general workup protocol, purified by flash column with 2.5% EtOAc/Hexanes to yield a light brown oil (339 mg, 78%). To the

4-(*tert*-butyl)-2-iodo-*N*-methylaniline (240 mg, 0.83 mmol, 1.2 equiv), $n\text{Bu}_4\text{NBr}$ (267 mg, 0.83 mmol, 1.2 equiv), K_2CO_3 (152 mg, 1.1 mmol, 1.5 equiv), allyl acetate (0.75 mmol, 75 mg) in DMA (5 mL) was added $\text{Pd}(\text{OAc})_2$ (30 mg, 16 mol%) in a sealed tube. The mixture was heated to 100 °C for 24 h. After the reaction was complete, the mixture was filtered through a celite pad, washed with EtOAc (100 mL) and subjected to the standard workup protocol, the crude was purified by flash column to yield the final product **IV-22-SM** as a yellow solid (79 mg, 47%).

$^1\text{H-NMR}$ (500 MHz, CDCl_3): δ 7.50 (dd, $J = 1.9, 0.7$ Hz, 1H), 7.21 (dd, $J = 8.6, 1.9$ Hz, 1H), 7.16 (dd, $J = 8.6, 0.7$ Hz, 1H), 6.15 (s, 1H), 3.62 (s, 3H), 2.38 (s, 3H), 1.35 (s, 9H).

$^{13}\text{C-NMR}$ (126 MHz, CDCl_3): δ 142.04, 136.83, 135.51, 127.69, 118.52, 115.61, 108.15, 99.47, 34.52, 32.01, 29.38, 12.76.

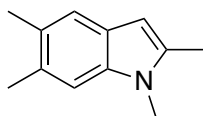


6-Isopropyl-1,2-dimethylindole (**IV-27-SM**)

The title compound was prepared according to *procedure 8* starting from 3-isopropylaniline (675 mg, 5 mmol), I_2 (1.4 g, 5.5 mmol), NaHCO_3 (462 mg, 5.5 mmol) to yield a mixture of 2-iodo-5-isopropylaniline and 2-iodo-5-isopropylaniline. The mixture was taken to the next 2 steps without purification. Final product **IV-27-SM** was isolated only in trace amount (44 mg).

$^1\text{H-NMR}$ (500 MHz, CDCl_3): δ 7.40 (d, $J = 8.0$ Hz, 1H), 7.06 (s, 1H), 6.94 (d, $J = 8.1$ Hz, 1H), 6.17 (s, 1H), 3.63 (s, 3H), 3.00 (hept, $J = 6.9$ Hz, 1H), 2.38 (s, 3H), 1.30 (d, $J = 7.0$ Hz, 6H).

$^{13}\text{C-NMR}$ (126 MHz, CDCl_3): δ 141.62, 137.48, 136.27, 126.04, 119.28, 118.42, 105.99, 99.17, 34.53, 29.29, 24.67, 12.77.



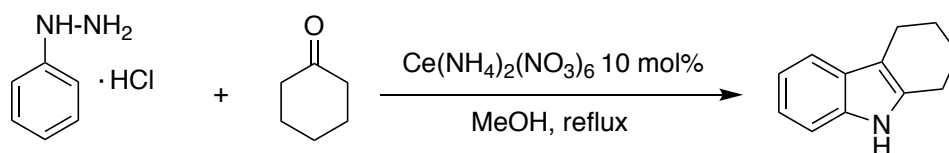
1,2,5,6-Tetramethylindole (**IV-28-SM**)

The title compound was prepared according to *procedure 8* starting from 3,4-dimethyl aniline (605 mg, 5 mmol), I_2 (1.4 g, 5.5 mmol), NaHCO_3 (462 mg, 5.5 mmol) to yield 2-iodo-4,5-dimethylaniline (1.05 g, 85%). The previous product (4.3 mmol) was subjected to lithium methylation as described in *procedure 8*, yielding 946 mg (85% yield). Following *procedure 8*, a 0.8 mmol scale Pd catalyzed cyclization reaction yielded the final product **IV-28-SM** as a yellow solid (62 mg, 45%).

$^1\text{H-NMR}$ (500 MHz, CDCl_3): δ 7.24 (s, 1H), 7.00 (s, 1H), 6.11 (s, 1H), 3.59 (s, 3H), 2.36 (s, 3H), 2.35 (s, 3H), 2.31 (s, 3H).

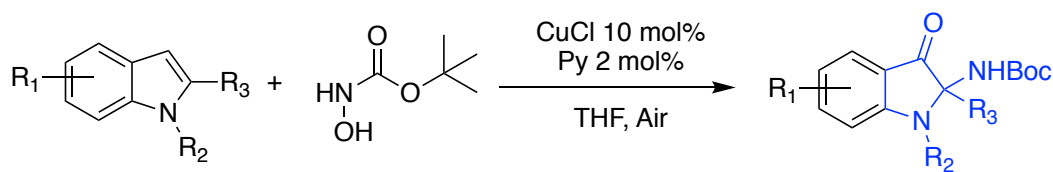
$^{13}\text{C-NMR}$ (126 MHz, CDCl_3): δ 136.29, 135.83, 129.17, 127.58, 126.18, 119.78, 109.27, 98.65, 29.34, 20.60, 20.02, 12.74

IV.7.2.9 Procedure 9⁶¹



Typical procedure: to a round bottom flask with cyclohexanone (3.1 mL, 30 mmol) in MeOH (40 mL), phenylhydrazine hydrochloride (4.34 g, 30 mmol, 1 equiv) and cerium ammonium nitrate (CAN) (1.52 g, 10 mol%) were added separately. The mixture was heated to reflux for 4 h, then cool down to the rt and quenched with water, extracted by EtOAc (3*100 mL), washed with brine and dried over Na₂SO₄. The crude product was purified by flash column to yield the final product (2.93 g, 57%). Methylation as described in *procedure 1* led to the isolated indole.

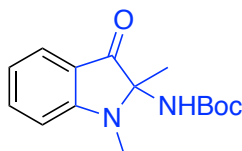
IV.7.3 Oxindole product characterization



General procedure 1: In a Pyrex test tube (12 * 75 mm size) was added 1,2-dimethyl indole (15 mg, 0.1 mmol), *tert*-butyl hydroxycarbamate (22 mg, 0.2 mmol, 2 equiv) and 20 μ L pyridine/THF stock solution (2 mol %) in THF containing copper chloride (1 mg, 10 mol%). The reaction was stirred open to air at rt and monitored by TLC. Time for completion this reaction was between 10-30 h. After the reaction was complete, the solution was concentrated and then passed through a short celite pad to remove the copper catalyst. The strong green fluorescent product was separated by prep-TLC with

EtOAc/Hexanes (30%) as eluent. Some substrates may require extra HPLC separation to get the pure form.

Note: Methanol- d_4 and methylene chloride- d_2 are recommended for NMR studies. Trace amount of the acids in CDCl_3 may cause slow decomposition of the product. We observed the bright color slowly changed to green while using CDCl_3 . Boc protecting group in the product normally was observed as a broad peak merged together with the C-2 methyl group. The aminal carbon in most of the product was not to be observed, while the water peak was normally observed in most of the traces due to the difficulty in its removal.



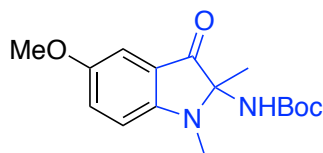
tert-Butyl (1,2-dimethyl-3-oxoindolin-2-yl) carbamate (**IV-19**)

The title compound was prepared according to the *general procedure 1*. 1,2-dimethylindole (15 mg, 0.1 mmol) yielded a yellow solid product **IV-19** (16.5 mg, 60%) after prep-TLC purification with EtOAc/Hexanes (30%).

$^1\text{H-NMR}$ (500 MHz, Methanol- d_4): δ 7.53 (m, 2H), 6.83 (d, $J = 8.5$ Hz, 1H), 6.73 (t, $J = 7.4$ Hz, 1H), 2.95 (s, 3H), 1.51 – 1.08 (m, 12H, Boc and CH_3).

$^{13}\text{C-NMR}$ (126 MHz, Methanol- d_4): δ 201.45, 159.36, 154.35, 137.82, 124.17, 117.92, 116.67, 108.19, 75.36, 27.00, 25.30, 19.11.

HRMS (ESI+): calcd for $\text{C}_{15}\text{H}_{21}\text{N}_2\text{O}_3$ $[\text{M}+\text{H}]^+$ 277.1552, found 277.1563; calcd for $\text{C}_{15}\text{H}_{20}\text{N}_2\text{O}_3\text{Na}$ $[\text{M}+\text{Na}]^+$ 299.1372, found 299.1377



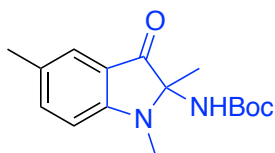
tert-Butyl (5-methoxy-1,2-dimethyl-3-oxoindolin-2-yl) carbamate (**IV-20**)

The title compound was prepared according to the *general procedure 1*. 5-methoxy-1,2-dimethylindole (17.5 mg, 0.1 mmol) yielded yellow solid product **IV-20** (22 mg, 72%) after prep-TLC purification with EtOAc/Hexanes (30%).

$^1\text{H-NMR}$ (500 MHz, CDCl_3): δ 7.12 (dd, $J = 8.8, 2.7$ Hz, 1H), 7.06 (d, $J = 2.7$ Hz, 1H), 6.65 (d, $J = 8.8$ Hz, 1H), 5.16 (s, 1H), 3.73 (s, 3H), 2.87 (s, 3H), 1.29 (s, 12H, Boc and CH_3).

$^{13}\text{C-NMR}$ (126 MHz, CDCl_3): δ 199.73, 155.06, 152.11, 127.92, 117.95, 111.62, 109.79, 105.55, 75.74, 55.87, 27.97, 27.13, 20.89.

HRMS (ESI+): calcd for $\text{C}_{16}\text{H}_{23}\text{N}_2\text{O}_4$ $[\text{M}+\text{H}]^+$ 307.1658, found 307.1658.



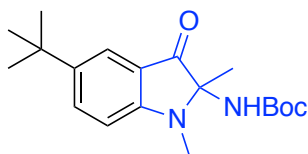
tert-Butyl (1,2,5-trimethyl-3-oxoindolin-2-yl)carbamate (**IV-21**)

The title compound was prepared according to the *general procedure 1*. 5-methyl-1,2-dimethylindole (16 mg, 0.1 mmol) yielded yellow solid product **IV-21** (20.6 mg, 71%) after prep-TLC purification with EtOAc/Hexanes (30%).

$^1\text{H-NMR}$ (500 MHz, Methanol- d_4): δ 7.37 (dd, $J = 8.4, 1.9$ Hz, 1H), 7.31 (s, 1H), 6.75 (d, $J = 8.4$ Hz, 1H), 2.90 (s, 3H), 2.26 (s, 3H), 1.25 (m, 12H, Boc and CH_3).

$^{13}\text{C-NMR}$ (126 MHz, Methanol- d_4): δ 201.49, 158.36, 154.19, 137.79, 124.40, 117.58, 116.24, 108.03, 75.34, 35.00, 27.07, 20.32, 13.18.

HRMS (ESI+): calcd for $\text{C}_{16}\text{H}_{23}\text{N}_2\text{O}_3$ $[\text{M}+\text{H}]^+$ 291.1709, found 291.1695.



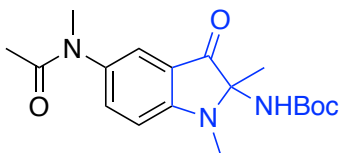
tert-Butyl (5-(*tert*-butyl)-1,2-dimethyl-3-oxoindolin-2-yl)carbamate (**IV-22**)

The title compound was prepared according to the *general procedure 1*. 5-(*tert*-Butyl)-1,2-dimethylindole (20 mg, 0.1 mmol) yielded a yellow solid product **IV-22** (23 mg, 69%) after prep-TLC purification with EtOAc/Hexanes (30%).

$^1\text{H-NMR}$ (500 MHz, Methanol- d_4): δ 7.65 (d, $J = 8.7$ Hz, 1H), 7.53 (s, 1H), 6.78 (d, $J = 8.8$ Hz, 1H), 2.91 (s, 3H), 1.42 – 1.06 (m, 21H, Boc and $\text{CH}_3 \times 3$).

$^{13}\text{C-NMR}$ (126 MHz, Methanol- d_4): δ 201.77, 157.95, 154.39, 140.02, 135.97, 119.93, 117.43, 108.12, 78.46, 75.68, 33.57, 30.36, 26.98, 25.45, 19.14.

HRMS (ESI+): calcd for $\text{C}_{19}\text{H}_{29}\text{N}_2\text{O}_3$ $[\text{M}+\text{H}]^+$ 333.2178, found 333.2166.



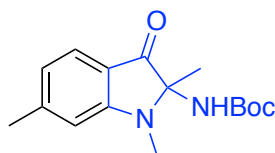
tert-Butyl (1,2-dimethyl-5-(*N*-methylacetamido)-3-oxoindolin-2-yl) carbamate (**IV-23**):

The title compound was prepared according to the *general procedure 1*. *N*-(1,2-Dimethylindol-5-yl)-*N*-methylacetamide (21.6 mg, 0.1 mmol) yielded a yellow solid product **IV-23** (13.3 mg, 38%) after prep-TLC purification with EtOAc/Hexanes (30%).

¹H-NMR (500 MHz, Methanol-*d*₄): δ 7.44 (m, 2H), 6.92 (d, *J* = 8.6 Hz, 1H), 3.22 (s, 3H), 2.98 (s, 3H), 1.90 (s, 3H), 1.35 (m, 12H, Boc and CH₃).

¹³C-NMR (126 MHz, Methanol-*d*₄): δ 200.53, 172.13, 158.16, 154.31, 136.55, 133.70, 118.37, 109.28, 75.94, 36.32, 27.07, 25.33, 20.86, 18.98.

HRMS (ESI⁺): calcd for C₁₈H₂₆N₃O₄ [M+H]⁺ 348.1923, found 348.1941. HRMS (ESI⁺): calcd for C₁₈H₂₅N₃O₄Na [M+Na]⁺ 370.1743, found 370.1756.



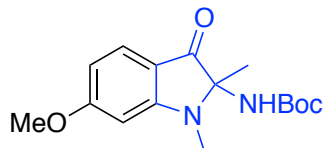
tert-Butyl (1,2,6-trimethyl-3-oxoindolin-2-yl) carbamate (**IV-24**)

The title compound was prepared according to the *general procedure 1*. 6-Methyl-1,2-dimethylindole (16 mg, 0.1 mmol) yielded yellow solid product **IV-24** (17.6 mg, 61%) after prep-TLC purification with EtOAc/Hexanes (30%).

¹H-NMR (500 MHz, Methanol-*d*₄): δ 7.39 (d, *J* = 7.9 Hz, 1H), 6.64 (s, 1H), 6.56 (d, *J* = 8.0 Hz, 1H), 2.91 (s, 3H), 2.36 (s, 3H), 1.26 (m, 12H, Boc and CH₃).

¹³C-NMR (126 MHz, Methanol-*d*₄): δ 200.77, 159.80, 154.32, 149.82, 124.03, 118.41, 115.65, 108.22, 75.67, 27.24, 25.27, 21.32, 19.25.

HRMS (ESI⁺): calcd for C₁₆H₂₃N₂O₃ [M+H]⁺ 291.1709, found 291.1729



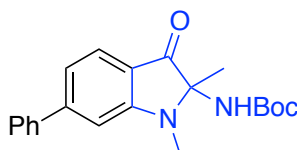
tert-Butyl (6-methoxy-1,2-dimethyl-3-oxoindolin-2-yl) carbamate (**IV-25**):

The title compound was prepared according to the *general procedure 1*. 6-Methoxy-1,2-dimethylindole (17.5 mg, 0.1 mmol) yielded a yellow solid product **IV-25** (21.6 mg, 71%) after prep-TLC purification with EtOAc/Hexanes (30%).

$^1\text{H-NMR}$ (500 MHz, Methanol- d_4): δ 7.44 (d, $J = 8.6$ Hz, 1H), 6.37 – 6.25 (m, 2H), 3.90 (s, 3H), 2.95 (s, 3H), 1.32 (m, 12H, Boc and CH_3).

$^{13}\text{C-NMR}$ (126 MHz, Methanol- d_4): δ 199.08, 169.08, 161.69, 154.29, 125.97, 111.21, 106.69, 106.49, 76.03, 54.86, 27.05, 25.29, 19.44.

HRMS (ESI+): calcd for $\text{C}_{16}\text{H}_{23}\text{N}_2\text{O}_4$ $[\text{M}+\text{H}]^+$ 307.1658, found 307.1663. HRMS (ESI+): calcd for $\text{C}_{16}\text{H}_{22}\text{N}_2\text{O}_4\text{Na}$ $[\text{M}+\text{Na}]^+$ 329.1477, found 329.1483.



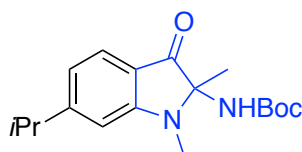
tert-Butyl (1,2-dimethyl-3-oxo-6-phenylindolin-2-yl) carbamate (**IV-26**):

The title compound was prepared according to the *general procedure 1*. 6-Phenyl-1,2-dimethylindole (22 mg, 0.1 mmol) yielded a yellow solid product **IV-26** (18.7 mg, 53%) after prep-TLC purification with EtOAc/Hexanes (30%).

$^1\text{H-NMR}$ (500 MHz, Methanol- d_4): δ 7.69 (d, $J = 8.8$ Hz, 2H), 7.60 (d, $J = 8.0$ Hz, 1H), 7.45 (m, 3H), 7.00 (dd, $J = 10.6, 2.7$ Hz, 2H), 3.01 (s, 3H), 1.50 – 1.05 (m, 12H, Boc and CH_3).

$^{13}\text{C-NMR}$ (126 MHz, Methanol- d_4): δ 200.94, 159.67, 154.39, 151.23, 140.74, 128.50, 128.12, 126.93, 124.59, 116.90, 116.41, 106.30, 75.83, 27.06, 25.36, 19.23.

HRMS (ESI+): calcd for $\text{C}_{21}\text{H}_{24}\text{N}_2\text{O}_3\text{Na}$ $[\text{M}+\text{Na}]^+$ 375.1685, found 375.1691.



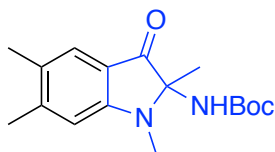
tert-Butyl (6-*isopropyl*-1,2-dimethyl-3-oxoindolin-2-yl) carbamate (**IV-27**):

The title compound was prepared according to the *general procedure 1*. 6-*isoPropyl*-1,2-dimethylindole (18.7 mg, 0.1 mmol) yielded a yellow solid product **IV-27** (20.7 mg, 65%) after prep-TLC purification with EtOAc/Hexanes (30%).

$^1\text{H-NMR}$ (500 MHz, Methanol- d_4): δ 7.45 (d, $J = 8.0$ Hz, 1H), 6.69 (s, 1H), 6.66 (d, $J = 8.1$ Hz, 1H), 2.99 – 2.90 (m, 4H, CH and CH_3), 1.29 (m, 18H, Boc, CH_3^*3).

$^{13}\text{C-NMR}$ (126 MHz, Methanol- d_4): δ 200.88, 160.84, 159.95, 154.37, 124.26, 116.02, 115.97, 105.68, 79.98, 75.68, 35.15, 27.25, 25.28, 22.50, 22.49, 19.25.

HRMS (ESI+): calcd for $\text{C}_{18}\text{H}_{27}\text{N}_2\text{O}_3$ $[\text{M}+\text{H}]^+$ 319.2022, found 319.2035. HRMS (ESI+): calcd for $\text{C}_{18}\text{H}_{26}\text{N}_2\text{O}_3\text{Na}$ $[\text{M}+\text{Na}]^+$ 341.1841, found 341.1849



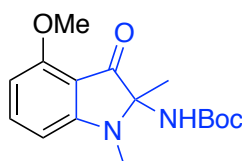
tert-Butyl (1,2,5,6-tetramethyl-3-oxoindolin-2-yl) carbamate (**IV-28**):

The title compound was prepared according to the *general procedure 1*. 1,2,5,6-Tetramethylindole (17.3 mg, 0.1 mmol) yielded a yellow solid product **IV-28** (21.6 mg, 71%) after prep-TLC purification with EtOAc/Hexanes (30%).

$^1\text{H-NMR}$ (500 MHz, Methanol- d_4): δ 7.28 (s, 1H), 6.67 (s, 1H), 2.91 (s, 3H), 2.33 (s, 3H), 2.21 (s, 3H), 1.46 – 1.08 (m, 12H, Boc and CH_3).

$^{13}\text{C-NMR}$ (126 MHz, Methanol- d_4): δ 200.96, 158.73, 154.35, 149.01, 125.75, 123.97, 115.88, 109.04, 79.97, 75.59, 27.24, 25.46, 20.13, 19.28, 17.65.

HRMS (ESI+): calcd for $\text{C}_{17}\text{H}_{25}\text{N}_2\text{O}_3$ $[\text{M}+\text{H}]^+$ 305.1865, found 305.1861. HRMS (ESI+): calcd for $\text{C}_{17}\text{H}_{24}\text{N}_2\text{O}_3\text{Na}$ $[\text{M}+\text{Na}]^+$ 327.1685, found 327.1689.



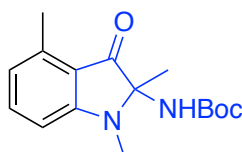
tert-Butyl (4-methoxy-1,2-dimethyl-3-oxoindolin-2-yl) carbamate (**IV-29**):

The title compound was prepared according to the *general procedure 1*. 4-Methoxy-1,2-dimethylindole (17.5 mg, 0.1 mmol) yielded yellow solid product **IV-29** (17.4 mg, 60%) after prep-TLC purification with EtOAc/Hexanes (30%).

$^1\text{H-NMR}$ (500 MHz, Methanol- d_4): δ 7.46 (t, $J = 8.2$ Hz, 1H), 6.38 (d, $J = 8.3$ Hz, 1H), 6.24 (d, $J = 8.0$ Hz, 1H), 3.89 (s, 3H), 2.92 (s, 3H), 1.47 – 1.15 (m, 12H, Boc and CH_3).

$^{13}\text{C-NMR}$ (126 MHz, Methanol- d_4): δ 201.77, 157.95, 154.39, 140.02, 135.97, 119.94, 117.43, 108.14, 75.68, 33.57, 30.36, 27.26, 25.45, 19.14.

HRMS (ESI+): calcd for $\text{C}_{16}\text{H}_{23}\text{N}_2\text{O}_4$ $[\text{M}+\text{H}]^+$ 307.1658, found 307.1648.



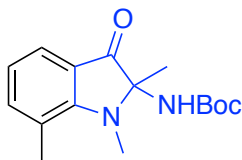
tert-Butyl (1,2,4-trimethyl-3-oxoindolin-2-yl) carbamate (**IV-30**)

The title compound was prepared according to the *general procedure 1*. 4-Methyl-1,2-dimethylindole (16 mg, 0.1 mmol) yielded a yellow solid product **IV-30** (18.9 mg, 65%) after prep-TLC purification with EtOAc/Hexanes (30%).

$^1\text{H-NMR}$ (500 MHz, Methanol- d_4): δ 7.33 (m, 1H), 6.59 (d, $J = 8.3$ Hz, 1H), 6.45 (d, $J = 7.3$ Hz, 1H), 2.89 (s, 3H), 2.49 (s, 3H), 1.24 (s, 12H, Boc and CH_3).

$^{13}\text{C-NMR}$ (126 MHz, Methanol- d_4): δ 201.62, 159.82, 154.40, 139.60, 137.11, 118.36, 116.03, 107.43, 105.36, 75.11, 26.95, 25.38, 19.32, 17.15.

HRMS (ESI+): calcd for $\text{C}_{16}\text{H}_{23}\text{N}_2\text{O}_3$ $[\text{M}+\text{H}]^+$ 291.1709, found 291.1713. HRMS (ESI+): calcd for $\text{C}_{16}\text{H}_{22}\text{N}_2\text{O}_3\text{Na}$ $[\text{M}+\text{Na}]^+$ 313.1528, found 313.1530.



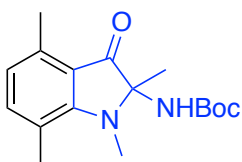
tert-Butyl (1,2,7-trimethyl-3-oxoindolin-2-yl) carbamate (**IV-31**)

The title compound was prepared according to the *general procedure 1*. 7-Methyl-1,2-dimethylindole (16 mg, 0.1 mmol) yielded a yellow solid product **IV-31** (13.7 mg, 47%) after prep-TLC purification with EtOAc/Hexanes (30%).

¹H-NMR (500 MHz, Methanol-*d*₄): δ 7.39 (d, *J* = 7.7 Hz, 1H), 7.28 (d, *J* = 7.2 Hz, 1H), 6.64 (t, *J* = 7.4 Hz, 1H), 3.23 (s, 3H), 2.55 (s, 3H), 1.44 – 1.06 (m, 12H, Boc and CH₃).

¹³C-NMR (126 MHz, Methanol-*d*₄): δ 202.01, 158.31, 154.37, 140.41, 122.13, 120.73, 119.08, 117.25, 75.90, 28.72, 28.67, 19.64, 18.95.

HRMS (ESI⁺): calcd for C₁₆H₂₃N₂O₃ [M+H]⁺ 291.1709, found 291.1718. HRMS (ESI⁺): calcd for C₁₆H₂₂N₂O₃Na [M+Na]⁺ 313.1528, found 313.1532



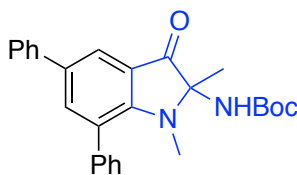
tert-Butyl (1,2,4,7-tetramethyl-3-oxoindolin-2-yl) carbamate (**IV-32**)

The title compound was prepared according to the *general procedure 1*. 1,2,4,7-Tetramethylindole (17.3 mg, 0.1 mmol) yielded a yellow solid product **IV-32** (23.3 mg, 77%) after prep-TLC purification with EtOAc/Hexanes (30%).

$^1\text{H-NMR}$ (500 MHz, Methanol- d_4): δ 7.11 (d, $J = 7.5$ Hz, 1H), 6.40 (d, $J = 7.4$ Hz, 1H), 3.21 (s, 3H), 2.50 (s, 3H), 2.48 (s, 3H), 1.48 – 1.10 (m, 12H, Boc and CH_3).

$^{13}\text{C-NMR}$ (126 MHz, Methanol- d_4): δ 202.17, 158.72, 154.41, 139.90, 137.29, 118.92, 118.75, 117.53, 117.08, 75.65, 28.80, 27.25, 19.91, 18.87, 17.09.

HRMS (ESI+): calcd for $\text{C}_{17}\text{H}_{24}\text{N}_2\text{O}_3\text{Na}$ $[\text{M}+\text{Na}]^+$ 327.1685, found 327.1691.



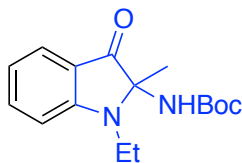
tert-Butyl (1,2-dimethyl-3-oxo-5,7-diphenylindolin-2-yl) carbamate (**IV-33**)

The title compound was prepared according to the *general procedure 1*. 1,2-Dimethyl-5,7-diphenylindole (30 mg, 0.1 mmol) yielded a yellow solid product **IV-33** (27.3 mg, 77%) after prep-TLC purification with EtOAc/Hexanes (30%).

$^1\text{H-NMR}$ (500 MHz, Methylene Chloride- d_2): δ 7.64 (s, 1H), 7.28 (q, $J = 3.0$ Hz, 3H), 7.25 – 7.19 (m, 5H), 7.14 – 7.10 (m, 2H), 6.80 (s, 1H), 3.01 (s, 3H), 1.37 (m, 12H, Boc and CH_3).

$^{13}\text{C-NMR}$ (126 MHz, Methylene Chloride- d_2): δ 198.75, 157.79, 153.23, 150.31, 141.66, 141.04, 130.50, 129.86, 129.49, 127.82, 127.72, 127.16, 126.09, 125.98, 117.66, 110.05, 75.41, 27.77, 26.54, 20.61.

HRMS (ESI+): calcd for $\text{C}_{27}\text{H}_{29}\text{N}_2\text{O}_3$ $[\text{M}+\text{H}]^+$ 429.2178, found 429.2194. HRMS (ESI+): calcd for $\text{C}_{27}\text{H}_{28}\text{N}_2\text{O}_3\text{Na}$ $[\text{M}+\text{Na}]^+$ 451.1998, found 451.1998.



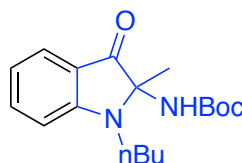
tert-Butyl (1-ethyl-2-methyl-3-oxoindolin-2-yl) carbamate (**IV-34**)

The title compound was prepared according to the *general procedure 1*. 1-Ethyl-2-methylindole (16 mg, 0.1 mmol) yielded a yellow solid product **IV-34** (17.4 mg, 60%) after prep-TLC purification with EtOAc/Hexanes (30%).

$^1\text{H-NMR}$ (500 MHz, Methanol- d_4): δ 7.54 – 7.46 (m, 2H), 6.80 (d, J = 8.4 Hz, 1H), 6.68 (ddd, J = 7.9, 7.2, 0.8 Hz, 1H), 3.44 (tp, J = 14.7, 7.4 Hz, 2H), 1.28 (m, 15H, Boc and 2*CH₃).

$^{13}\text{C-NMR}$ (126 MHz, Methanol- d_4): δ 201.49, 158.36, 154.19, 137.79, 124.40, 117.58, 116.24, 108.03, 75.34, 35.00, 27.07, 20.32, 13.18.

HRMS (ESI+): calcd for C₁₆H₂₃N₂O₃ [M+H]⁺ 291.1709, found 291.1696.



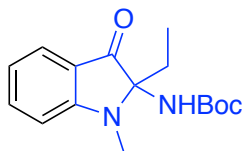
tert-Butyl (1-butyl-2-methyl-3-oxoindolin-2-yl) carbamate (**IV-35**):

The title compound was prepared according to the *general procedure 1*. 1-Butyl-2-methylindole (19 mg, 0.1 mmol) yielded a yellow solid product **IV-35** (11.8 mg, 37%) after prep-TLC purification with EtOAc/Hexanes (30%).

$^1\text{H-NMR}$ (500 MHz, Methanol- d_4): δ 7.61 – 7.45 (m, 2H), 6.81 (d, J = 8.3 Hz, 1H), 6.71 (t, J = 7.4 Hz, 1H), 3.39 (dd, J = 14.9, 7.7 Hz, 2H), 1.73 – 1.60 (m, 2H), 1.48 – 1.29 (m, 14H), 1.01 (t, J = 7.4 Hz, 3H).

$^{13}\text{C-NMR}$ (126 MHz, cd_3od): δ 201.36, 158.84, 154.17, 137.73, 124.36, 117.65, 116.31, 108.27, 75.48, 40.89, 31.11, 27.25, 20.17, 19.96, 12.85.

HRMS (ESI+): calcd for $\text{C}_{18}\text{H}_{27}\text{N}_2\text{O}_3$ $[\text{M}+\text{H}]^+$ 319.2022, found 319.2024. HRMS (ESI+): calcd for $\text{C}_{18}\text{H}_{26}\text{N}_2\text{O}_3\text{Na}$ $[\text{M}+\text{Na}]^+$ 341.1841, found 341.1843.



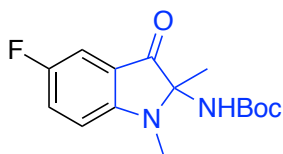
tert-Butyl (2-ethyl-1-methyl-3-oxoindolin-2-yl) carbamate (**IV-36**)

The title compound was prepared according to the *general procedure 1*. 2-Ethyl-1-methylindole (16 mg, 0.1 mmol) yielded yellow a solid product **IV-36** (14.3 mg, 49%) after prep-TLC purification with EtOAc/Hexanes (30%).

$^1\text{H-NMR}$ (500 MHz, Methanol- d_4): δ 7.57 – 7.44 (m, 2H), 6.82 (d, J = 8.2 Hz, 1H), 6.70 (t, J = 7.4 Hz, 1H), 2.94 (s, 3H), 1.90 – 1.76 (m, 2H), 1.45 – 0.99 (m, 9H), 0.61 (t, J = 7.5 Hz, 3H).

$^{13}\text{C-NMR}$ (126 MHz, Methanol- d_4): δ 201.54, 160.62, 154.38, 137.89, 123.50, 119.58, 116.32, 107.45, 78.14, 27.54, 26.97, 25.18, 5.79.

HRMS (ESI+): calcd for $\text{C}_{16}\text{H}_{23}\text{N}_2\text{O}_3$ $[\text{M}+\text{H}]^+$ 291.1709, found 291.1713. HRMS (ESI+): calcd for $\text{C}_{16}\text{H}_{22}\text{N}_2\text{O}_3\text{Na}$ $[\text{M}+\text{Na}]^+$ 313.1528, found 313.1537.



tert-Butyl (5-fluoro-1,2-dimethyl-3-oxoindolin-2-yl) carbamate (**IV-37**):

The title compound was prepared according to the *general procedure 1*. 5-Fluoro-1-methylindole (16.3 mg, 0.1 mmol) yielded a yellow solid product **IV-37** (5 mg, 17%) after prep-TLC purification with EtOAc/Hexanes (30%).

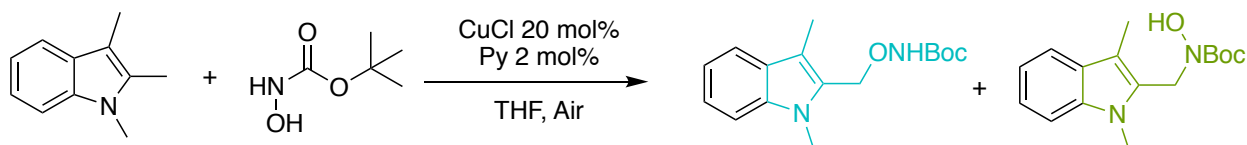
$^1\text{H-NMR}$ (500 MHz, Methanol- d_4): δ 7.34 (td, $J = 9.0, 2.7$ Hz, 1H), 7.22 (dd, $J = 7.5, 2.7$ Hz, 1H), 6.85 (dd, $J = 9.0, 3.7$ Hz, 1H), 2.93 (s, 3H), 1.28 (m, 12H, Boc and CH_3).

$^{13}\text{C-NMR}$ (126 MHz, Methanol- d_4): δ 200.96, 158.86, 156.33, 156.24, 154.45, 154.34, 125.15, 117.86, 109.52, 109.46, 108.83, 108.64, 79.99, 76.00, 27.25, 25.58, 19.01.

$^{19}\text{F-NMR}$ (470 MHz, Methanol- d_4): δ -126.11.

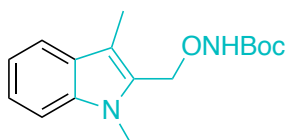
HRMS (ESI+): calcd for $\text{C}_{16}\text{H}_{21}\text{FN}_2\text{O}_3$ $[\text{M}+\text{H}]^+$ 331.1435, found 331.1434.

IV.7.4 Indole C-H functionalization product characterization



General procedure 2: To a Pyrex test tube (13 * 100 mm size) was added 1,2,3-trimethyl indole (32 mg, 0.2 mmol), *tert*-butyl hydroxycarbamate (106 mg, 0.8 mmol, 4 equiv) and 120 μL pyridine/THF stock solution (2 mol %) in THF (4 mL) containing copper chloride (4 mg, 20 mol%). The reaction was stirred open to air at rt, monitored by TLC. Time to

completion for this reaction was between 12-24 h. After the reaction was complete, the solution was concentrated and then passed through a short celite pad to remove the copper catalyst. Regio-selectivity was measured at its crude form by $^1\text{H-NMR}$. The two products were separated by flash column.



tert-Butyl ((1,3-dimethylindol-2-yl)methoxy) carbamate (**IV-40-O**) and *tert*-butyl ((1,3-dimethylindol-2-yl)methyl)(hydroxy) carbamate (**IV-40-N**):

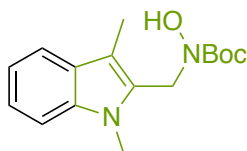
The title compound was prepared according to the *general procedure 2*. 1,2,3-Trimethylindole (32 mg, 0.2 mmol) yielded a white solid product **IV-40-O** (38.2 mg, 66%) and a white solid product **IV-40-N** (17.8 mg, 31%) after flash column purification.

tert-Butyl ((1,3-dimethylindol-2-yl)methoxy) carbamate (**IV-40-O**):

$^1\text{H-NMR}$ (500 MHz, CDCl_3): δ 7.56 (d, $J = 8.0$, 1H), 7.31 – 7.26 (m, 1H), 7.26 – 7.20 (m, 1H), 7.10 (dd, $J = 7.9$, 6.8 Hz, 1H), 7.07 (s, 1H), 5.04 (s, 2H), 3.79 (s, 3H), 2.34 (s, 3H), 1.45 (s, 9H).

$^{13}\text{C-NMR}$ (126 MHz, CDCl_3): δ 156.59, 137.27, 129.51, 127.53, 122.57, 119.30, 118.88, 112.55, 109.13, 81.82, 66.97, 29.86, 28.20, 8.75.

HRMS (ESI⁺): calcd for $\text{C}_{16}\text{H}_{22}\text{N}_2\text{O}_3\text{Na}$ $[\text{M}+\text{Na}]^+$ 313.1528, found 313.1525.

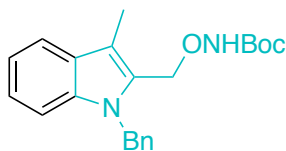


tert-Butyl ((1,3-dimethylindol-2-yl)methyl)(hydroxy) carbamate (**IV-40-N**):

¹H-NMR (500 MHz, CDCl₃): δ 7.53 (dt, *J* = 7.8, 1.0 Hz, 1H), 7.27 – 7.24 (m, 1H), 7.20 (m, 1H), 7.08 (dd, *J* = 7.9, 6.9 Hz, 1H), 6.22 (s, 1H), 4.80 (s, 2H), 3.72 (s, 3H), 2.33 (s, 3H), 1.47 (s, 9H).

¹³C-NMR (126 MHz, CDCl₃): δ 156.24, 137.01, 130.04, 127.76, 121.97, 118.89, 118.82, 110.88, 109.00, 82.42, 43.71, 29.87, 28.26, 8.80.

HRMS (ESI+): calcd for C₁₆H₂₂N₂O₃Na [M+Na]⁺ 313.1528, found 313.1524.



tert-Butyl ((1-benzyl-3-methylindol-2-yl)methoxy) carbamate (**IV-42-O**) and *tert*-butyl ((1-benzyl-3-methylindol-2-yl)methyl)(hydroxy) carbamate (**IV-42-N**)

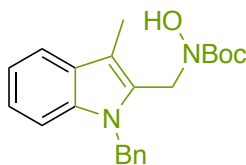
The title compound was prepared according to the *general procedure 2*. 1-Benzyl-2,3-dimethylindole (47 mg, 0.2 mmol) yielded an oil product **IV-42-O** (41 mg, 56%) and a white solid product **IV-42-N** (30 mg, 41%) after flash column purification.

tert-Butyl ((1-benzyl-3-methylindol-2-yl)methoxy) carbamate (**IV-42-O**):

¹H-NMR (500 MHz, CDCl₃): δ 7.60 (d, *J* = 7.8 Hz, 1H), 7.26 – 7.16 (m, 5H), 7.12 (m, 1H), 6.99 – 6.96 (m, 3H), 5.48 (s, 2H), 4.95 (s, 2H), 2.38 (s, 3H), 1.44 (s, 9H).

¹³C-NMR (126 MHz, CDCl₃): δ 156.56, 138.33, 137.19, 129.41, 128.68, 127.82, 127.21, 126.05, 122.91, 119.42, 119.18, 113.50, 109.66, 81.80, 67.07, 46.76, 28.18, 8.83.

HRMS (ESI+): calcd for C₂₂H₂₆N₂O₃Na [M+Na]⁺ 389.1841, found 389.1843.

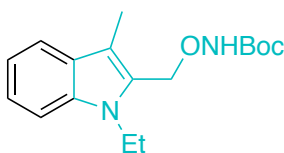


tert-Butyl ((1-benzyl-3-methylindol-2-yl)methyl)(hydroxy) carbamate (**IV-42-N**)

$^1\text{H-NMR}$ (500 MHz, CDCl_3): δ 7.61 – 7.56 (m, 1H), 7.24 – 7.07 (m, 6H), 6.89 (m, 2H), 5.78 (s, 1H), 5.43 (s, 2H), 4.75 (s, 2H), 2.37 (s, 3H), 1.40 (s, 9H).

$^{13}\text{C-NMR}$ (126 MHz, CDCl_3): δ 156.05, 138.42, 136.89, 129.77, 128.70, 128.08, 127.12, 125.64, 122.32, 119.15, 119.01, 111.82, 109.52, 82.37, 46.58, 43.81, 28.21, 8.88.

HRMS (ESI⁺): calcd for $\text{C}_{22}\text{H}_{26}\text{N}_2\text{O}_3\text{Na}$ [$\text{M}+\text{Na}$]⁺ 389.1841, found 389.1841.



tert-Butyl ((1-ethyl-3-methylindol-2-yl)methoxy) carbamate (**IV-43-O**) and *tert*-butyl ((1-ethyl-3-methylindol-2-yl)methyl)(hydroxy) carbamate (**IV-43-N**)

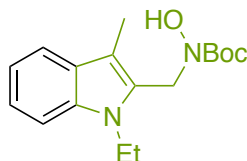
The title compound was prepared according to the *general procedure 2*. 1-Ethyl-2,3-dimethylindole (35 mg, 0.2 mmol) yielded an oil product **IV-43-O** (34 mg, 56%) and a white solid product **IV-43-N** (15 mg, 25%) after flash column purification.

tert-Butyl ((1-ethyl-3-methylindol-2-yl)methoxy) carbamate (**IV-43-O**):

$^1\text{H-NMR}$ (500 MHz, CDCl_3): δ 7.57 (dt, $J = 7.9, 1.0$ Hz, 1H), 7.31 (dt, $J = 8.4, 0.9$ Hz, 1H), 7.27 – 7.22 (m, 1H), 7.10 (ddd, $J = 7.9, 6.9, 1.0$ Hz, 1H), 7.05 (s, 1H), 5.03 (s, 2H), 4.27 (q, $J = 7.2$ Hz, 2H), 2.34 (s, 3H), 1.47 (s, 9H), 1.35 (t, $J = 7.2$ Hz, 3H).

$^{13}\text{C-NMR}$ (126 MHz, CDCl_3): δ 156.53, 136.10, 128.68, 127.77, 122.52, 119.42, 118.84, 112.71, 109.28, 81.80, 66.90, 38.17, 28.22, 15.63, 8.76.

HRMS (ESI+): calcd for $\text{C}_{17}\text{H}_{24}\text{N}_2\text{O}_3\text{Na}$ $[\text{M}+\text{Na}]^+$ 327.1685, found 327.1684.

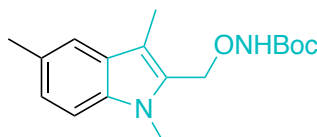


tert-Butyl ((1-ethyl-3-methylindol-2-yl)methyl)(hydroxy)carbamate (**IV-43-N**)

$^1\text{H-NMR}$ (500 MHz, CDCl_3): δ 7.54 (dt, $J = 7.8, 1.0$ Hz, 1H), 7.28 (d, $J = 8.2$ Hz, 1H), 7.20 (ddd, $J = 8.2, 6.9, 1.2$ Hz, 1H), 7.08 (ddd, $J = 7.9, 7.0, 1.0$ Hz, 1H), 5.77 (s, 1H), 4.81 (s, 2H), 4.23 (q, $J = 7.2$ Hz, 2H), 2.33 (s, 3H), 1.51 (s, 9H), 1.30 (t, $J = 7.2$ Hz, 3H).

$^{13}\text{C-NMR}$ (126 MHz, CDCl_3): δ 156.07, 135.83, 129.11, 128.02, 121.96, 119.03, 118.80, 111.13, 109.13, 82.44, 43.71, 37.96, 28.31, 15.43, 8.76.

HRMS (ESI+): calcd for $\text{C}_{17}\text{H}_{24}\text{N}_2\text{O}_3\text{Na}$ $[\text{M}+\text{Na}]^+$ 327.1685, found 327.1683.



tert-Butyl ((1,3,5-trimethylindol-2-yl)methoxy) carbamate (**IV-44-O**) and *tert*-butyl hydroxy((1,3,5-trimethylindol-2-yl)methyl) carbamate (**IV-44-N**):

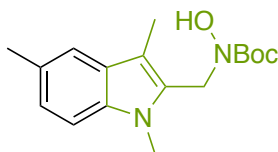
The title compound was prepared according to the *general procedure 2*. 1,2,3,5-Tetramethylindole (35 mg, 0.2 mmol) yielded an oil product **IV-44-O** (28 mg, 46%) and a white solid product **IV-44-N** (7 mg, 11%) after flash column purification.

tert-Butyl ((1,3,5-trimethylindol-2-yl)methoxy) carbamate (**IV-44-O**):

$^1\text{H-NMR}$ (500 MHz, CDCl_3): δ 7.34 (s, 1H), 7.17 (d, $J = 8.3$ Hz, 1H), 7.07 (dd, $J = 8.3, 1.6$ Hz, 1H), 7.05 (s, 1H), 5.02 (s, 2H), 3.76 (s, 3H), 2.45 (s, 3H), 2.31 (s, 3H), 1.45 (s, 9H).

$^{13}\text{C-NMR}$ (126 MHz, CDCl_3): δ 156.56, 135.73, 129.50, 128.09, 127.68, 124.22, 118.88, 112.01, 108.84, 81.77, 66.96, 29.87, 28.21, 27.98, 21.44, 8.73.

HRMS (ESI+): calcd for $\text{C}_{17}\text{H}_{24}\text{N}_2\text{O}_3\text{Na}$ $[\text{M}+\text{Na}]^+$ 327.1685, found 327.1679.

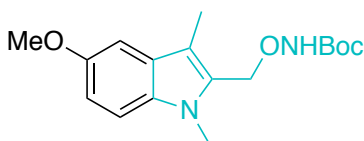


tert-Butyl hydroxy((1,3,5-trimethylindol-2-yl)methyl)carbamate (**IV-44-N**):

$^1\text{H-NMR}$ (500 MHz, CDCl_3): δ 7.31 (s, 1H), 7.15 (d, $J = 8.4$ Hz, 1H), 7.03 (d, $J = 8.3$ Hz, 1H), 4.80 (s, 2H), 3.70 (s, 3H), 2.44 (s, 4H), 2.31 (s, 3H), 1.52 (s, 9H).

$^{13}\text{C-NMR}$ (126 MHz, CDCl_3): δ 156.13, 135.45, 129.93, 128.07, 127.88, 123.62, 118.55, 110.43, 108.71, 82.39, 43.68, 29.89, 28.31, 28.19, 21.44, 8.76.

HRMS (ESI+): calcd for $\text{C}_{17}\text{H}_{24}\text{N}_2\text{O}_3\text{Na}$ $[\text{M}+\text{Na}]^+$ 327.1685, found 327.1685.



tert-Butyl ((5-methoxy-1,3-dimethylindol-2-yl)methoxy) carbamate (**IV-45-O**) and *tert*-butyl hydroxy((5-methoxy-1,3-dimethylindol-2-yl)methyl) carbamate (**IV-45-N**):

The title compound was prepared according to the *general procedure 2*. 5-Methoxy-1,2,3-trimethylindole (38 mg, 0.2 mmol) yielded a yellow solid product **IV-45-O**

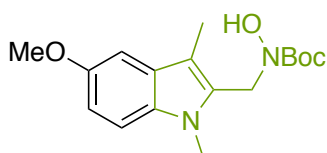
(30.7 mg, 48%) and a white solid product **IV-45-N** (7.3 mg, 11%) after flash column purification.

tert-Butyl ((5-methoxy-1,3-dimethylindol-2-yl)methoxy) carbamate (**IV-45-O**):

¹H-NMR (500 MHz, CDCl₃): δ 7.17 (d, *J* = 8.9 Hz, 1H), 7.08 (s, 1H), 6.98 (d, *J* = 2.4 Hz, 1H), 6.90 (dd, *J* = 8.8, 2.4 Hz, 1H), 5.01 (s, 2H), 3.85 (s, 3H), 3.75 (s, 3H), 2.31 (s, 3H), 1.45 (s, 9H).

¹³C-NMR (126 MHz, CDCl₃): δ 156.60, 153.71, 132.68, 130.10, 127.63, 112.96, 111.94, 109.95, 100.82, 81.79, 67.02, 55.96, 29.97, 28.20, 8.81.

HRMS (ESI+): calcd for C₁₇H₂₄N₂O₄Na [M+Na]⁺ 343.1634, found 343.1637.

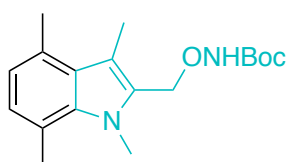


tert-Butyl hydroxy((5-methoxy-1,3-dimethylindol-2-yl)methyl) carbamate (**IV-45-N**):

¹H-NMR (500 MHz, CDCl₃): δ 7.15 (d, *J* = 8.9 Hz, 1H), 6.96 (d, *J* = 2.4 Hz, 1H), 6.87 (dd, *J* = 8.8, 2.5 Hz, 1H), 5.65 (s, 1H), 4.80 (s, 2H), 3.85 (s, 3H), 3.70 (s, 3H), 2.30 (s, 3H), 1.51 (s, 9H).

¹³C-NMR (126 MHz, CDCl₃): δ 156.11, 153.74, 132.38, 130.56, 127.86, 112.25, 110.45, 109.81, 100.68, 82.44, 55.99, 43.68, 29.99, 28.31, 8.85.

HRMS (ESI+): calcd for C₁₇H₂₅N₂O₄ [M+H]⁺ 321.1814, found 321.1815.



tert-Butyl ((1,3,4,7-tetramethylindol-2-yl)methoxy) carbamate (**IV-46-O**) and *tert*-butyl hydroxy((1,3,4,7-tetramethylindol-2-yl)methyl) carbamate (**IV-46-N**)

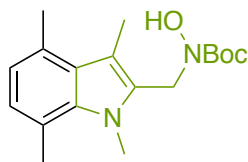
The title compound was prepared according to the *general procedure 2*. 1,2,3,4,7-Pentamethylindole (37 mg, 0.2 mmol) yielded a white solid product **IV-46-O** (26.6 mg, 42%) and a white solid product **IV-46-N** (13.4 mg, 21%) after flash column purification.

tert-Butyl ((1,3,4,7-tetramethylindol-2-yl)methoxy) carbamate (**IV-46-O**):

¹H-NMR (500 MHz, CDCl₃): δ 7.05 (s, 1H), 6.77 (d, *J* = 7.2 Hz, 1H), 6.64 (d, *J* = 7.2 Hz, 1H), 5.00 (s, 2H), 4.03 (s, 3H), 2.71 (s, 3H), 2.66 (s, 3H), 2.50 (s, 3H), 1.47 (s, 9H).

¹³C-NMR (126 MHz, CDCl₃): δ 156.61, 136.57, 129.81, 129.58, 126.77, 125.53, 120.67, 118.81, 113.75, 81.80, 66.67, 33.00, 28.23, 20.58, 20.55, 12.05.

HRMS (ESI+): calcd for C₁₈H₂₆N₂O₃Na [M+Na]⁺ 341.1841, found 341.1841.

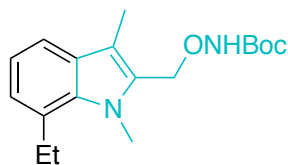


tert-Butyl hydroxy((1,3,4,7-tetramethylindol-2-yl)methyl) carbamate (**IV-46-N**)

¹H-NMR (500 MHz, CDCl₃): δ 6.74 (dd, *J* = 7.1, 1.0 Hz, 1H), 6.63 (dd, *J* = 7.2, 1.0 Hz, 1H), 5.65 (s, 1H), 4.78 (s, 2H), 3.95 (s, 3H), 2.70 (s, 3H), 2.65 (s, 3H), 2.50 (s, 3H), 1.51 (s, 9H).

¹³C-NMR (126 MHz, CDCl₃): δ 156.21, 136.32, 130.13, 129.21, 126.92, 125.11, 120.71, 118.65, 112.30, 82.38, 43.47, 32.96, 28.32, 20.67, 20.55, 12.05.

HRMS (ESI+): calcd for C₁₈H₂₆N₂O₃Na [M+Na]⁺ 341.1841, found 341.1840.



tert-Butyl ((7-ethyl-1,3-dimethylindol-2-yl)methoxy) carbamate (**IV-47-O**) and *tert*-butyl ((7-ethyl-1,3-dimethylindol-2-yl)methyl)(hydroxy) carbamate (**IV-47-N**):

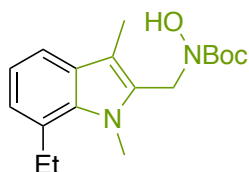
The title compound was prepared according to the *general procedure 2*. 7-Ethyl-1,2,3-trimethylindole (37 mg, 0.2 mmol) yielded a white solid product **IV-47-O** (30.2 mg, 47%) and a white solid product **IV-47-N** (12.8 mg, 20%) after flash column purification.

tert-Butyl ((7-ethyl-1,3-dimethylindol-2-yl)methoxy) carbamate (**IV-47-O**):

¹H-NMR (500 MHz, CDCl₃): δ 7.40 (dd, *J* = 6.7, 2.4 Hz, 1H), 7.08 (s, 1H), 7.04 – 6.98 (m, 2H), 5.03 (s, 2H), 4.03 (s, 3H), 3.11 (q, *J* = 7.5 Hz, 2H), 2.31 (s, 3H), 1.46 (s, 9H), 1.33 (t, *J* = 7.5 Hz, 3H).

¹³C-NMR (126 MHz, CDCl₃): δ 156.58, 135.41, 129.96, 128.65, 127.70, 124.03, 119.10, 117.29, 113.05, 81.81, 67.06, 32.80, 28.22, 25.99, 16.75, 8.87.

HRMS (ESI⁺): calcd for C₁₈H₂₆N₂O₃Na [M+Na]⁺ 341.1841, found 341.1844.

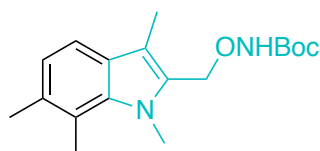


tert-Butyl ((7-ethyl-1,3-dimethylindol-2-yl)methyl)(hydroxy)carbamate (**IV-47-N**):

¹H-NMR (500 MHz, CDCl₃): δ 7.38 (dd, *J* = 7.5, 1.5 Hz, 1H), 7.05 – 6.94 (m, 2H), 5.73 (s, 1H), 4.81 (s, 2H), 3.95 (s, 3H), 3.10 (q, *J* = 7.5 Hz, 2H), 2.31 (s, 3H), 1.51 (s, 9H), 1.33 (t, *J* = 7.5 Hz, 3H).

^{13}C -NMR (126 MHz, CDCl_3): δ 156.25, 135.17, 130.35, 128.88, 127.53, 123.60, 119.08, 116.92, 111.64, 82.42, 43.90, 32.72, 28.30, 26.04, 16.80, 8.90.

HRMS (ESI+): calcd for $\text{C}_{18}\text{H}_{26}\text{N}_2\text{O}_3\text{Na}$ $[\text{M}+\text{Na}]^+$ 341.1841, found 341.1847.



tert-Butyl ((1,3,6,7-tetramethylindol-2-yl)methoxy) carbamate (**IV-48-O**) and *tert*-butyl hydroxy((1,3,6,7-tetramethylindol-2-yl)methyl) carbamate (**IV-48-N**):

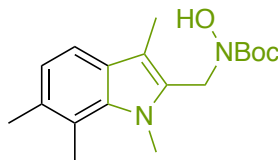
The title compound was prepared according to the *general procedure 2*. 1,2,3,6,7-Pentamethylindole (37 mg, 0.2 mmol) yielded a white solid product **IV-48-O** (30.3 mg, 48%) and a white solid product **IV-48-N** (11.7 mg, 18%) after flash column purification.

tert-Butyl ((1,3,6,7-tetramethylindol-2-yl)methoxy) carbamate (**IV-48-O**):

^1H -NMR (500 MHz, CDCl_3): δ 7.26 (d, $J = 8.0$ Hz, 1H), 7.04 (s, 1H), 6.91 (d, $J = 8.0$ Hz, 1H), 5.00 (s, 2H), 4.04 (s, 3H), 2.65 (s, 3H), 2.39 (s, 3H), 2.27 (s, 3H), 1.46 (s, 9H).

^{13}C -NMR (126 MHz, CDCl_3): δ 156.55, 137.09, 131.32, 129.70, 127.07, 122.24, 119.21, 116.41, 112.73, 81.76, 67.15, 33.59, 28.22, 20.56, 15.06, 8.78.

HRMS (ESI+): calcd for $\text{C}_{18}\text{H}_{27}\text{N}_2\text{O}_3$ $[\text{M}+\text{H}]^+$ 319.2022, found 319.2020.

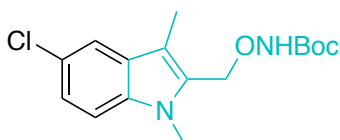


tert-Butyl hydroxy((1,3,6,7-tetramethylindol-2-yl)methyl) carbamate (**IV-48-N**):

¹H-NMR (500 MHz, CDCl₃): δ 7.25 (d, *J* = 8.0 Hz, 1H), 6.90 (d, *J* = 8.0 Hz, 1H), 5.49 (s, 1H), 4.78 (s, 2H), 3.95 (s, 3H), 2.64 (s, 3H), 2.38 (s, 3H), 2.27 (s, 3H), 1.52 (s, 9H).

¹³C-NMR (126 MHz, CDCl₃): δ 156.19, 136.96, 130.82, 130.06, 127.31, 122.19, 119.10, 116.04, 111.31, 82.35, 44.00, 33.56, 28.32, 20.55, 15.13, 8.81.

HRMS (ESI⁺): calcd for C₁₈H₂₆N₂O₃Na [M+Na]⁺ 341.1841, found 341.1841.



tert-Butyl ((5-chloro-1,3-dimethylindol-2-yl)methoxy) carbamate (**IV-49-O**) and *tert*-butyl ((5-chloro-1,3-dimethylindol-2-yl)methyl)(hydroxy) carbamate (**IV-49-N**):

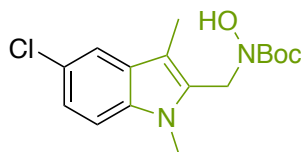
The title compound was prepared according to the *general procedure 2*. 5-Chloro-1,2,3-trimethylindole (39 mg, 0.2 mmol) yielded a white solid product **IV-49-O** (15 mg, 23%) and a white solid product **IV-49-N** (34.4 mg, 53%) after flash column purification.

tert-Butyl ((5-chloro-1,3-dimethylindol-2-yl)methoxy) carbamate (**IV-49-O**):

¹H-NMR (500 MHz, CDCl₃): δ 7.50 (dd, *J* = 1.8, 0.8 Hz, 1H), 7.21 – 7.16 (m, 2H), 7.07 (s, 1H), 5.00 (s, 2H), 3.78 (s, 3H), 2.29 (s, 3H), 1.44 (s, 9H).

¹³C-NMR (126 MHz, CDCl₃): δ 156.63, 135.63, 130.95, 128.50, 124.59, 122.77, 118.74, 112.04, 110.17, 81.96, 66.96, 30.07, 28.17, 8.67.

HRMS (ESI⁺): calcd for C₁₆H₂₁N₂O₃NaCl [M+Na]⁺ 347.1138, found 347.1141.

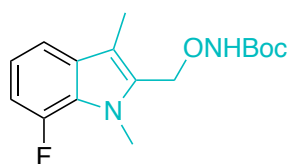


tert-Butyl ((5-chloro-1,3-dimethylindol-2-yl)methyl)(hydroxy) carbamate (**IV-49-N**):

$^1\text{H-NMR}$ (500 MHz, CDCl_3): δ 7.48 (d, $J = 1.5$ Hz, 1H), 7.18 – 7.11 (m, 2H), 6.16 (s, 1H), 4.77 (s, 2H), 3.70 (s, 3H), 2.28 (s, 3H), 1.47 (s, 9H).

$^{13}\text{C-NMR}$ (126 MHz, CDCl_3): δ 156.22, 135.39, 131.51, 128.75, 124.55, 122.15, 118.37, 110.54, 110.03, 82.64, 43.66, 30.07, 28.24, 8.70.

HRMS (ESI+): calcd for $\text{C}_{16}\text{H}_{21}\text{N}_2\text{O}_3\text{NaCl}$ $[\text{M}+\text{Na}]^+$ 347.1138, found 347.1138.



tert-Butyl ((7-fluoro-1,3-dimethylindol-2-yl)methoxy) carbamate (**IV-50-O**) and *tert*-butyl ((7-fluoro-1,3-dimethylindol-2-yl)methyl)(hydroxy) carbamate (**IV-50-N**)

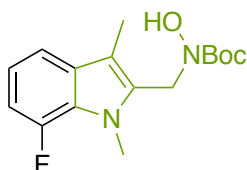
The title compound was prepared according to the *general procedure 2*. 7-Fluoro-1,2,3-trimethylindole (35 mg, 0.2 mmol) yielded an oil product **IV-50-O** (9 mg, 19%) and a white solid product **IV-50-N** (31.5 mg, 51%) after flash column purification.

tert-Butyl ((7-fluoro-1,3-dimethylindol-2-yl)methoxy) carbamate (**IV-50-O**):

$^1\text{H-NMR}$ (500 MHz, CDCl_3): δ 7.28 (d, $J = 7.8$ Hz, 1H), 7.06 (s, 1H), 6.94 (td, $J = 7.8, 4.5$ Hz, 1H), 6.86 (ddd, $J = 13.0, 7.7, 1.0$ Hz, 1H), 5.00 (s, 2H), 4.00 (d, $J = 1.2$ Hz, 3H), 2.31 (s, 3H), 1.44 (s, 9H).

^{13}C -NMR (126 MHz, CDCl_3): δ 156.64, 151.06, 149.12, 131.44, 131.39, 130.88, 125.27, 125.20, 118.83, 118.78, 115.04, 115.02, 113.37, 113.35, 108.18, 108.04, 81.94, 66.69, 43.44, 32.47, 32.41, 28.17, 8.96.

HRMS (ESI+): calcd for $\text{C}_{16}\text{H}_{21}\text{N}_2\text{O}_3\text{NaF}$ $[\text{M}+\text{Na}]^+$ 331.1434, found 331.1436.

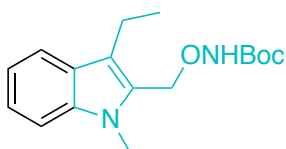


tert-Butyl ((7-fluoro-1,3-dimethylindol-2-yl)methyl)(hydroxy)carbamate (**IV-50-N**):

^1H -NMR (500 MHz, CDCl_3): δ 7.25 (d, $J = 7.4$ Hz, 1H), 6.93 (td, $J = 7.8, 4.4$ Hz, 1H), 6.83 (ddd, $J = 13.0, 7.7, 0.9$ Hz, 1H), 6.34 (s, 1H), 4.76 (s, 2H), 3.92 (d, $J = 1.1$ Hz, 3H), 2.30 (s, 3H), 1.46 (s, 9H).

^{13}C -NMR (126 MHz, CDCl_3): δ 156.26, 151.01, 149.07, 131.70, 131.65, 131.35, 124.91, 124.84, 118.77, 118.72, 114.66, 114.64, 111.87, 107.68, 107.53, 82.58, 43.46, 32.46, 32.41, 28.22, 8.99.

HRMS (ESI+): calcd for $\text{C}_{16}\text{H}_{21}\text{N}_2\text{O}_3\text{NaF}$ $[\text{M}+\text{Na}]^+$ 331.1434, found 331.1435.



tert-Butyl ((3-ethyl-1-methylindol-2-yl)methoxy) carbamate (**IV-51-O**) and *tert*-butyl ((3-ethyl-1-methylindol-2-yl)methyl)(hydroxy) carbamate (**IV-51-N**):

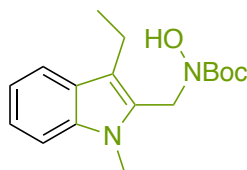
The title compound was prepared according to the *general procedure 2*. 3-Ethyl-1,2-dimethylindole (35 mg, 0.2 mmol) yielded an oil product **IV-51-O** (29.1 mg, 48%) and a yellow solid product **IV-51-N** (18.9 mg, 31%) after flash column purification.

tert-Butyl ((3-ethyl-1-methylindol-2-yl)methoxy) carbamate (**IV-51-O**):

¹H-NMR (500 MHz, CDCl₃): δ 7.61 (d, *J* = 7.9 Hz, 1H), 7.29 (d, *J* = 8.3 Hz, 1H), 7.26 – 7.21 (m, 1H), 7.13 – 7.03 (m, 2H), 5.03 (s, 2H), 3.79 (s, 3H), 2.81 (q, *J* = 7.6 Hz, 2H), 1.45 (s, 8H), 1.25 (t, *J* = 7.6 Hz, 3H).

¹³C-NMR (126 MHz, CDCl₃): δ 156.61, 137.37, 128.92, 126.56, 122.45, 119.43, 119.35, 118.84, 109.24, 81.81, 67.01, 29.84, 28.20, 17.60, 16.44.

HRMS (ESI+): calcd for C₁₇H₂₄N₂O₃Na [M+Na]⁺ 327.1685, found 327.1685.

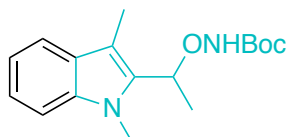


tert-Butyl ((3-ethyl-1-methylindol-2-yl)methyl)(hydroxy) carbamate (**IV-51-N**):

¹H-NMR (500 MHz, CDCl₃): δ 7.58 (d, *J* = 7.8 Hz, 1H), 7.27 (d, *J* = 8.3 Hz, 1H), 7.23 – 7.17 (m, 1H), 7.12 – 7.04 (m, 1H), 5.95 (s, 1H), 4.81 (s, 2H), 3.72 (s, 3H), 2.82 (q, *J* = 7.5 Hz, 2H), 1.50 (s, 9H), 1.23 (t, *J* = 7.5 Hz, 3H).

¹³C-NMR (126 MHz, CDCl₃): δ 156.17, 137.14, 129.28, 126.79, 122.45, 121.91, 119.06, 118.81, 117.80, 109.12, 82.46, 43.57, 29.81, 28.29, 17.50, 16.04.

HRMS (ESI+): calcd for C₁₇H₂₄N₂O₃Na [M+Na]⁺ 327.1685, found 327.1687.



tert-Butyl (1-(1,3-dimethylindol-2-yl)ethoxy) carbamate (**IV-52-O**) and *tert*-butyl (1-(1,3-dimethylindol-2-yl)ethyl)(hydroxy) carbamate (**IV-52-N**):

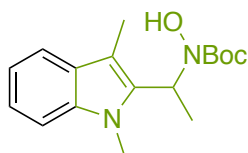
The title compound was prepared according to the *general procedure 2*. 2-Ethyl-1,3-dimethylindole (35 mg, 0.2 mmol) yielded a white solid product **IV-52-O** (41 mg, 67%) and an oil product **IV-52-N** (13.8 mg, 21%) after flash column purification.

tert-Butyl (1-(1,3-dimethylindol-2-yl)ethoxy) carbamate (**IV-52-O**):

$^1\text{H-NMR}$ (500 MHz, CDCl_3): δ 7.55 (d, $J = 7.9$ Hz, 1H), 7.33 – 7.21 (m, 2H), 7.11 (t, $J = 7.4$ Hz, 1H), 6.94 (s, 1H), 5.41 (q, $J = 6.9$ Hz, 1H), 3.81 (s, 3H), 2.32 (s, 3H), 1.68 (d, $J = 7.0$ Hz, 3H), 1.43 (s, 9H).

$^{13}\text{C-NMR}$ (126 MHz, CDCl_3): δ 156.35, 137.46, 133.16, 127.90, 122.22, 118.97, 118.89, 110.52, 108.92, 81.69, 75.59, 30.80, 28.18, 18.99, 8.70.

HRMS (ESI+): calcd for $\text{C}_{17}\text{H}_{24}\text{N}_2\text{O}_3\text{Na}$ $[\text{M}+\text{Na}]^+$ 327.1685, found 327.1687.



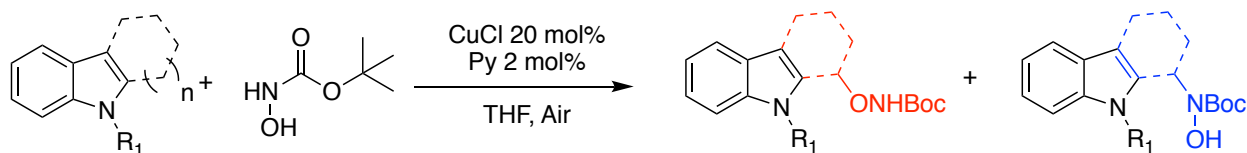
tert-Butyl (1-(1,3-dimethylindol-2-yl)ethyl)(hydroxy) carbamate (**IV-52-N**):

$^1\text{H-NMR}$ (500 MHz, CDCl_3): δ 7.53 (d, $J = 7.9$ Hz, 1H), 7.24 (m, 1H), 7.20 (ddd, $J = 8.2, 6.8, 1.2$ Hz, 1H), 7.08 (ddd, $J = 7.9, 6.8, 1.2$ Hz, 1H), 5.82 (s, 1H), 5.62 (q, $J = 7.2$ Hz, 1H), 3.74 (s, 3H), 2.42 (s, 3H), 1.76 (d, $J = 7.2$ Hz, 3H), 1.46 (s, 9H).

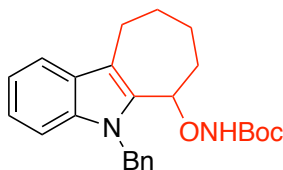
^{13}C -NMR (126 MHz, CDCl_3): δ 155.67, 136.64, 133.01, 128.22, 121.94, 118.78, 118.62, 109.82, 108.95, 82.23, 51.04, 30.21, 28.29, 16.18, 9.65.

HRMS (ESI+): calcd for $\text{C}_{17}\text{H}_{24}\text{N}_2\text{O}_3\text{Na}$ $[\text{M}+\text{Na}]^+$ 327.1685, found 327.1689.

IV.7.5 Ring fused indoles substrates



The same procedure was used for C-2 functionalization reaction of alkyl indoles. Regio-selectivity was measured by crude ^1H -NMR.



tert-Butyl ((5-benzyl-5,6,7,8,9,10-hexahydrocyclohepta[*b*]indol-6-yl)oxy) carbamate (**IV-53-O**):

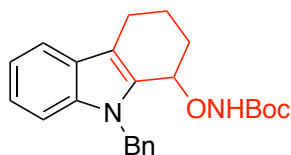
The title compound was prepared according to the *general procedure 2*. 5-Benzyl-5,6,7,8,9,10-hexahydrocyclohepta[*b*]indole (55 mg, 0.2 mmol) yielded a white solid product **IV-53-O** (48 mg, 60%) after flash column purification.

^1H -NMR (500 MHz, CDCl_3): δ 7.58 (d, $J = 7.8$ Hz, 1H), 7.27 – 7.14 (m, 4H), 7.10 (ddd, $J = 7.9, 6.9, 1.0$ Hz, 1H), 6.96 (d, $J = 7.1$ Hz, 2H), 6.90 (s, 1H), 5.72 (d, $J = 17.4$ Hz, 1H), 5.45 (d, $J = 17.4$ Hz, 1H), 5.12 (dd, $J = 5.6, 2.0$ Hz, 1H), 3.03 (ddd, $J = 15.5, 6.2, 2.4$ Hz, 1H), 2.85 (ddd, $J = 15.2, 11.7, 2.8$ Hz, 1H), 2.42 (dtd, $J = 14.1, 5.3, 2.6$ Hz, 1H), 2.05

(dtq, $J = 12.9, 9.6, 3.1$ Hz, 2H), 1.83 (ddd, $J = 16.8, 7.9, 3.5$ Hz, 1H), 1.69 – 1.60 (m, 2H), 1.46 (s, 9H).

^{13}C -NMR (126 MHz, CDCl_3): δ 156.87, 138.70, 136.44, 133.86, 128.67, 127.37, 127.09, 125.87, 122.36, 119.13, 118.96, 117.79, 109.65, 81.70, 77.65, 46.25, 46.20, 29.62, 28.22, 28.12, 24.11, 23.95.

HRMS (ESI+): calcd for $\text{C}_{25}\text{H}_{30}\text{N}_2\text{O}_3\text{Na}$ $[\text{M}+\text{Na}]^+$ 429.2154, found 429.2155.



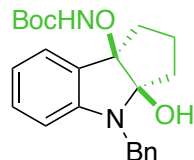
tert-Butyl ((9-benzyl-2,3,4,9-tetrahydrocarbazol-1-yl)oxy) carbamate (**IV-54-O**):

The title compound was prepared according to the *general procedure 2*. 9-Benzyl-2,3,4,9-tetrahydrocarbazole (52 mg, 0.2 mmol) yielded a white solid product **IV-54-O** (39 mg, 53%) after flash column purification.

^1H -NMR (500 MHz, CDCl_3): δ 7.56 (dt, $J = 7.9, 1.0$ Hz, 1H), 7.26 – 7.13 (m, 5H), 7.10 – 7.05 (m, 3H), 7.01 (s, 1H), 5.85 (d, $J = 16.9$ Hz, 1H), 5.48 (d, $J = 16.8$ Hz, 1H), 4.95 (t, $J = 3.1$ Hz, 1H), 2.91 (ddd, $J = 16.0, 5.4, 2.4$ Hz, 1H), 2.71 – 2.60 (m, 1H), 2.42 (ddt, $J = 14.4, 5.0, 2.8$ Hz, 1H), 2.01 (dtdd, $J = 13.7, 11.3, 5.4, 2.7$ Hz, 1H), 1.88 (dddd, $J = 13.0, 7.2, 5.4, 2.9$ Hz, 1H), 1.80 – 1.71 (m, 1H), 1.47 (s, 9H).

^{13}C -NMR (126 MHz, CDCl_3): δ 157.07, 138.88, 137.42, 131.18, 128.52, 126.96, 126.42, 126.40, 122.62, 119.12, 118.99, 114.92, 109.94, 81.76, 74.67, 46.49, 28.24, 27.21, 21.20, 18.22.

HRMS (ESI+): calcd for $\text{C}_{24}\text{H}_{28}\text{N}_2\text{O}_3\text{Na}$ $[\text{M}+\text{Na}]^+$ 415.1998, found 415.1996.



tert-Butyl (((3a,8b)-4-benzyl-3a-hydroxy-2,3,3a,4-tetrahydrocyclopenta[*b*]indol-8b-yl)oxy) carbamate (**IV-55**):

The title compound was prepared according to the *general procedure 2*. 4-Benzyl-1,2,3,4-tetrahydrocyclopenta[*b*]indole (52 mg, 0.2 mmol) yielded white solid product **IV-55** (52.6 mg, 70%) after flash column purification.

$^1\text{H-NMR}$ (500 MHz, CDCl_3): δ 7.32 – 7.29 (m, 2H), 7.26 – 7.22 (m, 2H), 7.21 – 7.15 (m, 2H), 7.04 (ddd, $J = 7.9, 7.5, 1.3$ Hz, 1H), 6.94 (s, 1H), 6.68 (td, $J = 7.4, 1.0$ Hz, 1H), 6.11 (dt, $J = 8.0, 0.7$ Hz, 2H), 4.63 (d, $J = 15.9$ Hz, 1H), 4.07 (d, $J = 15.9$ Hz, 1H), 2.37 – 2.24 (m, 2H), 2.10 – 2.03 (m, 1H), 1.94 – 1.82 (m, 2H), 1.49 – 1.45 (m, 1H), 1.42 (s, 9H).

$^{13}\text{C-NMR}$ (126 MHz, CDCl_3): δ 158.41, 150.82, 139.41, 130.54, 128.34, 126.92, 126.64, 126.19, 124.40, 117.61, 107.67, 100.40, 95.13, 82.88, 47.57, 37.08, 35.26, 28.20, 28.13, 21.12.

HRMS (ESI+): calcd for $\text{C}_{23}\text{H}_{28}\text{N}_2\text{O}_4\text{Na}$ [$\text{M}+\text{Na}$] $^+$ 419.1947, found 419.1945.

IV.7.6 X-Ray Crystallographic Data

tert-Butyl (1,2-dimethyl-3-oxoindolin-2-yl)carbamate (**IV-19**): A suitable yellow plate-shaped crystal (0.32×0.28×0.11) of **IV-19** was selected and mounted on a nylon loop with paratone oil on a Bruker APEX-II CCD diffractometer. The crystal was kept at $T = 173(2)$ K during data collection. Using Olex2 (Dolomanov et al., 2009), the structure was solved with the olex2.solve (Bourhis et al., 2015) structure solution program, using

the Charge Flipping solution method. The model was refined with XL (Sheldrick, 2008) using Least Squares minimisation.

The crystal structure was deposited into the CCDC database (CCDC No. 1566683).

Compound	IV-19
Formula	C ₁₅ H ₂₀ N ₂ O ₃
$D_{calc.}/\text{g cm}^{-3}$	1.235
$/\text{mm}^{-1}$	0.705
Formula Weight	276.33
Colour	yellow
Shape	plate
Max Size/mm	0.32
Mid Size/mm	0.28
Min Size/mm	0.11
T/K	173(2)
Crystal System	triclinic
Space Group	P-1
$a/\text{\AA}$	6.29480(10)
$b/\text{\AA}$	10.9955(2)
$c/\text{\AA}$	11.2044(2)
$\alpha/^\circ$	81.2899(9)
$\beta/^\circ$	89.5727(10)
$\gamma/^\circ$	75.9519(9)
$V/\text{\AA}^3$	743.29(2)
Z	2
Z'	1
$\Theta_{min}/^\circ$	3.993
$\Theta_{max}/^\circ$	71.947
Measured Refl.	10414
Independent Refl.	2808
Reflections Used	2559
R_{int}	0.0230
Parameters	186
Restraints	0
Largest Peak	0.348
Deepest Hole	-0.343
Goof	1.044
wR_2 (all data)	0.0988
wR_2	0.0959
R_1 (all data)	0.0402
R_1	0.0369

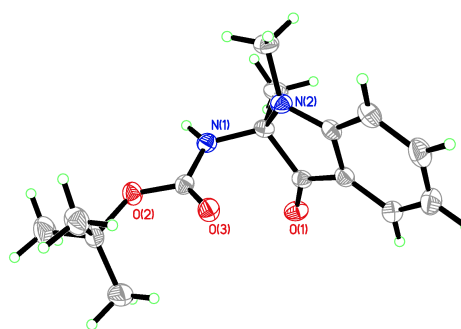


Figure IV-22. Crystal structure of IV-19.

Table IV-3. Crystal data and structure refinement for IV-19

Atom	x	y	z	U_{eq}
O1	2689.8(14)	3576.4(9)	9439.5(8)	29.4(2)
O2	331.9(14)	7526.1(8)	8128.9(8)	28.0(2)
O3	2279.4(14)	5979.8(8)	7123.5(8)	28.1(2)
N1	-725.0(16)	5746.3(9)	8192.6(9)	23.4(2)
N2	-638.8(17)	4271.5(9)	6778.1(9)	23.8(2)
C1	-482.5(19)	4435.3(11)	8051.2(10)	22.0(3)
C2	1826.2(19)	3593.7(11)	8466.6(10)	22.2(2)
C3	2604(2)	2873.3(11)	7501.8(11)	23.4(3)
C4	4519(2)	1939.1(12)	7415.4(12)	29.5(3)
C5	4880(2)	1439.7(13)	6351.0(14)	36.0(3)
C6	3332(2)	1867.8(13)	5397.7(13)	35.3(3)
C7	1410(2)	2777.3(12)	5468.5(11)	29.2(3)
C8	1064(2)	3308.3(11)	6539.9(11)	22.8(3)
C9	-2723(2)	4621.5(12)	6112.2(12)	29.6(3)
C10	-2191(2)	3925.5(13)	8811.7(12)	30.0(3)
C11	789.3(19)	6385.3(11)	7758.9(10)	21.7(2)
C12	1637(2)	8457.0(11)	7741.0(12)	27.4(3)
C13	1363(3)	8863.2(13)	6387.6(13)	38.1(3)
C14	570(3)	9539.9(14)	8408.2(16)	47.0(4)
C15	4017(2)	7929.9(14)	8137.2(14)	39.1(3)

Table IV-4: Fractional atomic coordinates ($\times 10^4$) and equivalent isotropic displacement parameters ($\text{\AA}^2 \times 10^3$) for **IV-19**. U_{eq} is defined as $1/3$ of the trace of the orthogonalised U_{ij} .

tert-butyl ((1,3-dimethylindol-2-yl)methoxy)carbamate (IV-41-O): Single colourless needle-shaped crystals of **IV-41-O** were used as received. A suitable crystal ($0.50 \times 0.15 \times 0.06$) mm³ was selected and mounted on a nylon loop with paratone oil on a Bruker APEX-II CCD diffractometer. The crystal was kept at $T = 173(2)$ K during data collection. Using Olex2 (Dolomanov et al., 2009), the structure was solved with the ShelXS (Sheldrick, 2008) structure solution program, using the Direct Methods solution method. The model was refined with version of XL (Sheldrick, 2008) using Least Squares minimisation.

The crystal structure was deposited into the CCDC database (CCDC No. 1566685).

Compound	IV-41-O
Formula	C ₁₆ H ₂₂ N ₂ O ₃
$D_{calc}/\text{g cm}^{-3}$	1.230
$/\text{mm}^{-1}$	0.692
Formula Weight	290.35
Colour	colourless
Shape	needle
Size/ mm^3	0.50x0.15x0.06
T/K	173(2)
Crystal System	monoclinic
Space Group	P2 ₁ /c
$a/\text{Å}$	10.0850(2)
$b/\text{Å}$	17.2469(3)
$c/\text{Å}$	9.1930(2)
$\alpha/^\circ$	90
$\beta/^\circ$	101.3510(10)
$\gamma/^\circ$	90
$V/\text{Å}^3$	1567.71(5)
Z	4
Z'	1
Wavelength/ Å	1.541838
Radiation type	
$\theta_{min}/^\circ$	4.472
$\theta_{max}/^\circ$	72.287
Measured Refl.	12193
Independent Refl.	3080
Reflections Used	2293
R_{int}	0.0623
Parameters	195
Restraints	0
Largest Peak	0.301
Deepest Hole	-0.316
Goof	1.025
wR_2 (all data)	0.1276
wR_2	0.1141
R_1 (all data)	0.0669
R_1	0.0461

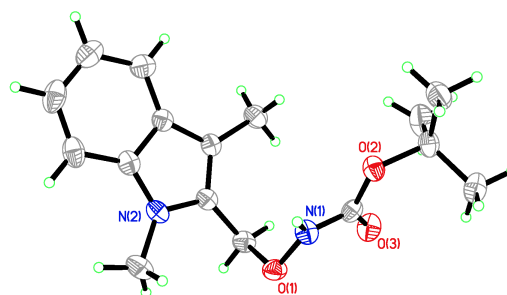


Figure IV-23. Crystal structure of IV-41-O.

Table IV-5. Crystal data and structure refinement for IV-41-O.

Atom	x	y	z	U_{eq}
O1	5055.4(12)	7362.2(8)	5726.2(15)	32.4(3)
O2	1748.2(12)	8054.4(8)	4968.9(14)	30.6(3)
O3	3374.1(14)	8164.7(9)	3565.8(15)	37.5(3)
N1	3771.6(14)	7613.3(10)	5863.0(17)	29.6(3)
N2	4870.2(14)	5610.9(10)	6679.7(16)	29.4(3)
C1	4978.6(18)	6662.8(11)	4826(2)	30.8(4)
C2	4274.8(17)	6010.0(11)	5406.8(19)	26.9(4)
C3	3040.2(17)	5691.2(11)	4830.3(19)	27.1(4)
C4	2858.2(17)	5055.5(11)	5765(2)	27.7(4)
C5	1836(2)	4503.0(12)	5727(2)	35.8(4)
C6	1989(2)	3939.7(12)	6815(3)	42.2(5)
C7	3142(2)	3917.7(13)	7945(2)	44.0(5)
C8	4164(2)	4453.5(13)	8017(2)	37.9(5)
C9	4019.2(18)	5023.0(11)	6915(2)	29.2(4)
C10	6125.7(19)	5823.7(14)	7662(2)	41.4(5)
C11	2046(2)	5955.8(13)	3488(2)	40.8(5)
C12	2988.7(18)	7961.1(10)	4678.2(19)	27.0(4)
C13	729.4(19)	8535.7(11)	3987(2)	31.6(4)
C14	1233(2)	9361.5(13)	3986(3)	42.4(5)
C15	407(3)	8185.9(15)	2433(2)	51.1(6)
C16	-475(2)	8478.8(14)	4742(2)	42.7(5)

Table IV-6: Fractional atomic coordinates ($\times 10^4$) and equivalent isotropic displacement parameters ($\text{\AA}^2 \times 10^3$) for **IV-41-O**. U_{eq} is defined as 1/3 of the trace of the orthogonalised U_{ij} .

***tert*-butyl ((1,3-dimethylindol-2-yl)methyl)(hydroxy)carbamate (IV-41-N)**

Single colourless needle-shaped crystals of **IV-41-N** were used as received. A suitable crystal ($0.44 \times 0.10 \times 0.04$) mm³ was selected and mounted on a nylon loop with paratone oil on a Bruker APEX-II CCD diffractometer. The crystal was kept at $T = 173(2)$ K during data collection. Using Olex2 (Dolomanov et al., 2009), the structure was solved with the XT (Sheldrick, 2015) structure solution program, using the Intrinsic Phasing solution method. The model was refined with version of XL (Sheldrick, 2008) using Least Squares minimisation.

The crystal structure was deposited into the CCDC database (CCDC No. 1566684).

Compound	IV-41-N
Formula	C ₁₆ H ₂₂ N ₂ O ₃
$D_{calc.}/\text{g cm}^{-3}$	1.241
$/\text{mm}^{-1}$	0.698
Formula Weight	290.35
Colour	colourless
Shape	needle
Size/ mm^3	0.44×0.10×0.04
T/K	173(2)
Crystal System	monoclinic
Space Group	$P2_1/c$
$a/\text{Å}$	12.1198(5)
$b/\text{Å}$	16.2040(7)
$c/\text{Å}$	7.9546(3)
$\alpha/^\circ$	90
$\beta/^\circ$	96.038(2)
$\gamma/^\circ$	90
$V/\text{Å}^3$	1553.53(11)
Z	4
Z'	1
Wavelength/Å	1.541838
Radiation type	
$\theta_{min}/^\circ$	3.667
$\theta_{max}/^\circ$	70.139
Measured Refl.	17025
Independent Refl.	2942
Reflections Used	2410
R_{int}	0.0528
Parameters	199
Restraints	0
Largest Peak	0.249
Deepest Hole	-0.177
Goof	1.029
wR_2 (all data)	0.1035
wR_2	0.0961
R_1 (all data)	0.0496
R_1	0.0382

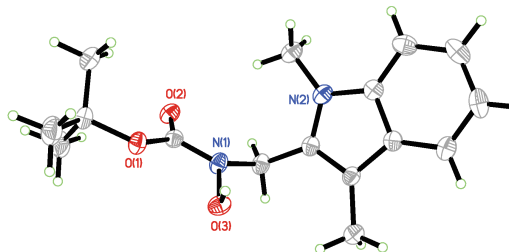


Figure IV-24. Crystal structure of IV-41-N.

Table IV-7. Crystal data and structure refinement for IV-41-N.

Atom	x	y	z	U_{eq}
O1	7920.5(8)	1979.4(6)	4842.6(12)	27.2(2)
O2	6840.3(8)	1438.2(6)	2593.6(12)	27.6(2)
O3	7070.0(9)	3430.1(6)	4292.1(13)	28.3(2)
N1	6565.6(10)	2732.0(7)	3509.5(15)	25.4(3)
N2	3890.5(10)	2615.0(7)	3520.6(15)	26.6(3)
C1	7118.7(11)	2009.7(8)	3566.7(17)	22.6(3)
C2	5657.6(12)	2926.2(9)	2217.4(17)	26.2(3)
C3	4624.1(11)	3180.2(9)	2953.4(17)	23.5(3)
C4	4260.0(11)	3969.2(9)	3172.8(17)	23.7(3)
C5	3237.0(11)	3899.4(9)	3900.1(17)	24.5(3)
C6	2493.9(13)	4483.8(10)	4431.2(19)	31.1(3)
C7	1564.7(13)	4205.1(12)	5126(2)	38.2(4)
C8	1362.8(13)	3360.4(12)	5302(2)	38.8(4)
C9	2081.7(13)	2771(1)	4795(2)	33.2(4)
C10	3025.2(12)	3050.5(9)	4095.5(17)	24.9(3)
C11	4805.1(13)	4750.8(10)	2708(2)	34.2(4)
C12	3950.0(13)	1715.1(9)	3436.8(19)	31.0(3)
C13	8629.8(12)	1229.9(9)	5112.0(19)	29.4(3)
C14	9293.3(14)	1128.5(12)	3607(2)	42.3(4)
C15	7931.6(14)	480.7(10)	5434(2)	39.1(4)
C16	9374.9(14)	1454.9(11)	6704(2)	41.9(4)

Table IV-8: Fractional atomic coordinates ($\times 10^4$) and equivalent isotropic displacement parameters ($\text{\AA}^2 \times 10^3$) for **IV-41-N**. U_{eq} is defined as 1/3 of the trace of the orthogonalised U_{ij} .

tert-butyl (((3a,8b)-4-benzyl-3a-hydroxy-2,3,3a,4-tetrahydrocyclopenta[*b*]indol-8b-yl)oxy) carbamate (IV-55):

Single colourless needle-shaped crystals of **IV-55** were used as received. A suitable crystal ($0.28 \times 0.10 \times 0.04$) mm³ was selected and mounted on a nylon loop with paratone oil on a Bruker APEX-II CCD diffractometer. The crystal was kept at $T = 173(2)$ K during data collection. Using Olex2 (Dolomanov et al., 2009), the structure was solved with the ShelXS (Sheldrick, 2008) structure solution program, using the Direct Methods solution method. The model was refined with version of XL (Sheldrick, 2008) using Least Squares minimisation.

The crystal structure was deposited into the CCDC database (CCDC No. 1566686).

Compound	IV-55
Formula	C ₂₃ H ₂₈ N ₂ O ₄
<i>D</i> _{calc.} /g cm ⁻³	1.268
/mm ⁻¹	0.087
Formula Weight	396.47
Colour	colourless
Shape	needle
Size/mm ³	0.28×0.10×0.04
<i>T</i> /K	173(2)
Crystal System	triclinic
Space Group	P-1
<i>a</i> /Å	7.435(3)
<i>b</i> /Å	11.892(4)
<i>c</i> /Å	12.646(5)
<i>α</i> /°	106.665(5)
<i>β</i> /°	98.361(5)
<i>γ</i> /°	98.555(5)
<i>V</i> /Å ³	1038.2(7)
<i>Z</i>	2
<i>Z</i> '	1
Wavelength/Å	0.710730
Radiation type	
<i>θ</i> _{min} /°	1.715
<i>θ</i> _{max} /°	25.482
Measured Refl.	3836
Independent Refl.	3836
Reflections Used	2500
<i>R</i> _{int}	.
Parameters	274
Restraints	0
Largest Peak	0.632
Deepest Hole	-0.339
Goof	1.030
<i>wR</i> ₂ (all data)	0.1442
<i>wR</i> ₂	0.1245
<i>R</i> ₁ (all data)	0.1047
<i>R</i> ₁	0.0600

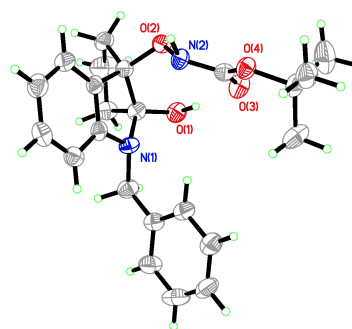


Figure IV-25. Crystal structure of IV-55.

Table IV-9. Crystal data and structure refinement for IV-55.

Atom	x	y	z	U_{eq}
O1	2340(3)	7397.1(19)	1444(2)	39.6(6)
O2	3936(3)	9114.6(18)	542.0(16)	32.8(5)
O3	4462(3)	6838(2)	-202(2)	45.1(6)
O4	7252(3)	7638.9(18)	-490.2(18)	36.7(5)
N1	4813(3)	8558(2)	2949(2)	33.1(6)
N2	5718(3)	8848(2)	499(2)	32.1(6)
C1	3095(4)	8532(3)	2209(3)	32.5(7)
C2	1554(4)	8946(3)	2817(3)	41.4(8)
C3	505(6)	9472(4)	2055(4)	71.2(13)
C4	1905(4)	10118(3)	1584(3)	39.4(8)
C5	3624(4)	9553(3)	1687(2)	30.6(7)
C6	5342(4)	10309(3)	2516(2)	30.5(7)
C7	5947(4)	9681(3)	3226(3)	30.4(7)
C8	7502(4)	10180(3)	4079(3)	36.1(8)
C9	8440(5)	11333(3)	4212(3)	41.5(8)
C10	7853(5)	11961(3)	3503(3)	44.3(9)
C11	6293(4)	11446(3)	2651(3)	38.7(8)
C12	4730(4)	7910(3)	3764(3)	39.9(8)
C13	6180(4)	7151(3)	3805(3)	35.0(8)
C14	7268(4)	6920(3)	3007(3)	39.9(8)
C15	8521(5)	6165(3)	3045(3)	46.9(9)
C16	8665(5)	5636(3)	3885(3)	49.5(10)
C17	7588(5)	5864(3)	4685(3)	56.9(10)
C18	6368(5)	6632(3)	4652(3)	46.4(9)
C19	5679(4)	7674(3)	-99(3)	33.1(7)
C20	7757(4)	6485(3)	-1062(3)	39.6(8)
C21	6363(5)	5862(4)	-2147(3)	67.5(12)
C22	7894(5)	5753(3)	-267(3)	55.8(10)
C23	9640(4)	6893(3)	-1297(3)	45.5(9)

Table IV-10: Fractional atomic coordinates ($\times 10^4$) and equivalent isotropic displacement parameters ($\text{\AA}^2 \times 10^3$) for **IV-55**. U_{eq} is defined as 1/3 of the trace of the orthogonalised U_{ij} .

REFERENCES

REFERENCES

1. Vitaku, E.; Smith, D. T.; Njardarson, J. T., Analysis of the Structural Diversity, Substitution Patterns, and Frequency of Nitrogen Heterocycles among US FDA Approved Pharmaceuticals. *J Med Chem* **2014**, *57* (24), 10257-10274.
2. Kaushik, N. K.; Kaushik, N.; Attri, P.; Kumar, N.; Kim, C. H.; Verma, A. K.; Choi, E. H., Biomedical Importance of Indoles. *Molecules* **2013**, *18* (6), 6620-6662.
3. Tong, K.; Liu, X. D.; Zhang, Y.; Yu, S. Y., Visible-Light-Induced Direct Oxidative C-H Amidation of Heteroarenes with Sulfonamides. *Chem-Eur J* **2016**, *22* (44), 15669-15673.
4. Yamaguchi, T.; Yamaguchi, E.; Itoh, A., Cross-Dehydrogenative C-H Amination of Indoles under Aerobic Photo-oxidative Conditions. *Org Lett* **2017**, *19* (6), 1282-1285.
5. Li, Y. X.; Wang, H. X.; Ali, S.; Xia, X. F.; Liang, Y. M., Iodine-mediated regioselective C2-amination of indoles and a concise total synthesis of (+/-)-folicanthine. *Chem Commun* **2012**, *48* (17), 2343-2345.
6. Shen, T.; Zhang, Y. Q.; Liang, Y. F.; Jiao, N., Direct Tryptophols Synthesis from 2-Vinylanilines and Alkynes via C C Triple Bond Cleavage and Dioxygen Activation. *J Am Chem Soc* **2016**, *138* (40), 13147-13150.
7. Alam, R.; Diner, C.; Jonker, S.; Eriksson, L.; Szabo, K. J., Catalytic Asymmetric Allylboration of Indoles and Dihydroisoquinolines with Allylboronic Acids: Stereodivergent Synthesis of up to Three Contiguous Stereocenters. *Angew Chem Int Edit* **2016**, *55* (46), 14417-14421.
8. Liu, W. P.; Bang, J.; Zhang, Y. J.; Ackermann, L., Manganese(I)- Catalyzed C-H Aminocarbonylation of Heteroarenes. *Angew Chem Int Edit* **2015**, *54* (47), 14137-14140.
9. Liu, C.; Yi, J. C.; Zheng, Z. B.; Tang, Y.; Dai, L. X.; You, S. L., Enantioselective Synthesis of 3a-Amino-Pyrroloindolines by CopperCatalyzed Direct Asymmetric Dearomative Amination of Tryptamines. *Angew Chem Int Edit* **2016**, *55* (2), 751-754.
10. Ilies, L.; Isomura, M.; Yamauchi, S. I.; Nakamura, T.; Nakamura, E., Indole Synthesis via Cyclative Formation of 2,3-Dizincindoles and Regioselective Electrophilic Trapping. *J Am Chem Soc* **2017**, *139* (1), 23-26.
11. Leitch, J. A.; Bhonoah, Y.; Frost, C. G., Beyond C2 and C3: Transition-Metal-Catalyzed C-H Functionalization of Indole. *Acs Catal* **2017**, *7* (9), 5618-5627.

12. Jiang, X. J.; Yang, J. J.; Zhang, F.; Yu, P.; Yi, P.; Sun, Y. W.; Wang, Y. Q., Synthesis of Quaternary 3,3-Disubstituted 2-Oxindoles from 2-Substituted Indole Using Selectfluor. *Org Lett* **2016**, *18* (13), 3154-3157.
13. Zhang, C. H.; Li, S. L.; Bures, F.; Lee, R.; Ye, X. Y.; Jiang, Z. Y., Visible Light Photocatalytic Aerobic Oxygenation of Indoles and pH as a Chemoselective Switch. *Acs Catal* **2016**, *6* (10), 6853-6860.
14. Zhu, X. Y.; Li, M.; Han, Y. P.; Chen, S.; Li, X. S.; Liang, Y. M., Copper-Catalyzed Oxidative Cyclization of Alkynes with Sulfonylhydrazides Leading to 2-Sulfonated 9H-pyrrolo[1,2-a]indol-9-ones. *J Org Chem* **2017**, *82* (16), 8761-8768.
15. Wu, P. L.; Hsu, Y. L.; Jao, C. W., Indole alkaloids from *Cephalanceropsis gracilis*. *J Nat Prod* **2006**, *69* (10), 1467-1470.
16. Hutchison, A. J.; Kishi, Y., Stereospecific Total Synthesis of DI-Austamide. *J Am Chem Soc* **1979**, *101* (22), 6786-6788.
17. Shu, C.; Li, L.; Xiao, X. Y.; Yu, Y. F.; Ping, Y. F.; Zhou, J. M.; Ye, L. W., Flexible and practical synthesis of 3-oxyindoles through gold-catalyzed intermolecular oxidation of o-ethynylanilines. *Chem Commun* **2014**, *50* (63), 8689-8692.
18. Goriya, Y.; Ramana, C. V., Synthesis of pseudo-indoxyl derivatives via sequential Cu-catalyzed SNAr and Smalley cyclization. *Chem Commun* **2013**, *49* (57), 6376-6378.
19. Li, Y. J.; Yan, N.; Liu, C. H.; Yu, Y.; Zhao, Y. L., Gold/Copper-Co-catalyzed Tandem Reactions of 2-Alkynylanilines: A Synthetic Strategy for the C2-Quaternary Indolin-3-ones. *Org Lett* **2017**, *19* (5), 1160-1163.
20. Zhang, M. L.; Duan, Y. Q.; Li, W. P.; Cheng, Y. X.; Zhu, C. J., Visible-light-induced aerobic dearomatative reaction of indole derivatives: access to heterocycle fused or spirocyclic indolones. *Chem Commun* **2016**, *52* (26), 4761-4763.
21. Kong, L. K.; Wang, M. D.; Zhang, F. F.; Xu, M. R.; Li, Y. Z., Copper-Catalyzed Oxidative Dearomatization/Spirocyclization of Indole-2-Carboxamides: Synthesis of 2-Spiro-pseudoindoxyls. *Org Lett* **2016**, *18* (23), 6124-6127.
22. Guchhait, S. K.; Chaudhary, V.; Rana, V. A.; Priyadarshani, G.; Kandekar, S.; Kashyap, M., Oxidative Dearomatization of Indoles via Pd-Catalyzed C-H Oxygenation: An Entry to C2-Quaternary Indolin-3-ones. *Org Lett* **2016**, *18* (7), 1534-1537.
23. Huang, H. W.; Cai, J. H.; Ji, X. C.; Xiao, F. H.; Chen, Y.; Deng, G. J., Internal Oxidant-Triggered Aerobic Oxygenation and Cyclization of Indoles under Copper Catalysis. *Angew Chem Int Edit* **2016**, *55* (1), 307-311.

24. Itahara, T.; Ouya, H.; Kozono, K., The Oxidation of the 2-Methyl Group of 3-Substituted 2-Methylindoles by Autoxidation and with Silver Acetate in Carboxylic-Acids. *B Chem Soc Jpn* **1982**, *55* (12), 3861-3864.
25. Higuchi, K.; Tayu, M.; Kawasaki, T., Active thionium species mediated functionalization at the 2 alpha-position of indole derivatives. *Chem Commun* **2011**, *47* (23), 6728-6730.
26. Tayu, M.; Higuchi, K.; Inaba, M.; Kawasaki, T., Sulfoxide-TFAA and nucleophile combination as new reagent for aliphatic C-H functionalization at indole 2alpha-position. *Org Biomol Chem* **2013**, *11* (3), 496-502.
27. Jiang, L.; Xie, X. N.; Zu, L. S., tert-Butyl hypochlorite mediated diastereoselective oxidative coupling: access to 1-functionalized tetrahydrocarbazoles. *Rsc Adv* **2015**, *5* (12), 9204-9207.
28. Gulzar, N.; Klusmann, M., Aerobic C-H amination of tetrahydrocarbazole derivatives via photochemically generated hydroperoxides. *Org Biomol Chem* **2013**, *11* (27), 4516-4520.
29. Hansen, C. L.; Ohm, R. G.; Olsen, L. B.; Ascic, E.; Tanner, D.; Nielsen, T. E., Catalytic Enantioselective Synthesis of Tetrahydrocarbazoles and Exocyclic Pictet-Spengler-Type Reactions. *Org Lett* **2016**, *18* (23), 5990-5993.
30. Adam, W.; Krebs, O., The nitroso ene reaction: a regioselective and stereoselective allylic nitrogen functionalization of mechanistic delight and synthetic potential. *Chem Rev* **2003**, *103* (10), 4131-46.
31. Zuman, P.; Shah, B., Addition, Reduction, and Oxidation Reactions of Nitrosobenzene. *Chem Rev* **1994**, *94* (6), 1621-1641.
32. Xu, C. M.; Zhang, L.; Luo, S. Z., Catalytic Asymmetric Oxidative alpha-C-H N,O-Ketalization of Ketones by Chiral Primary Amine. *Org Lett* **2015**, *17* (17), 4392-4395.
33. Good, S. N.; Sharpe, R. J.; Johnson, J. S., Highly Functionalized Tricyclic Oxazinanones via Pairwise Oxidative Dearomatization and N-Hydroxycarbamate Dehydrogenation: Molecular Diversity Inspired by Tetrodotoxin. *J Am Chem Soc* **2017**, *139* (36), 12422-12425.
34. Ghorpade, S.; Liu, R. S., Copper-Catalyzed Oxidative Dimerizations of 3-N-Hydroxy-aminoprop-1-enes to form 1,4-Dihydroxy-2,3-diaminocyclohexanes with C-2 Symmetry. *Angew Chem Int Edit* **2014**, *53* (47), 12885-12888.
35. Sun, Q. S.; Zhu, H.; Chen, Y. J.; Yang, X. D.; Sun, X. W.; Lin, G. Q., Squaramide-Catalyzed Synthesis of Enantioenriched Spirocyclic Oxindoles via Ketimine

- Intermediates with Multiple Active Sites. *Angew Chem Int Edit* **2015**, *54* (45), 13253-13257.
36. Pous, J.; Courant, T.; Bernadat, G.; Iorga, B. I.; Blanchard, F.; Masson, G., Regio-, Diastereo-, and Enantioselective Nitroso-Diels-Alder Reaction of 1,3-Diene-1-carbamates Catalyzed by Chiral Phosphoric Acids. *J Am Chem Soc* **2015**, *137* (37), 11950-11953.
 37. Palmer, L. I.; Frazier, C. P.; de Alaniz, J. R., Developments in Nitrosocarbonyl Chemistry: Mild Oxidation of N-Substituted Hydroxylamines Leads to New Discoveries. *Synthesis-Stuttgart* **2014**, *46* (3), 269-280.
 38. Leach, A. G.; Houk, K. N., Diels-Alder and ene reactions of singlet oxygen, nitroso compounds and triazolinediones: transition states and mechanisms from contemporary theory. *Chem Commun* **2002**, (12), 1243-1255.
 39. Leach, A. G.; Houk, K. N., The ene reactions of nitroso compounds involve polarized diradical intermediates. *J Am Chem Soc* **2002**, *124* (50), 14820-14821.
 40. Seymour, C. A.; Greene, F. D., On the Reaction of the Nitroso Group with Olefins - Mechanisms of Ene Reactions. *J Org Chem* **1982**, *47* (26), 5226-5227.
 41. Roche, S. P.; Tendoung, J. J. Y.; Treguier, B., Advances in dearomatization strategies of indoles. *Tetrahedron* **2015**, *71* (22), 3549-3591.
 42. Cohen, A. D.; Zeng, B. B.; King, S. B.; Toscano, J. P., Direct observation of an acyl nitroso species in solution by time-resolved IR spectroscopy. *J Am Chem Soc* **2003**, *125* (6), 1444-1445.
 43. Kirby, G. W., Electrophilic C-Nitroso-Compounds. *Chem Soc Rev* **1977**, *6* (1), 1-24.
 44. Frazier, C. P.; Engelking, J. R.; de Alaniz, J. R., Copper-Catalyzed Aerobic Oxidation of Hydroxamic Acids Leads to a Mild and Versatile AcylNitroso Ene Reaction. *J Am Chem Soc* **2011**, *133* (27), 10430-10433.
 45. Petermayer, C.; Thumser, S.; Kink, F.; Mayer, P.; Dube, H., Hemiindigo: Highly Bistable Photoswitching at the Biooptical Window. *J Am Chem Soc* **2017**, *139* (42), 15060-15067.
 46. Ximenes, V. F.; Campa, A.; Catalani, L. H., The oxidation of indole derivatives catalyzed by horseradish peroxidase is highly chemiluminescent. *Arch Biochem Biophys* **2001**, *387* (2), 173-179.

47. Matsumoto, S.; Samata, D.; Akazome, M.; Ogura, K., Synthesis and physical properties of various organic dyes derived from a single core skeleton, 1,2-dihydroindol-3-one. *Tetrahedron Lett* **2009**, *50* (1), 111-114.
48. Shao, Y. H.; Gan, Z. T.; Epifanovsky, E.; Gilbert, A. T. B.; Wormit, M.; Kussmann, J.; Lange, A. W.; Behn, A.; Deng, J.; Feng, X. T.; Ghosh, D.; Goldey, M.; Horn, P. R.; Jacobson, L. D.; Kaliman, I.; Khaliullin, R. Z.; Kus, T.; Landau, A.; Liu, J.; Proynov, E. I.; Rhee, Y. M.; Richard, R. M.; Rohrdanz, M. A.; Steele, R. P.; Sundstrom, E. J.; Woodcock, H. L.; Zimmerman, P. M.; Zuev, D.; Albrecht, B.; Alguire, E.; Austin, B.; Beran, G. J. O.; Bernard, Y. A.; Berquist, E.; Brandhorst, K.; Bravaya, K. B.; Brown, S. T.; Casanova, D.; Chang, C. M.; Chen, Y. Q.; Chien, S. H.; Closser, K. D.; Crittenden, D. L.; Diedenhofen, M.; DiStasio, R. A.; Do, H.; Dutoi, A. D.; Edgar, R. G.; Fatehi, S.; Fusti-Molnar, L.; Ghysels, A.; Golubeva-Zadorozhnaya, A.; Gomes, J.; Hanson-Heine, M. W. D.; Harbach, P. H. P.; Hauser, A. W.; Hohenstein, E. G.; Holden, Z. C.; Jagau, T. C.; Ji, H. J.; Kaduk, B.; Khistyayev, K.; Kim, J.; Kim, J.; King, R. A.; Klunzinger, P.; Kosenkov, D.; Kowalczyk, T.; Krauter, C. M.; Lao, K. U.; Laurent, A. D.; Lawler, K. V.; Levchenko, S. V.; Lin, C. Y.; Liu, F.; Livshits, E.; Lochan, R. C.; Luenser, A.; Manohar, P.; Manzer, S. F.; Mao, S. P.; Mardirossian, N.; Marenich, A. V.; Maurer, S. A.; Mayhall, N. J.; Neuscamman, E.; Oana, C. M.; Olivares-Amaya, R.; O'Neill, D. P.; Parkhill, J. A.; Perrine, T. M.; Peverati, R.; Prociuk, A.; Rehn, D. R.; Rosta, E.; Russ, N. J.; Sharada, S. M.; Sharma, S.; Small, D. W.; Sodt, A.; Stein, T.; Stuck, D.; Su, Y. C.; Thom, A. J. W.; Tsuchimochi, T.; Vanovschi, V.; Vogt, L.; Vydrov, O.; Wang, T.; Watson, M. A.; Wenzel, J.; White, A.; Williams, C. F.; Yang, J.; Yeganeh, S.; Yost, S. R.; You, Z. Q.; Zhang, I. Y.; Zhang, X.; Zhao, Y.; Brooks, B. R.; Chan, G. K. L.; Chipman, D. M.; Cramer, C. J.; Goddard, W. A.; Gordon, M. S.; Hehre, W. J.; Klamt, A.; Schaefer, H. F.; Schmidt, M. W.; Sherrill, C. D.; Truhlar, D. G.; Warshel, A.; Xu, X.; Aspuru-Guzik, A.; Baer, R.; Bell, A. T.; Besley, N. A.; Chai, J. D.; Dreuw, A.; Dunietz, B. D.; Furlani, T. R.; Gwaltney, S. R.; Hsu, C. P.; Jung, Y. S.; Kong, J.; Lambrecht, D. S.; Liang, W. Z.; Ochsenfeld, C.; Rassolov, V. A.; Slipchenko, L. V.; Subotnik, J. E.; Van Voorhis, T.; Herbert, J. M.; Krylov, A. I.; Gill, P. M. W.; Head-Gordon, M., Advances in molecular quantum chemistry contained in the Q-Chem 4 program package. *Mol Phys* **2015**, *113* (2), 184-215.
49. Shiri, M.; Farajpour, B.; Bozorgpour-Savadjani, Z.; Shintre, S. A.; Koobanally, N. A.; Kruger, H. G.; Notash, B., Transition-metal free highly selective aerobic oxidation of hindered 2-alkylindoles. *Tetrahedron* **2015**, *71* (34), 5531-5537.
50. Prasad, B.; Adepur, R.; Sharma, A. K.; Pal, M., Creation of molecular complexities via a new Cu-catalyzed cascade reaction: a direct access to novel 2,2'-spirobiindole derivatives. *Chem Commun* **2015**, *51* (7), 1259-1262.
51. Peng, Y. D.; Li, Y. D.; Cheng, G. L.; Wang, L. H.; Cui, X. L., Copper-Catalyzed Synthesis of 2-Arylquinazolinones from 2-Arylindoles with Amines or Ammoniums. *J Org Chem* **2015**, *80* (14), 7099-7107.

52. Yamashita, M.; Iida, A., Copper-mediated oxidative tandem reactions with molecular oxygen: synthesis of 2-arylbenzoxazinone derivatives from indoles. *Tetrahedron Lett* **2014**, *55* (18), 2991-2993.
53. Esaki, H.; Ito, N.; Sakai, S.; Maegawa, T.; Monguchi, Y.; Sajiki, H., General method of obtaining deuterium-labeled heterocyclic compounds using neutral D₂O with heterogeneous Pd/C. *Tetrahedron* **2006**, *62* (47), 10954-10961.
54. Baidya, M.; Griffin, K. A.; Yamamoto, H., Catalytic Enantioselective O-Nitrosocarbonyl Aldol Reaction of beta-Dicarbonyl Compounds. *J Am Chem Soc* **2012**, *134* (45), 18566-18569.
55. Allen, S. E.; Walvoord, R. R.; Padilla-Salinas, R.; Kozlowski, M. C., Aerobic Copper-Catalyzed Organic Reactions. *Chem Rev* **2013**, *113* (8), 6234-6458.
56. Dobbs, A., Total synthesis of indoles from *Tricholoma* species via Bartoli/heteroaryl radical methodologies. *J Org Chem* **2001**, *66* (2), 638-641.
57. Challis, B. C.; Rosa, E.; Iley, J.; Norberto, F., Kinetics and Mechanism of the Hydrolysis of N-Methyl-N-Nitroamides in Aqueous Sulfuric-Acid. *J Chem Soc Perk T 2* **1990**, (1), 179-183.
58. Bonnamour, J.; Bolm, C., Iron(II) Triflate as a Catalyst for the Synthesis of Indoles by Intramolecular C-H Amination. *Org Lett* **2011**, *13* (8), 2012-2014.
59. Stokes, B. J.; Dong, H. J.; Leslie, B. E.; Pumphrey, A. L.; Driver, T. G., Intramolecular C-H amination reactions: Exploitation of the Rh-2(II)-Catalyzed decomposition of azidoacrylates. *J Am Chem Soc* **2007**, *129* (24), 7500-7501.
60. Liu, Y.; Yao, B.; Deng, C. L.; Tang, R. Y.; Zhang, X. G.; Li, J. H., Palladium-Catalyzed Selective Heck-Type Diarylation of Allylic Esters with Aryl Halides Involving a beta-OAc Elimination Process. *Org Lett* **2011**, *13* (5), 1126-1129.
61. Varma, P. P.; Sherigara, B. S.; Mahadevan, K. M.; Hulikal, V., Efficient and Straightforward Synthesis of Tetrahydrocarbazoles and 2,3-Dimethyl Indoles Catalyzed by CAN. *Synthetic Commun* **2009**, *39* (1), 158-165.

Chapter V: Engineering Large Stokes Shift Heptamethine Cyanine Dyes for Transparent Luminescent Solar Concentrators (LSCs)

V.1 Introduction of LSCs

Solar energy harvesting systems play an important role in green chemistry. Amongst many elegant devices, transparent solar concentrators (LSCs) have attracted significant attention due to their easy installation and lower cost. This new approach harvests solar energy in a transparent fashion, which could have a huge impact on improving building energy efficiency and mobile electronics performance.¹⁻⁵

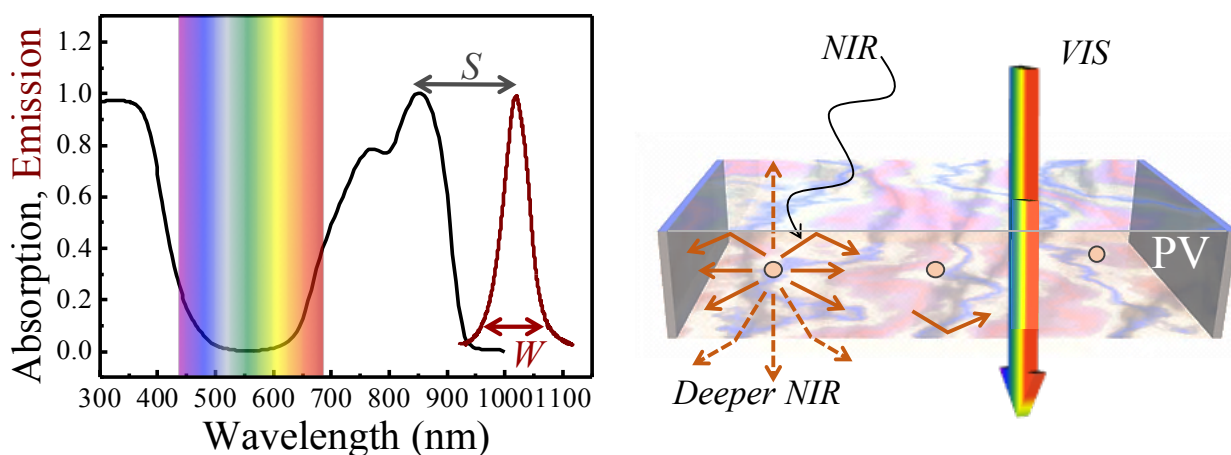


Figure V-1. Working model of LSCs. Both UV and near IR light can be harvested. S stands for Stokes shift and W stands for dye emission width.

LSCs let all visible light to pass through while converting the non-visible light, such as UV light and near IR light, into electricity (**Figure V-1**). The design criteria of the material for LSCs are less absorption and emission in the visible range. Working principle of such devices is using the material that is incorporated on the surface of the glasses to harvest either UV or near IR light, then the re-emitted light can be absorbed by the PV cells on the edge of the glasses and transferred into electricity (**Figure V-1**). This work

was pioneered by Prof. Lunt (Chemical Engineering Department, Michigan State University). Our lab has been collaborating with Prof. Lunt's lab on this cutting edge project. Our efforts have been focused on the organic materials design and synthesis for the transparent solar cells. **Chapter V** is mainly focused on materials development for LSCs.

There are two parts of energy we can potentially harvest with LSCs, one is the UV region and the other is the near IR light. Lunt's lab has successfully used nanoclusters to harvest UV light in LSCs systems. Our research has been focused on the near IR light harvesting. In order to harvest near IR light energy, heptamethine cyanine dyes were chosen due to their unique photophysical properties and broad research interests.⁶ Generally, cyanine dyes can absorb near IR light and emit deep IR light. These dyes have been widely used in the biomedical engineering and imaging projects due to their deeper penetration properties in the living tissues.⁷⁻⁹

We are interested in the abilities of these dyes to absorb near IR light and emit deeper IR light.¹⁰ However, most cyanine dyes exhibit small Stokes shift. This may not be a serious issue for imaging or biomedical engineering purposes. But, if we directly apply such dyes into the transparent solar cells, it can lower the overall solar cell efficiency. As shown in **Figure V-2**, the calculated optical efficiency as a function of LSC length has a direct correlation with the Stokes shift from the material.¹¹ Such impact is more emphasized with the increasing length of LSCs. This decrease in optical efficiency is caused by the self-quenching process of the small Stokes shift materials in the device.

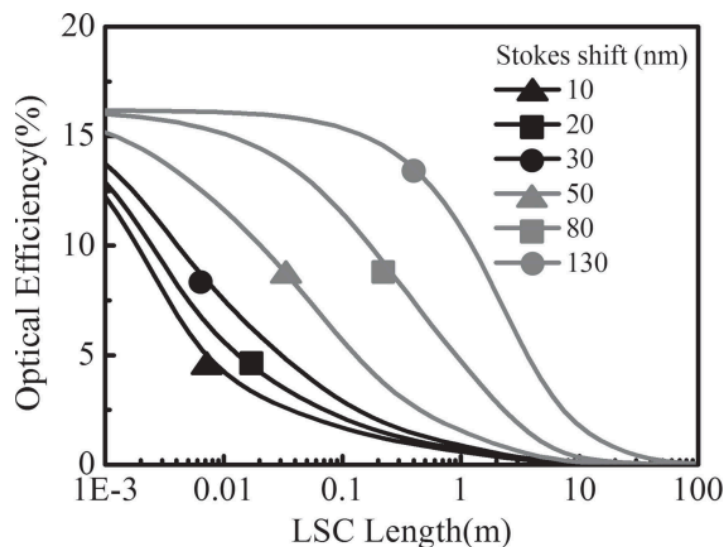
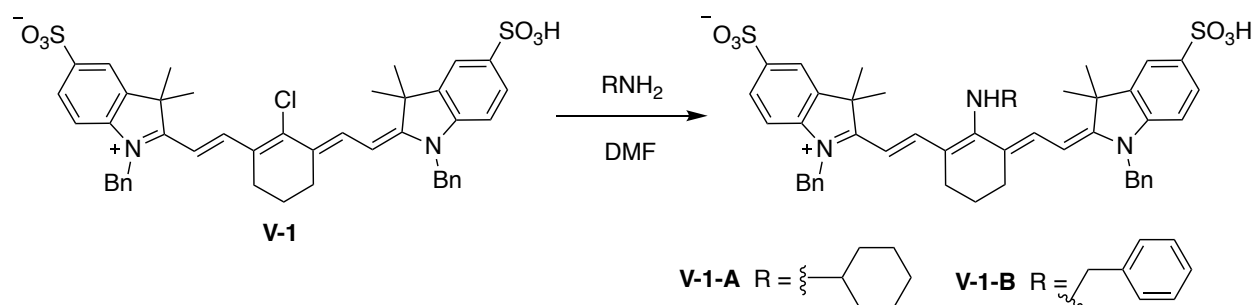


Figure V-2. Calculated Stokes shift impact on LSCs.

Thus, developing large Stokes shift cyanine dyes to minimize self-quenching process is highly desired for our devices. We are aiming to develop novel cyanine dyes which exhibit both near IR absorption and large Stokes shift properties.

V.2 Literature precedence for large Stokes shift cyanine dyes

The first large Stokes shift cyanine dyes were reported by Peng's group in 2005.¹² In this report, they used simple primary amines (cyclohexanemethylamine and benzyl amine) substitution reaction to replace the chloride on Cy-7 (**V-1**) to yield new cyanine dyes with massive Stokes shifts. Both of these two products exhibit large Stokes shift (**V-1-A** and **V-1-B** exhibits 155nm and 140 nm Stokes shift, respectively). However, the detailed mechanism of such large Stokes shift change was not well understood. The authors suggested that structural change of the bridgehead amines (pyramidal geometry on the excited state) lead to the significant Stokes shift change.



Dye	Absorption (nm)	Emission (nm)	Stokes shift (nm)
V-1	783	803	20
V-1-A	602	757	155
V-1-B	617	757	140

Figure V-3. Large Stokes shift cyanine dyes. Absorption and emission were measured in methanol solution.

Another elegant study of spectroscopic properties of cyanine dyes was carried out by Maury's group.¹³ They introduced a new bis-dipole form of the polymethine cyanine dyes. This argument is based on the observation that the cyanine dyes absorption can change based on a variety of substitutions patterns. As shown in **Figure V-4**, with halide, thioether and ether substituents, general cyanine dyes absorptions were observed. However, replacing the halide with different electron donating amines led to a blueshift of absorption. A correlation between the middle substituent electron donating ability and dye absorption wavelength was observed ($\lambda_{\text{abs}} \text{OMe} < \lambda_{\text{abs}} \text{H} < \lambda_{\text{abs}} \text{CF}_3 < \lambda_{\text{abs}} \text{NO}_2$). More blue-shifted dyes can be achieved by breaking the polymethine conjugation via ketone or imine substituents. This study is also supported by computational analysis and ¹³C chemical shifts.

However, detailed fluorescence data for all the dyes in Maury's work were not reported, thus we do not know the impact of these substituents to the Stokes shift.

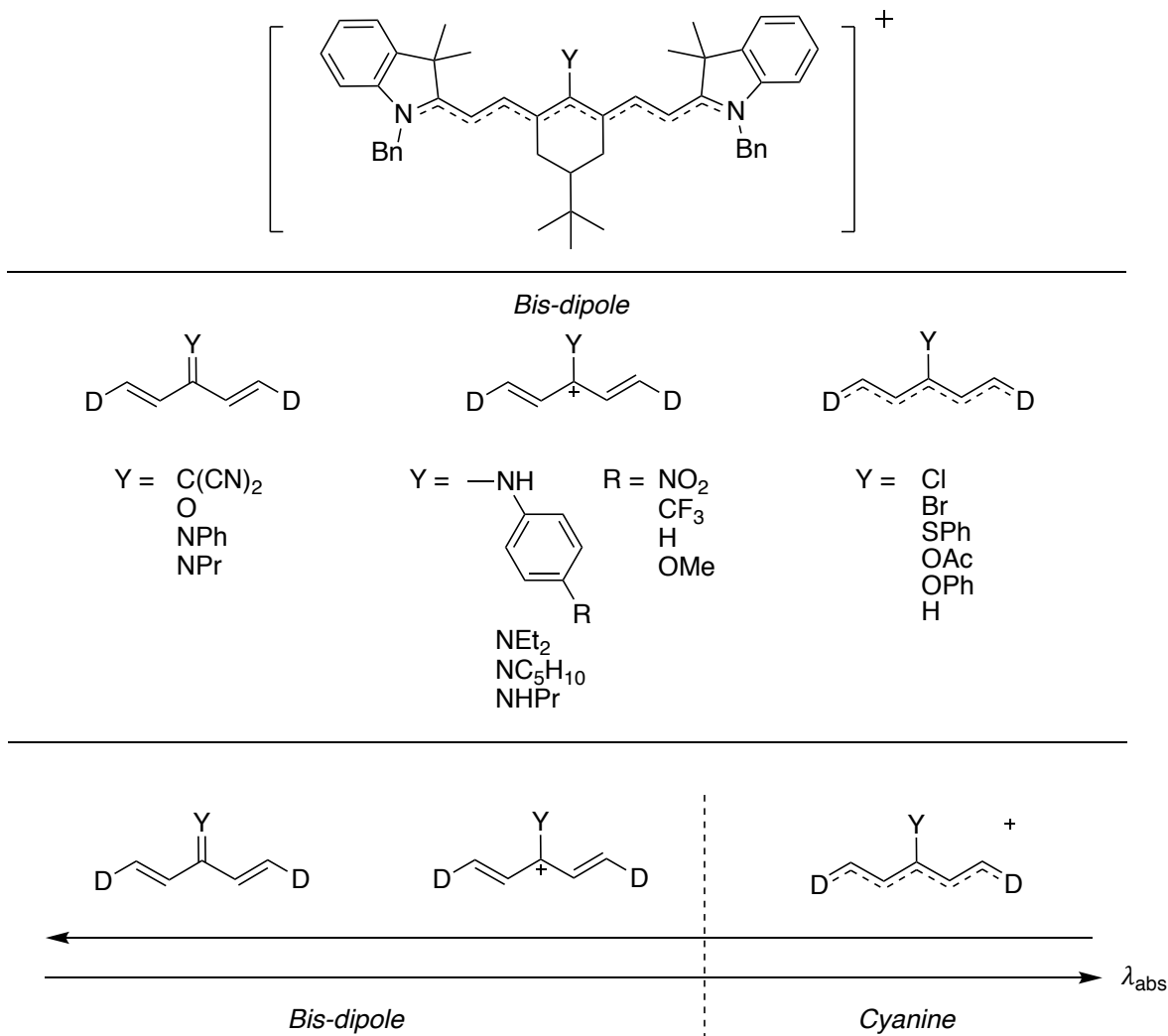
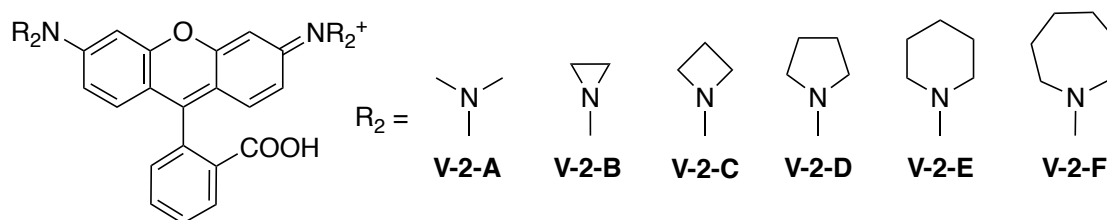


Figure V-4. Bis-dipole form of cyanine dyes.

V.2.1 Literature precedence on improving quantum yield

We were surprised to find out that heptamethine cyanine dye has attracted limited research interest so far and its Stokes shift related photo properties have not been well studied. However, a work reported by Lionnet and Lavis' groups that focused on improving quantum yield of fluorophores caught our attention. In this report, different amine substituents were installed on rhodamine dyes and a significant quantum yield improvement was observed when the dye is derivatized with an azetidine ring.¹⁴ Among

5 different ring sizes, the four-member ring azetidine gave the best result as compared with other substrates (88% quantum yield, **V-2-B**). Although the absorption wavelength varies among the different substrates, Stokes shifts of these dyes remained almost unchanged. They also reported this effect can be duplicated with other dyes with similar rhodamine cores.



Dye	λ_{\max} (nm)	λ_{em} (nm)	ϵ ($\text{M}^{-1} \text{cm}^{-1}$)	ϕ	τ (ns)
V-2-A	548	572	78,000	0.41	2.21
V-2-B	–	–	–	–	–
V-2-C	549	571	101,000	0.88	3.84
V-2-D	553	576	76,000	0.74	3.60
V-2-E	560	586	80,000	0.10	0.59
V-2-F	560	583	106,000	0.25	1.62

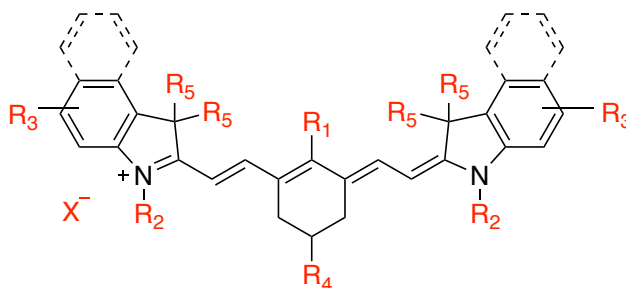
Figure V-5. Spectroscopic data of different rhodamine derivate. ϕ , quantum yield; τ , fluorescence lifetime. **V-2-B** did not show appreciable absorption or emission.

V.3 Engineering large Stokes shift cyanine dyes

V.3.1 Series 1 cyanine dyes

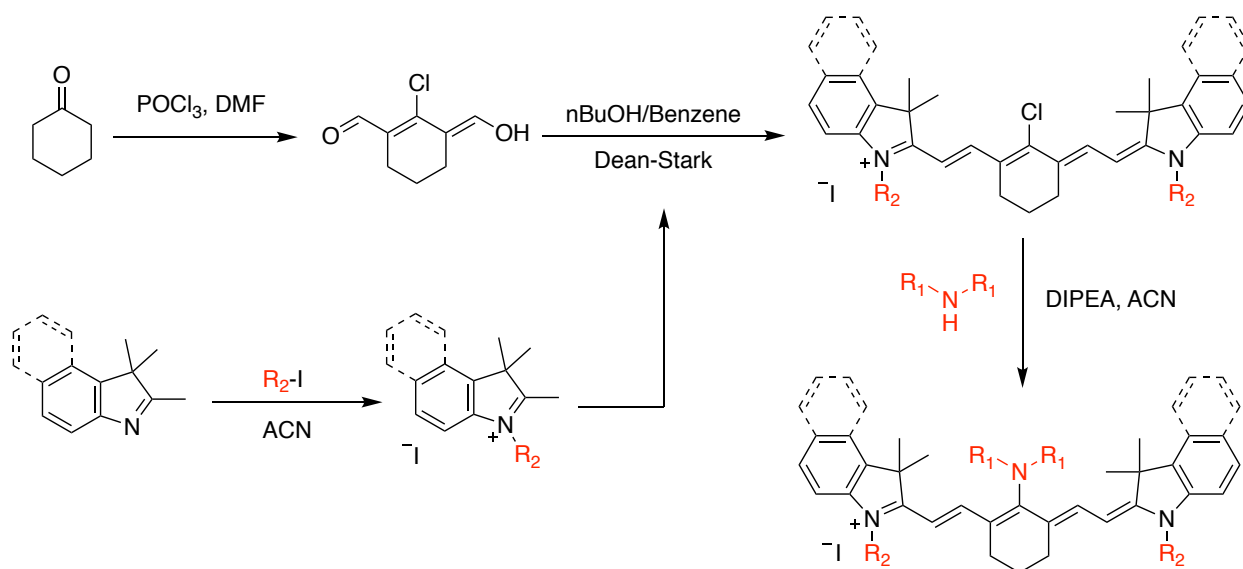
Inspired by the literature described above, we decided to test cyclic amine substituted ring size effects on cyanine dyes. We believed that altering the ring size can also affect the photo properties of polymethine cyanine dyes.

Cyanine dyes have a rich history, with several positions on the dyes that have been well explored before. A brief summary of cyanine dye modificationa is listed below (**Scheme V-1**): R_1 is the common position to functionalize a variety of cyanine dyes; R_2 with different alkyl chains can be used to change the water solubility; Different substituents can be installed on the indolium ring (R_3) to redshift cyanine dyes or improve water solubility; There is no detailed study for the R_4 position. H and *t*-butyl groups are commonly installed on this position. The R_5 position is normally substituted with a methyl group, while there is no detailed study for this position; different counter anion X^- can affect the stability of the cyanine dyes.¹⁵⁻²⁵



Scheme V-1. Positions on the cyanine dyes that can be modified.

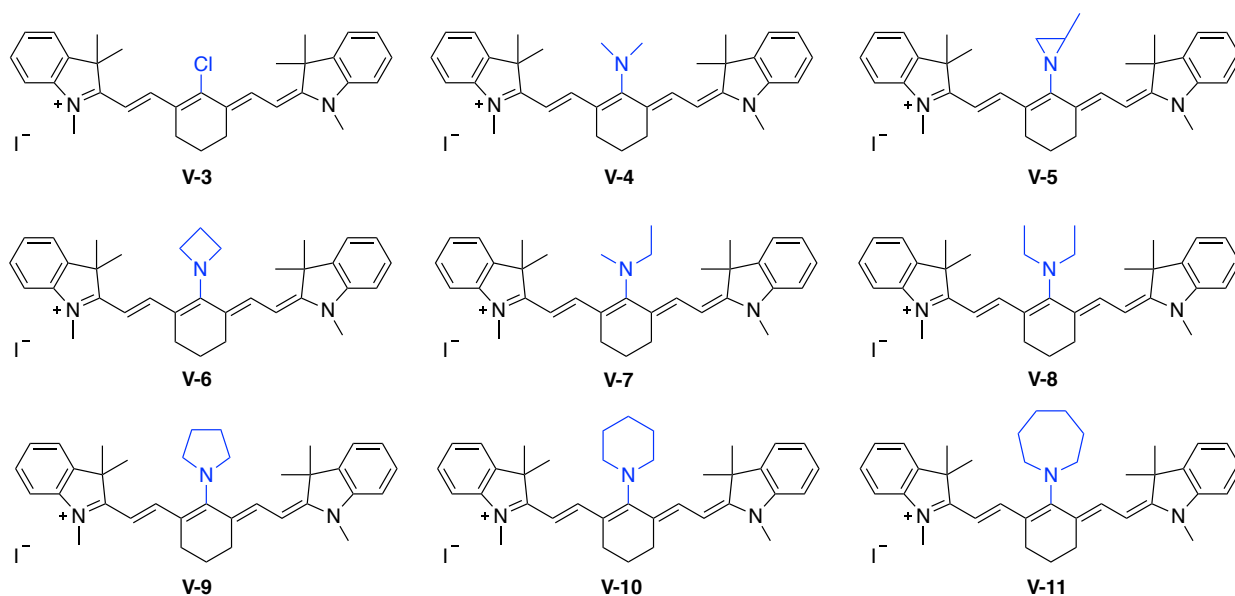
After analyzing all the positions on cyanine dyes, we proposed that the best position to begin with is R_1 , which can be easily functionalized and lead to a direct impact to the conjugated polymethine chain. To test our hypothesis, we began our investigation with Cy-7 dyes, which can be prepared according to literature procedures. A general scheme for the synthesis of cyanine dyes is shown below (**Scheme V-2**).¹⁶



Scheme V-2. General scheme for cyanine dyes synthesis. DIPEA = N,N-Diisopropylethylamine.

The R₂ position on cyanine dyes can be easily substituted with different alkyl halides. For this study, we used small groups such as methyl or ethyl groups. Cy-7-Cl (**V-3**) substitution reactions were carried out in a sealed tube with different secondary amines. The synthesized series 1 cyanine dyes structures are summarized in **Scheme V-3**. Overall, we have synthesized two different categories of series 1 cyanine dyes: secondary amines with alkyl chains and cyclic rings. Dyes with alkyl chains include dimethyl (**V-4**), methyl ethyl (**V-7**) and diethyl groups (**V-8**) whereas cyclic rings include methylaziridine (**V-5**), azetidine (**V-6**), pyrrolidine (**V-9**) and piperidine (**V-10**). The 7-member ring (**V-11**) substrate was not stable in our hands and we were not able to record the photo chemical property for this substrate in its pure form.

Series 1:



Scheme V-3. Series 1 cyanine dyes.

After the successful synthesis of series 1 dyes, we began testing the photoproperties of these dyes. To our surprise, while dyes **V-4** and **V-5** share similar structure, they behave different spectroscopically (**Figure V-6**). Dye **V-4** absorbs at 664 nm and emits at 777 nm in dichloromethane, leading to a 113 nm Stokes shift. However, dye **V-5** only has a 24 nm Stokes shift. Interestingly, quantum yield of these two dyes are similar (28% for dye **V-4** and 25% for dye **V-5**). At this point, we speculated that the ring structure may lead to a lower Stokes shift value.

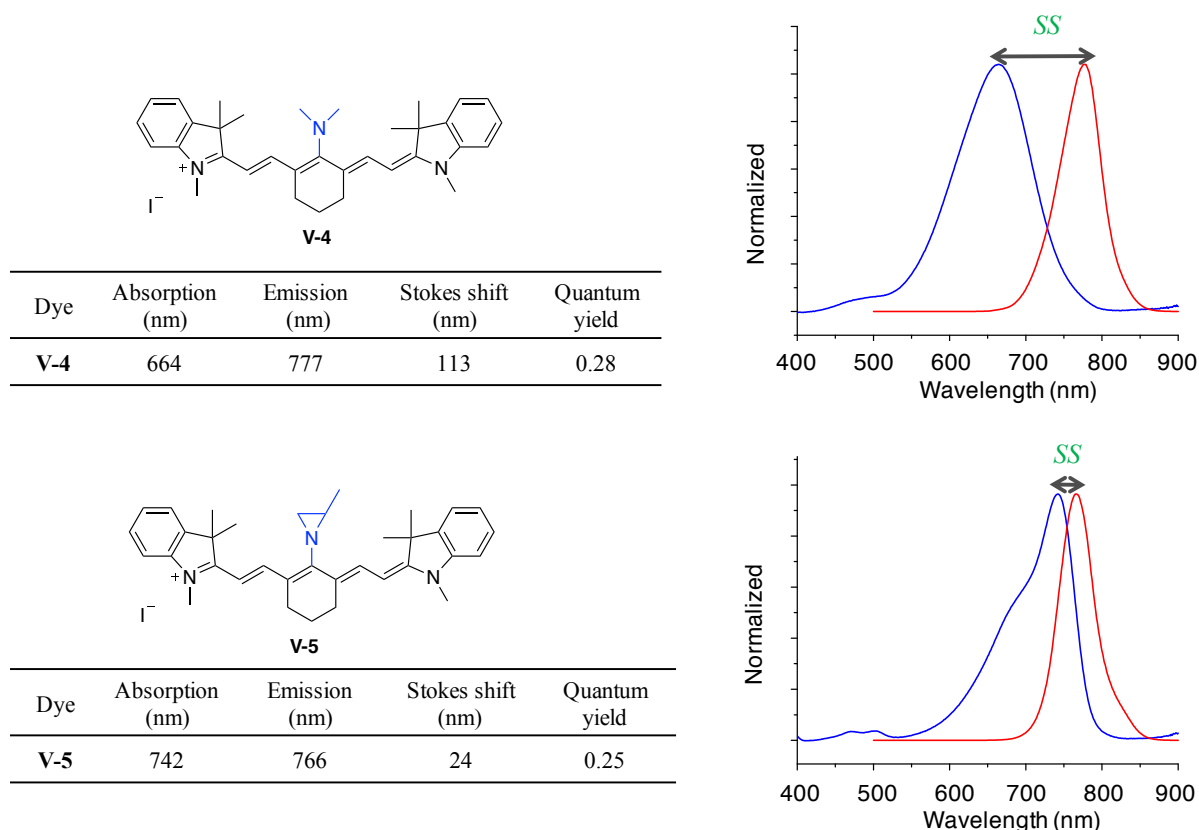


Figure V-6. Spectroscopic data for dye **V-4** and **V-5**. Absorption, emission and quantum yield were measured in DCM. SS= Stokes shift.

To our surprise, when **V-8** and **V-9** were made, we observed the opposite trend (**Figure V-7**). Diethylamine substrate **V-8** yielded a 79 nm Stokes shift (absorption at 699 nm and emission at 778 nm). However, cyclic pyrrolidine substrate **V-9** led to an even larger Stokes shift (180 nm). Interestingly, their quantum yields are still similar (31% for **V-8** and 33% for **V-9**). These observations were encouraging since it appears that Stokes shift of cyanine dyes can be easily tuned by their amine substituents. Meanwhile the opposite trends observed with the linear and cyclic senses were puzzling.

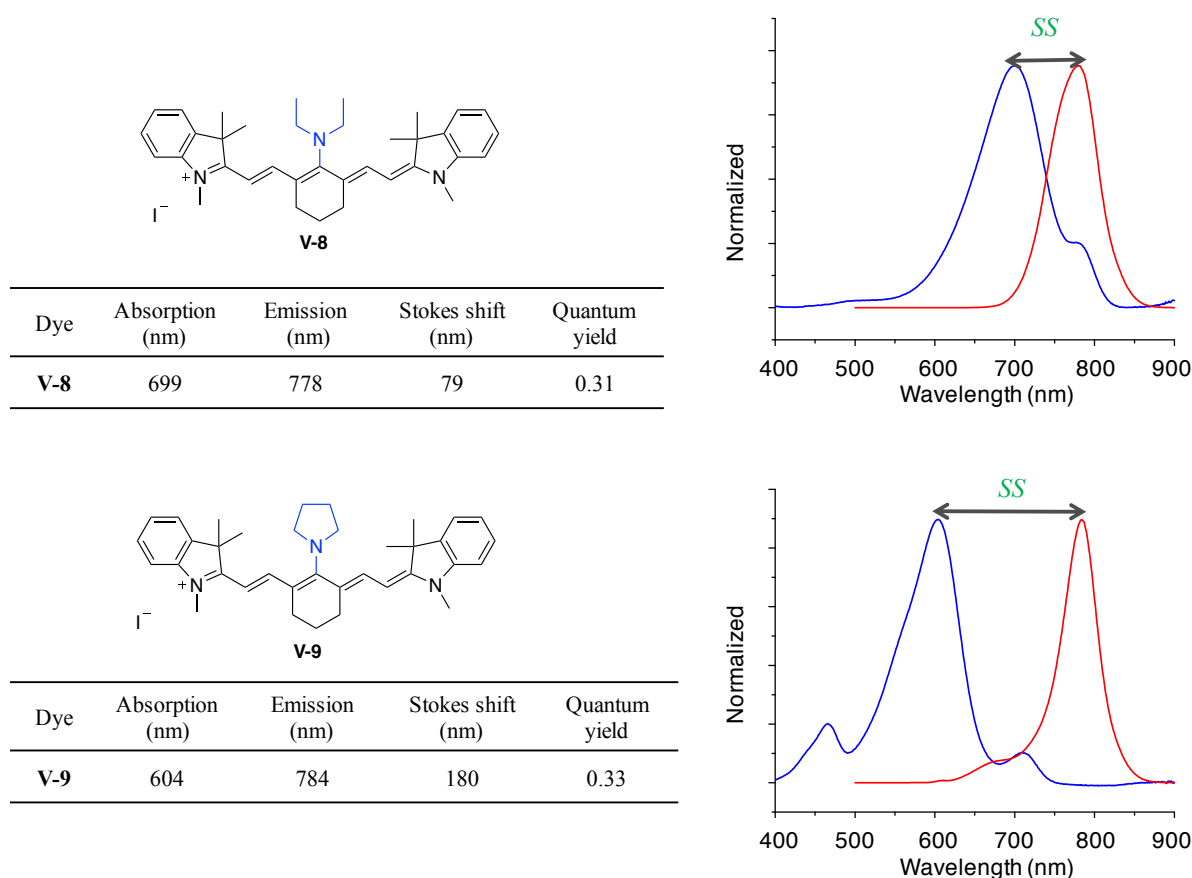


Figure V-7. Spectroscopic data for dye **V-8** and **V-9**. Absorption, emission and quantum yield were measured in DCM. SS= Stokes shift.

The summarized spectroscopic data for series 1 cyanine dyes is listed in **Table V-1**. Surprisingly, the 3-member ring aziridine dye **V-5** yields the smallest Stokes shift, while the 5-member ring piperidine dye **V-9** yields the largest Stokes shift. For the open chain alkyl amine dyes, dimethyl amine dye **V-4** yields 113 nm Stokes shift. With one more carbon, dye **V-7** yields a slightly lower Stokes shift (94 nm). With two more carbons, dye **V-8** yields the lowest Stokes shift (79 nm). Increasing the carbon numbers on the open chain amine substrates leads to a decreasing of the Stokes shift. On the other hand, there is no clear trend for cyclic amine dyes. Another interesting photoproperty is that most of

these dyes (except **V-6**) share similar emission wavelength (around 770 nm). The change in Stokes shift is dictated mainly by the blueshift of the absorption. Thus, we speculated that these dyes may have different ground state geometries but share similar excited state geometries.

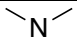
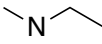
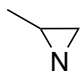

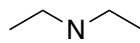
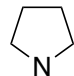
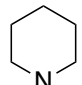
Dye	Amine substrates	Absorption (nm)	Emission (nm)	Stokes shift (nm)	QY (%)
V-4		664	777	113	28
V-7		684	778	94	29
V-5		742	766	24	25
V-6		615	704	89	26
V-8		699	778	79	31
V-9		604	784	180	33
V-10		668	785	117	23

Table V-1. Spectroscopic data for series 1 cyanine dyes. Absorption, emission and quantum yield were measured in DCM. QY = quantum yield.

During the purification of these compounds, we found that azetidine substrate **V-6** exhibits interesting solvatochromic properties with different colors in DCM and methanol solutions. This was not observed for other dyes. Thus, we tested absorption and emission of dye **V-6** in various solvents (**Figure V-8**). Among polar solvents, DCM redshifts the absorption to 615 nm and leads to the lowest Stokes shift. Acetone, ethyl acetate, methanol and benzene blueshift the absorption and yield larger Stokes shift. There was almost no fluorescence in non-polar solvents such as n-hexanes and methyl cyclohexane.

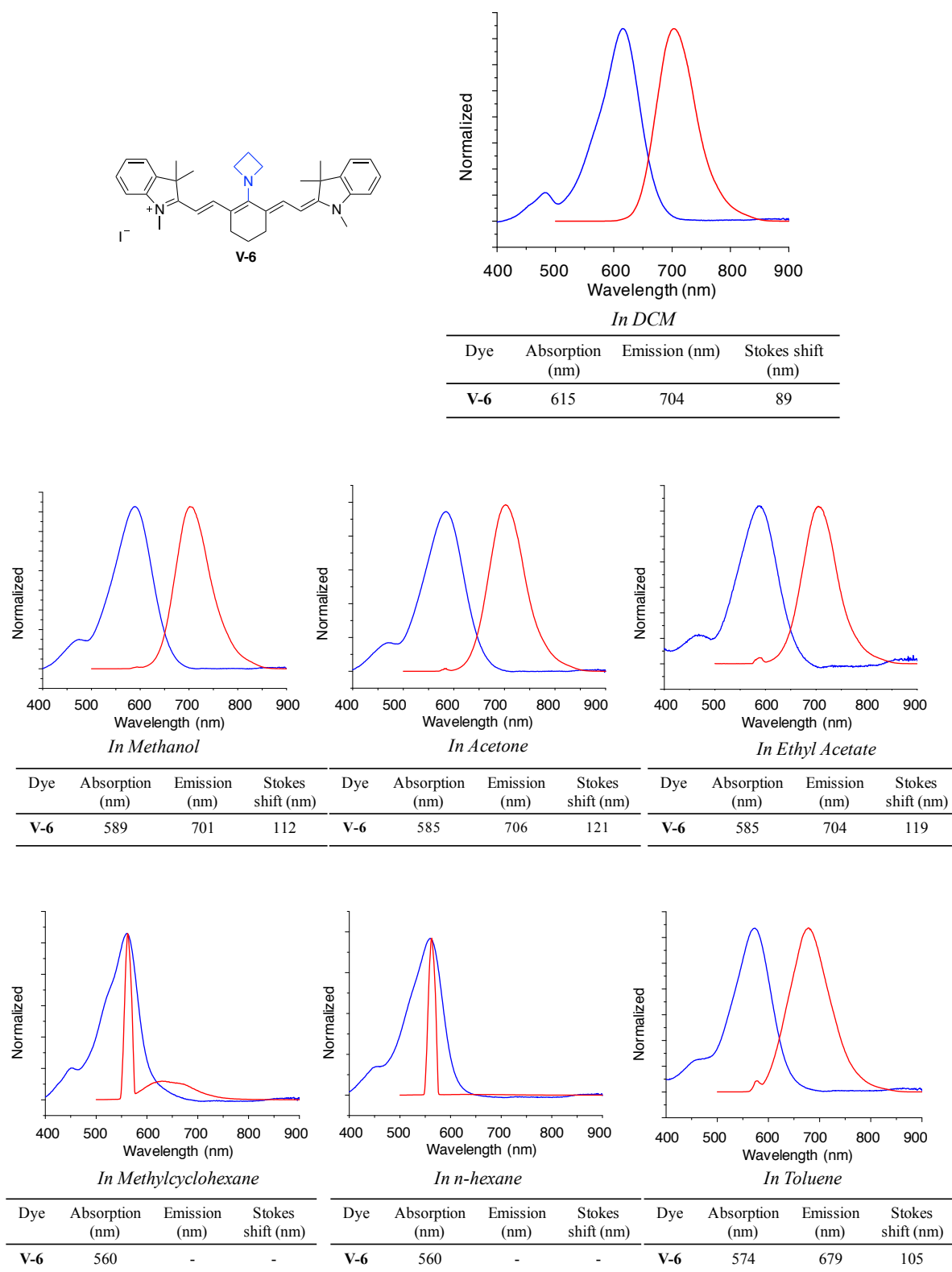
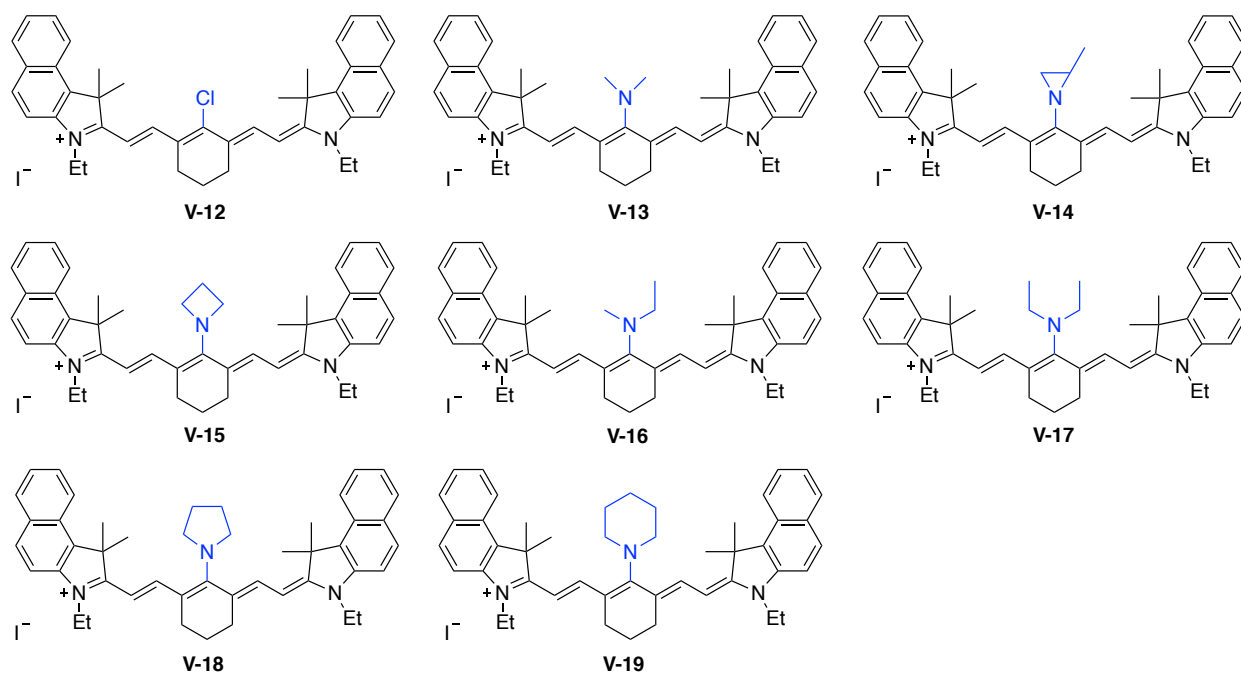


Figure V-8. Spectroscopic data of dye **V-6** in various solvents.

V.3.2 Series 2 cyanine dyes

In order to examine whether the same trend observed in series 1 dyes still persists, we synthesized series 2 cyanine dyes (**Scheme V-4**) which have a more conjugated aryl rings according to the general synthesis (**Scheme V-2**).



Scheme V-4. Series 2 cyanine dyes.

Indeed, we did observe a similar trend in series 2 cyanine dyes. For example, in **Figure V-9**, dyes **V-4** and **V-13** share dimethylamine substituents and they have the same Stokes shift (113 nm) and similar quantum yield (24% for **V-13** and 28% for **V-4**). But the absorption and emission spectra of **V-13** is red-shifted as a result of the larger aryl ring.

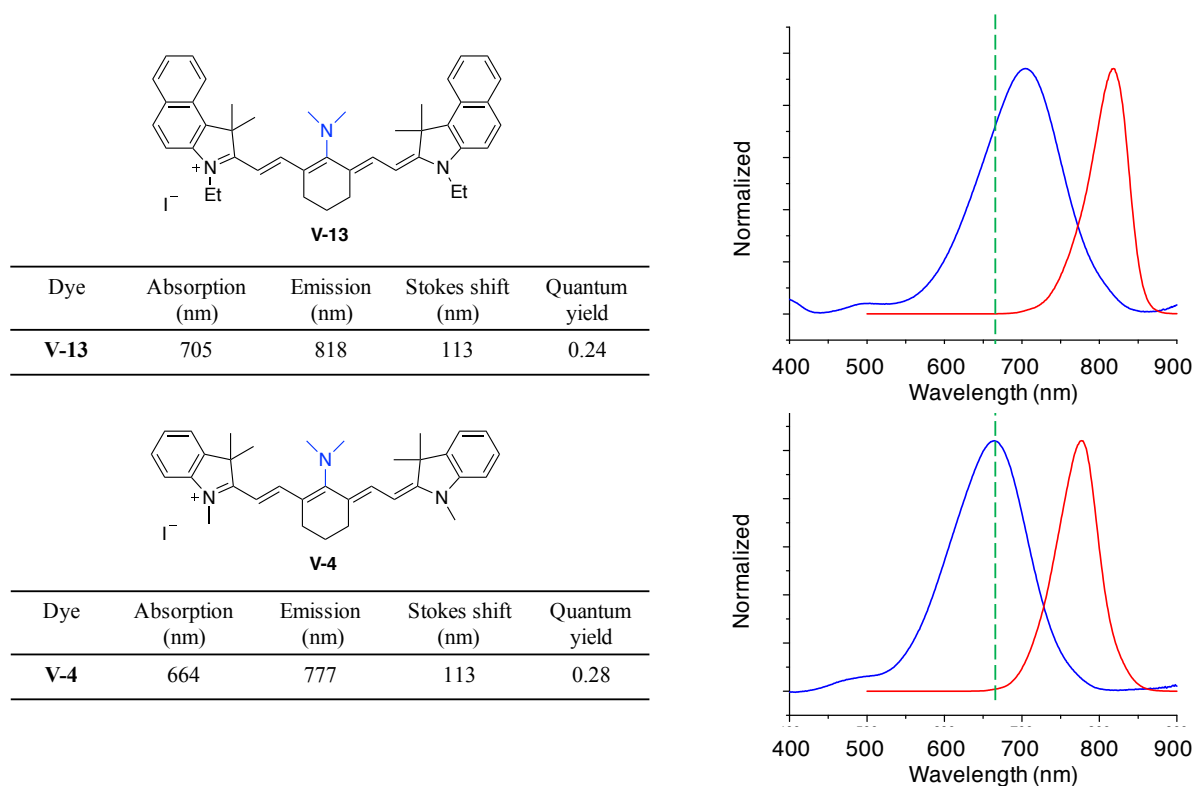


Figure V-9. Spectroscopic data for similar dye **V-13** and **V-4**. Absorption, emission and quantum yield were measured in DCM.

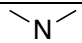
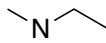
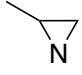

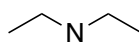
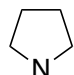
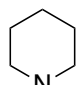
Dye	Amine substrates	Absorption (nm)	Emission (nm)	Stokes shift (nm)	QY (%)
V-13		705	818	113	24
V-16		724	816	92	26
V-14		746	802	56	24
V-15		649	737	88	30
V-17		739	819	80	24
V-18		636	823	187	25
V-19		708	824	116	21

Table V-2. Spectroscopic data for series 2 cyanine dyes. Absorption, emission and quantum yield were measured in DCM. QY = quantum yield.

Spectroscopic data for series 2 cyanine dyes are summarized in **Table V-2**. The largest Stokes shift comes from dye **V-18** and lowest is the aziridine dye **V-14**. Most of the dyes from series 1 have a slightly higher quantum yield than its series 2 analog. Only azetidone substituent dye **V-15** yields slightly higher quantum yield (30%) than **V-6** (26%). In general, Stokes shift of these two series remains the same.

V.4 Theoretical calculation

In order to investigate the mechanism for the observed change in the Stokes shift, we carried out a series of computational studies.²⁶ High level calculation of cyanine dyes remains a challenging tasks in the computational field.²⁷ For example, commonly used TD-DFT methods can not provide accurate transition energies of cyanine dyes and overestimate energies by 0.5 -1.0 eV. Other hybrid functionals also have their own limits.²⁸ In this regard, we decided not to focus on absolute results for each dye. Instead, a relative trend among these cyanine dyes could be more instructive. Prof. Levine (Department of Chemistry, Michigan State University, our computational collaborator on this project) is performing high level calculations. The data presented in **Chapter V** were collected in our lab, using the described computational setups.

V.4.1 Cyanine *s-trans* and *s-cis* geometries

Series 1 and 2 cyanine dyes share the same trend in the observed Stokes shifts. In order to save computational time, we focused on all series 1 cyanine dyes. Cyanine dye with *s-cis* geometry were observed in crystal structures.²⁹ Thus, whether the nitrogen substituents may affect the most stable conformation between *s-cis* and *s-trans* was tested (**Figure V-10**). We first examined the indolium geometry in all series 1 dyes. The

most stable conformers of *s-cis* and *s-trans* are obtained at DFT/B3LYP/6-31G*/CPCM(H₂O) level.

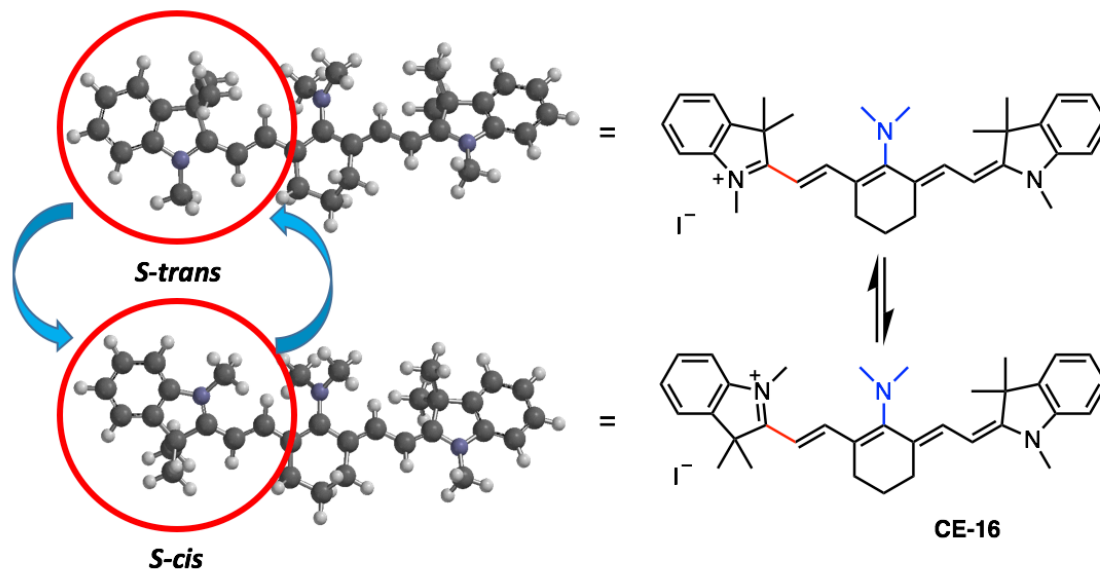


Figure V-10. Two possible *s-cis* and *s-trans* conformers of dye **V-4**. The lowest energies of these two conformers are computed at DFT/B3LYP/6-31G*/CPCM(H₂O) level from SPARTAN 16 software.

After the calculation of all series 1 dyes, we found that all *s-trans* conformers are more stable than *s-cis* conformers in all these cases by an average of 2 Kcal/mol (dye **V-3** to **V-10**, **Figure V-11**). Thus, we believe that *s-trans* conformation is the most stable conformation for these dyes, and thus, the Stokes shift change is not caused by the indolium ring flipping.

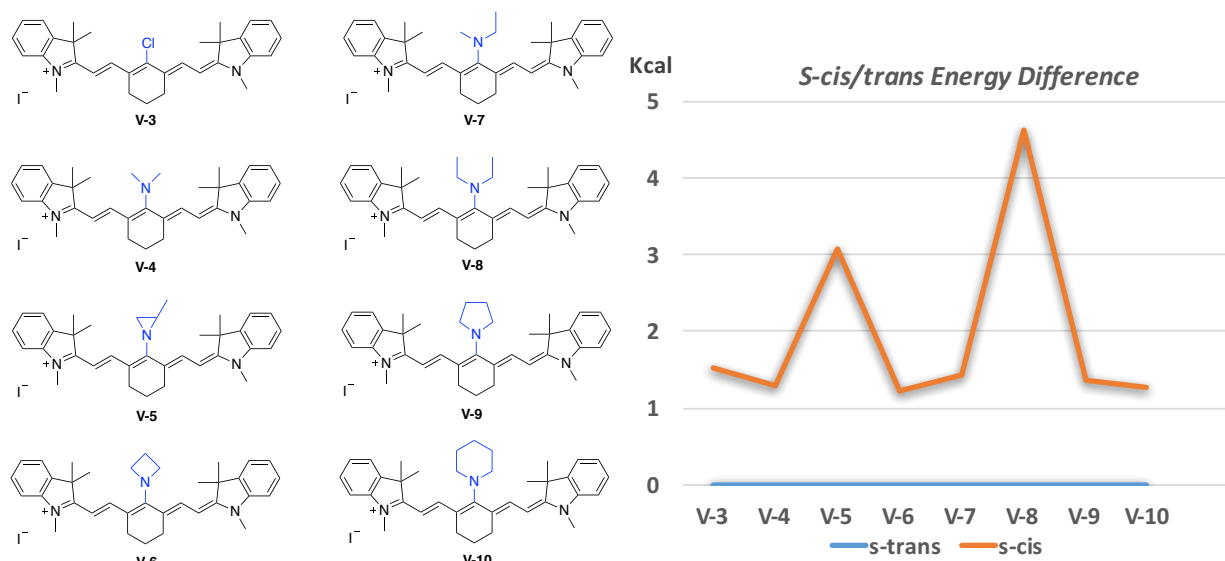


Figure V-11. Calculated relative energy difference between the most stable *s-cis* and *s-trans* conformation at DFT/B3LYP/6-31G*/CPCM (H₂O) level.

V.4.2 Effect of twisting and bending

Due in part to the similar structures shared by series 1 cyanine dyes and close emission wavelengths, we believed the key reason to cause this dramatic Stokes shifts most probably originates from differences in their ground states rather than the excited states.³⁰ Thus, we carried out a series of computational analyses to evaluate the ground states structures of these dyes.

To begin the study, we screened several calculation levels by comparing the vertical excitation energy between the most stable ground state and its geometry at the first excited state. Dye **V-4** which exhibits a large Stokes shift (λ_{abs} 664 nm, λ_{em} 777nm, Stokes shift 113 nm) was chosen for this screening study.

Calculation level	Dihedral Angle	Helical Twist	HOMO (eV)	LUMO (eV)	Gap (eV)	E(S0) (Hartree)	E(S1) (Hartree)	Vertical Excitation (eV)	Wavelength (nm)
DFT/B3LYP/6-31G*/CPCM	42.62	53.60	-4.84	-2.47	2.37	-1485.029667	-1484.945249	2.297	540
CAM/B3LYP/6-31G*/CPCM	38.32	51.89	-6.16	-1.65	4.51	-1484.195136	-1484.096904	2.673	464
PBE0/6-31+G*/CPCM	41.13	52.60	-5.21	-2.56	2.65	-1483.306214	-1483.212912	2.539	489
ω B97X-D/6-31+G*/CPCM	36.95	47.91	-6.70	-1.08	5.62	-1484.603544	-1484.503249	2.729	455
M06-2X/6-31+G*/CPCM	35.45	42.10	-6.11	-1.97	4.14	-1484.397212	N/A	N/A	N/A
MP2/6-31G*	39.45	61.25	-8.97	-1.77	7.20	-1479.984896	N/A	N/A	N/A
MP2/6-31G* ^a	39.45	61.27	-4.99 ^a	-2.56 ^a	2.43 ^a	-1484.977390 ^a	-1485.062772 ^a	2.323 ^a	534 ^a

Table V-3. Screening computation functionals of cyanine dye **V-4**. ^aOptimized geometry from MP2 level was subject to energy calculation at B3LYP/6-31+G*/CPCM level. Water is chosen for all the solvation models. E(S0) was calculated as singlet at ground state. E(S1) was calculated as singlet at excited state.

Due to the fact that the MP2 level can not support computational analysis at excited state, we subjected the optimized structure from MP2 level to DFT in order to obtain the final absorption wavelength. After comparing the calculated absorption wavelength of dye **V-4**, both DFT and MP2 (energy at DFT) level led to closer energies with the experimental result (**Table V-3**). PBE0 also performed well, but not as good as DFT. However, other functionals such as ω B97X-D and CAM overestimated the direct absorption energy. As for M06-2X, we were not able to locate the first excited energies due to computer hardware limitation. Thus, we chose the DFT and MP2 levels to optimize the ground state geometries of the rest of series 1 cyanine dyes.

In order to evaluate the conformational differences between these similar dyes, we introduced 3 different parameters to quantify them (**Figure V-12**). First parameter is the dihedral angle $\angle_{C-N-C-C}$ between the substituent and the cyanine dyes. For example, dye **V-4** has two dihedral angles (42.62 and 41.38) as a result of the secondary amine structure (**Figure V-12**). This angle can be used to quantify the geometry of different substituents and potentially the location of the electrons from the nitrogen. Second parameter is the twisting angle between the two indolium rings. This angle was measured between C-N-N-C (highlighted in the **Figure V-12**). It reflects the overall impact of the substituent on the cyanine dyes. The last parameter is the $\sum Bending$ angle. This angle is the sum up of each methine bending angle between two indolium rings. It can also reflect the flatness of the cyanine dye structure.

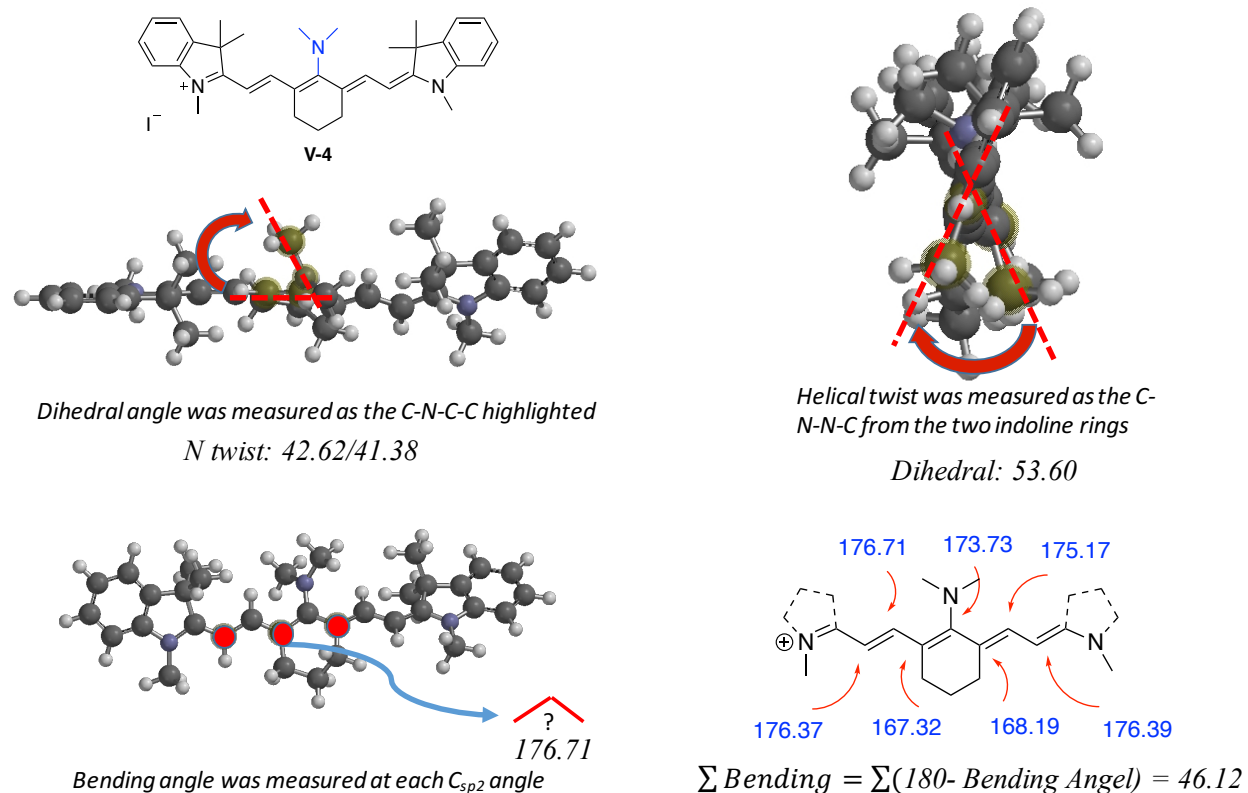


Figure V-12. Using different parameters to evaluate series 1 cyanine dyes.

Summarized data at DFT and MP2 levels are shown in **Table V-4** and **Table V-5**, respectively. Interestingly, if we just focus on one of the parameters, we could not find a correlation with the Stokes shift, especially considering the dihedral angles. However, the sum of the $\sum Bending$ with the twisting angle together yields a trend that corresponds to the Stokes shift. For example, dye **V-3** and **V-5** both have small bending and twisting angles (33.33 for dye **V-3** and 72.27 for dye **V-5** at DFT level), exhibiting small Stokes shift (21 nm for **V-3** and 24 nm for **V-5**, respectively). All the rest of the dyes which have large bending and twisting angles (greater than 80 degrees obtained at DFT level) lead to a larger Stokes shift (highlighted in the **Table V-4**). We did observe the same trend at

MP2 level as well (**Table V-5**). Another interesting result is that dye **V-6** has the largest Σ Bending angle among all of the series 1 dyes. Both calculated results showed that the entire dye was bent in a “V” shape at its ground state. Such a large bending was not observed in other dyes. Indeed, dye **V-6** has the lowest emission wavelength (704 nm, **Table V-2**) among all series 1 dyes. We speculated that such large bending angle cannot be relaxed even in the excited state. Thus, blue shifted emission wavelength was observed (experimental emission result of dye **V-6** is 704 nm, falls lower than the rest of the dyes).

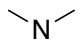
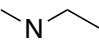
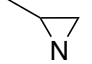
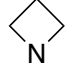
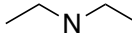
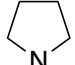
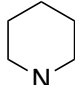
Dye	Substrate	Dihedral angles	Twisting angle	Total Bending angle	Twisting + bending	Stokes shift (nm)
V-3	Cl	-	4.91	26.42	31.33	21
V-4		42.60/41.38	53.6	46.12	99.72	113
V-7		45.11/47.34	43.84	45.70	89.54	94
V-5		61.74/46.37	7.39	64.88	72.27	24
V-6		18.11/19.17	0.49	95.18	95.67	89
V-8		49.59/48.63	42.24	40.98	83.22	79
V-9		51.19/49.38	51.89	46.49	98.38	180
V-10		45.22/45.76	56.27	50.02	106.29	117

Table V-4. Summarized 3 parameters data for series 1 cyanine dyes at DFT/B3LYP/6-31G*/CPCM(H₂O) level. Calculated results from SPARTAN 16 software.

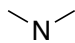
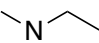
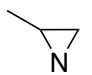
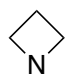
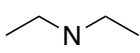
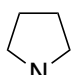
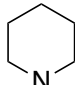
Dye	Substrate	Dihedral angles	Twisting angle	Total Bending angle	Twisting + bending	Stokes shift (nm)
V-3	Cl	--	0.7	24.63	25.33	21
V-4		39.45/38.38	61.25	51.11	112.36	113
V-7		42.51/41.67	59.80	49.85	109.65	94
V-5		64.23/50.02	3.42	61.84	65.26	24
V-6		21.82/21.90	0.12	90.8	90.92	89
V-8		43.27/44.26	57.47	49.72	107.19	79
V-9		43.97/43.63	65.16	52.17	117.33	180
V-10		38.97/38.96	67.72	57.35	125.07	117

Table V-5. Summarized 3 parameters data for series 1 cyanine dyes at MP2 level. Calculated results from SPARTAN 16 software.

However, we still can not explain why the 6-member ring dye **V-10**, which has the largest twisting and bending angle yields lower Stokes shift than the 5-member ring dye **V-9**. But a relative trend can be described as: if the substrate caused more impact (twisting or $\sum Bending$) to the heptamethine cyanine chain, a greater Stokes shift can be expected.

V.4.3 Geometry at the nitrogen atom

During the computational analysis, we found that the nitrogen atom of the substituent can adopt either the sp^2 or the sp^3 hybridization in series 1 cyanine dyes. For example, the dye with the smallest Stokes shift (**V-5**) adopts a more sp^3 hybridized nitrogen whereas other larger Stokes shift dyes **V-4** and **V-8** adopt more sp^2 hybridized nitrogen. Thus, we proposed that the geometry of the nitrogen can be another useful tool to quantify the Stokes shift of these dyes. More sp^2 hybridized nitrogen indicates the long

pairs are prone to be donated to the conjugated polyenes, thus, breaking the cyanine dye conjugation can yield a bis-dipole structure and blueshift the absorption. On the other hand, more sp^3 hybridized nitrogen indicates less lone pair donations to the polyenes, leading to a less bis-dipole structure which can potentially yield smaller Stokes shift.

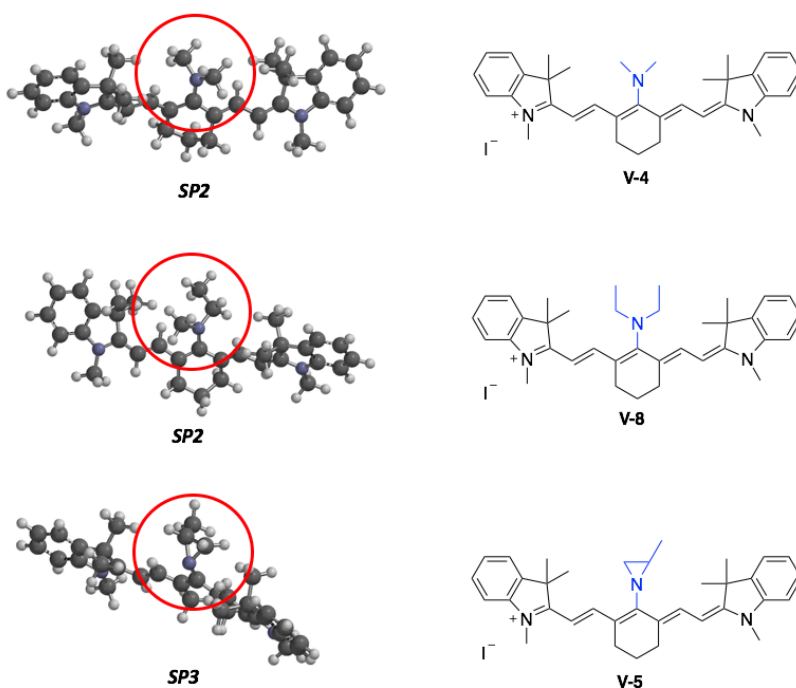


Figure V-13. Optimized ground state geometries of dye **V-4**, **V-8** and **V-5** from SPARTAN 16.

Since series 1 cyanine dyes share similar structures, an empirical D3 dispersion correlation was utilized to include the Van der Waals energy in the computational analysis. Structures that optimized at B3LYP/6-31G*/CPCM(H₂O) level were subject to either B3LYP-D3/6-31G*/CPCM(H₂O) or PBE-D3/6-31G*/CPCM(H₂O) level to yield the final optimal ground state geometry. We were able to obtain all the optimized ground state geometries for series 1 cyanine dyes at both computational levels.

Locating the lone pair position or quantifying numbers of electron that are donated from different nitrogen substituents was almost impossible. Indeed, we did try several different indirect methods to quantify the nitrogen lone pair donation. Mulliken charges and electrostatic calculation on either N or first carbon that attached to N substituent were analyzed. However, we did not obtain a clear correlation from these trials (**Figure V-14**). Attempts to fit these data only lead to poor linear regressions ($R^2 < 0.5$).

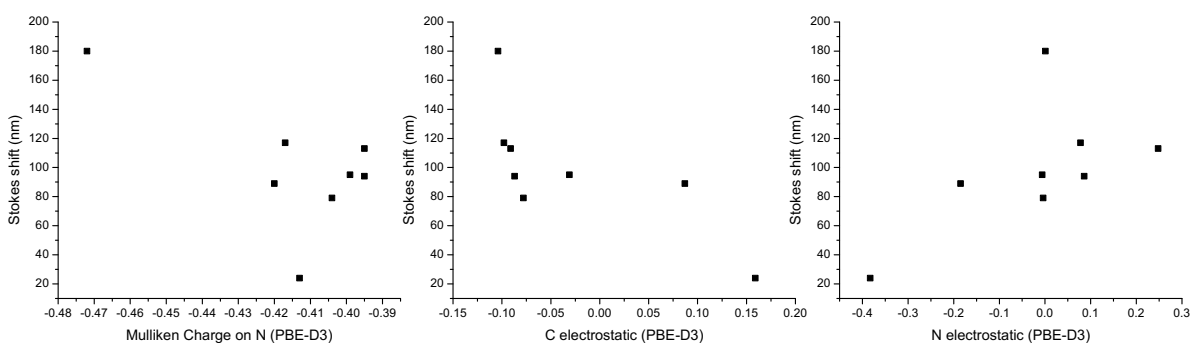
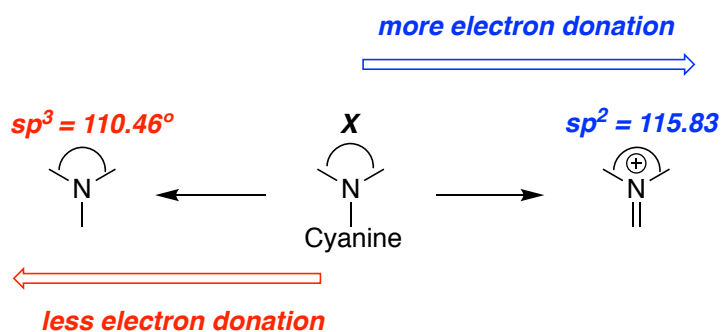


Figure V-14. Calculated Mulliken charge and electrostatic values of series 1 cyanine dyes at PBE-D3/6-31G*/CPCM(H₂O) level. No clear trend was observed in these attempts.

Next, we turned our attention to the geometry of the nitrogen. For example, a fully sp^3 hybridized trimethylamine adopts \angle_{C-N-C} 110.46° and fully sp^2 hybridized trimethylamine adopts \angle_{C-N-C} 115.83° . Thus, we can measure the \angle_{C-N-C} angle obtained from **V-4** to quantify the electron donation from the nitrogen to the cyanine dye (**Scheme V-5**). More importantly, this angle also includes the natural geometrical properties from different N substituents. Parameter $angle_{donation}$ was proposed as the subtraction between the \angle_{C-N-C} from the computed dye structure and the fully sp^3 hybridized N substituents.



$$\text{Angle}_{\text{donation}} = \text{Angle}_x - \text{Angle}_{\text{sp}^3}$$

Scheme V-5. New parameter is established to quantify the electron donation from different nitrogen substituents.

Dye	Free amine	Fully sp^3 angle ^a	$\angle_{\text{C-N-C}}$ ^b	Charged Imine	Fully sp^2 angle ^a	Angle _{donation}	Stokes shift (nm)
V-4		110.46	113.72		115.83	3.26	113
V-20		111.61	115.37		116.77	3.76	95
V-7		111.63	115.43		116.90	3.8	94
V-8		111.08	117.91		117.91	6.83	79
V-5		60.98	61.30		49.03	0.32	24
V-6		89.41	92.64		92.69	3.23	89
V-10		110.36	116.38		115.01	6.02	117
V-11		103.49	111.74		110.76	8.25	180

Table V-6. Summarized data for series 1 cyanine dyes. ^aFully sp^2 and sp^3 hybridized angles were obtained from SPRATN 16 at MP2/6-31G* level. ^bCyanine $\angle_{\text{C-N-C}}$ angle was measured at PBE-D3/6-31G*/CPCM(H₂O) level.

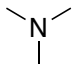
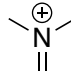
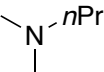
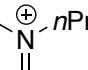
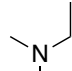
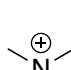
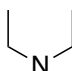
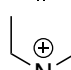
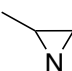
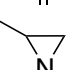
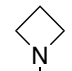

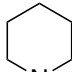
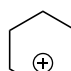

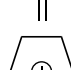
Dye	Free amine	Fully sp ³ angle ^a	$\angle_{\text{C-N-C}}$ ^b	Charged Imine	Fully sp ² angle ^a	Angle _{donation}	Stokes shift (nm)
V-4		110.46	114.05		115.83	3.59	113
V-20		111.61	115.33		116.77	3.72	95
V-7		111.63	115.64		116.90	4.01	94
V-8		111.08	116.30		117.91	5.22	79
V-5		60.98	61.16		49.03	0.18	24
V-6		89.41	92.59		92.69	3.18	89
V-10		110.36	117.00		115.01	6.64	117
V-11		103.49	112.94		110.76	9.45	180

Table V-7. Summarized data for series 1 cyanine dyes. ^aFully sp² and sp³ hybridized angles were obtained from SPRATN 16 at MP2/6-31G* level. ^bCyanine $\angle_{\text{C-N-C}}$ angle was measured at B3LYP-D3/6-31G*/CPCM(H₂O) level.

In order to make equal datasets for both open chain and cyclic ring substituents, we synthesized dye **V-20** and added it to the computational analysis. Herein, we summarized all the data at two different computational levels (PBE-D3 and DFT-D3) in **Table V-6** and **Table V-7**. Both computational levels yielded a similar result that angle_{donation} has a direct correlation with the Stokes shift. For example, **V-5** which has the smallest Stokes shift and has 0.18 angle_{donation} value from DFT-D3 calculation (0.32 angle_{donation} value at PBE-D3 level). This value indicates the nitrogen is sp³ hybridized on the cyanine dye. **V-11** which has the largest Stokes shift has a 9.45 angle_{donation} value

from DFT-D3 calculation (8.25 angle_{donation} value at PBE-D3 level) indicating that the N is almost fully sp² hybridized and fully donates its electrons into the cyanine dye.

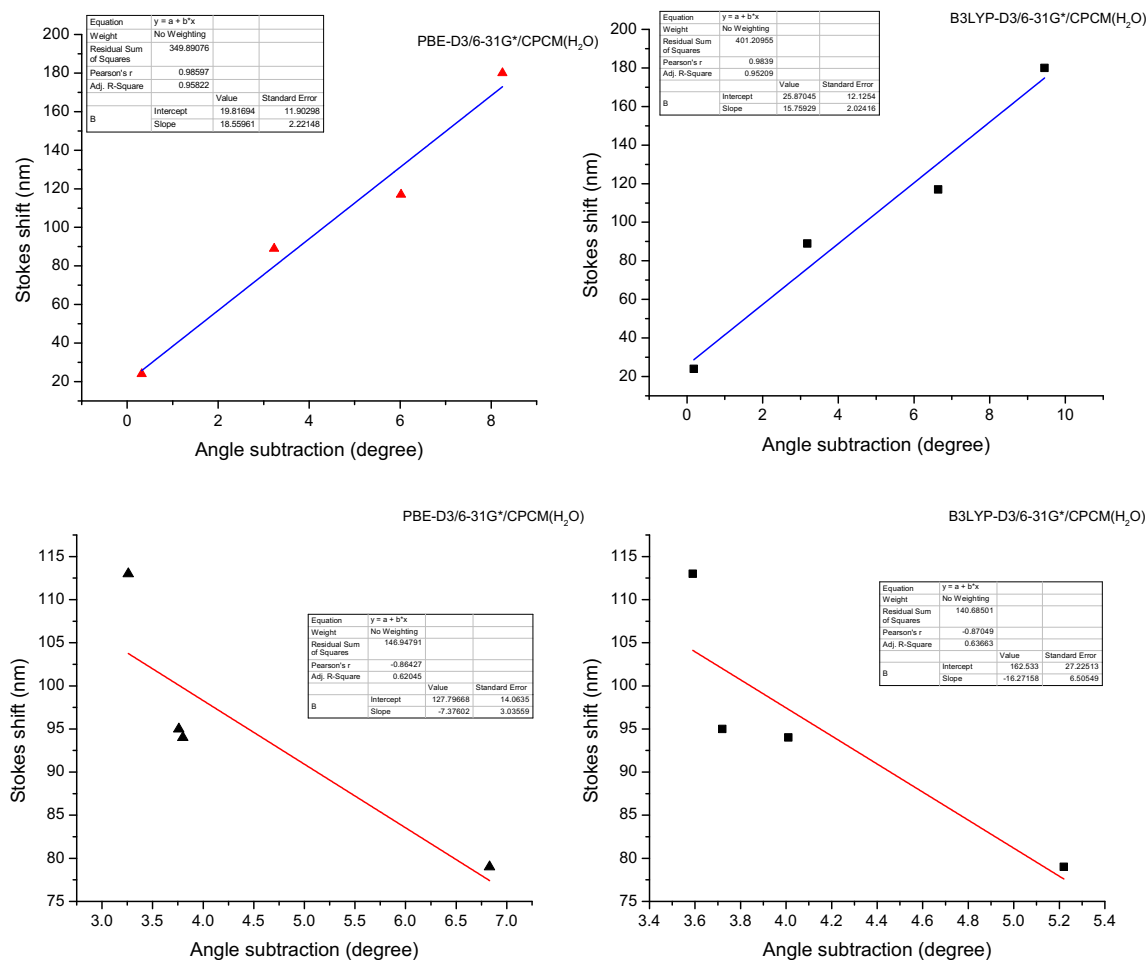


Figure V-15. Linear correlation between the angle subtraction (angle_{donation}) and Stokes shift at DFT-D3 and PBE-D3 levels. Top figures: cyclic ring substrates; bottom figures: open chain substrates.

Curiously, the two categories (open chain and cyclic rings) exhibit opposite trends analyzed as described above. For example, **V-4**, **V-20**, **V-7** and **V-8**, all open chain substituents, can have free alkyl rotations and are not restricted by the ring strain. A higher angle_{donation} value for these dyes leads to lower Stokes shift. However, cyclic ring substrates **V-5**, **V-6**, **V-10** and **V-11** may suffer from the ring strain to limit the free rotations.

In these cases, a higher angle_{donation} value correlates to a higher Stokes shift. The plotted angle_{donation} against Stokes shifts are shown in **Figure V-15**. At both computational levels, we observed the that angle_{donation} values have two opposite trends for the two series groups of dyes good linear correlations.

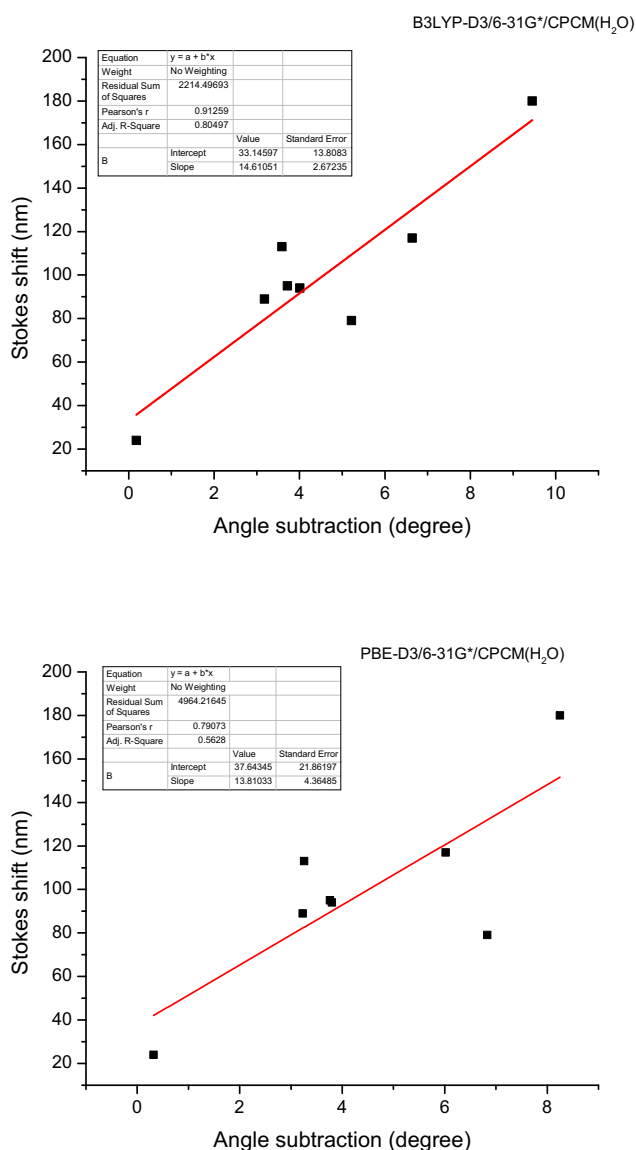


Figure V-16. Linear correlation between the angle subtraction (angle_{donation}) and Stokes shift at DFT-D3 and PBE-D3 levels. Top figures: DFT-D3/B3LYP/6-31G*/CPCM(H₂O) level; bottom figures: PBE-D3/B3LYP/6-31G*/CPCM(H₂O) level.

In another attempt, we plotted all data from series 1 cyanine dyes as a function of Stokes shift (**Figure V-16**). B3LYP-D3 level yields better linear correlations than PBE-D3 level ($R^2 = 0.80$ at DFT, $R^2 = 0.56$ at PBE). Based on the latter correlations, we can argue that a larger angle_{donation} value can lead to a larger Stokes shift but they may behave differently depending on the structures of the substituent.

This study provides a glimpse into selective engineering of Stokes shifts for cyanine dyes, which are of importance in biomedical engineering and imaging projects to reduce background noise. Some of the cyanine dyes described here have already been tested in the LSCs systems and afforded good results. More detailed studies on tuning Stokes shifts of such dyes are still ongoing in our lab.

V.5 Experimental Section

V.5.1 Materials and general instrumentations

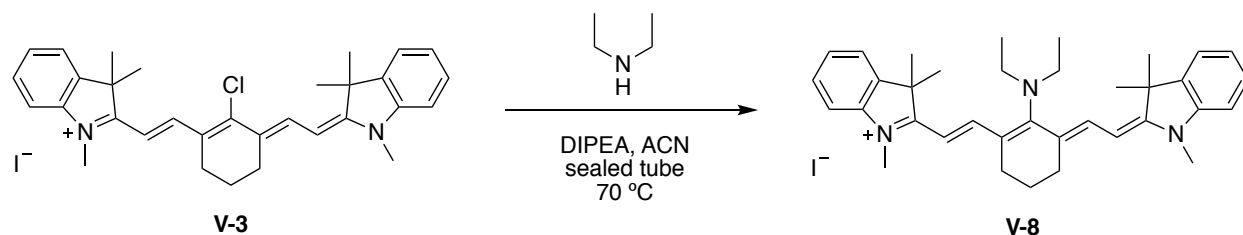
Solvents and reagents used for reactions were purchased from commercial sources. Acetonitrile (ACN) for reactions was HPLC grade from Sigma-Aldrich. Column chromatography was performed using SiliCycle silica gel (230-400 mesh). Thin layer chromatography (TLC) with fluorescent indicator was purchased from Analtech. $^1\text{H-NMR}$ and $^{13}\text{C-NMR}$ spectra were obtained on Varian Inova 500 MHz instruments and were reported in parts per million (ppm) relative to the solvent resonances (δ), with coupling constants (J) in Hertz (Hz). HRMS analysis was performed on a Q-TOF Ultima system using electrospray ionization in positive mode. UV-Vis was performed on Agilent Cary 100 series machine and PL was recorded on Fluorolog by ISA instrument. Quantum yield measurement was performed on absolute PL quantum yield spectrometer C11347 by Hamamatsu.

V.5.2 Computational analysis

Commercial available PC with 15 core Intel Xeon X5647 @2.93 GHz with 48 G memory on a Kernel Linux platform, equipped with SPRATN 16 software was used for the computational study. Conformer distribution calculations were performed at the MMFF level of theory, followed by energy calculation at HF/6-31G*. The top four most stable conformers were screened and then subjected to DFT/B3LYP/6-31G*/CPCM(H_2O) level to obtain the optimized ground state geometry. Other ground state geometry optimizations were based on the most stable conformer obtained from the DFT level.

V.5.3 General dye synthesis

General procedure for series 1 and series 2 cyanine dyes:



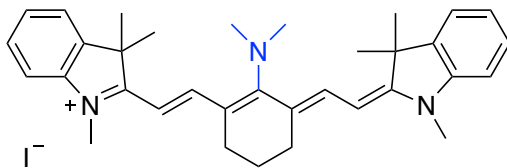
2-((E)-2-((E)-2-(diethylamino)-3-(2-((E)-1,3,3-trimethylindolin-2-ylidene)ethylidene)cyclohex-1-en-1-yl)vinyl)-1,3,3-trimethyl-3H-indol-1-ium iodide. (**V-8**)

Compound **V-3** is synthesized according to the previous reported procedures. To a solution of **V-3** (74 mg, 0.10 mmol), diisopropylethylamine (DIPEA) (35 μL , 2 equiv, 0.20 mmol) in acetonitrile (2 mL) was added freshly distilled diethylamine (206 μL , 20 equiv, 2.0 mmol) under nitrogen. The mixture was stirred at 70 $^\circ\text{C}$ and the reaction was monitored by LC-MS. Upon completion, typically in 48 h, the mixture was concentrated under reduced pressure and purified by flash column (100% DCM gradually to 5% MeOH/DCM). The product was isolated as a dark solid (21 mg, 0.032 mmol, 32%).

$^1\text{H-NMR}$ (500 MHz, Chloroform- d): δ 7.52 (d, J = 13.6 Hz, 2H), 7.34 – 7.26 (m, 4H), 7.11 (m, 2H), 7.02 (d, J = 7.9 Hz, 2H), 5.80 (d, J = 13.6 Hz, 2H), 3.65 (q, J = 6.9 Hz, 4H), 3.52 (s, 6H), 2.49 (t, J = 6.5 Hz, 4H), 1.82 (p, J = 6.5 Hz, 2H), 1.60 (s, 12H), 1.28 (t, J = 6.9 Hz, 6H).

$^{13}\text{C-NMR}$ (126 MHz, Chloroform- d): δ 174.15, 169.83, 143.19, 142.52, 140.06, 128.57, 125.76, 123.76, 121.97, 109.50, 96.95, 49.47, 48.03, 31.36, 29.07, 24.88, 21.98, 14.84.

HRMS(ESI $^+$): calcd for $\text{C}_{36}\text{H}_{46}\text{N}_3^+$ [M] $^+$ 520.3690, found 520.3692.



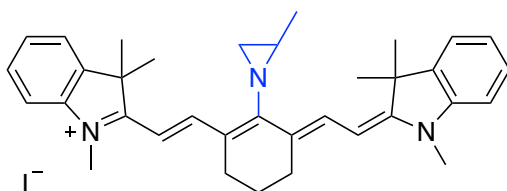
2-((E)-2-((E)-2-(dimethylamino)-3-(2-((E)-1,3,3-trimethylindolin-2-ylidene)ethylidene)cyclohex-1-en-1-yl)vinyl)-1,3,3-trimethyl-3H-indol-1-ium iodide (**V-4**)

The title compound was prepared according to the general procedure at 0.1 mmol scale. Product **V-4** was isolated as a dark solid product (40 mg, 0.064 mmol, 64%).

$^1\text{H-NMR}$ (500 MHz, Chloroform-*d*): δ 7.40 (d, $J = 13.1$ Hz, 2H), 7.23 (td, $J = 8.1$, 7.4, 1.5 Hz, 4H), 7.01 (t, $J = 7.4$ Hz, 2H), 6.88 (d, $J = 7.9$ Hz, 2H), 5.56 (d, $J = 13.1$ Hz, 2H), 3.61 (s, 6H), 3.39 (s, 6H), 2.46 (t, $J = 6.6$ Hz, 4H), 1.79 (p, $J = 6.6$ Hz, 2H), 1.59 (s, 12H).

$^{13}\text{C-NMR}$ (126 MHz, Chloroform-*d*): δ 175.55, 167.84, 143.54, 140.28, 139.84, 128.22, 122.73, 122.08, 121.97, 108.50, 94.06, 53.53, 47.86, 47.60, 29.48, 25.40, 21.56.

HRMS(ESI+): calcd for $\text{C}_{34}\text{H}_{42}\text{N}_3^+$ $[\text{M}]^+$ 492.3379, found 492.3378.



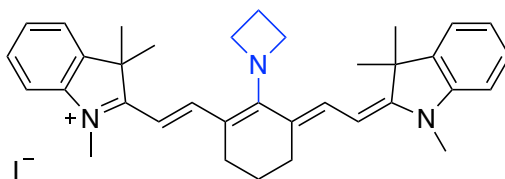
1,3,3-Trimethyl-2-((E)-2-((E)-2-(2-methylaziridin-1-yl)-3-(2-((E)-1,3,3-trimethylindolin-2-ylidene)ethylidene)cyclohex-1-en-1-yl)vinyl)-3H-indol-1-ium iodide (**V-5**)

The title compound was prepared according to the general procedure at 0.1 mmol scale. Product **V-5** was isolated as a dark solid product (30 mg, 0.047 mmol, 47%).

$^1\text{H-NMR}$ (500 MHz, Chloroform-*d*): δ 8.01 (d, $J = 13.7$ Hz, 2H), 7.38 – 7.26 (m, 4H), 7.14 (t, $J = 7.4$ Hz, 2H), 7.05 (d, $J = 7.9$ Hz, 2H), 5.88 (d, $J = 13.7$ Hz, 2H), 3.57 (s, 6H), 2.57 (t, $J = 6.0$ Hz, 4H), 1.84 – 1.76 (m, 3H), 1.69 – 1.59 (m, 14H), 1.46 (d, $J = 5.4$ Hz, 3H).

$^{13}\text{C-NMR}$ (126 MHz, Chloroform-*d*): δ 170.91, 170.12, 143.07, 140.20, 139.76, 128.61, 124.61, 124.14, 121.99, 109.76, 98.11, 48.27, 39.06, 36.94, 31.66, 28.61, 28.47, 25.95, 20.86, 18.09.

HRMS(ESI+): calcd for $\text{C}_{35}\text{H}_{42}\text{N}_3^+$ $[\text{M}]^+$ 504.3379, found 504.3375.



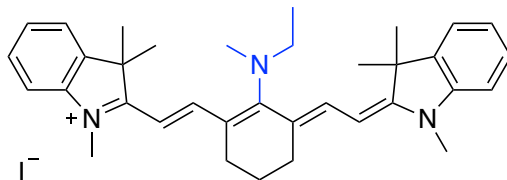
2-((*E*)-2-((*E*)-2-(azetidin-1-yl)-3-(2-((*E*)-1,3,3-trimethylindolin-2-ylidene)ethylidene)cyclohex-1-en-1-yl)vinyl)-1,3,3-trimethyl-3*H*-indol-1-ium iodide (**V-6**)

The title compound was prepared according to the general procedure at 0.1 mmol scale. Product **V-6** was isolated as a dark solid product (49 mg, 0.078 mmol, 78%).

$^1\text{H-NMR}$ (500 MHz, Chloroform-*d*): δ 7.24 – 7.16 (m, 6H), 6.96 (t, $J = 7.5$ Hz, 2H), 6.77 (d, $J = 7.7$ Hz, 2H), 5.32 (d, $J = 12.8$ Hz, 2H), 4.93 (t, $J = 7.6$ Hz, 4H), 3.25 (s, 6H), 2.71 (p, $J = 7.6$ Hz, 2H), 2.56 – 2.49 (m, 4H), 1.86 – 1.83 (m, 2H), 1.64 (s, 12H).

$^{13}\text{C-NMR}$ (126 MHz, Chloroform-*d*): δ 169.77, 165.86, 143.70, 139.75, 134.78, 127.96, 121.99, 121.95, 107.61, 92.32, 62.46, 47.02, 29.83, 29.27, 27.22, 20.79, 19.31.

HRMS(ESI+): calcd for $\text{C}_{35}\text{H}_{42}\text{N}_3^+$ $[\text{M}]^+$ 504.3379, found 504.3382.



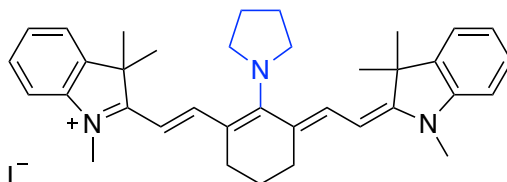
2-((*E*)-2-((*E*)-2-(ethyl(methyl)amino)-3-(2-((*E*)-1,3,3-trimethylindolin-2-ylidene)ethylidene)cyclohex-1-en-1-yl)vinyl)-1,3,3-trimethyl-3*H*-indol-1-ium iodide (**V-7**).

The title compound was prepared according to the general procedure at 0.1 mmol scale. Product **V-7** was isolated as a dark solid product (39 mg, 0.062 mmol, 62%).

$^1\text{H-NMR}$ (500 MHz, Chloroform-*d*): δ 7.46 (d, $J = 13.4$ Hz, 2H), 7.33 – 7.24 (m, 4H), 7.08 (t, $J = 7.4$ Hz, 2H), 6.97 (d, $J = 7.9$ Hz, 2H), 5.72 (d, $J = 13.4$ Hz, 2H), 3.79 (q, $J = 7.0$ Hz, 2H), 3.48 (s, 6H), 3.41 (s, 3H), 2.47 (t, $J = 6.5$ Hz, 4H), 1.81 (p, $J = 6.6$ Hz, 2H), 1.60 (s, 12H), 1.37 (t, $J = 7.0$ Hz, 3H).

$^{13}\text{C-NMR}$ (126 MHz, Chloroform-*d*): δ 175.03, 169.15, 143.30, 141.83, 139.94, 128.44, 124.26, 123.41, 121.97, 109.15, 95.86, 53.52, 47.90, 44.73, 31.24, 29.27, 24.94, 21.83, 14.98.

HRMS(ESI+): calcd for $\text{C}_{35}\text{H}_{44}\text{N}_3^+$ [M] $^+$ 506.3535, found 506.3525.



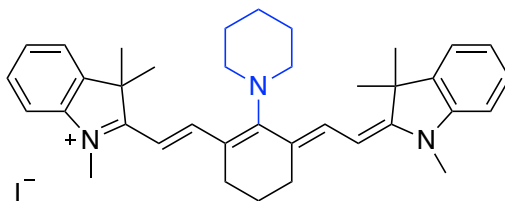
1,3,3-Trimethyl-2-((*E*)-2-((*E*)-2-(pyrrolidin-1-yl)-3-(2-((*E*)-1,3,3-trimethylindolin-2-ylidene)ethylidene)cyclohex-1-en-1-yl)vinyl)-3*H*-indol-1-ium iodide (**V-9**).

The title compound was prepared according to the general procedure at 0.1 mmol scale. Product **V-9** was isolated as a dark solid product (15 mg, 0.023 mmol, 23%).

$^1\text{H-NMR}$ (500 MHz, Chloroform-*d*): δ 7.42 (d, $J = 12.7$ Hz, 2H), 7.19 (m, 4H), 6.94 (t, $J = 7.4$ Hz, 2H), 6.73 (d, $J = 8.0$ Hz, 2H), 5.27 (d, $J = 12.7$ Hz, 2H), 4.32 (d, $J = 6.5$ Hz, 4H), 3.22 (s, 6H), 2.59 (t, $J = 6.2$ Hz, 4H), 2.10 (m, 4H), 1.79 (t, $J = 6.3$ Hz, 2H), 1.70 (s, 12H).

$^{13}\text{C-NMR}$ (126 MHz, cdcl_3): δ 173.07, 165.22, 143.92, 140.02, 135.14, 127.72, 122.03, 121.53, 121.22, 107.08, 91.76, 55.86, 46.98, 29.58, 29.43, 28.77, 24.16, 20.91.

HRMS(ESI+): calcd for $\text{C}_{36}\text{H}_{44}\text{N}_3^+$ [M] $^+$ 518.3535, found 518.3536.



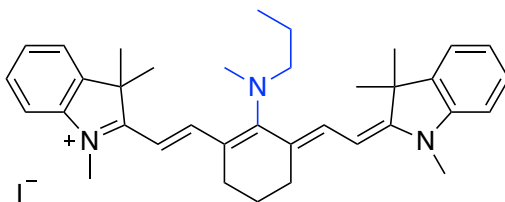
1,3,3-Trimethyl-2-((*E*)-2-((*E*)-2-(piperidin-1-yl)-3-(2-((*E*)-1,3,3-trimethylindolin-2-ylidene)ethylidene)cyclohex-1-en-1-yl)vinyl)-3*H*-indol-1-ium iodide (**V-10**)

The title compound was prepared according to the general procedure at 0.1 mmol scale. Product **V-10** was isolated as a dark solid product (72 mg, 0.054 mmol, 54%).

$^1\text{H-NMR}$ (500 MHz, Chloroform-*d*): δ 7.50 (d, $J = 13.2$ Hz, 2H), 7.33 – 7.22 (m, 4H), 7.06 (t, $J = 7.4$ Hz, 2H), 6.95 (d, $J = 7.9$ Hz, 2H), 5.68 (d, $J = 13.2$ Hz, 2H), 3.85 (t, $J = 5.0$ Hz, 4H), 3.46 (s, 6H), 2.47 (t, $J = 6.7$ Hz, 4H), 1.96-1.92 (m, 2H), 1.90-1.86 (m, 4H), 1.84-1.82 (m, 2H), 1.62 (s, 12H).

$^{13}\text{C-NMR}$ (126 MHz, Chloroform-*d*): δ 175.57, 168.39, 143.43, 140.15, 139.75, 128.36, 123.79, 123.06, 121.89, 108.84, 95.03, 56.80, 47.63, 28.96, 28.15, 24.94, 24.28, 21.63, 18.91.

HRMS(ESI+): calcd for C₃₇H₄₆N₃⁺ [M]⁺ 532.3692, found 532.3690.



1,3,3-Trimethyl-2-((*E*)-2-((*E*)-2-(methyl(propyl)amino)-3-(2-((*E*)-1,3,3-trimethylindolin-2-ylidene)ethylidene)cyclohex-1-en-1-yl)vinyl)-3*H*-indol-1-ium iodide (**V-20**)

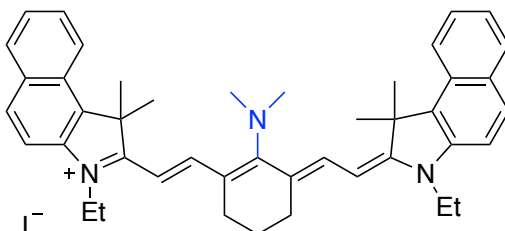
The title compound was prepared according to the general procedure at 0.1 mmol scale. Product **V-20** was isolated as a dark solid product (58 mg, 0.090 mmol, 90%).

¹H-NMR (500 MHz, Chloroform-*d*): δ 7.47 (d, *J* = 13.4 Hz, 2H), 7.32 – 7.24 (m, 4H), 7.07 (t, *J* = 7.4 Hz, 2H), 6.97 (d, *J* = 7.9 Hz, 2H), 5.71 (d, *J* = 13.3 Hz, 2H), 3.69 (t, *J* = 7.2 Hz, 2H), 3.47 (s, 6H), 3.44 (s, 3H), 2.46 (t, *J* = 6.5 Hz, 4H), 1.80 – 1.76 (m, 4H), 1.59 (s, 12H), 0.92 (t, *J* = 7.3 Hz, 3H).

¹³C-NMR (126 MHz, Chloroform-*d*): δ 175.41, 169.07, 143.30, 141.79, 139.94, 128.44, 123.89, 123.38, 121.97, 109.13, 95.70, 60.80, 47.86, 45.58, 31.21, 29.28, 24.85, 22.45, 21.82, 11.29.

HRMS(ESI+): calcd for C₃₆H₄₆N₃⁺ [M]⁺ 520.3692, found 520.3685.

Series 2 cyanine dyes:



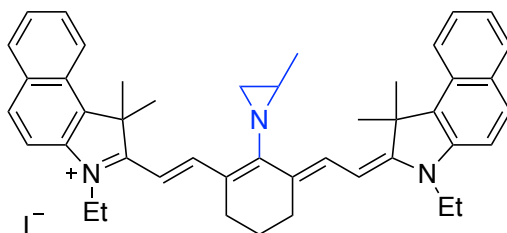
2-((*E*)-2-((*E*)-2-(dimethylamino)-3-((*E*)-2-(3-ethyl-1,1-dimethyl-1,3-dihydro-2*H*-benzo[*e*]indol-2-ylidene)ethylidene)cyclohex-1-en-1-yl)vinyl)-3-ethyl-1,1-dimethyl-1*H*-benzo[*e*]indol-3-ium iodide (**V-13**).

The title compound was prepared according to the general procedure at 0.1 mmol scale. Product **V-13** was isolated as a dark solid product (41 mg, 0.055 mmol, 55%).

¹H-NMR (500 MHz, Chloroform-*d*): δ 8.07 (d, *J* = 8.5 Hz, 2H), 7.83 (dd, *J* = 8.5, 4.4 Hz, 4H), 7.57 (d, *J* = 13.3 Hz, 2H), 7.51 (ddd, *J* = 8.3, 6.8, 1.3 Hz, 2H), 7.34 (t, *J* = 7.5 Hz, 2H), 7.23 (d, *J* = 8.4 Hz, 2H), 5.69 (d, *J* = 13.3 Hz, 2H), 4.04 (q, *J* = 7.2 Hz, 4H), 3.65 (s, 6H), 2.50 (t, *J* = 6.6 Hz, 4H), 1.93 (s, 12H), 1.86 – 1.81 (m, 2H), 1.40 (t, *J* = 7.2 Hz, 6H).

¹³C-NMR (126 MHz, Chloroform-*d*): δ 174.46, 168.95, 140.52, 139.85, 131.82, 130.89, 130.18, 129.89, 128.49, 127.41, 123.90, 122.00, 121.91, 109.74, 93.65, 49.72, 47.83, 38.59, 28.97, 25.34, 21.74, 12.03.

HRMS(ESI⁺): calcd for C₄₄H₅₀N₃⁺ [M]⁺ 620.4005, found 620.4008.



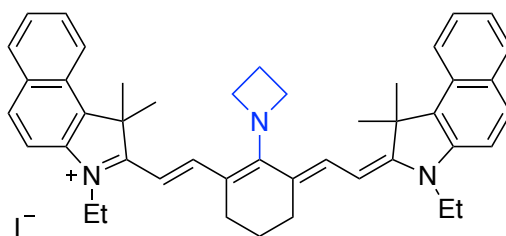
3-Ethyl-2-((*E*)-2-((*E*)-3-((*E*)-2-(3-ethyl-1,1-dimethyl-1,3-dihydro-2*H*-benzo[*e*]indol-2-ylidene)ethylidene)-2-(2-methylaziridin-1-yl)cyclohex-1-en-1-yl)vinyl)-1,1-dimethyl-1*H*-benzo[*e*]indol-3-ium iodide (**V-14**)

The title compound was prepared according to the general procedure at 0.1 mmol scale. Product **V-14** was isolated as a dark solid product (36 mg, 0.047 mmol, 47%).

$^1\text{H-NMR}$ (500 MHz, Chloroform-*d*): δ 8.14 (d, $J = 13.7$ Hz, 2H), 8.10 – 8.04 (m, 2H), 7.88 (dd, $J = 8.5, 4.2$ Hz, 4H), 7.55 (ddd, $J = 8.3, 6.8, 1.3$ Hz, 2H), 7.39 (ddd, $J = 8.0, 6.8, 1.0$ Hz, 2H), 7.35 (d, $J = 8.8$ Hz, 2H), 5.94 (d, $J = 13.7$ Hz, 2H), 4.18 (q, $J = 7.3$ Hz, 4H), 2.79 – 2.77 (m, 1H), 2.70 (d, $J = 5.8$ Hz, 1H), 2.58 (t, $J = 6.2$ Hz, 4H), 2.43 (d, $J = 3.5$ Hz, 1H), 1.98 (d, $J = 7.4$ Hz, 13H), 1.86 – 1.82 (m, 2H), 1.56 (d, $J = 5.4$ Hz, 3H), 1.44 (t, $J = 7.2$ Hz, 6H).

$^{13}\text{C-NMR}$ (126 MHz, Chloroform-*d*): δ 170.68, 170.28, 139.50, 139.11, 132.75, 131.45, 130.61, 130.07, 128.30, 127.64, 124.54, 124.01, 121.93, 110.27, 97.17, 50.26, 39.37, 37.12, 28.16, 28.04, 25.94, 20.92, 18.37, 12.33.

HRMS(ESI+): calcd for $\text{C}_{45}\text{H}_{50}\text{N}_3^+$ [M] $^+$ 632.4005, found 632.4009.



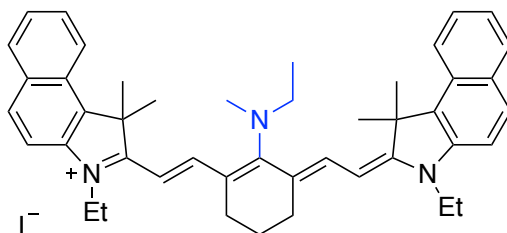
2-((*E*)-2-((*E*)-2-(azetidin-1-yl)-3-((*E*)-2-(3-ethyl-1,1-dimethyl-1,3-dihydro-2*H*-benzo[*e*]indol-2-ylidene)ethylidene)cyclohex-1-en-1-yl)vinyl)-3-ethyl-1,1-dimethyl-1*H*-benzo[*e*]indol-3-ium iodide (**V-15**)

The title compound was prepared according to the general procedure at 0.1 mmol scale. Product **V-15** was isolated as a dark solid product (64 mg, 0.084 mmol, 84%).

$^1\text{H-NMR}$ (500 MHz, Chloroform-*d*): δ 8.07 (d, $J = 8.6$ Hz, 2H), 7.78 (dd, $J = 13.7$, 8.4 Hz, 4H), 7.48 (ddd, $J = 8.3$, 6.8, 1.3 Hz, 2H), 7.38 (d, $J = 12.8$ Hz, 2H), 7.29 (ddd, $J = 8.0$, 6.8, 1.0 Hz, 2H), 7.11 (d, $J = 8.7$ Hz, 2H), 5.43 (d, $J = 12.7$ Hz, 2H), 5.01 (t, $J = 7.5$ Hz, 4H), 3.88 (q, $J = 7.2$ Hz, 4H), 2.75 (p, $J = 7.5$ Hz, 2H), 2.55 (t, $J = 6.2$ Hz, 4H), 1.96 (s, 12H), 1.90 – 1.84 (m, 2H), 1.31 (t, $J = 7.2$ Hz, 6H).

$^{13}\text{C-NMR}$ (126 MHz, Chloroform-*d*): δ 169.26, 166.64, 140.07, 134.72, 131.06, 130.49, 129.81, 129.72, 128.65, 127.24, 123.39, 122.06, 117.62, 109.25, 91.46, 62.48, 49.04, 37.71, 28.66, 27.22, 20.84, 19.31, 11.59.

HRMS(ESI+): calcd for $\text{C}_{45}\text{H}_{50}\text{N}_3^+$ [M] $^+$ 632.4005, found 632.4007.



3-Ethyl-2-((*E*)-2-((*E*)-2-(ethyl(methyl)amino)-3-((*E*)-2-(3-ethyl-1,1-dimethyl-1,3-dihydro-2*H*-benzo[*e*]indol-2-ylidene)ethylidene)cyclohex-1-en-1-yl)vinyl)-1,1-dimethyl-1*H*-benzo[*e*]indol-3-ium iodide (**V-16**).

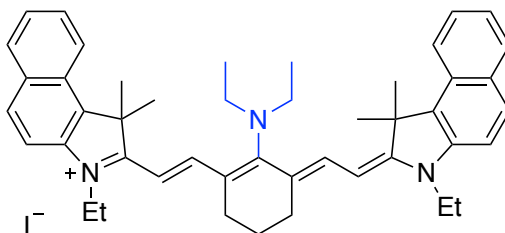
The title compound was prepared according to the general procedure at 0.1 mmol scale. Product **V-16** was isolated as a dark solid product (57 mg, 0.075 mmol, 75%).

$^1\text{H-NMR}$ (500 MHz, Chloroform-*d*): δ 8.06 (d, $J = 8.4$ Hz, 2H), 7.86 (dd, $J = 8.7$, 2.1 Hz, 4H), 7.63 (d, $J = 13.6$ Hz, 2H), 7.53 (ddd, $J = 8.4$, 6.8, 1.3 Hz, 2H), 7.36 (ddd, $J = 8.1$, 6.9, 1.1 Hz, 2H), 7.30 (d, $J = 8.8$ Hz, 2H), 5.82 (d, $J = 13.6$ Hz, 2H), 4.11 (q, $J = 7.2$

Hz, 4H), 3.80 (q, $J = 7.0$ Hz, 2H), 3.42 (s, 3H), 2.50 (t, $J = 6.4$ Hz, 4H), 1.92 (s, 12H), 1.85 (p, $J = 6.5$ Hz, 2H), 1.43 – 1.40 (m, 9H).

^{13}C -NMR (126 MHz, Chloroform-*d*): δ 173.76, 170.16, 141.76, 139.68, 132.27, 131.18, 130.46, 130.02, 128.35, 127.53, 124.33, 124.23, 121.83, 110.09, 95.39, 53.44, 49.99, 44.59, 39.03, 24.99, 21.96, 15.12, 12.24.

HRMS(ESI⁺): calcd for $\text{C}_{45}\text{H}_{52}\text{N}_3^+$ [M]⁺ 634.4161, found 634.4171.



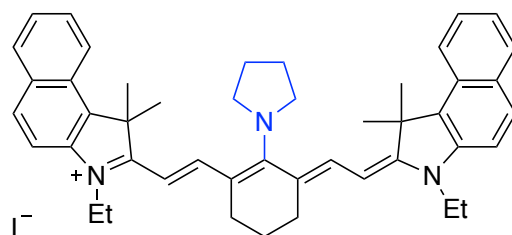
2-((*E*)-2-((*E*)-2-(diethylamino)-3-((*E*)-2-(3-ethyl-1,1-dimethyl-1,3-dihydro-2*H*-benzo[*e*]indol-2-ylidene)ethylidene)cyclohex-1-en-1-yl)vinyl)-3-ethyl-1,1-dimethyl-1*H*-benzo[*e*]indol-3-ium iodide (**V-17**)

The title compound was prepared according to the general procedure at 0.1 mmol scale. Product **V-16** was isolated as a dark solid product (36 mg, 0.046 mmol, 46%).

^1H -NMR (500 MHz, Chloroform-*d*): δ 8.07 (d, $J = 8.5$ Hz, 2H), 7.89 (d, $J = 8.9$ Hz, 4H), 7.69 (d, $J = 13.7$ Hz, 2H), 7.58 – 7.51 (m, 2H), 7.42 – 7.37 (m, 2H), 7.34 (d, $J = 8.8$ Hz, 2H), 5.89 (d, $J = 13.7$ Hz, 2H), 4.15 (q, $J = 7.2$ Hz, 4H), 3.70 (q, $J = 6.9$ Hz, 4H), 2.53 (t, $J = 6.4$ Hz, 4H), 1.93 (s, 12H), 1.89 – 1.85 (m, 2H), 1.44 (t, $J = 7.2$ Hz, 6H), 1.35 (t, $J = 6.9$ Hz, 6H).

^{13}C -NMR (126 MHz, Chloroform-*d*): δ 173.00, 170.56, 142.05, 139.64, 132.46, 131.29, 130.56, 130.10, 128.33, 127.57, 125.62, 124.37, 121.82, 110.20, 96.22, 50.06, 49.39, 39.18, 28.59, 28.44, 25.01, 22.05, 14.96, 12.31.

HRMS (ESI+): calcd for $\text{C}_{46}\text{H}_{54}\text{N}_3^+$ $[\text{M}]^+$ 648.4319, found 648.4318.



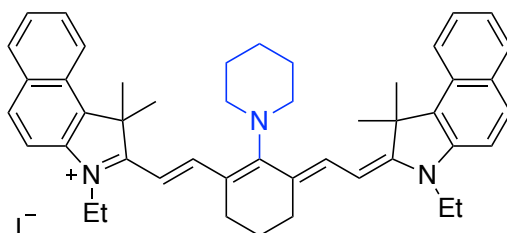
3-Ethyl-2-((*E*)-2-((*E*)-3-((*E*)-2-(3-ethyl-1,1-dimethyl-1,3-dihydro-2*H*-benzo[*e*]indol-2-ylidene)ethylidene)-2-(pyrrolidin-1-yl)cyclohex-1-en-1-yl)vinyl)-1,1-dimethyl-1*H*-benzo[*e*]indol-3-ium iodide (**V-18**).

The title compound was prepared according to the general procedure at 0.1 mmol scale. Product **V-18** was isolated as a dark solid product (56 mg, 0.072 mmol, 72%).

^1H -NMR (500 MHz, Chloroform-*d*): δ 8.08 (d, $J = 8.6$ Hz, 2H), 7.75 (dd, $J = 16.0$, 8.4 Hz, 4H), 7.53 (d, $J = 12.7$ Hz, 2H), 7.44 (dd, $J = 8.4$, 6.8 Hz, 2H), 7.25 (t, $J = 7.5$ Hz, 2H), 7.08 (d, $J = 8.7$ Hz, 2H), 5.38 (d, $J = 12.7$ Hz, 2H), 4.34 (d, $J = 6.4$ Hz, 4H), 3.84 (q, $J = 7.6$, 7.0 Hz, 4H), 2.62 (t, $J = 6.1$ Hz, 4H), 2.12 (q, $J = 4.7$, 3.1 Hz, 4H), 1.99 (s, 12H), 1.81 (p, $J = 6.4$ Hz, 2H), 1.29 (t, $J = 7.3$ Hz, 6H).

^{13}C -NMR (126 MHz, Chloroform-*d*): δ 172.74, 165.92, 140.25, 135.05, 130.89, 130.28, 129.65, 129.62, 128.76, 127.03, 123.10, 122.11, 120.64, 109.17, 91.03, 55.93, 48.99, 37.51, 28.81, 28.78, 24.30, 20.89, 11.50.

HRMS (ESI+): calcd for $\text{C}_{46}\text{H}_{52}\text{N}_3^+$ $[\text{M}]^+$ 646.4161, found 646.4163.



3-Ethyl-2-((*E*)-2-((*E*)-3-((*E*)-2-(3-ethyl-1,1-dimethyl-1,3-dihydro-2*H*-benzo[*e*]indol-2-ylidene)ethylidene)-2-(piperidin-1-yl)cyclohex-1-en-1-yl)vinyl)-1,1-dimethyl-1*H*-benzo[*e*]indol-3-ium iodide (**V-19**).

The title compound was prepared according to the general procedure at 0.1 mmol scale. Product **V-18** was isolated as a dark solid product (66 mg, 0.084 mmol, 84%).

¹H-NMR (500 MHz, Chloroform-*d*): δ 8.06 (d, *J* = 8.6 Hz, 2H), 7.84 (d, *J* = 8.5 Hz, 4H), 7.68 (d, *J* = 13.3 Hz, 2H), 7.51 (ddd, *J* = 8.3, 6.8, 1.3 Hz, 2H), 7.34 (ddd, *J* = 8.0, 6.8, 1.0 Hz, 2H), 7.27 (d, *J* = 8.7 Hz, 2H), 5.78 (d, *J* = 13.3 Hz, 2H), 4.07 (q, *J* = 7.2 Hz, 4H), 3.79 (t, *J* = 4.8 Hz, 4H), 2.48 (t, *J* = 6.6 Hz, 4H), 1.95 – 1.80 (m, 20H), 1.40 (t, *J* = 7.2 Hz, 6H).

¹³C-NMR (126 MHz, Chloroform-*d*): δ 174.14, 169.56, 140.35, 139.77, 131.99, 131.07, 130.38, 129.99, 128.39, 127.46, 124.08, 124.04, 121.86, 110.03, 94.84, 56.78, 49.78, 38.85, 28.48, 28.23, 25.07, 24.57, 21.83, 12.18.

HRMS (ESI+): calcd for C₄₇H₅₄N₃⁺ [M]⁺ 660.4318, found 660.4318.

REFERENCES

REFERENCES

1. Yang, C. C.; Lunt, R. R., Limits of Visibly Transparent Luminescent Solar Concentrators. *Adv Opt Mater* **2017**, *5* (8), 1600851.
2. Traverse, C. J.; Pandey, R.; Barr, M. C.; Lunt, R. R., Emergence of highly transparent photovoltaics for distributed applications (vol 2, pg 849, 2017). *Nat Energy* **2018**, *3* (2), 157-157.
3. Suddard-Bangsund, J.; Traverse, C. J.; Young, M.; Patrick, T. J.; Zhao, Y. M.; Lunt, R. R., Organic Salts as a Route to Energy Level Control in Low Bandgap, High Open-Circuit Voltage Organic and Transparent Solar Cells that Approach the Excitonic Voltage Limit. *Adv Energy Mater* **2016**, *6* (1), 1501659.
4. Ooyama, Y.; Harima, Y., Photophysical and Electrochemical Properties, and Molecular Structures of Organic Dyes for Dye-Sensitized Solar Cells (vol 13, pg 4032, 2012). *Chemphyschem* **2013**, *14* (5), 871-871.
5. Sharma, M.; Gungor, K.; Yeltik, A.; Olutas, M.; Guzelturk, B.; Kelestemur, Y.; Erdem, T.; Delikanli, S.; McBride, J. R.; Demir, H. V., Near-Unity Emitting Copper-Doped Colloidal Semiconductor Quantum Wells for Luminescent Solar Concentrators. *Adv Mater* **2017**, *29* (30), 1700821.
6. Geiger, T.; Schoger, I.; Rentsch, D.; Veron, A. C.; Oswald, F.; Meyer, T.; Nuesch, F., Unsymmetrical Heptamethine Dyes for NIR Dye-Sensitized Solar Cells. *Int J Photoenergy* **2014**, 258984.
7. Shi, C. H.; Wu, J. B.; Pan, D. F., Review on near-infrared heptamethine cyanine dyes as theranostic agents for tumor imaging, targeting, and photodynamic therapy. *J Biomed Opt* **2016**, *21* (5), 50901.
8. Hong, G. S.; Antaris, A. L.; Dai, H. J., Near-infrared fluorophores for biomedical imaging. *Nat Biomed Eng* **2017**, *1* (1), 0010.
9. Yuan, L.; Lin, W. Y.; Zheng, K. B.; He, L. W.; Huang, W. M., Far-red to near infrared analyte-responsive fluorescent probes based on organic fluorophore platforms for fluorescence imaging. *Chem Soc Rev* **2013**, *42* (2), 622-661.
10. Sun, W.; Guo, S. G.; Hu, C.; Fan, J. L.; Peng, X. J., Recent Development of Chemosensors Based on Cyanine Platforms. *Chem Rev* **2016**, *116* (14), 7768-7817.
11. Zhao, Y. M.; Meek, G. A.; Levine, B. G.; Lunt, R. R., Near-Infrared Harvesting Transparent Luminescent Solar Concentrators. *Adv Opt Mater* **2014**, *2* (7), 606-611.

12. Peng, X. J.; Song, F. L.; Lu, E.; Wang, Y. N.; Zhou, W.; Fan, J. L.; Gao, Y. L., Heptamethine cyanine dyes with a large Stokes shift and strong fluorescence: A paradigm for excited-state intramolecular charge transfer. *J Am Chem Soc* **2005**, *127* (12), 4170-4171.
13. Pascal, S.; Haefele, A.; Monnereau, C.; Charaf-Eddin, A.; Jacquemin, D.; Le Guennic, B.; Andraud, C.; Maury, O., Expanding the Polymethine Paradigm: Evidence for the Contribution of a Bis-Dipolar Electronic Structure. *J Phys Chem A* **2014**, *118* (23), 4038-4047.
14. Grimm, J. B.; English, B. P.; Chen, J. J.; Slaughter, J. P.; Zhang, Z. J.; Revyakin, A.; Patel, R.; Macklin, J. J.; Normanno, D.; Singer, R. H.; Lionnet, T.; Lavis, L. D., A general method to improve fluorophores for live-cell and single-molecule microscopy. *Nat Methods* **2015**, *12* (3), 244-250.
15. Arjona-Esteban, A.; Stolte, M.; Wurthner, F., Conformational Switching of π -Conjugated Junctions from Merocyanine to Cyanine States by Solvent Polarity. *Angew Chem Int Edit* **2016**, *55* (7), 2470-2473.
16. Das, R. K.; Samanta, A.; Ha, H. H.; Chang, Y. T., Solid phase synthesis of ultra-photostable cyanine NIR dye library. *Rsc Adv* **2011**, *1* (4), 573-575.
17. Funabiki, K.; Yagi, K.; Ueta, M.; Nakajima, M.; Horiuchi, M.; Kubota, Y.; Mastui, M., Rational Molecular Design and Synthesis of Highly Thermo- and Photostable Near-Infrared-Absorbing Heptamethine Cyanine Dyes with the Use of Fluorine Atoms. *Chem-Eur J* **2016**, *22* (35), 12282-12285.
18. Konig, S. G.; Kramer, R., Accessing Structurally Diverse Near-Infrared Cyanine Dyes for Folate Receptor-Targeted Cancer Cell Staining. *Chem-Eur J* **2017**, *23* (39), 9306-9312.
19. Nani, R. R.; Gorke, A. P.; Nagaya, T.; Yamamoto, T.; Ivanic, J.; Kobayashi, H.; Schnermann, M. J., In Vivo Activation of Duocarmycin-Antibody Conjugates by Near-Infrared Light. *Acs Central Sci* **2017**, *3* (4), 329-337.
20. Pascal, S.; Denis-Quanquin, S.; Appaix, F.; Duperray, A.; Grichine, A.; Le Guennic, B.; Jacquemin, D.; Cuny, J.; Chi, S. H.; Perry, J. W.; van der Sanden, B.; Monnereau, C.; Andraud, C.; Maury, O., Keto-polymethines: a versatile class of dyes with outstanding spectroscopic properties for in cellulo and in vivo two-photon microscopy imaging. *Chem Sci* **2017**, *8* (1), 381-394.
21. Lou, Z. R.; Li, P.; Song, P.; Han, K. L., Ratiometric fluorescence imaging of cellular hypochlorous acid based on heptamethine cyanine dyes. *Analyst* **2013**, *138* (21), 6291-6295.

22. Zheng, L. H.; Wang, L. Q.; Wang, P. J.; Sun, Q.; Liu, X. L.; Zhang, X. B.; Qiu, S. B., Substitution nitrogen for chlorine of heptamethine cyanines for large Stokes shift fluorescent probes. *Tetrahedron Lett* **2016**, *57* (8), 932-936.
23. Michie, M. S.; Gotz, R.; Franke, C.; Bowler, M.; Kumari, N.; Magidson, V.; Levitus, M.; Loncarek, J.; Sauer, M.; Schnermann, M. J., Cyanine Conformational Restraint in the Far-Red Range. *J Am Chem Soc* **2017**, *139* (36), 12406-12409.
24. Samanta, A.; Vendrell, M.; Das, R.; Chang, Y. T., Development of photostable near-infrared cyanine dyes. *Chem Commun* **2010**, *46* (39), 7406-7408.
25. Bouit, P. A.; Aronica, C.; Toupet, L.; Le Guennic, B.; Andraud, C.; Maury, O., Continuous Symmetry Breaking Induced by Ion Pairing Effect in Heptamethine Cyanine Dyes: Beyond the Cyanine Limit. *J Am Chem Soc* **2010**, *132* (12), 4328-4335.
26. Shao, Y. H.; Gan, Z. T.; Epifanovsky, E.; Gilbert, A. T. B.; Wormit, M.; Kussmann, J.; Lange, A. W.; Behn, A.; Deng, J.; Feng, X. T.; Ghosh, D.; Goldey, M.; Horn, P. R.; Jacobson, L. D.; Kaliman, I.; Khaliullin, R. Z.; Kus, T.; Landau, A.; Liu, J.; Proynov, E. I.; Rhee, Y. M.; Richard, R. M.; Rohrdanz, M. A.; Steele, R. P.; Sundstrom, E. J.; Woodcock, H. L.; Zimmerman, P. M.; Zuev, D.; Albrecht, B.; Alguire, E.; Austin, B.; Beran, G. J. O.; Bernard, Y. A.; Berquist, E.; Brandhorst, K.; Bravaya, K. B.; Brown, S. T.; Casanova, D.; Chang, C. M.; Chen, Y. Q.; Chien, S. H.; Closser, K. D.; Crittenden, D. L.; Diedenhofen, M.; DiStasio, R. A.; Do, H.; Dutoi, A. D.; Edgar, R. G.; Fatehi, S.; Fusti-Molnar, L.; Ghysels, A.; Golubeva-Zadorozhnaya, A.; Gomes, J.; Hanson-Heine, M. W. D.; Harbach, P. H. P.; Hauser, A. W.; Hohenstein, E. G.; Holden, Z. C.; Jagau, T. C.; Ji, H. J.; Kaduk, B.; Khistyayev, K.; Kim, J.; Kim, J.; King, R. A.; Klunzinger, P.; Kosenkov, D.; Kowalczyk, T.; Krauter, C. M.; Lao, K. U.; Laurent, A. D.; Lawler, K. V.; Levchenko, S. V.; Lin, C. Y.; Liu, F.; Livshits, E.; Lochan, R. C.; Luenser, A.; Manohar, P.; Manzer, S. F.; Mao, S. P.; Mardirossian, N.; Marenich, A. V.; Maurer, S. A.; Mayhall, N. J.; Neuscamman, E.; Oana, C. M.; Olivares-Amaya, R.; O'Neill, D. P.; Parkhill, J. A.; Perrine, T. M.; Peverati, R.; Prociuk, A.; Rehn, D. R.; Rosta, E.; Russ, N. J.; Sharada, S. M.; Sharma, S.; Small, D. W.; Sodt, A.; Stein, T.; Stuck, D.; Su, Y. C.; Thom, A. J. W.; Tsuchimochi, T.; Vanovschi, V.; Vogt, L.; Vydrov, O.; Wang, T.; Watson, M. A.; Wenzel, J.; White, A.; Williams, C. F.; Yang, J.; Yeganeh, S.; Yost, S. R.; You, Z. Q.; Zhang, I. Y.; Zhang, X.; Zhao, Y.; Brooks, B. R.; Chan, G. K. L.; Chipman, D. M.; Cramer, C. J.; Goddard, W. A.; Gordon, M. S.; Hehre, W. J.; Klamt, A.; Schaefer, H. F.; Schmidt, M. W.; Sherrill, C. D.; Truhlar, D. G.; Warshel, A.; Xu, X.; Aspuru-Guzik, A.; Baer, R.; Bell, A. T.; Besley, N. A.; Chai, J. D.; Dreuw, A.; Dunietz, B. D.; Furlani, T. R.; Gwaltney, S. R.; Hsu, C. P.; Jung, Y. S.; Kong, J.; Lambrecht, D. S.; Liang, W. Z.; Ochsenfeld, C.; Rassolov, V. A.; Slipchenko, L. V.; Subotnik, J. E.; Van Voorhis, T.; Herbert, J. M.; Krylov, A. I.; Gill, P. M. W.; Head-Gordon, M., Advances in molecular quantum chemistry contained in the Q-Chem 4 program package. *Mol Phys* **2015**, *113* (2), 184-215.

27. Adamo, C.; Jacquemin, D., The calculations of excited-state properties with Time-Dependent Density Functional Theory. *Chem Soc Rev* **2013**, *42* (3), 845-856.
28. Le Guennic, B.; Jacquemin, D., Taking Up the Cyanine Challenge with Quantum Tools. *Accounts Chem Res* **2015**, *48* (3), 530-537.
29. Davydenko, I.; Barlow, S.; Sharma, R.; Benis, S.; Simon, J.; Allen, T. G.; Cooper, M. W.; Khurstalev, V.; Jucov, E. V.; Castaneda, R.; Ordonez, C.; Li, Z. A.; Chi, S. H.; Jang, S. H.; Parker, T. C.; Timofeeva, T. V.; Perry, J. W.; Jen, A. K. Y.; Hagan, D. J.; Van Stryland, E. W.; Marder, S. R., Facile Incorporation of Pd(PPh₃)₂Hal Substituents into Polymethines, Merocyanines, and Perylene Diimides as a Means of Suppressing Intermolecular Interactions. *J Am Chem Soc* **2016**, *138* (32), 10112-10115.
30. Liu, X. G.; Qiao, Q. L.; Tian, W. M.; Liu, W. J.; Chen, J.; Lang, M. J.; Xu, Z. C., Aziridiny Fluorophores Demonstrate Bright Fluorescence and Superior Photostability by Effectively Inhibiting Twisted Intramolecular Charge Transfer. *J Am Chem Soc* **2016**, *138* (22), 6960-6963.